A STABLE ISOTOPIC ANALYSIS OF SYN-TECTONIC FLUID REGIMES IN THE DOGTOOTH, WESTERN, AND MAIN RANGES OF SOUTHEASTERN BRITISH COLUMBIA

by

STUART R. KNOOP

B.A., Oberlin College, 1992

A THESIS SUBMITTED IN PARTIAL FULFILLMENT OF THE REQUIREMENTS FOR

THE DEGREE OF MASTER OF SCIENCE

in

THE FACULTY OF GRADUATE STUDIES

(Department of Earth and Ocean Sciences)

We accept this thesis as conforming to the required standard

THE UNIVERSITY OF BRITISH COLUMBIA

June, 2000

In presenting this thesis in partial fulfilment of the requirements for an advanced degree at the University of British Columbia, I agree that the Library shall make it freely available for reference and study. I further agree that permission for extensive copying of this thesis for scholarly purposes may be granted by the head of my department or by his or her representatives. It is understood that copying or publication of this thesis for financial gain shall not be allowed without my written permission.

Department of Earth + Ocean Sciences

The University of British Columbia
Vancouver, Canada

Date July 7, 2000

DE-6 (2/88)

ABSTRACT

Stable isotope data from syn-kinematic veins, cataclasites, and wall rocks in the Dogtooth, Western, and Main Ranges of southeastern British Columbia document fluid migration across local and large-scale (100's of meters to 10's of kilometers) distances during Mesozoic contraction. Sampling was conducted across a ~30 km long western transect, which includes siliciclastic-dominated assemblages of the Dogtooth Range and carbonate units of the Western Ranges, and a ~5 km long eastern transect in carbonates and meta-pelites of the western Main Ranges. Syn-tectonic veins throughout the study area are comprised primarily of quartz and calcite and conform to three morphologies: i) laminated, bedding-parallel veins and syntaxial tension gashes, ii) boudinaged, cleavage-parallel veins, and iii) cataclasites and fault-parallel veins.

In the Dogtooth Range, the oxygen isotopic composition of whole rock carbonates is ~5 ‰ lower than accepted sedimentary protolith values. Vein calcite is generally depleted in ^{18}O, whereas vein quartz is equally enriched and depleted compared with host rocks. Fluid-assisted isotopic exchange between siliciclastic and less-abundant carbonate assemblages across outcrops has lowered carbonate signatures and yielded quartz vein values that are more homogeneous than those of wall rocks. Hydrogen isotopes suggest that the fluids involved were metamorphic in origin with a possible meteoric component.

In comparison, the Western Ranges exhibit an abrupt, mean $\delta^{18}O$ increase of ~ 4.5 ‰ and a trend of gradually heavier values with distance up-section and eastward from the Dogtooth Range. Neither variation in age nor mineral abundance can fully explain this phenomenon. Moreover, isotope and solvus thermometry indicate that veins were in thermal equilibrium with

their host rocks (~300°C - 380°C). Hinterland-driven infiltration of low-$\delta^{18}O$, low X_{CO2} fluid into the Western Ranges best explains this trend, and analytical modeling places time-integrated fluid fluxes at 10^4 - 10^5 mol H_2O/cm^2.

In the Main Ranges, oxygen values are more heterogeneous and reflect multiple fluid sources. Vein signatures as low as 6 ‰ indicate minor focussing of meteoric fluids downward into some fault zones. Variable vein quartz and wall rock carbonate values in other outcrops, in conjunction with a metamorphic hydrogen signature from vein chlorite, suggest that lower-$\delta^{18}O$, metamorphic fluids were channeled upward under conditions of heterogeneous time-integrated fluid flux.

TABLE OF CONTENTS

LIST OF TABLES

LIST OF FIGURES

LIST OF PLATES

ACKNOWLEDGEMENTS

I am indebted to my supervisory committee, Lori Kennedy, Greg Dipple, and Steve Rowins, whose patience and encouragement have kept me blind to the toil that has encompassed these last six months. Above all, I thank Lori and Greg for their camaraderie and continued intellectual and financial investment in this project. Their good humor, pep talks, and ability to integrate the big picture with the seemingly endless minutia of data and transmutations thereof are qualities to be emulated by all supervisors.

Phil Simony displayed enormous generosity in taking the time to teach me about the geology of the eastern Cordillera the way it should be taught, in the field. Kurt Kyser and Kerry Klassen at Queen's were always quick with their analyses and very responsive to my questions, both relevant and irrelevant. Mati Raudsepp and Elisabetta Pani were unbegrudging about teaching me the same things over and over on the SEM and microprobe. Hans Machel at U. of Alberta was remarkably approachable and enthusiastic about allowing me use of his cathodoluminescence equipment. Chris Akelaitis and Jenny Dicus were not only tireless pack mules and patient brunton bearers, but also wise field geologists who quickly corrected me when I was caught staring at the sun too long.

Praise Maile Smith for being Lori's first graduate student. Thanks to Steve Israel for his friendship and contagious iron will when it comes to forging through the Disneyland of graduate school. Finally, thanks to Dana Ayotte, to whom I owe most of my well-grounded lunacy these past few years. Without her, I would've been gone long ago.

CHAPTER 1

INTRODUCTION

1.1 Context of study

Over the past 20 years, much has been written about the role of fluid migration in deformation and orogenesis. Theoretical models suggest that fluids are potentially rate-controlling factors for strain during pressure solution [*Etheridge et al.,* 1984], brittle faulting [*Hubbert and Rubey*, 1959; *Sibson*, 1990, 1996], and ductile shear [*McCaig*, 1988] and might be transported across vast distances during accretionary and mountain building events [*Koons and Craw*, 1991]. Specifically, fluid migration is at least partially responsible for the maintenance of elevated pore fluid pressure and mass transport that drive the development of faults and pressure solution cleavage associated with major orogenic events. The questions of how much fluid is involved, how far it has travelled, and from whence it originated are an ongoing topic of discussion in the literature and the focus of this thesis.

Chemical alteration in stable (e.g., O, C, H, and N) and radiogenic isotopes (e.g., Sr), as well as major, minor, and trace elements, has provided some of the best evidence that the above mentioned scenarios adequately describe hydromechanical processes within some terranes. This study utilizes oxygen, carbon, and to a lesser degree, hydrogen isotopes to document fluid advection across a scale of centimeters, meters, and kilometers during the Late Jurassic through Early Cretaceous contractional event that affected the northern Purcell and western Rocky Mountains of southeastern British Columbia. Over the course of two field seasons, syn-kinematic veins, wall rocks, and samples of fault breccia were collected for isotopic analysis along 100 - 500 m traverses across regional faults and local fault and fracture zones in the Dogtooth, Western, and Main Ranges. *Balkwill* [1969,1972], *Simony and Wind* [1970], *Cook* [1975],

Gardner [1977], *Stewart* [1989], and *Kubli and Simony* [1992, 1994] have thoroughly investigated the stratigraphy, structure, and regional geology of the study area. This well constrained geological history permits robust interpretations about the chronology and flowpath of fluid events that affected the region.

In total, 170 analyses were obtained from 21 localities that were spread nearly 60 km across strike. Detailed observations about the relative timing of veins and comparisons between the isotopic composition of veins and wall rocks within individual outcrops were crucial in constraining the degree of disequilibrium (i.e., chemical buffering) between fluids and rocks during deformation. Kilometer-scale trends in isotope composition were also addressed within the context of an abrupt, regional isotopic shift across the Purcell Thrust Fault, which separates the Dogtooth Range in its hanging wall from Western Ranges' structures in its footwall. Where large scale fluid migration through the shallow crust is normally obscured during isotopic buffering by homogeneous rock reservoirs, a geochemical boundary such as this can result in an isotopic front, which records fluid infiltration as rock alteration and disequilibrium among veins and wall rocks. Moreover, the geometry and lateral extent of the alteration front carries important implications about the total time-integrated fluid flux and degree of kinetic dispersion that were involved during the flow event. A focus on local vein-rock relationships and a regional isotopic front distinguishes this study from previous work by *Nesbitt and Muehlenbachs* [1995, 1997], who provided a more generalized isotopic analysis of veins in the Rocky and Purcell Mountains.

1.2 Organization of thesis

This thesis presents observations and interpretations from two isotopic transects. The western transect, discussed in Chapters 2-4, includes localities in the Dogtooth and Western Ranges and represents the bulk of the isotope data collected in this study. Outcrops in the western Main Ranges comprise the eastern transect.

Chapter 2 provides a comprehensive discussion of fluid regimes in the western transect solely based upon oxygen isotope data. It has been written as a stand-alone paper for submission for publication and can be read without reference to other chapters. The objectives of Chapter 2 are to (i) document and explore the implications of the isotopic shift across the Purcell Thrust, (ii) investigate isotopic relationships between veins and wall rocks at each locality as a means of identifying open versus closed system fluid regimes, and (iii) formulate conclusions about the magnitude of fluid advection and the source of fluids based on large-scale patterns of isotopic alteration and an analytical transport model.

Chapter 3 uses additional data from carbon and, to a lesser degree, hydrogen isotopes to expand upon the conclusions of Chapter 2 and further discuss fluid sources in the western transect.

Chapter 4 provides results from a cathodoluminescence study that was performed on veins and cataclasites to elucidate geochemical patterns at the microstructural scale in the western transect.

Chapter 5 presents oxygen and carbon isotope data from the eastern transect. Here, the objectives are to (i) compare wall rock signatures with those expected from similar rocks of the same age, (ii) investigate the isotopic relationship between veins and wall rocks in order to cite

possible evidence for the infiltration of exotic fluids into the local fluid-rock system, and (iii) compare these findings with observations from the western transect.

A complete data set and an extended description and synthesis of the geological context and isotope systematics at each sample locality are provided in the Appendices.

CHAPTER 2

FLUID REGIMES ACROSS THE DOGTOOTH AND WESTERN RANGES AS INFERRED FROM OXYGEN ISOTOPES

2.1 Introduction

Numerous studies have explored the potential for large-scale fluid migration during orogenesis and its role in the generation of geochemical fronts, mineral deposits, and hydrocarbon reservoirs [e.g., *Oliver*, 1986; *Bradbury and Woodwell*, 1987; *Ferry*, 1992; *Machel et al.*, 1996; *Oliver*, 1996]. Because of the large buffering capacity of silicate and carbonate rocks in the cold, brittle crust, the use of oxygen isotopes to track fluids as they alter wall rocks and precipitate veins is problematic. Studies in the foreland [*Nesbitt and Muehlenbachs*, 1995] and Front Ranges [*Woodwell*, 1985; *Kirschner and Kennedy*, in press] of the Canadian Rockies have focussed on lithologically, and therefore isotopically, homogeneous domains where enormous carbonate reservoirs can easily diminish the isotopic imprint of through-going fluids. This study utilizes oxygen isotopes from over 100 samples of wall rock, syn-kinematic veins, and fault breccia to interpret both outcrop-scale (< 500 m) and regional (> 1 km) fluid regimes across the hinterland-foreland transition of the Canadian Cordillera. I capitalize upon an abrupt, regional isotopic change in wall rock composition, where transport theory dictates that alteration from fluid migration will be most conspicous [e.g., *Bickle and McKenzie*, 1987]. This lateral shift occurs across a structural boundary that loosely coincides with the hinterland-foreland transition and exposes the subtle effects of a km-scale, deformation-driven fluid event in the Canadian Rockies that went previously undetected.

The sampling transect extends 30 km across strike from the Dogtooth Range in the northern Purcell Mountains, across the Rocky Mountain Trench (RMT), and into the Western Ranges of the Rocky Mountain foreland (Figures 2.1 and 2.2). The Purcell Thrust, an out of sequence fault that separates predominantly siliciclastic sedimentary rocks of the Dogtooth Range from younger, calcite dominated sequences in the RMT and Western Ranges, delineates an abrupt, regionally significant structural, stratigraphic, and isotopic boundary. This provides an excellent opportunity to test for km-scale fluid migration across the shift in the form of an isotopic alteration front. This paper expands upon prior studies in the region that have used stable isotope and fluid inclusion data to address the origin and timing of vein forming fluids [*Nesbitt and Muehlenbachs*, 1994, 1995, 1997]. Specifically, this contribution (1) documents an isotopic shift and explores in detail the implications of this structurally defined boundary, (2) places explicit constraints on the timing of veins and fault-related fabrics and links them with geochemical data, and (3) provides extensive analysis and discussion of the isotopic composition of lithologically diverse wall rocks.

These results carry implications for similar thin-skinned fold and thrust belts that incorporate sediments deposited within a passive continental margin/continental rift setting. The lateral (and vertical) change from calcareous sequences, which were emplaced along a carbonate platform, into siliceous, turbiditic/pelagic (miogeoclinal) sediments is a feature observed in orogenic belts throughout the world (e.g., MacKenzie-Selwyn fold and thrust belts, Ouachita fold and thrust belt, Alice Springs orogen). However, this transition is frequently distorted by subsequent deformation events or distended across vast lateral distances. The uplift and exposure of deep-water sediments by the Purcell Thrust therefore permits investigation of this

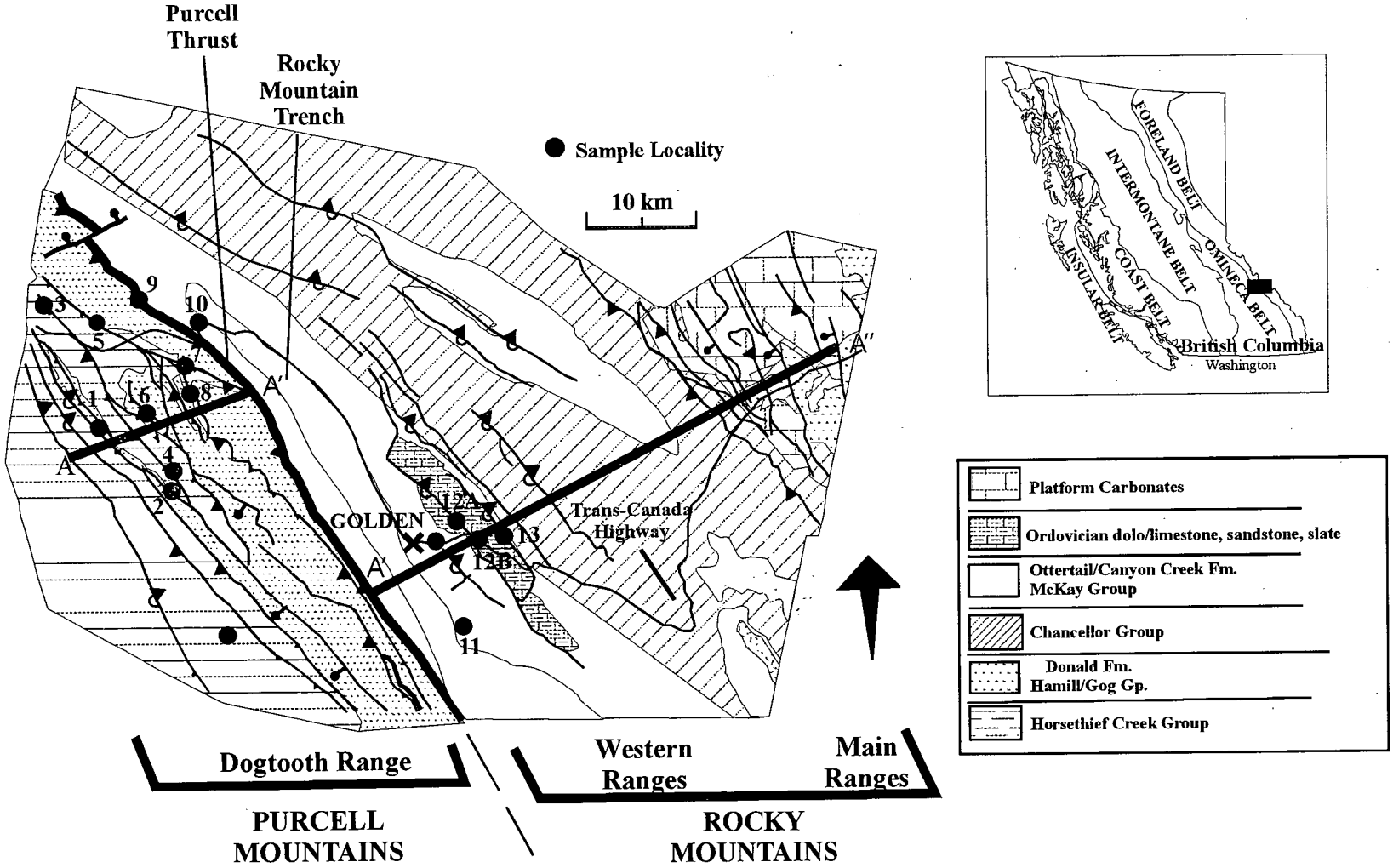

Figure 2.1: Regional map of study area including sample locations denoted by solid circles. Modified from *Price and Simony*, 1971.

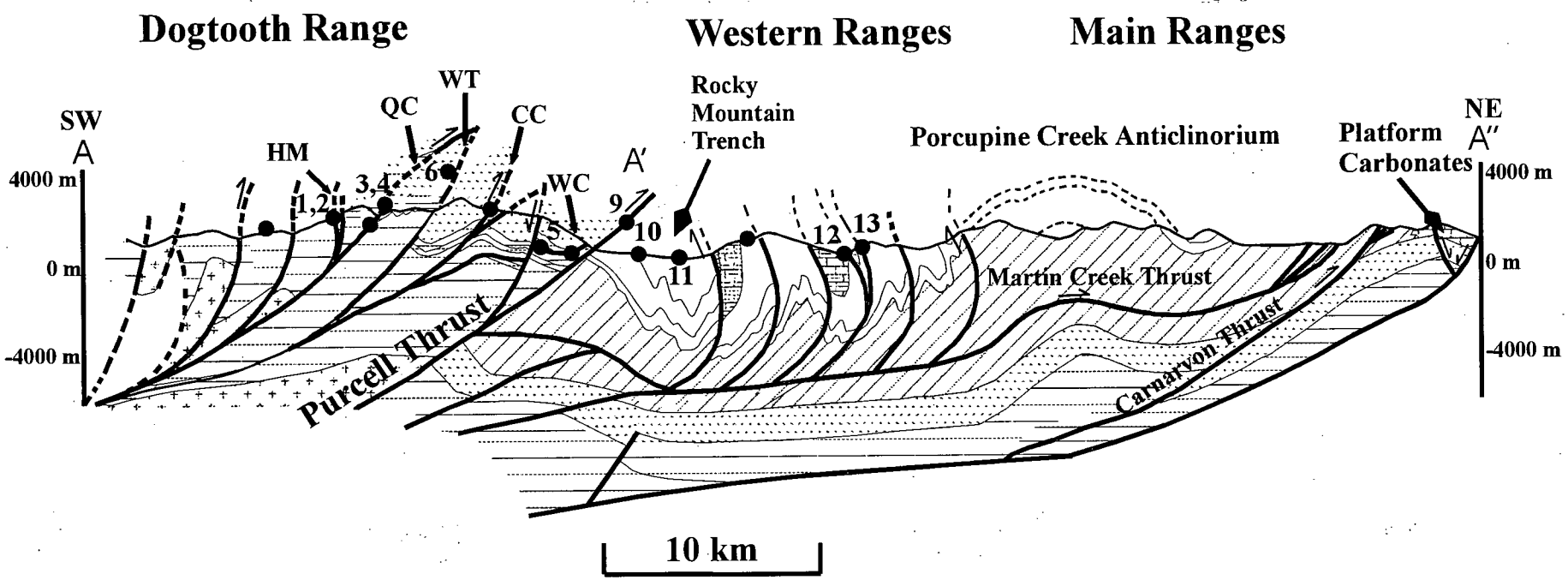

Figure 2.2: Simplified cross-section of study area. Solid circles denote sample localities. Circles above topography reflect localities away from line of section. Modified from *Kubli* [1990], *Kubli and Simony* [1994], *Price and Simony* [1971], *Balkwill* [1969], and *Cook* [1970]. HM=Heather Mountain Thrust; QC=Quartz Creek Thrust;WT= Wall Thrust; CC=Cirque Creek Thrust; WC=Wiseman Creek Thrust.

juxtaposition between geochemically distinct sedimentary packages and its relevance to the paleohydrology of a deforming orogen.

Nesbitt and Muehlenbachs [1995,1997] used data from fluid inclusions and hydrogen and oxygen isotopes to assert that fluid flow during Mesozoic contraction in the Purcell and Rocky Mountains was minimal. They argued that most veins record either a pre-tectonic phase of fluid flow related to early metamorphism or result from the channeling of meteoric waters down dip along normal faults during Early Tertiary extension. On the basis of textural and cross-cutting relationships between veins, faults, and regional foliation, I propose an alternative scenario in which fluctuating pore fluid pressure and fluid supply yielded several distinct generations of veins during the bulk shortening that affected the Dogtooth and Western Ranges between Late-Jurassic and Early Cretaceous time. By focussing on syn-kinematic veins, I assess the importance of deformation-driven fluid advection in its capacity to promote wall rock alteration along local pressure gradients at individual outcrops, and simultaneously drive a large hydrothermal cell across several thrust sheets.

Numerous researchers cite systematic oxygen isotope depletions and large changes in major element concentration within both basement and supracrustal shear zones to justify deep (upper greenschist to granulite facies) and voluminous ($\cong 10^4$-10^5 m^3/m^2) infiltration of meteoric and metamorphic fluids during contraction [e.g., *Burkhard and Kerrich*, 1988; *Marquer and Burkhard*, 1992; *Dipple and Ferry*, 1992a; *Cartwright and Buick*, 1999]. From their study of shallow level (200-300°C) carbonates in the Swiss Alps, *Marquer and Burkhard* [1992] have interpreted isotope depletions in late-stage veins and mylonites as evidence that km-scale interconnectedness between shear zones was a mitigating factor in promoting fluid expulsion upwards from crystalline basement. In addition, isotopic evidence suggests that stylolites can

behave as conduits that transmit a significant volume ($\cong 10^9$ m^3/m^2) of metamorphic water [*Bradbury and Woodwell*, 1987].

Other case studies infer that regional deformation by pressure solution and faulting need not be accompanied by extreme volume loss or a large time-integrated fluid flux. Based on low isotopic fractionation between veins and wall rocks near thrust faults, *Cartwright et al.* [1994] concluded that fluid circulation beyond 10's to 100's of meters was unlikely during tectonism in parts of the Alice Spring Orogen in central Australia. *Waldron and Sandiford* [1988] performed strain analysis on porphyroclasts in the Ballarat slate belt of southeastern Australia to show that volume was conserved during deformation, thereby minimizing mass transport into and out of the local fluid-rock system. In a dramatic example from the Lachlan fold belt of southeastern Australia, *Gray et al.* [1991] demonstrated that diffusion and advection over relatively small distances (10's-100's of meters) combined to promote the isotopic homogenization of quartz veins in thrust sheets and faults throughout 80,000 km^2. Finally, *Kirschner and Kennedy* [in press] found no isotopic evidence for extensive fluid advection outside of very narrow shear zones in the Front Ranges of the Canadian Rockies.

Here, I interpret isotopic relationships across the scale of centimeters (vein-wall rock pairs), tens of meters (outcrops), and kilometers (regional comparisons) to reconcile the quandary of closed versus open-system fluid regimes for a segment of the Canadian Cordillera. By analysis of rocks and veins located various distances away from thrust faults I assess the role of brittle faulting as a mechanism for channeling large volumes of fluids during displacement. Finally, this study has implications for structurally similar terranes in which cleavage development played a pre-eminent role in tectonic shortening and also serves as a basis for

comparison with studies from different structural domains such as the Rocky Mountain Front Ranges.

2.2 Regional Overview

The study area encompasses 1100 km^2 from the western Dogtooth Range near Glacier National Park to the central Western Ranges east of Golden, BC, and straddles a major tectonic boundary between two morphogeological belts of the Canadian Cordillera (Figure 2.1). The Dogtooth Range occupies the eastern extent of the Omineca Belt, a province that contains the suture of marine sediments from the Upper Proterozoic and Lower Cambrian North American rift margin with accreted island arcs and oceanic crust of Late Paleozoic to Early Mesozoic age. The Western Ranges form the western boundary of the Foreland Belt, which is characterized for its thin-skinned style of tectonism with broad, regional folds that overlie shallow-dipping decollements. Together, the Dogtooth and Western Ranges represent a structural transition from the poly-deformed, greenschist to amphibolite grade rocks that comprise the Selkirk Complex in the west to the fault-dominated, foreland-style tectonism that affects sub-greenschist assemblages in the platform carbonates of the Rocky Mountain Main and Front Ranges [*Gabrielse and Yorath*, 1992].

Wall rock composition varies substantially between the Dogtooth Range, where slate, phyllite, and sandstone possess < 20 vol. % carbonate minerals, and the Western Ranges, which are comprised of pelite, limestone, and dolostone with > 50 vol. % calcite and dolomite. In the Dogtooth Range, the northwest trending Wall Thrust delineates a boundary between a >3000 m thick succession of quartz, muscovite, and chlorite rich turbidites that belong to the Upper Proterozoic Horsethief Creek Group in the west and a 950-1750 m thick package of

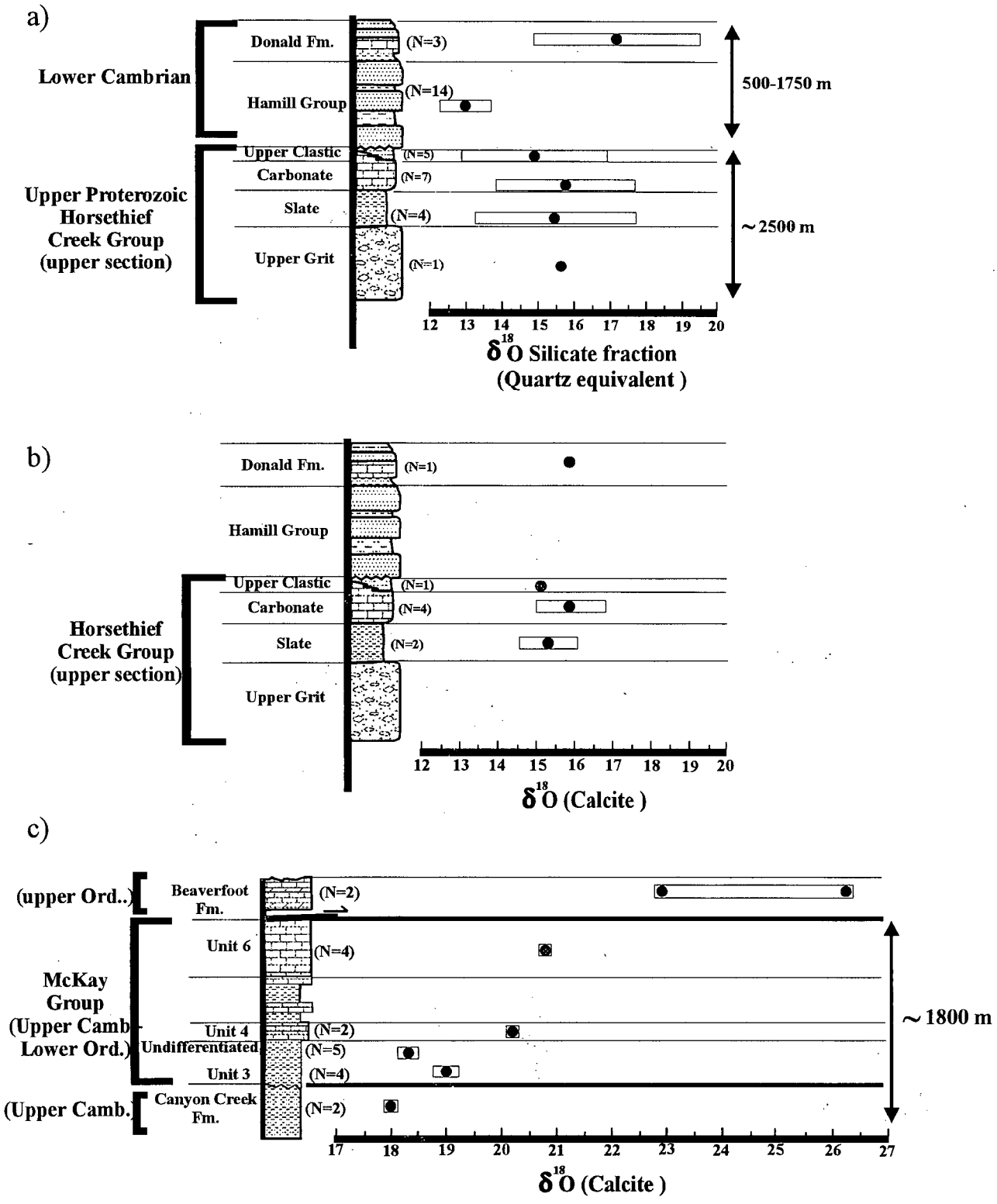

Figure 2.3: Distribution of oxygen isotope values by stratigraphic horizon. Bars denote 1σ of population.(a) and (b) Units from the Dogtooth Range exhibit no isotopic trend with decreasing age. Stratigraphic section modified from *Kubli and Simony* [1992]. (c) Units in the Western Ranges show isotopic enrichmentin younger units. Section modified from *Cook* [1975].

predominantly quartzite, siltstone, and shale from the Lower Cambrian Hamill Group and Donald Formation [Figures 2.2 and 2.3 - *Simony and Wind*, 1970; *Kubli*, 1990]. All units possess minor calcite and dolomite, which are either disseminated within pelites or occur as discrete interbeds that range in thickness between decimeters and tens of meters. Pervasive chlorite and siderite record lower greenschist facies metamorphism, and *Kubli* [1990] used structural restorations to constrain the minimum depth of burial as 10 km at 3 kbar. Based on calcite-dolomite solvus thermometry in wall rocks, *Kubli* [1990] deduced a maximum burial temperature of 360°C to 375°C.

The Western Ranges host an 1800 m thick succession of Upper Cambrian through Lower Ordovician shallow marine pelites and thin, nodular limestone beds assigned to the Canyon Creek Formation and McKay Group [Figure 2.3 - *Balkwill*, 1972; *Gardner et al.*, 1976]. These two designations are established on lithological rather than temporal grounds, and *Balkwill* [1969] inferred that the Canyon Creek Formation is probably correlative with the middle McKay Group. *Gardner* [1977] used phase equilibria and calcite-dolomite solvus thermometry to estimate maximum P-T conditions that were consistent with chlorite grade metamorphism, with temperatures no greater than 365°C to 420°C and pressures of at least 2.5 kbar.

The evolution of the Dogtooth Duplex, located at the northern terminus of the northwest trending Purcell Anticlinorium, resulted in approximately 18 – 23 km or 50 % shortening. *Kubli and Simony* [1994] propose that the region evolved as a hinterland-dipping duplex during a main phase of contraction (D1) between late Jurassic and early Cretaceous time. Its deformation history is relatively simple, and consists of a prolonged phase of northeast-directed imbricate thrust faulting and associated regional folding with locally intense ductile shear [*Kubli and Simony*, 1994]. During D1-deformation, out-of-sequence displacement on major faults, such as

the Quartz Creek Thrust in the central duplex, resulted in the tightening and overturning of structures in the west. Regional detachments that were examined in this study include, from west to east, the Heather Mountain, Quartz Creek, Cirque Creek, and Wiseman Creek Thrusts (Figure 2.2).

At some time between D1 and the development of a secondary foliation, which formed during a transtensional phase, more than 10 km of displacement on the out-of-sequence Purcell Thrust led to the offset of faults and fabrics in the eastern Dogtooth Duplex and their juxtaposition against Upper Cambrian units of the Western Ranges [*Simony and Wind*, 1970; *Kubli and Simony*, 1994]. Approximately 3800 m of Middle Cambrian pelites from the Chancellor Formation, which separate units from the Dogtooth and Western Ranges, have been truncated by the Purcell Thrust and are therefore unexposed in this portion of the study area [Figure 2.2 - *Balkwill*, 1972; *Gardner*, 1977].

The style of deformation in the Western Ranges reflects the incompetent rheology of the units that comprise them. Bulk strain has resulted in 30 km of shortening [*Kubli and Simony*, 1994] and is partitioned mainly into cleavage formed during pressure solution of quartz and calcite and recrystallization of muscovite and chlorite. Pervasive isoclinal folding and minor displacement (<3 km) on regional thrust faults occurred in conjunction with cleavage development [*Cook*, 1975].

The exact timing of metamorphism with respect to deformation in the Dogtooth and Western Ranges is ambiguous. However, inclusion trails within siderite porphyroblasts from the Dogtooth Range demonstrate that peak metamorphism in the west occurred either during, or shortly after D1-deformation [*Kubli*, 1990]. Given that the main phase of deformation was likely synchronous in the Dogtooth and Western Ranges [*Kubli and Simony*, 1994]; deformation

initiated when sediments were at their maximum depth of burial; and penetrative cleavage is pervasive in the Western Ranges, it is reasonable to assume that metamorphism and associated devolatization reactions were coeval with D1 and vein development throughout the study area.

Finally, the Western Ranges' western margin coincides with the Rocky Mountain Trench, a northwest trending, topographically defined lineament that extends across more than 1600 km [*van der Velden and Cook*, 1996]. The trench is a relatively late (Tertiary) feature associated with minor transform and extensional faulting in the southern Rockies. Importantly, major structures have been correlated directly across the trench near the latitude of this study on the basis of seismic reflection data [*van der Velden and Cook*, 1996], and therefore minimal strike-slip faulting does not hinder conclusions about Mesozoic fluid migration between the Dogtooth and Western Ranges.

2.3 Methodology for Sample Selection

Because the scope of this study is limited to fluid regimes that evolved with structures during Mesozoic contraction, constraints on the timing of veining events were essential. Since Late Proterozoic time, at least two phases of extension (Late Proterozoic-Early Cambrian and Early Tertiary) and two compressional events (Devonian and Late Jurassic-Early Cretaceous) have been documented in the eastern Cordillera. Furthermore, a large-scale fluid event in pre-Jurassic time caused the dolomitization of Cambrian platform carbonates directly east of the study area [*Nesbitt and Muehlenbachs*, 1994; *Yao and Demicco*, 1995,1997]. In this paper, the term "syn-kinematic" will therefore denote events concurrent with the main phase of northeast-directed compression.

Sampling localities have been chosen to highlight patterns of isotopic disequilibrium across the structural contact between the Dogtooth and Western Ranges, across individual faults, and within dense fracture zones of thrust sheets. Two types of settings are emphasized:

(1) outcrops where regional thrust faults are exposed, including the Purcell Thrust, five faults in the Dogtooth Range, and two thrusts in the Western Ranges, and

(2) exposures within thrust sheets where vein density is high (>10%), and cross-cutting relationships between axial planar cleavage, minor faults, and veins permit robust timing constraints to be placed upon fluid events.

2.4 The geometry and timing of veins

The style and prevalence of veining across the transect is heavily contingent upon the competence of host rocks and the mechanisms by which they deform. In the Dogtooth Range, veins are more prominent in coarse, brittle units such as quartzite, massive carbonate, and siltstone, whereas in the Western Ranges, they are equally distributed throughout slate, micrite, and siltstone. Macroscopic veining within Proterozoic slate and phyllite from the Dogtooth Range is sparse, whereas similar lithologies in the Western Ranges commonly host dense fracture networks that record multiple fluid events. This contrast suggests that fine-grained meta-sediments in the Western Ranges experienced greater chemical potential gradients along which dissolved calcite could either diffuse or advect into vein openings.

Vein density rarely correlates with increased proximity to regional faults, although veins are more common in outcrops that host minor splays and faults with meter-scale offset. Quartz and carbonate bearing veins are common on both sides of the Purcell Thrust. However, quartz is more abundant in veins and wall rocks in the Dogtooth Range, whereas calcite and dolomite are

the dominant vein constituents in the Western Ranges. Accessory vein-filling minerals include chlorite, muscovite, apatite, and pyrite. Based on their cross-cutting relationship with S1-cleavage, folds, and faults, I categorize veins as early to syn-tectonic, syn-tectonic, and late tectonic (Plate 2.1).

Type 1: Early to syn-tectonic veins

These include: (a) kinked and sigmoidal veins oriented oblique to bedding and cleavage, (b) syntaxial, calcite-filled tension gashes oriented perpendicular to bedding, and (c) laminated to massive, bedding-parallel veins.

Type 1a veins are 1 – 5 cm wide and occur within broadly folded beds of quartzite and siltstone (Plate 2.1(a)). A consistent southwest trending orientation suggests a dilation direction parallel to the regional fold axis (i.e., NW-SE). Intragranular strain in the form of rotated sub-grains and deformation lamellae, and elongated, recrystallized grains oriented parallel to local cleavage indicate early tectonic development. Quartz fibers are "stretched" and oriented orthogonal or oblique to vein walls, and replacement muscovite that rims quartz grains reflects subsequent pressure solution. Latent calcite precipitates in fractures that cross-cut quartz fibers.

Type 1b veins between 30 μm and 3 mm wide are typically offset or dissolved along cleavage planes, where they are rimmed by a thin residue of chlorite, muscovite, and opaque minerals (Plate 2.1(c)). Because they are usually vertical and commonly occur near the hinges of cm-scale folds, I suspect that they either precipitated while bedding was horizontal, consistent with *Gardner's* [1977] conclusions, or formed later during extension perpendicular to fold axes. These are cross-cut by 2 - 6 cm wide, Type 1c veins that form northwest trending, open to isoclinal folds (Plate 2.1(b)). The hinges of folded veins are usually truncated by pressure

solution and dissolved along their contacts with wall rock. Successive generations of fibrous calcite, euhedral quartz and calcite, and very fine grained, disseminated apatite record a prolonged history of fluid infiltration by crack-seal and open fracture filling mechanisms.

Type 2: Syn-tectonic veins

Variably distended, cleavage-parallel veins occur within slate and phyllite throughout the transect (Plate 2.1(e)). For the following reasons, I suggest that this geometry reflects precipitation during, rather than preceeding, cleavage development. I observed neither consistent folding of local bedding into parallelism with cleavage nor evidence of fold closure within veins, thereby nullifying the counter-argument that pre- to early-tectonic veins were isoclinally folded into parallelism with axial planar cleavage. Also, veins are not limited to outcrops where cleavage is vertical, as would be expected if they originated as mode I style tensile cracks perpendicular to bedding. Instead, I propose a scenario in accordance with *Valenta* [1989], who justified vein dilation parallel to the maximum principle stress direction (σ_1) by invoking the transient condition of a simultaneous rise in pore fluid pressure with a decrease in differential stress. Boudinage records subsequent flattening or elongation in the plane of cleavage (i.e. the XY plane).

In the Dogtooth Range, syn-tectonic veins are locally concentrated where axial planar cleavage (S1) has been folded or faulted, and wall rocks have been sporadically altered to chlorite. The ratio in thickness between boudins and necks varies from 4.0 to 8.0, with a maximum width of 15 cm. In the western portion of the study area, Type 2 veins contain mildly strained blocky quartz with overprinting, dendritic chlorite and dolomite that infill microcracks and grain boundaries. Chlorite apophesies that extend outward into the wall rock merge into

parallelism with cleavage, while dolomite is truncated along dissolution seams. Thus, chloritization and dolomitization were synchronous with cleavage development. Near the Quartz Creek Thrust, intense dynamic recrystallization of elongate quartz grains parallel to foliation and the growth of an incipient C-fabric demand that veins formed prior to the cessation of contraction (Plate 2.1(d)).

In the Western Ranges, cleavage-parallel veins are more pervasive and exhibit milder intragranular strain compared with those in the west. Some show laminated textures, which were observed in Type 1 veins discussed above, and host recrystallized quartz and calcite grains that are elongated parallel to cleavage. Massive veins are continuously boudinaged and reflect later-stage infiltration of silica-rich fluids as overprinting, fine-grained quartz and quartz-filled microcracks. Progressive phases of fluid infiltration or chemical diffusion and corresponding mineral replacement have possibly erased strain features within vein material.

Type 3: Late-tectonic veins

Fault-parallel veins and densely fractured and stylolitized breccia zones, which cross-cut all other vein types, document the youngest phase of contraction-related fluid infiltration in the study area. In the Dogtooth Range, I documented Type 3 veins at the Quartz Creek, Cirque Creek, and Wiseman Creek Thrusts (Plate 2.1(f)). At each locality, thrust-parallel veins are often discontinuous along strike, indicative of high variability in the degree of fluid channeling into and along faults.

At the Quartz Creek Thrust, cleavage-parallel quartz veins and a local, microscopic strain fabric in the adjacent quartzite concentrate within 10 m of the fault contact. Veins are typically 1-5 cm wide and discontinuous with an arrhythmic pinch and swell morphology. Vein quartz is

blocky and shows evidence of sub-grain rotation and grain boundary migration. A dense network of microcracks, some replaced with dolomite and muscovite, align sub-perpendicular to cleavage. Entrained, foliated lenses of wall rock constrain the timing of vein formation to post-cleavage development.

Elsewhere in the Dogtooth Range, fault-parallel veins up to 3 m wide exhibit a penetrative fabric, which is defined by parallel, discontinuous muscovite seams and crystallographic preferred orientation in vein quartz. Quartz grains with an aspect ratio greater than 10:1 have been kinked and stretched into near parallelism with the local foliation. Cross-cutting, 100 μm wide veinlets document latent fracture and fluid infiltration. The Wiseman Creek Thrust contains a unique, 12 m wide zone, where quartzite matrix has been bulk replaced by vein quartz. At the fault, relict sedimentary textures are entirely overprinted by minimally strained, euhedral quartz that ranges in diameter from < 10 μm to 0.5 mm. Numerous sub-millimeter intra- and intergranular fractures document multiple phases of fracture and quartz precipitation.

In the Western Ranges, fault contacts are bounded by a resistant, ~50 cm wide "damage zone" of stylolites, mm-wide calcite veins, and calcite-dolomite matrix that has been both brecciated and dynamically recrystallized (Plate 2.1(g)). Mutually cross-cutting veins and stylolites are both parallel and orthogonal to the principle fabric, and disarticulated fragments of vein material grade into fine grained matrix, suggesting cycling between brittle and ductile processes during cataclasis. Matrix calcite has undergone intense grain size reduction from diameters of 0.4 mm to less than 10 μm and exhibits a strong shape preferred orientation parallel to the regional foliation. Twinning within the few relict coarser grains is moderate, indicating that solution transfer by pressure solution or Coble Creep was the dominant mechanism of

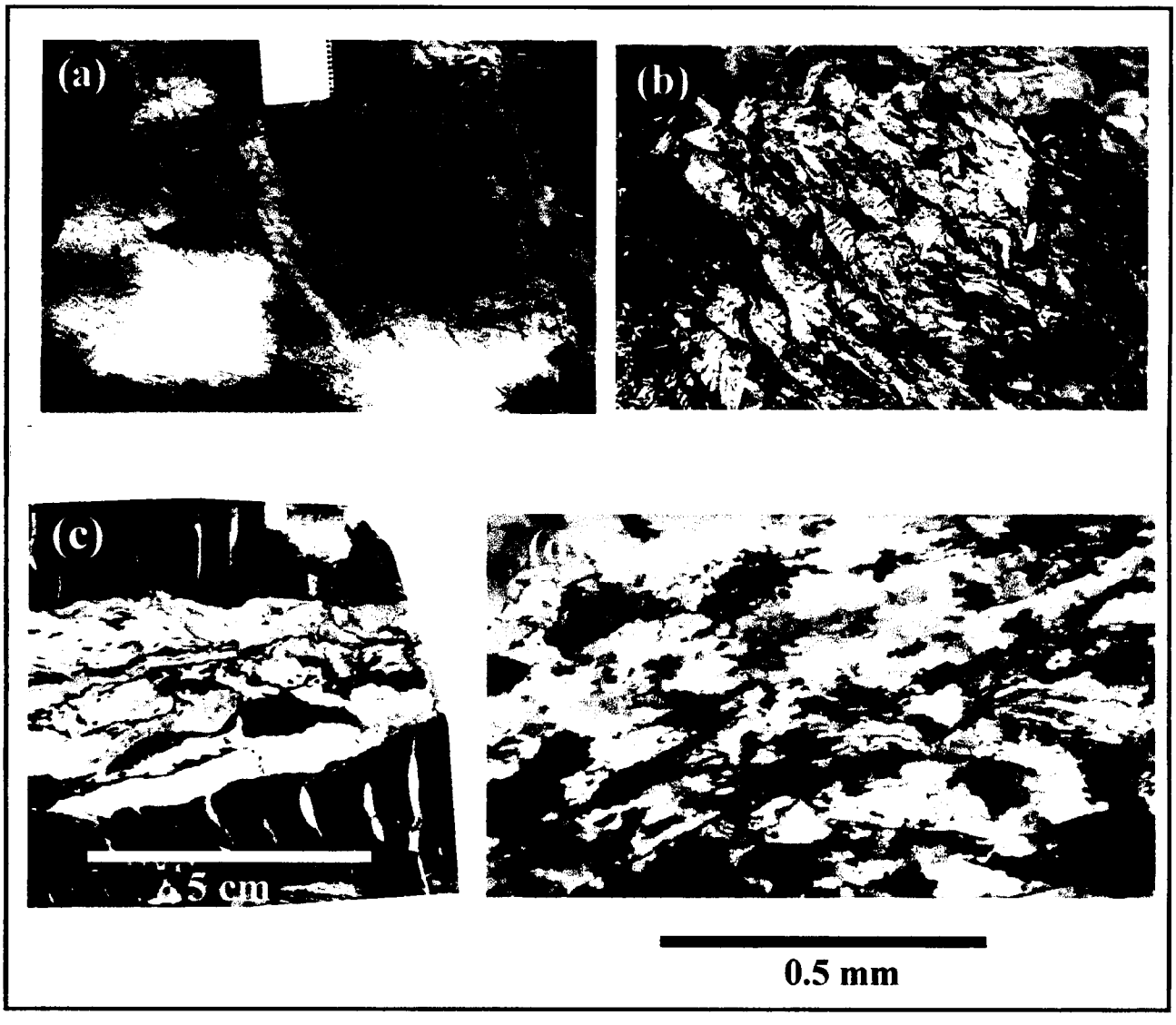

Plate 2.1: Representative veins from the Dogtooth and Western Ranges. (a) Fibrous quartz veins cross-cut folded siltstone layers near the Copperstain Syncline in the western Dogtooth Range. Field book for scale. (b) and (c) Laminated, bedding-parallel quartz-calcite veins near the Purcell Thrust. Note calcite tension gashes oriented perpendicular to bedding in (c). (d) Photomicrograph (x-polar) shows incipient S-fabric within a distended, cleavage-parallel quartz vein (shown in (e)) near the Quartz Creek Thrust.

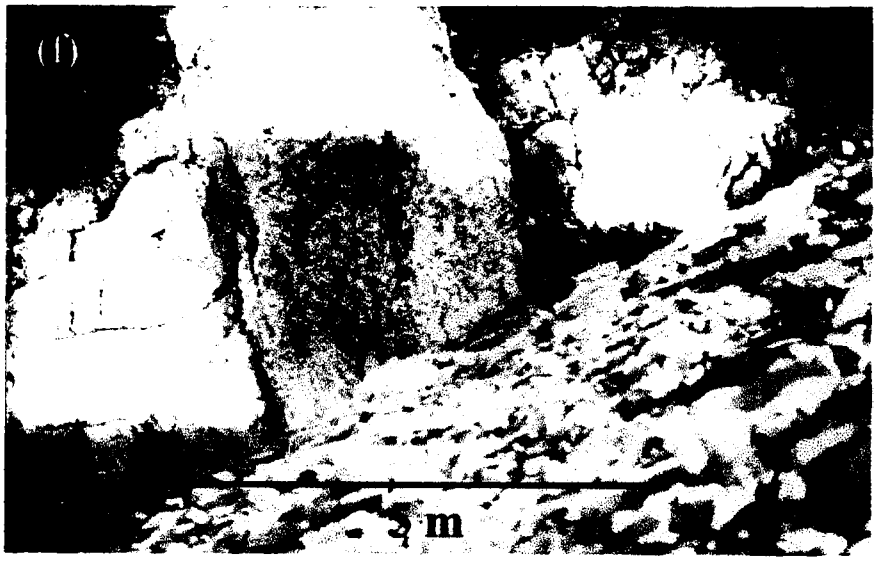

Plate 2.1 (con't): (e) Distended, cleavage-parallel vein near footwall splay of Quartz Creek Thrust. (f) Three meter thick fault-parallel vein near Cirque Creek Thrust in the eastern Dogtooth Range.

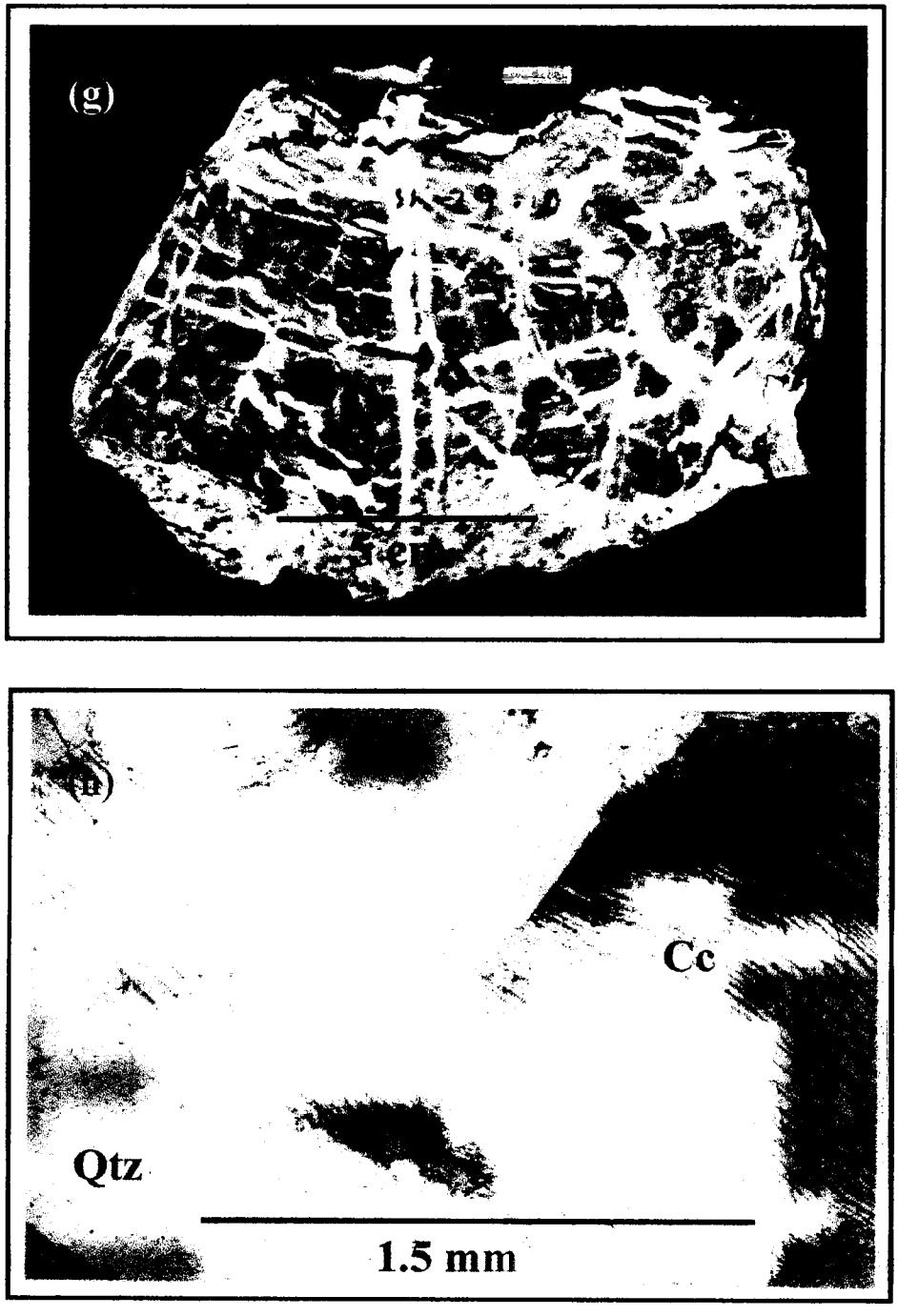

Plate 2.1 (con't): (g) Cataclasite from unnamed fault in the Western Ranges. Veins and stylolites are oriented oblique and parallel to the regional fabric. (h) Photomicrograph (plane light) of fault-parallel quartz (qtz)-calcite (cc) vein from a minor thrust near the Purcell Thrust. Calcite twins are kinked, indicative of high cumulative strain.

recrystallization. Laminated and massive veins between 5 and 10 cm in width also precipitate along meter-scale reverse faults at outcrops east of the Purcell Thrust. Within these, variably fibrous and euhedral calcite and quartz grains possess kinked twins, deformation lamellae, and sub-grains, which document the most intense microscopic strain observed in the Western Ranges (Plate 2.1(h)).

2.5 Stable Isotope Analysis

2.5.1 Analytical Methods

Results are based on 124 $\delta^{18}O$ analyses that were divided evenly between carbonates and silicates. Carbonates were also analyzed for $\delta^{13}C$. Silicates were crushed and powdered from ~ 8 cm^3 slabs. For samples that contained both quartz and carbonate, powders were reacted with dilute HCl (10 %) and flushed repeatedly with deionized water. All silicates were analyzed at the Queen's University Geochemistry Lab (Dr. T.K. Kyser, dir.) using the BrF_5 procedure described in *Clayton and Mayeda* [1963]. A 1σ uncertainty of 0.2 ‰ was reported for NBS-28, and repeated analyses of blind samples yielded a 1σ of 0.05 ‰ (N=4).

Carbonate powders were drilled from slabs using diamond impregnated drill bits in a Dremel tool. Powders were derived from less than 4 mm^3 of sampled material. Carbonates were analyzed at Queen's (N=37) and at the UBC Stable Isotope Lab (N=27)(Dr. T.F. Pedersen, dir.). Both labs used the techniques outlined in *McCrea* [1950] for liberation of CO_2 by reaction with H_3PO_4. A sample of vein calcite (44-4B) submitted to both labs yielded values identical to within 0.1 ‰ for $\delta^{18}O$ and 0.2 ‰ for $\delta^{13}C$. Both labs reported an uncertainty (1σ) of less than 0.1 ‰ for NBS-19. At Queen's, repeated analyses of blind samples yielded a 1σ of 0.1 ‰ and 0.06 ‰

(N=4) for $\delta^{18}O$ and $\delta^{13}C$, respectively. Similar accuracy was achieved at UBC, where the respective uncertainty for $\delta^{18}O$ and $\delta^{13}C$ was 0.1 ‰ and 0.08 ‰ (N=5). Values are reported in VSMOW and VPDB notation for $\delta^{18}O$ and $\delta^{13}C$, respectively.

2.5.2 Reporting of data and calculated uncertainty

Comparisons between data from whole rocks and vein quartz required normalization of the reported value from polyphase silicates with that of quartz. Otherwise, I risk basing erroneous interpretations of disequilibrium between veins and wall rocks on differences in ^{18}O partitioning between coexisting phases. Of 62 silicate analyses, 18 were from polyphase rocks that were too fine grained to permit the use of mineral separation techniques. All but one of these were from the Dogtooth Range. The following methodology was used to equate whole rock silicate values with that of quartz:

(a) Mineral modes for each phase were estimated within samples.

(b) Using molar volumes presented in *Berman* [1988], mineral mode was converted into the ratio: mol O in phase i vs. mol O in 100 cm^3 of sample.

(c) A $\delta^{18}O$ equivalent for quartz was calculated by simultaneously solving for mass balance (Eqn. 1) and isotopic fractionation between phase i and quartz (Eqn. 2):

$$(1)\quad \delta^{18}O_{wr} = \Sigma_{i=1} X_{O,i}\delta^{18}O_i$$

$$(2)\quad \delta^{18}O_{quartz} - \delta^{18}O_i = \Delta_{quartz\,-\,i}$$

where $\delta^{18}O_{wr}$ is the reported oxygen isotope composition of the whole rock sample; $X_{O,i}$ represents the molar fraction of oxygen contained within phase i over that within 100 cm^3 of sample; and $\Delta_{quartz\,-\,i}$ is the fractionation factor between phase i and quartz (as in *Rumble*, 1982).

Fractionation factors for the systems quartz-muscovite, quartz-clinochlore, and quartz-albite were taken from *Zheng* [1993]. Based on the results of calcite-dolomite solvus thermometry in *Kubli* [1990] and *Gardner* [1977] and isotope thermometry in this study (discussed below), we assigned a temperature of 370°C for isotopic equilibration across the transect. The above technique involves uncertainty in the estimation of mineral mode, the temperature of equilibration, and the selection of fractionation factors. I used the following strategy to account for each of these:

(i) In most cases, quartz, albite, muscovite, and chlorite were easily distinguished though a polarizing microscope, thereby enabling easy visual estimation of mineral mode. Thin-sections were cut perpendicular to foliation to avoid over-estimation of the concentration of sheet silicates. In very fine-grained slates, X-ray diffraction spectrometry confirmed relative abundances of chlorite and muscovite. Depending on the grain size and textural complexity within samples, an uncertainty of 5 - 20 % was assigned to each estimation of mineral mode.

(ii) Because peak conditions never exceeded chlorite grade metamorphism, 400°C represents a conservative maximum for temperatures in the study area. In the Dogtooth Range, the shallowest units reached a burial depth of at least 10 km [*Kubli*, 1990], which, assuming a geothermal gradient of +30°C/ km, is consistent with a minimum temperature of 300°C.

(iii) Finally, fractionation factors from *Zheng* [1993] were replaced with those of *Clayton and Kieffer* [1991; quartz-albite], *Wenner and Taylor* [1971; quartz-chlorite], and *Chacko et al.* [1996; quartz-muscovite] and substituted into the $\Delta_{quartz-i}$ term of Eqn. 2.

The predicted uncertainties, which arise from changing one of the above conditions (i - iii) while holding the other two constant, are presented in Table 2.1. Under these assumptions, the uncertainty exceeded +/- 0.5 ‰ and +/- 1.0 ‰ in only 6 and 2 samples, respectively. Of

those, the highest error was +/- 2.1 ‰ (sample 13-1A). In the following discussion, I attach the suffix "qtz. equivalent" to values that were derived using this method.

Table 2.1: Predicted uncertainties for converting whole rock $\delta^{18}O$ into quartz equivalent values.

Sample	Mineral Mode (+/- permil)	Temperature (+/- permil)	Fractionation Factor (+/- permil)
42-5B	0.15	0.4	0.3
17-3C	< 0.05	0.55	0.05
17-3G	0.15	**0.6**	0.05
17-3K	0.5	0.5	**0.65**
16-2D	0.45	0.55	0.15
16-2G	0.45	0.3	0.25
43-4A	0.2	0.05	< 0.1
34-1C	0.25	0.45	0.35
34-2A	0.25	0.1	<0.1
18-3B	< 0.05	0.5	0.25
18-3C	0.35	0.15	0.15
14-4C	0.2	0.2	0.1
14-4A	0.3	0.15	0.1
14-1F	0.45	0.2	0.15
13-1A	**2.1**	0.35	0.15
10-5C	1.3	0.2	0.15
34-5C	0.5	0.5	0.4
12-3C	0.25	0.3	< 0.05

Each column shows uncertainties generated by varying three separate input variables. In most cases, mineral mode was visually estimated. Temperatures were varied between 300°C and 400°C, and fractionation factors from *Zheng* [1993] are compared with those from *Clayton and Kieffer* [1991; quartz-albite], *Wenner and Taylor* [1971;quartz-chlorite], and *Chacko et al.* [1996; quartz-muscovite].

2.6 Results

2.6.1 Regional distribution of $\delta^{18}O$ in wall rocks

In this section, I highlight critical differences in the distribution of wall rock compositions both within the Dogooth and Western Ranges, and across the structural contact that divides them. Mean oxygen values are presented in Table 2.2, and a complete listing of isotopic

results are available in Appendix B. Figures 2.3 and 2.4 convey (i) a sharp eastward increase in $\delta^{18}O$ (calcite) across the Purcell Thrust, (ii) fairly consistent $\delta^{18}O$ (calcite and qtz. equivalent) values from sandstones and pelites both laterally and up-section within the Dogtooth Duplex, and (iii) a trend of gradual, eastward enrichment in $\delta^{18}O$ (calcite) up stratigraphic section and laterally across structural contacts in the Western Ranges.

Compared with carbonates in the Dogtooth Range that exhibit a mean $\delta^{18}O$ (calcite) of 15.6 +/- 0.8 ‰, those in the Western Ranges are consistently heavier in ^{18}O by 4.5 ‰, with an average of 20.1 +/- 2.3 ‰. I observed no compositional overlap between the two domains, with the highest signature in the Dogtooth Range, 17.3 ‰, recorded in a 10 m thick dolomite unit. By comparision, calcareous slate from the immediate footwall of the Purcell Thrust possessed a $\delta^{18}O$ of 17.9 ‰, the lowest in the Western Ranges. At the Purcell Thrust, where the eastern and western domains are directly juxtaposed, this shift is recorded in footwall slates that are enriched by 2.0 ‰ relative to carbonates ~150 m away in the hanging wall. Only one silicate analysis was obtained from wall rocks in the Western Ranges, where a phyllite from the Rocky Mountain Trench possessed a $\delta^{18}O$ (qtz. equivalent) of 17.4 ‰. Comparatively, pelites in the Dogtooth Range are depleted by 1.2 ‰, and therefore record a similar, albeit less constrained, trend of lower values as that observed in carbonates.

Siliciclastic rocks from the Horsethief Creek Group in the Dogtooth Range are, on average, relatively constant in composition regardless of their stratigraphic position or the thrust sheet in which they lie (Figure 2.3(a)). This suggests that differences in age, mineralogy, and sedimentary provenance between units leave no systematic imprint on their isotope signature or their effect has been overprinted by secondary processes. However, large standard deviations (~ 2.2 ‰) and a wide compositional range (13.4 ‰ – 19.9 ‰ (qtz. equivalent)) denote high isotopic

variability within each unit and might reflect the lithologic heterogeneity (i.e., interbedding among sandstones, pelites, and carbonate) evident over tens of meters. Figure 2.3(a) illustrates a shift in $\delta^{18}O$ across the sub-Cambrian unconformity, which separates Horsethief Creek rocks from the overlying Hamill Group. Hamill quartzites average 13.0 +/- 0.7 ‰ (qtz. equivalent) and possess the lowest signatures in the Dogtooth Range. The Hamill's locally distinctive and homogeneous lithology, pure quartzite (>95 % quartz) with minor plagioclase and muscovite, is the simplest explanation for the abrupt decrease in $\delta^{18}O$. Carbonate compositions in the Dogtooth Range are consistent across unit and structural contacts, but exhibit a much narrower spread (14.7 ‰ – 17.3 ‰ (calcite)) than silicates (Figures 2.3(b) and 2.4).

Finally, the $\delta^{18}O$ of calcite from wall rocks in the Western Ranges gradually rises with distance up-section and eastward across strike from the Purcell Thrust (Figures 2.3(c) and 2.4). Within calcareous slate and micrite of the McKay Group and its correlative Canyon Creek Formation, calcite exhibits an average $\delta^{18}O$ increase of ~3.0 ‰ across ~ 14 km of structural strike, from 17.9 ‰ to 20.8 ‰. Signatures as high as 25.1 ‰ were documented in the massive dolostones of the Late Ordivician Beaverfoot Formation. However, I focus on the Late Cambrian and Early Ordivician units, because of their stratigraphic continuity and lithologic similarity and the relatively narrow time interval over which they were deposited.

Wall rock compositions at each outcrop are distinctly homogeneous with standard deviations that are consistently less than 0.2 ‰. This implies that the observed regional trend, though subtle, is not an artifact of local, meter-scale variations in composition. That is, because samples of both micrite and calcareous slate were collected across 50 m to 200 m wide outcrops, the apparent increase cannot be attributed to minor lithologic changes over tens of meters, nor to compositional zoning across millimeters. It is noteworthy that all oxygen compositions from the

McKay and Canyon Creek samples fall either below or at the lower end of the 20-24 ‰ range that typifies Cambrian carbonates throughout the world [*Veizer*, 1983]. Samples collected east of the study area from older rocks in the underlying Chancellor Group exhibit values as high as 20.7 ‰ (see Chapter 5), thus increasing the likelihood that signatures in the McKay and Canyon Creek units are not pristine. I return to these points in later discussion regarding the cause for the observed pattern.

Table 2.2: $\delta^{18}O$ compositions in the Dogtooth and Western Ranges

Dogtooth Range Horsethief Creek Group				
	mean $\delta^{18}O$	**mean $\delta^{18}O$ (quartz equivalent)**	**range**	**n**
siliciclastics	12.7 +/- 2.1	15.1 +/- 1.8	13.4-19.9 (qtz.)	18
carbonates	15.6 +/- 0.8		14.7-17.3	7
vein calcite	**15.4 +/- 1.4**		**13.8-16.3**	**4**
vein quartz	**16.4 +/- 2.2**		**14.5-19.7**	**8**

Dogtooth Range Hamill Gp. and Donald Fm.				
	mean $\delta^{18}O$	**mean $\delta^{18}O$ (quartz equivalent)**	**range**	**n**
siliciclastics	12.8 +/- 1.4	13.8 +/- 1.9	11.5-19.8 (qtz)	18
carbonates	15.9			1
vein calcite	**16.2 +/- 0.1**		**16.2-16.3**	**3**
vein quartz	**14.6 +/- 2.5**		**12.5-18.8**	**11**

Western Ranges Canyon Creek Fm. and McKay Gp.				
	mean $\delta^{18}O$	**mean $\delta^{18}O$ (quartz equivalent)**	**range**	**n**
siliciclastics	15.7	17.4		1
carbonates	19.2 +/- 1.1		17.9-20.9	14
vein calcite/breccia	**18.1 +/- 1.1**		**16.2-20.0**	**20**
vein quartz	**19.9 +/- 1.6**		**18-22.3**	**6**

Uncertainty represented as 1σ of population. qtz=quartz equivalent.

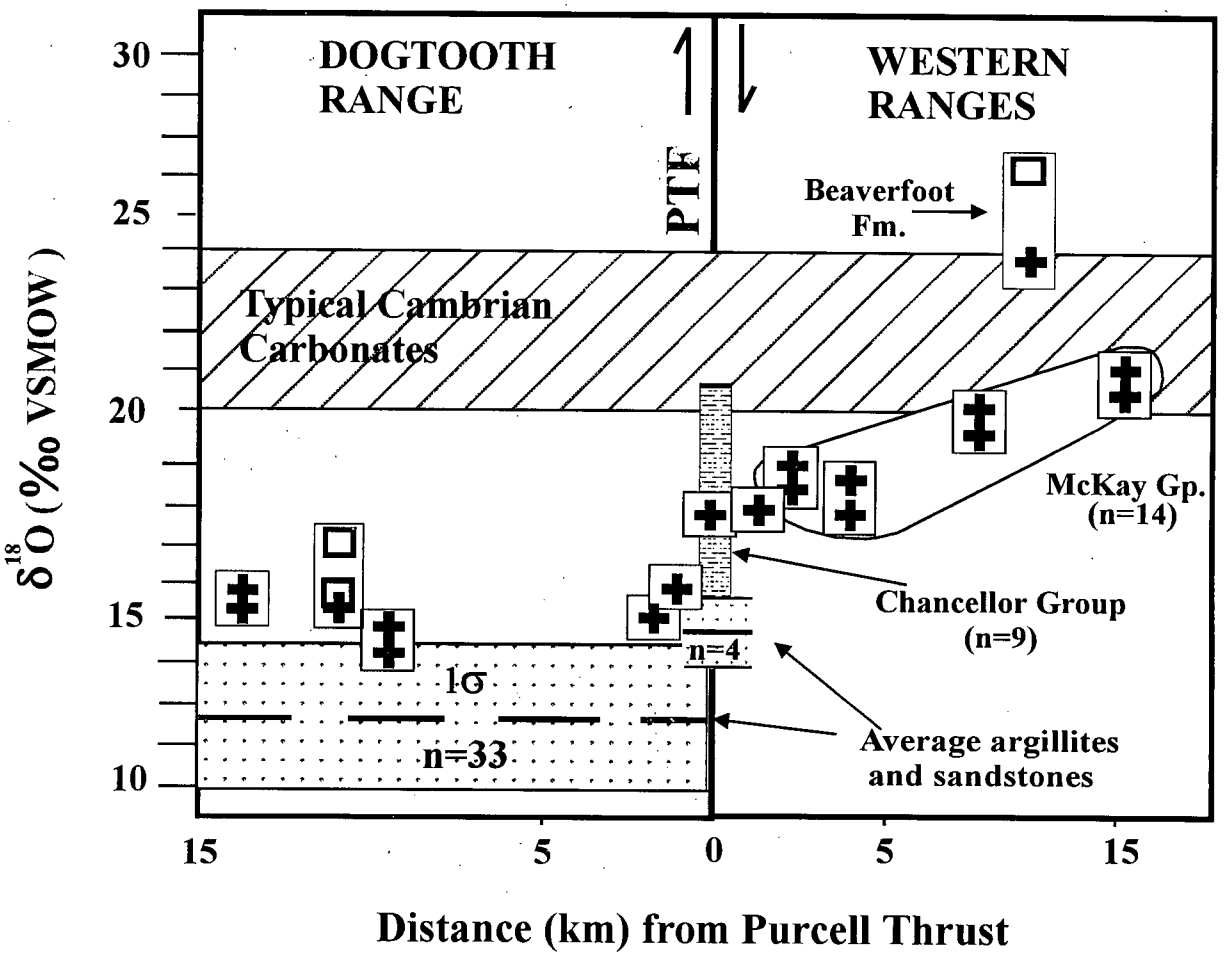

Figure 2.4: Oxygen isotope value of wall rock carbonates. PTF=Purcell Thrust Fautl. Crosses are calcite and open squares are dolomite. "Distance (km) from Purcell Thrust" is measured as distance across strike. The signature of carbonates from the Chancellor Group reflects the composition of middle Chancellor units below the upper Cambrian succession. Samples from the Chancellor Group were obtained 40 km east of the PTF in the Main Ranges (see Chapter 5).

2.6.2 Regional distribution of $\delta^{18}O$ in veins and vein-wall rock relationships

Here, I present isotope data from veins and cataclasites sampled across the transect, with specific attention given to vein-wall rock pairs, as well as general observations about the relationship between veins and host rocks at the outcrop-scale (Table 2.2; Appendix B1,2). In the Dogtooth Range, I observed: (1) a narrower range of $\delta^{18}O$ for veins than whole rocks, (2) no association between faults and the magnitude of vein-wall rock disequilibrium, and (3) no systematic relationship between vein and wall rock compositions. No evidence was found for the low-end quartz (12.1 ‰ -15.0 ‰) and calcite (6.4 ‰ -12.7 ‰) signatures that *Nesbitt and Muehlenbachs* [1997] recorded during their transect through the Proterozoic (Horsethief Creek) units of the northern Purcell Mountains. In fact, the $\delta^{18}O$ of veins lies within the compositional range of rocks sampled at individual outcrops in all but one case, and therefore indicates that vein-forming fluids were in general isotopic equilibrium with wall rocks.

In the Horsethief Creek Group, the $\delta^{18}O$ of quartz veins varies from 14.5 ‰ to 19.7 ‰ compared with that of wall rocks, which lies between 13.4 ‰ and 19.9 ‰ (qtz. equivalent). Similarly, quartz veins within the Hamill Group are distributed over a narrower compositional range, 12.5 ‰ – 14.1 ‰ (excluding an anomalously high value of 18.8 ‰), than that of their host quartzite, which varies from 12.5 ‰ to 14.7 ‰. In the Dogtooth Range, the only evidence for any systematic vein-wall rock disequilibrium occurs within calcite veins from the Horsethief Creek Group, where the range of vein compositions, 13.8 ‰ - 16.3 ‰, is modestly lower than that of limestone and calcareous shale, 14.7 ‰ – 17.3 ‰. In later discussion, I argue that this apparent depletion is not indicative of infiltration by externally sourced fluids, but instead reflects fluid migration across bedding contacts between siliclastic and carbonate units.

Compositional differences between veins associated with large regional detachment faults and their immediate wall rocks are subtle and inconsistent. Of four fault-parallel veins sampled at the Wiseman Creek and Quartz Creek Thrusts, three were enriched by 0.4 - 1.4 ‰ and the other was slightly depleted by 0.5 ‰. Furthermore, analysis of vein-wall rock pairs reveals no systematic trend of vein enrichment or depletion in the Dogtooth Range (Figure 2.5(a)). The fractionation of ^{18}O between veins and wall rocks, $\Delta_{\text{vein-wall rock}}$, varies widely from -3.5 ‰ to +5.9 ‰. Based on the above evidence that the range in $\delta^{18}O$ of veins is confined within that of wall rocks, the scatter in Figure 2.5(a) does not likely reflect multiple fluid regimes throughout the western transect. Instead, I attribute it to wide variations in rock composition at individual outcrops. That is, even though veins might be in apparent disequilibrium with their immediate host rocks, they are still equilibrated with overall bulk rock $\delta^{18}O$ across 10's to 100's of meters (i.e., the minimum distance sampled across each outcrop). This point is further developed in later discussion.

In the Western Ranges, quartz and calcite veins mimic the trend displayed by their host rock carbonate, with a gradual increase in $\delta^{18}O$ eastward and up-section from the Purcell Thrust (not shown-see Appendix B2 for vein values by outcrop). Within Cambrian strata, vein quartz and calcite increase from west to east by 2.5 ‰ and 2.1 ‰, respectively. Therefore, the $\delta^{18}O$ of vein forming fluids in the Western Ranges were at least partially imposed by the composition of wall rocks. However, the isotopic relationship between vein calcite and wall rocks is consistently and conspicuously different in the Western Ranges than in the Dogtooth Range. The average $\delta^{18}O$ of calcite veins from Canyon Creek, McKay, and Beaverfoot strata is less than that of wall rock carbonate by 1.6 ‰, 1.0 ‰, and 2.7 ‰, respectively (Table 2.2). Figure 2.5(b) illustrates that this depletion, though modest, is systematic and apparent at most outcrops. A maximum

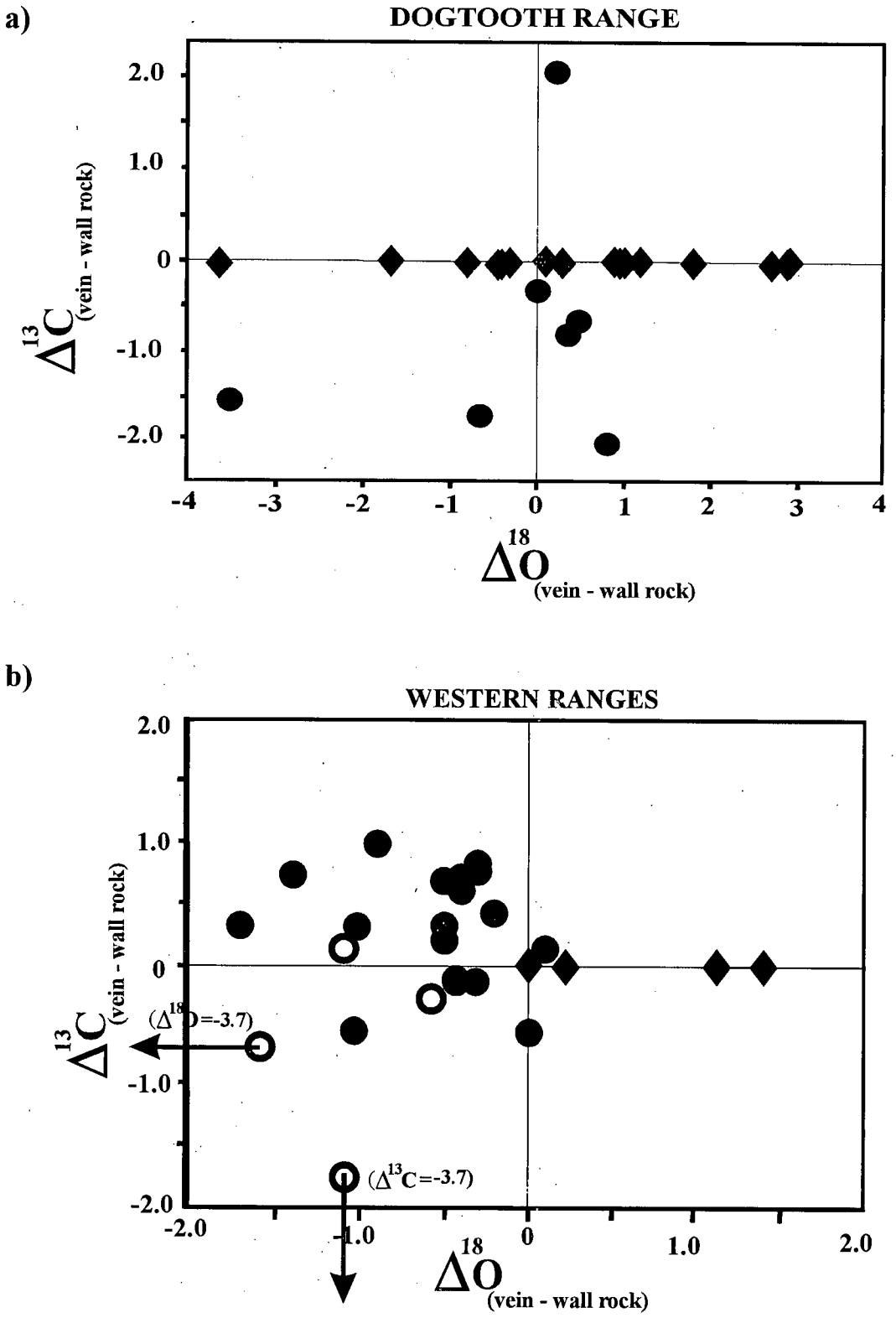

Figure 2.5: Fractionation of ^{18}O and ^{13}C between veins and wall rocks. Filled circles=vein calcite; diamonds=vein quartz; open circles=fault breccia and cataclasite. Note wide scatter in Dogtooth data compared with systematic oxygen depletion in the Western Ranges.

depletion of 3.7 ‰ was documented within a 1 mm wide veinlet from a cataclasite at an overturned thrust fault along the Trans-Canada Highway (locality 12B-Figure 2.1). Within the same sample, highly comminuted, very fine grained matrix material is also depleted by 1.1 ‰ compared with undeformed calcite 2 m away in the hanging wall. Similar style breccias from the two other fault zones that were sampled showed a $\Delta_{\text{vein-wall rock}}$ of ~ 1.0 ‰ (localities 12A and 13). Of 21 vein-wall rock pairs, oxygen enrichment (+ 0.1 ‰) was observed within only one calcite vein.

The magnitude of depletion is independent of vein type (Figure 2.6), a phenomenon that is best illustrated at an outcrop in the Rocky Mountain Trench ~ 4 km east of the Purcell Thrust (Figure 2.7). Vein density at this locality is unusually high (10-20 %), and at least five distinct generations of veins are associated with numerous meter-scale reverse faults. Despite evidence that vein precipitation progressed from early (tightly folded, bedding-parallel veins) into late (laminated, fault-parallel veins) tectonism, twelve samples from across 50 m demonstrate a remarkable uniformity in composition from 17.8 to 18.3 ‰. With the exception of a single sample of micrite that possesses a slightly lower $\delta^{18}O$ (- 0.1 ‰) than a neighboring vein, wall rocks consistently exhibit larger signatures than the veins with which they are in contact by 0.2 – 0.8 ‰.

To summarize, vein forming fluids were modestly, but systematically, displaced from isotopic equilibrium with surrounding carbonates in the Western Ranges. Depletions occur within all types of syn-kinematic veins, regardless of their geometry or timing relative to the main phase of tectonism. However, it is noteworthy that cataclasite from a regional fault exhibited the largest departure from equilibrium. These observations support either: (a) the presence of a fluid component that was partially exotic to the bulk rock isotopic system at each

outcrop or (b) a situation of prevailing thermal or kinetic disequilibrium between vein material and the fluids from which they precipitated.

2.6.3 Derivation of temperatures from quartz-calcite fractionation

Oxygen isotope thermometry was applied to nine quartz-calcite pairs that appeared to have co-precipitated in veins across the transect (fractionation factors taken from *Sharp and Kirschner* [1994]). Results are presented in Figure 2.8. For the most part, this data is compatible with calcite-dolomite solvus thermometry performed on wall rocks in the Dogtooth Range [*Kubli*, 1990] and a portion of the Western Ranges ~15 km north of the study area [*Gardner*, 1977]. The isotope data yields vein temperatures that range between 305°C and 420°C. Veins in which quartz and calcite clearly showed a cross-cutting relationship with each other gave predictably unrealistic temperatures. In addition, two measurements taken within a meter of each other on the same fault-parallel vein at the Purcell Thrust (34-5A/B) gave discordant temperatures of 420°C and 315°C. I suggest that the former value is unrealistically high, due to isotopic disequilibrium between quartz and calcite at the thrust contact. Calcite-dolomite solvus thermometry yielded a range of 260°-350°C from a single fibrous vein (17-3E) adjacent to the Heather Mountain Thrust and a maximum temperature of 290°C from a breccia-hosted veinlet (36-1B) in the Western Ranges (for methodology see *Anovitz and Essene* [1987]- results are tabulated in Appendix C). Isotope thermometry on 17-3E yielded a closing temperature of 400°C.

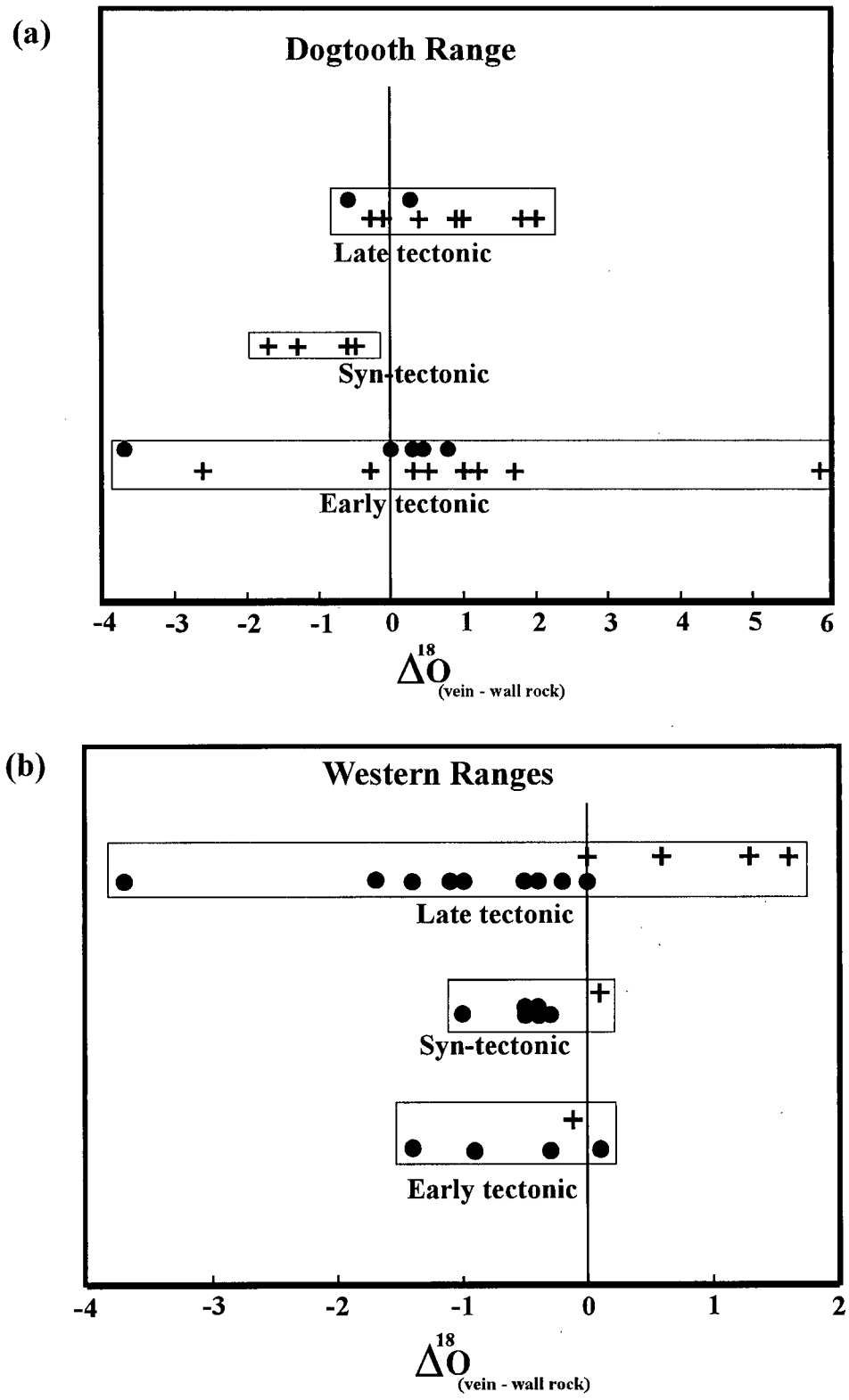

Figure 2.6: Oxygen fractionation between veins and wall rocks by vein type. Circles represent vein carbonate and crosses denote vein quartz. Systematic trends are lacking in both domains, although syn-tectonic (i.e. cleavage-parallel) veins in the Dogtooth Range are consistently depleted relative to wall rocks.

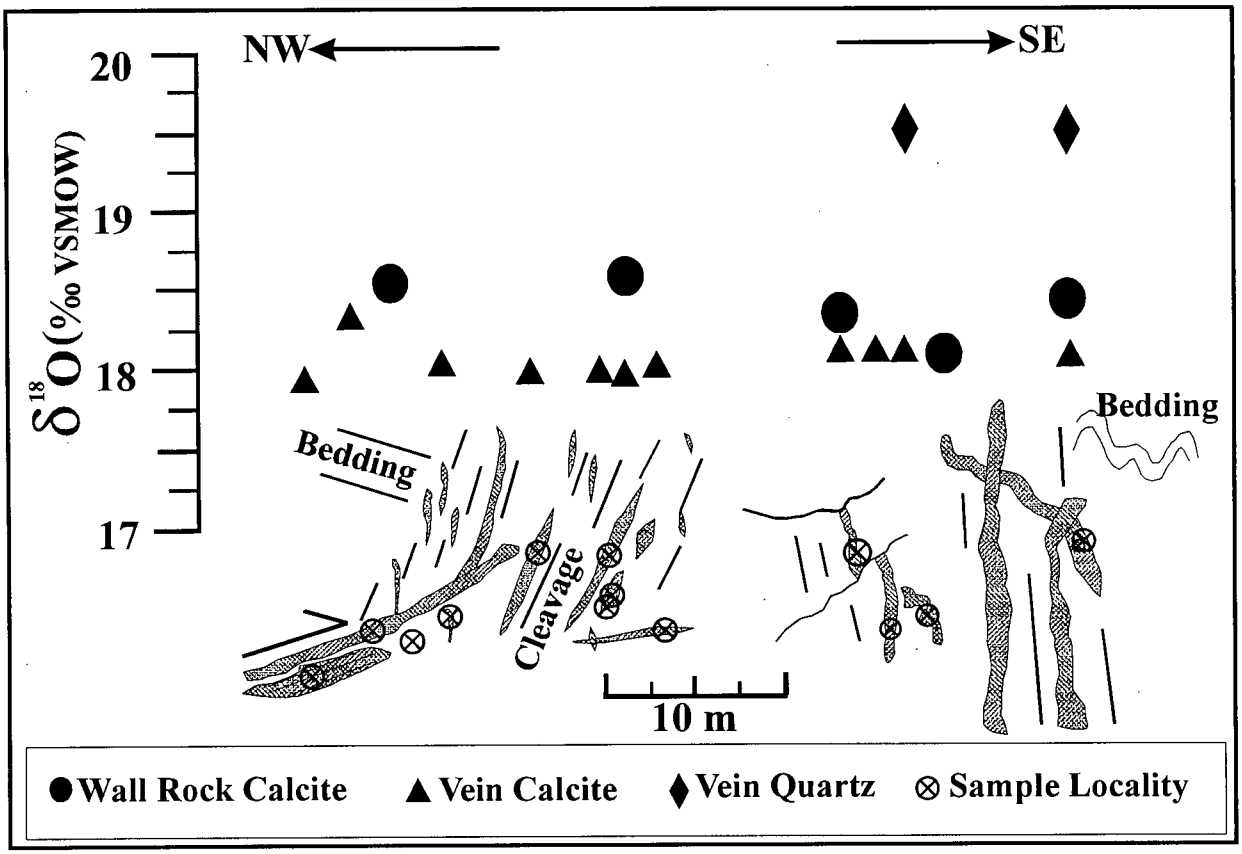

Figure 2.7: Oxygen isotope values at outcrop in Rocky Mountain Trench (11) 2.5 km from nearest thrust contact. Despite large temporal and morphological variations, veins are compositionally monotonous and generally lighter than their neighboring wall rocks.

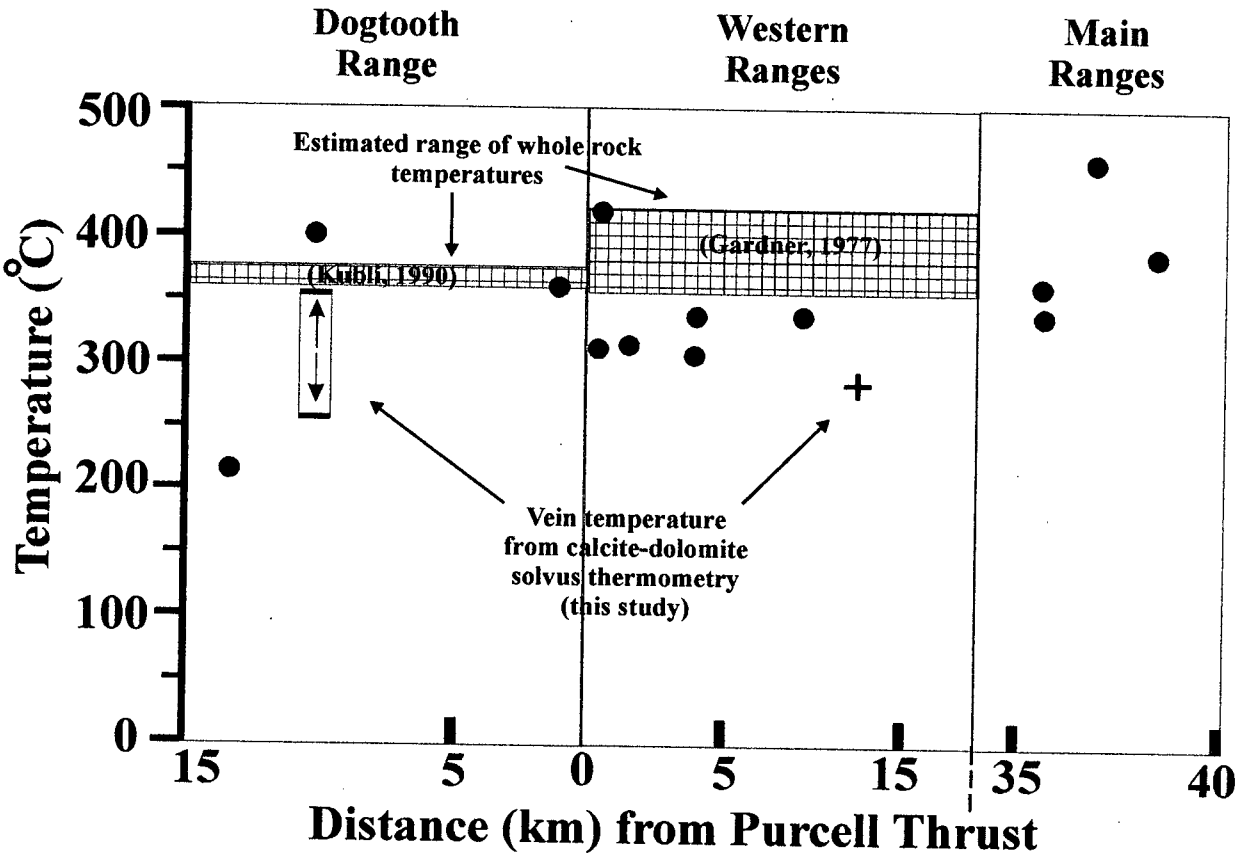

Figure 2.8: Estimated temperature of quartz-calcite veins from isotope and calcite-dolomite solvus thermometry. Fractionation factors for quartz-calcite taken from *Sharp and Kirschner* [1991]. Calcite-dolomite thermometer based upon that of *Anovitz and Essene* [1987]. Data from the Main Ranges are presented in Chapter 5..

2.7 Discussion

2.7.1 Potential catalysts for isotopic depletion

Anomalously low $\delta^{18}O$ (carbonate) values in the Dogtooth and Western Ranges and systematic depletions in vein calcite relative to wall rocks suggest several possible scenarios. Specifically, these include:

(i) the age dependence of carbonate $\delta^{18}O$, in accordance with the observation that older rocks tend to possess lower oxygen values,

(ii) exchange with low-$\delta^{18}O$, metamorphic fluids that were sourced from coexisting clay minerals during devolatilization reactions,

(iii) localized, fluid-assisted isotopic exchange with coexisting, lower-$\delta^{18}O$ phases such as quartz and muscovite,

(iv) down-temperature (i.e., up-section) flow of a fluid that was isotopically equilibrated, but hotter than surrounding wall rocks such that the veins which precipitated exhibited lower $\delta^{18}O$ than their host rocks,

(v) exchange with a fluid that was in thermal and isotopic equilibrium with wall rocks and flowed up a temperature gradient (i.e., down-section), and finally

(vi) exchange with an exotically derived, low-$\delta^{18}O$ fluid (i.e., open-system exchange).

Using specific examples from individual outcrops, the following sections incorporate a more detailed analysis of the isotopic data in order to identify the scenarios which best apply to syn-tectonic fluid regimes in the western transect.

2.7.2 Possible age controls on wall rock $\delta^{18}O$ (calcite)

Statistical studies have shown that Late Proterozoic and Phanerozoic carbonates follow a well constrained trend of declining $\delta^{18}O$ with increasing age [*Veizer and Hoefs*, 1976; *Veizer*, 1983]. Here, I address and refute the possibility that age plays a factor in (i) the apparently low isotopic composition of carbonates in the Dogtooth Range, and (ii) the pattern of eastward and up-section enrichment of $\delta^{18}O$ in the Western Ranges.

Figure 2.3(b) illustrates that the range of $\delta^{18}O$(calcite) is relatively constant throughout the Upper Proterozoic (Horsethief Creek) section, despite an extended depositional history that persisted through the latter half of the period between 850 Ma and 700 Ma [*Gabrielse and Campbell*, 1991]. The time span over which these sediments were deposited was therefore either too narrow to affect a significant shift in isotope value, or bulk rock $\delta^{18}O$ was grossly homogenized during deformation and greenschist metamorphism. A least-squares regression presented by *Veizer and Hoefs* [1976] predicts a $\delta^{18}O$ of 22 – 22.5 ‰ for 850-700 m.y. carbonates. In the same study, signatures below 18.5 ‰ are rare and never systematic in Proterozoic data. Furthermore, *Ghent and O'Neil* [1985] recorded an oxygen value of ~ 21 ‰ from the Horsethief Creek Group, and *Wickham and Peters* [1993] reported signatures of ~22 ‰ for marbles in correlative strata from Utah and Nevada. Therefore, it is unlikely that calcite and dolomite from the Dogtooth Range, which average 15.6 +/- 0.8 ‰, represent true protolith compositions that have been unaffected by secondary exchange with depleted fluids. An obvious local reservoir for low-$\delta^{18}O$ fluid is the abundant siliceous sandstone and meta-pelite present at each sample locality. Consistent with the notion of isotopic homogenization throughout the Horsethief Creek section, I contend that local fluid advection across at least tens of meters (i.e.

the maximum bed thickness for limestone) provoked exchange between siliciclastic rocks and subordinate carbonates, thereby lowering the $\delta^{18}O$ of carbonate wall rocks.

The composition of wall rocks from the Canyon Creek and McKay units in the Western Ranges falls either below or at the lower end of typical carbonates of similar age. Absolute age determinations for the Upper and Lower McKay Group are non-existent, but fossil evidence from trilobites [*Dean*, 1988; *Chatterton and Ludvigsen*, 1998] constrains deposition as having occured between Late Cambrian and Early Ordivician time. The maximum duration for deposition of the McKay Group was therefore no greater than 40 m.y. (527 - 487 m.a.). During this time span, the model of *Veizer and Hoefs* [1976] predicts a $\delta^{18}O$ decrease of 0.2 - 0.5 ‰ with increasing age. Clearly, the observed 3.0 ‰ decrease across the Western Ranges cannot be explained by age variation alone. As with samples from the Dogtooth Range, these too must have undergone secondary exchange with a medium that was depleted in ^{18}O. The extent of this exchange increased towards the west, where signatures near the Purcell Thrust show the greatest departure from the expected $\delta^{18}O$ of Upper Cambrian carbonates (Figure 2.4). However, the calcareous sediments in the Western Ranges contain no obvious local source for low-$\delta^{18}O$ fluids.

2.7.3 Fluid regimes in the Dogtooth Range

In this section, I build upon evidence from depleted isotopic signatures from whole rock carbonates to argue that fluid advection in the Dogtooth Range was active across a minimum of 1-10 meters, with the effect of altering the composition of vein forming fluids towards the average $\delta^{18}O$ of wall rocks over the same distance. Isotopic disequilibrium between veins and wall rocks near bedding contacts suggests localized fluid advection within individual outcrops. At the Heather Mountain Thrust (locality 1), a 1 cm wide, antitaxial quartz-carbonate vein is

depleted relative to its host dolomite by ~3.5 ‰ (Figure 2.9(a)). Thirty centimeters away, a quartz-arenite unit borders the dolomite and possesses a lower $\delta^{18}O$ of 13.8 ‰ (qtz. equivalent). Transport of fluid between the dolomite and sandstone best explains the intermediate oxygen value possessed by the vein (i.e., scenario (iii) above). Otherwise stated, the vein forming fluid had undergone isotopic exchange with both the sandstone and dolomite. Thus, the time-integrated fluid flux was sufficiently low to permit rock buffering of the silica and carbonate bearing species such that the signature of vein quartz and calcite approached that of the average bulk rock package (i.e., dolomite + quartzarenite). Although quartz precipitation by chemical diffusion has been documented in crack-seal veins [*Fisher and Brantley*, 1992], diffusion across more than a few cm's is relatively inefficient [*Etheridge et al.*, 1984] making advection the most viable transport mechanism for the $\delta^{18}O$-depleted fluid.

Figure 2.9(b) illustrates a similar phenomenon within a fibrous, cleavage-parallel vein at an unnamed thrust fault in the central Dogtooth Range (locality 6). The vein, which is depleted by 1.3 ‰ compared with surrounding wall rock, is hosted by a 10 cm wide phyllite that is isolated within an outcrop of quartzite. However, the vein is nearly equilibrated with nearby quartzite,

and therefore precipitated from a fluid that was almost entirely buffered by the dominant rock type within the outcrop.

Finally, a comparison between whole rock and vein signatures across the same outcrop reinforces the assertion that cm to meter-scale fluid flow homogenized vein compositions in the western transect. The $\delta^{18}O$ of wall rocks in Figure 2.9(b) ranges from 11.5 ‰ to 14.7 ‰, while vein quartz is more narrowly distributed between 12.5 ‰ and 13.4 ‰. In fact, with the exception

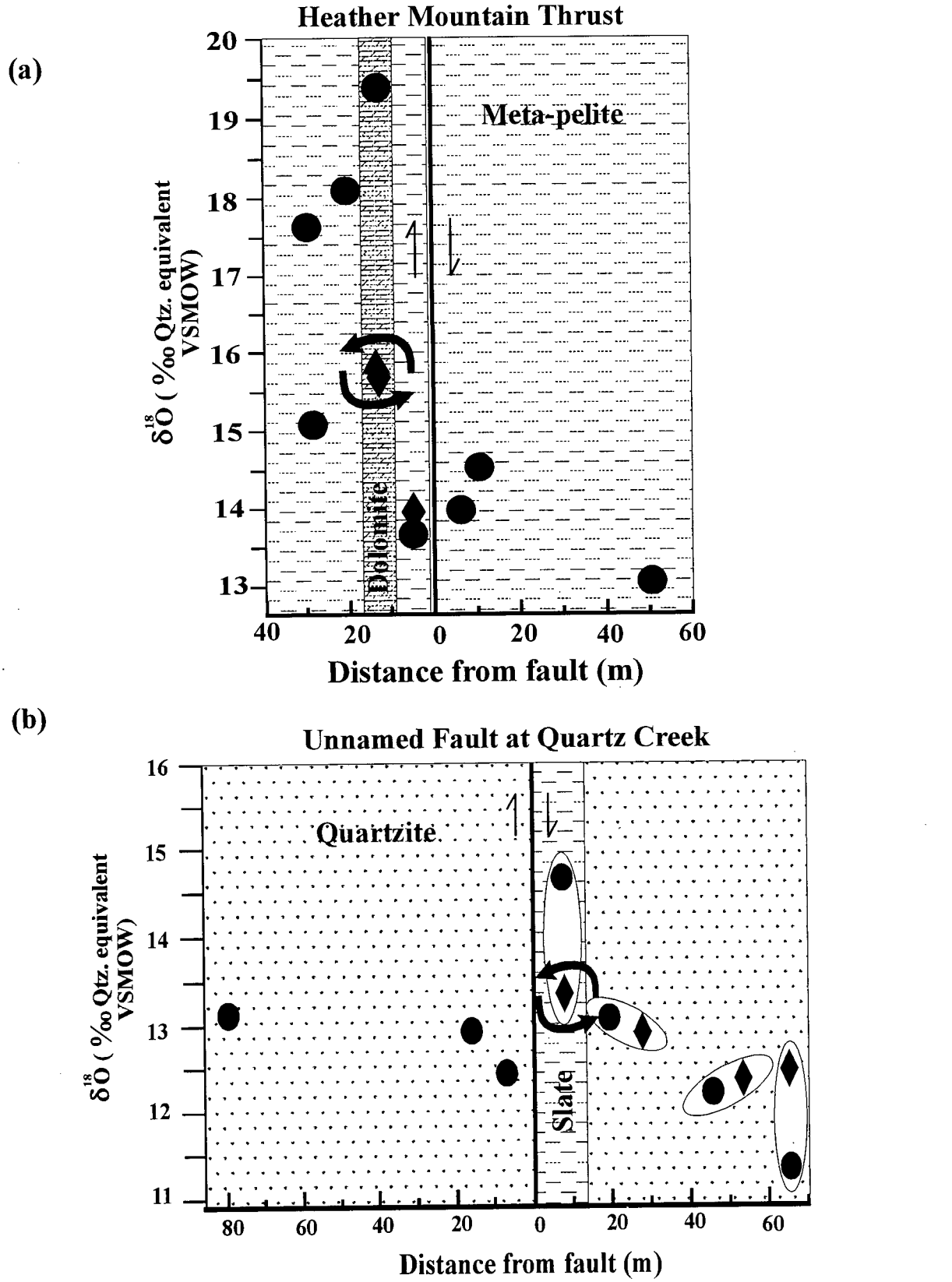

Figure 2.9: Isotopic evidence for fluid migration across bedding contacts and ≥ meter-scale homogenization at outcrops in the Dogtooth range. Solid circles represent wall rocks, diamonds denote quartz veins, and triangles are calcite veins..

of a single, anomalously high-$\delta^{18}O$ quartz vein (18.8 ‰), vein signatures at each outcrop sampled in the Dogtooth Range fell within the range of those for wall rocks (Appendix A). This subdued variation in the composition of veins and simultaneous disequilibrium between veins and their immediate host rocks (i.e. Figure 2.5(a)) suggests that vein-forming fluids had been in contact with wall rocks located at least a few, but possibly 10's to 100's of meters away from the site of quartz precipitation. The above examples support a scenario in which the $\delta^{18}O$ of veins, though in modest disequilibrium with the immediate host rock, approach the average bulk rock composition across at least a few meters.

2.7.4 Fluid regimes in the Western Ranges

The following section presents two possible scenarios for closed and open system fluid-rock exchange in the Western Ranges and assesses their validity. Data from wall rocks and veins are discussed separately.

I. Wall rock alteration during local fluid circulation and subsequent vein formation within a closed system

Under these conditions, isotopic alteration and dissolution-reprecipitation reactions are restricted to the pre-existing rock-fluid system, with no influx of fluid or solutes from external sources. In other words, there is no fluid communication between adjacent outcrops. In discussion, I restrict the size of the system to the limits of my sampling, i.e., individual outcrops ($\leq$ 100 m), although obviously it might be larger (e.g., the distance to the next outcrop sampled). Use of the terms closed- and open-system therefore refers to respective conditions of geochemical "isolation" versus exchange between outcrops.

Earlier, I refuted the notion that age variations are responsible for increasing wall rock depletion westward towards the Purcell Thrust, and must therefore propose a secondary process capable of altering and homogenizing rock compositions. Dehydration reactions, which occur during the formation of chlorite and muscovite from clays, are capable of generating a substantial volume of fluid during regional metamorphism and cleavage development [e.g., *Etheridge et al., 1984; Valley*, 1986; *Ferry*, 1992]. For example, *Ferry* [1992] estimated that Appalachian metacarbonates of similar grade to those in the Western Ranges experienced a time-integrated fluid flux of $4.0 \bullet 10^2$ mol H_2O/cm^2 during regional metamorphism. Pervasive circulation of locally derived metamorphic fluid can produce systematic carbonate depletions by: (a) promoting isotopic exchange between carbonates and coexisting, lower-$\delta^{18}O$ siliceous phases (i.e., scenario (iii) above) or (b) promoting isotopic exchange between carbonates and the metamorphic fluid itself (scenario (ii)). If either of these were the catalyst for the observed depletions, then outcrops towards the west would necessarily possess a higher concentration of siliceous phases that were capable of lowering the average bulk-rock $\delta^{18}O$ during devolatilization. Two lines of evidence might support some correlation between variations in lithology and oxygen composition.

In the Canyon Creek Formation, calcite occurs as laminae in slate and phyllite, whereas the McKay Group contains regular interbeds of massive and nodular limestone and tends to be more calcareous [*Balkwill*, 1969]. Correspondingly, at the stratigraphic contact between the two units (locality 10), wall rocks from the Canyon Creek Formation are depleted by 0.7 ‰ - 1.1 ‰ compared with McKay carbonates less than 100 meters away (Figure 2.10). Because outcrops in the Western Ranges tend to be strongly uniform in composition, this discrepancy is probably not a function of random variation. Instead, it reflects the effect of stratigraphy on $\delta^{18}O$ and suggests

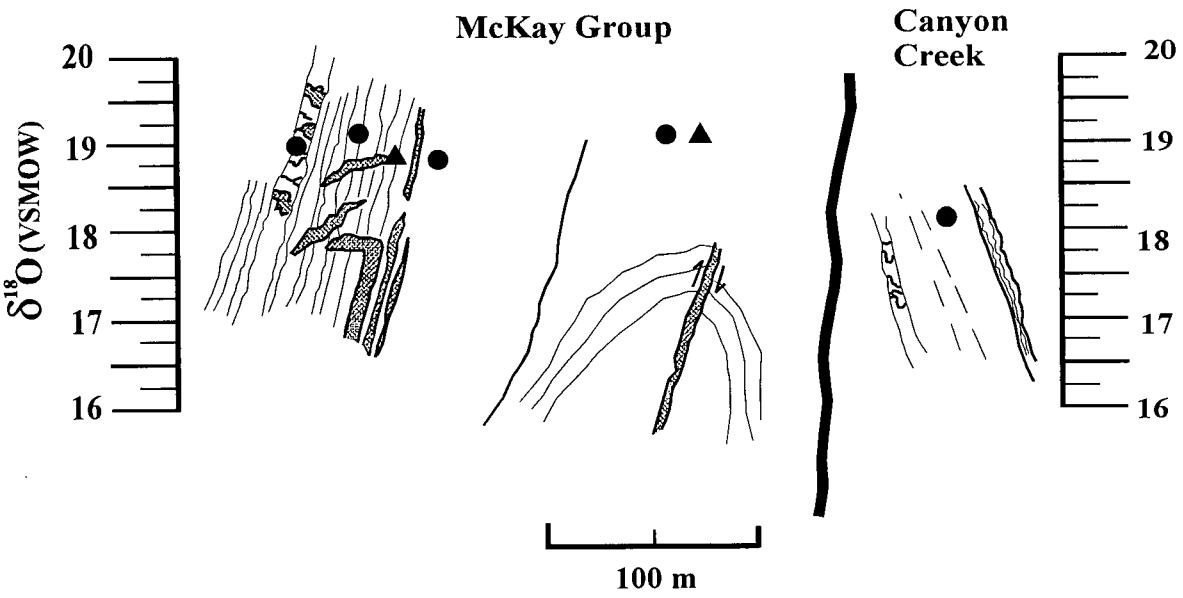

Figure 2.10: Stratigraphic contact between McKay Group and Canyon Creek Formation (locality 10). Note that oxygen composition is lower within Canyon Creek sediments, indicating that lithological differences partly affect isotopic values. Circles denote wall rock calcite and triangles represent vein calcite.

a)

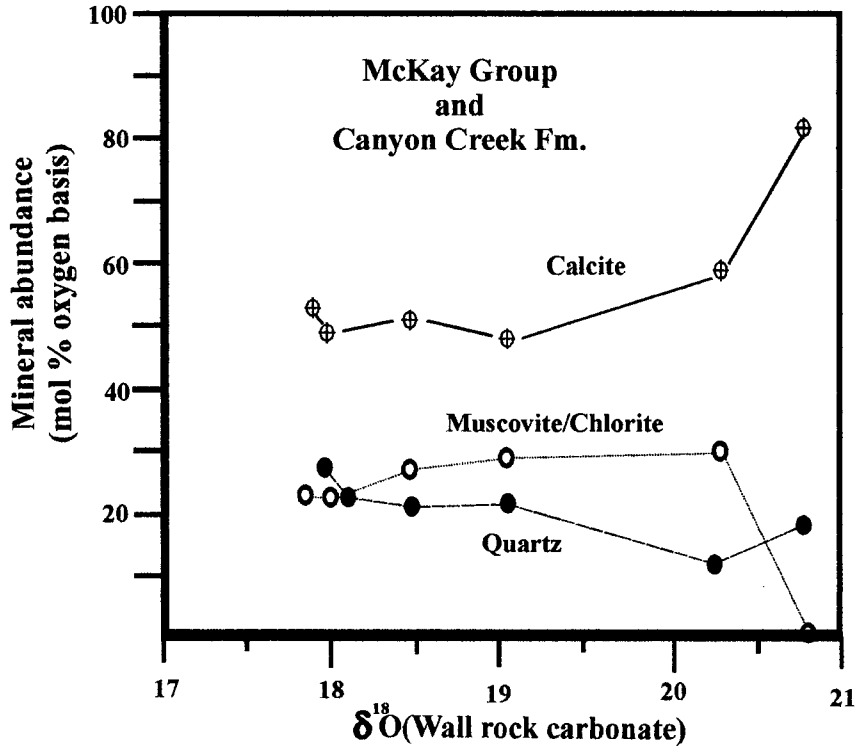

b)

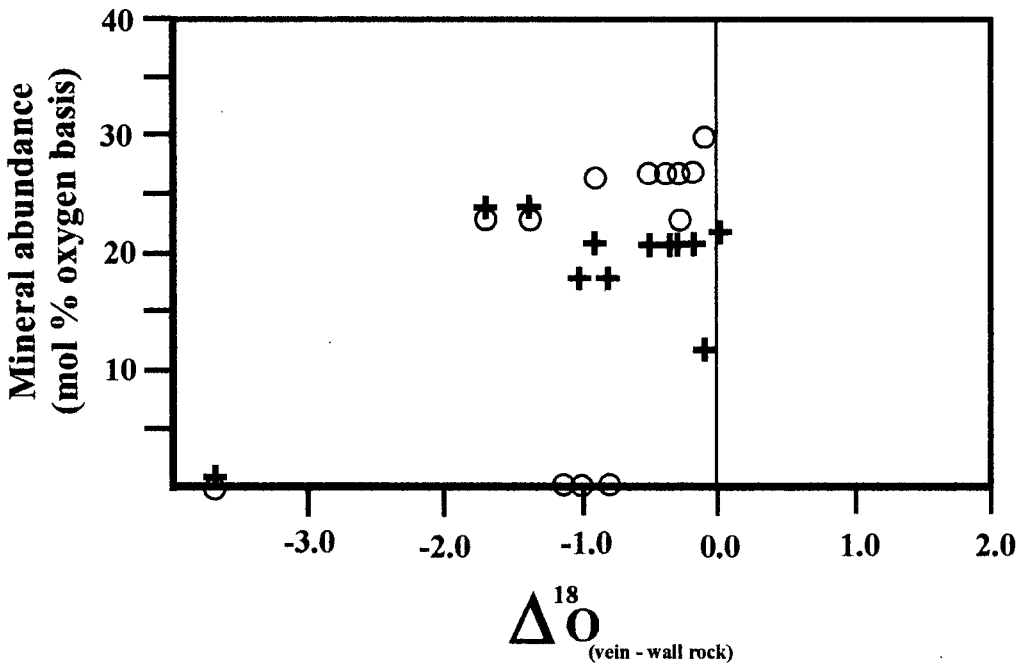

Figure 2.11: (a) Mineral content versus mean isotopic signature for Canyon Creek and McKay outcrops in the Western Ranges. With the exception of the two easternmost outcrops, a correlation between calcite and oxygen composition is lacking. (b) Mineral content versus vein-wall rock composition by sample. Open circles represent muscovite abundance and crosses denote chlorite abundance. The magnitude of depletions do not correlate with silicate composition as would be expected if vein signatures were rock buffered. mol % oxygen basis = mol O in mineral/mol O in rock

that more siliceous units are lower in oxygen composition. It also indicates that complete isotopic homogenization from local fluid circulation does not extend beyond 100 meters at this outcrop.

In Figure 2.11(a), a comparison between isotope signature and carbonate content at each outcrop containing McKay and Canyon Creek rocks shows a sharp positive correlation in the two eastern most localities. However, the trend among the other four outcrops either shows a positive correlation or is too subtle to be definitive given a 5 % uncertainty for estimation of mineral mode. The regional data therefore presents an ambiguous picture of the impact by quartz and mica on isotope composition. The sharp jump in $\delta^{18}O$ at the unit contact between the Canyon Creek and McKay and between the two eastern most localities indicates that local mineralogy probably did mildly affect the composition of wall rocks during localized fluid circulation and re-equilibration associated with metamorphism. However, this relationship is complex and non-linear, and other factors discussed later must also have been responsible for the alteration of calcite in wall rocks.

To assess the possibility that syntectonic veins precipitated from fluids derived from sources local to the bulk rock system, the systematic depletion observed in veins and breccia from three regional faults and two densely fractured outcrops must be explained. The regularity of this pattern and lack of corresponding enrichment preclude the effects of *random* kinetic disequilibrium between rocks and fluid as being the cause for isotopic discrepancies between veins and wall rocks. Potential factors for promoting systematic vein depletion within an isotopically closed-system include: (a) fluids derived locally from the dewatering of low-$\delta^{18}O$ hydrous phases (scenario (iii)), and (b) thermal disequilibrium between wall rock and fluids (scenario (iv)).

As previously stated, peak metamorphism in the Western Ranges was coeval with the main phase of deformation and vein development. If the hydrous phases were isotopically lighter than surrounding carbonates and the residence time of the metamorphic fluids was sufficiently brief to prevent homogenization with wall rocks, the resultant veins will exhibit a lower $\delta^{18}O$ than that of wall rock calcite [*Valley*, 1986]. Under such conditions, the local concentration of hydrous minerals would be proportional to the magnitude of vein depletion. In Figure 2.11(b), no correlation exists between vein depletion and the abundance of muscovite and chlorite at each outcrop. In fact, the two largest depletions occur in dolomite and limestone breccia from outcrops that contain less than 5 mol % hydrous minerals. Hence, closed system cycling of metamorphic fluid between sites of devolitization reactions and open fractures cannot fully explain systematic fluid-rock disequilibrium across the Western Ranges.

The fractionation of ^{18}O between water and calcite during vein precipitation is a temperature dependent process that is quantifiable by a partition coefficient. Fluids that are isotopically equilibrated with the rocks through which they pass can nevertheless produce relatively low-$\delta^{18}O$ veins if they are hotter than surrounding rocks [e.g., *Lee et al.*, 1997]. Assuming an ambient temperature of 350°C, depletions of 1.0 ‰ are possible in veins that precipitated from fluids elevated by 50°C - 60°C [*O'Neil et al.*, 1969; *Zheng*, 1993]. Given a geothermal gradient of 30°C/km, this requires that fluids ascending from a minimum of ~1.7 - 2 km below the dilation site travelled at rates high enough to prevent cooling. For fluid fluxes typical in metamorphic environments ($< 10^{-9}$ m/s), conduction has been shown to outweigh advection as a mechanism for heat transport [e.g., *Bickle and McKenzie*, 1987] making thermal perturbations from long distance fluid flow unlikely. Even for large fluxes of $\sim 10^{-8}$ m/s that are confined to within shear zones, modeling predicts that the temperature of an ascending fluid will

only be ~26°C hotter than the host rock [*Dipple and Ferry*, 1992a]. Distributed flow through a fracture network will result in even more subdued thermal perturbation [*Brady*, 1988]. Furthermore, vein temperatures deduced from isotope thermometry are consistently between 300° and 350°C, and therefore compatible with the estimated ambient rock temperature. Thus, the argument for a nearby source for depleted vein forming fluids is dubious. Moreover, while local hydrothermal circulation during metamorphism probably altered wall rock compositions to a degree, the influence of local lithology on $\delta^{18}O$ cannot fully explain westward carbonate depletion in the Western Ranges.

II. Open-system fluid regime: An eastward-migrating isotopic front

Here, I address the possibility that a large-scale, infiltration front propagated across the Western Ranges during Mesozoic contraction and consequently lowered wall rock compositions and promoted disequilibrium between veins and wall rocks. I argued above that a factor other than local homogenization between silicates and calcite is responsible for the westward decrease in $\delta^{18}O$. The most plausible alternative to this is the pervasive eastward flow of relatively low-$\delta^{18}O$ fluids across the transect and subsequent re-equilibration of host rocks. Circumstantial evidence for this can be seen in the outcrop from the Rocky Mountain Trench that is depicted in Figure 2.7. The density of fractures and faults is higher here (~10-20 %) than at any other locality, wall rocks possess the lowest $\delta^{18}O$ of all carbonates sampled from the McKay Group, and oxygen values across the outcrop are remarkably uniform. Elevated permeability from an interconnected network of micro- and meso-scale fractures apparently promoted efficient fluid flow and homogenization within the outcrop, and also permitted greater access to externally derived fluids [e.g., fault-fracture meshes in *Sibson*, 1996].

The distribution of whole rock compositions in Figure 2.4 fits the general profile of 1-D flow models described by isotope transport theory [*Dipple and Ferry*, 1992b; *Bowman et al.*, 1994]. An ascending, eastward-migrating, low-$\delta^{18}O$ fluid, which infiltrated Canyon Creek and McKay sediments from the west, could trigger the observed pattern of whole rock depletion across a flow path ≥ 14 km. The gradational nature of the profile is consistent with substantial fluid dispersion and/or retarded exchange kinetics during the flow event. Siliciclastic sequences in the Dogtooth Range represent an obvious, low-$\delta^{18}O$ reservoir from which this isotopic front could have been derived. A sample of calcareous siltstone from the Donald Formation, the shallowest and eastern most unit west of the Purcell Thrust, exhibits a signature of 16.0 ‰ (calcite) and best approximates the composition of rocks in equilibrium with fluids at their point of entry into the Middle and Upper Cambrian sequence. I therefore propose that low-$\delta^{18}O$ fluid was either expelled or siphoned from the Dogtooth Duplex during contraction, and migrated eastward and up-section into the carbonate sequences of the Western Ranges where it produced a ≥ 14 km wide zone of isotopic depletion.

The observed departure from equilibrium within veins is small enough to necessitate substantial buffering of fluids by wall rocks. However, the systematic nature of these depletions suggests that vein-forming fluids exchanged only partially with wall rocks and therefore retained a light isotopic component from the source. In an open-system flow regime, vein depletion reflects either (a) the infiltration of fluid that has travelled along a temperature gradient (i.e., scenario (v)), or (b) the infiltration of fluid derived from a low-$\delta^{18}O$ source (scenario (vi)).

Transport theory dictates that under conditions of thermal and kinetic equilibrium exchange between water and rock, fluid migrating up a temperature gradient, i.e. downwards through a stratigraphic package or along a fault, will drive $\delta^{18}O$ values downwards [*Dipple and*

Ferry, 1992b; *Bowman et al.*, 1994]. The magnitude of these shifts is a function of the time-integrated fluid flux and the profile of the geothermal gradient. The one-dimensional transport model developed by *Dipple and Ferry* [1992b] can be used to predict the time-integrated fluid flux required to effect the observed depletion in veins that precipitate from fluids migrating up a temperature gradient of +30°C/km. Fluxes of ~ 1-4 • 10^4 mol H_2O/cm^2 over a path length of 1-5 km will lower vein compositions by 1 ‰ - 3.7 ‰ relative to surrounding wall rocks. Some studies have documented the siphoning of large volumes of shallow fluid downward against a lithostatic gradient [*Burkhard and Kerrich*, 1988; *McCaig*, 1988; *Cartwright and Buick*, 1999]. For example, *Cartwright and Buick* [1999] used silica solubility to estimate a time-integrated fluid flux of 2.1 • 10^6 mol H_2O/cm^2 in ductile shear zones of the Alice Springs Orogen. However, most of these models invoke the channeling of fluids along high strain zones, such as mylonites, or demand a latent phase of stress relaxation and extensional faulting to justify fluid migration up a pressure gradient. Neither of these situations applies to localities in the Western Ranges. Furthermore, vein quartz, which is prevalent in the Western Ranges, is unlikely to have precipitated during up-temperature fluid flow. A more reasonable mechanism for promoting systematic vein depletion is the large-scale influx of fluid from a low-$\delta^{18}O$ source. In previous discussion, I identified such a reservoir in the siliceous units of the Dogtooth Range. Although the composition of veins is not low enough to resemble that of wall rocks in the Dogtooth Range (~14 ‰ - 16 ‰), the only source for fluids even mildly depleted in ^{18}O at each outcrop is within rocks located deeper and farther west.

If each outcrop was located within a km-scale fluid infiltration front that extended eastward from the Purcell Thrust and conditions of kinetic disequilibrium prevailed, the fluids from which these veins precipitated would be equilibrated with lower-$\delta^{18}O$ wall rocks farther

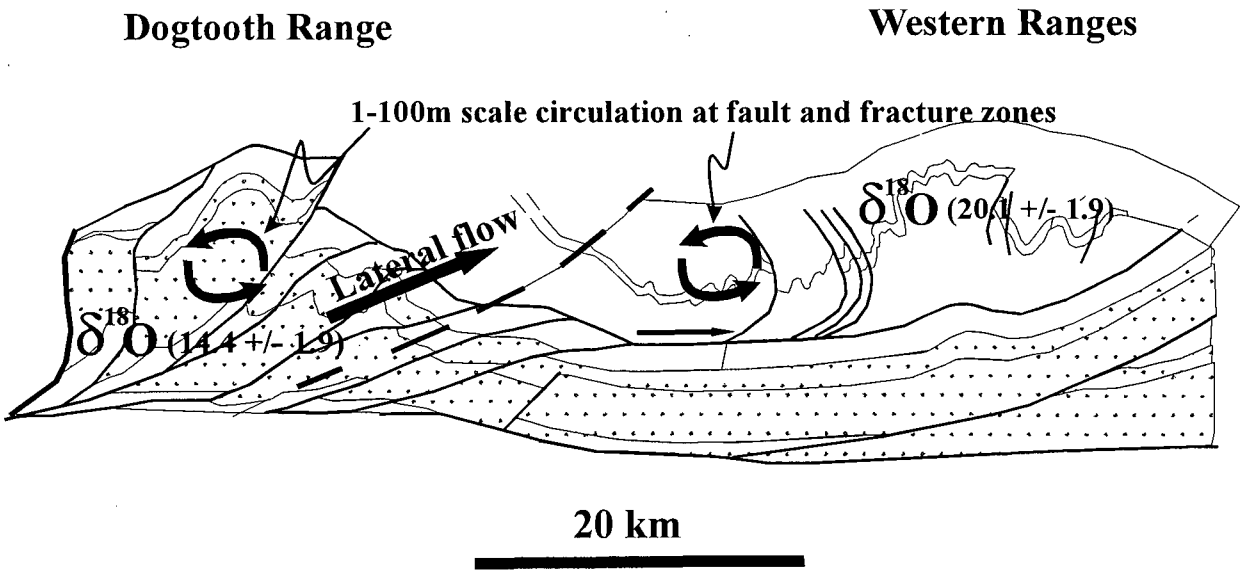

Figure 2.12: Proposed scenario of both local and large-scale fluid migration in the Dogtooth and Western Ranges. Cross-section reflects configuration prior to displacement on the Purcell Thrust. Modified from *Kubli and Simony* [1994].

upstream, i.e., deeper and westward, in the flow system. That is, the flux of westerly-derived fluids migrating towards isotopically heavier carbonates prevented them from fully equilibrating with the surrounding wall rocks. Instead, fluids exhibited a compositional "lag", recorded as depletions in vein calcite along their flow path. In conclusion, a gradual shift in isotope compositions and systematic vein depletions in the Western Ranges provide two lines of evidence to suggest that during Mesozoic tectonism, a substantial volume of fluid migrated eastward and up-section across a minimum distance of 14 km (Figure 2.12).

Table 2.3: Summary of catalysts for isotopic depletion in the Western Ranges

	Scenario		**Evidence**
i	shift in $\delta^{18}O$ is a function of age variability (closed-system)	no	observed isotopic spread is too large
ii	exchange with *locally-derived*, metamorphic fluids (closed-system)	partially responsible for outcrop-scale homogenization	correlation between $\delta^{18}O$ and silicate abundance in some outcrops, but no correlation between phyllosilicate concentration and magnitude of depletions
iii	exchange with low-$\delta^{18}O$ phases (closed-system)	partially responsible	evidence from McKay-Canyon Creek contact and correlation between $\delta^{18}O$ and silicate abundance in some outcrops
iv	fluid-rock thermal disequlibrium (closed- or open-system)	no	unrealistic given required temperature differential/vein geothermometry precludes this
v	up-temperature fluid flow (open-system)	no	quartz veins preclude up-T flow and required TIFF is too large
vi	exchange with low-$\delta^{18}O$, exotically derived fluid (open-system)	**yes**	likely source reservoir in the Dogtooth Range and similarity between observed isotopic profile and model-derived profiles for regional fluid migration

TIFF=time-integrated fluid flux

2.8 Model-derived constraints for time-integrated fluid flux and kinetic dispersion

2.8.1 Premise

Comparisons between idealized, model-derived curves and the $\delta^{18}O$ profile in this study would be fruitful in placing first-order constraints on time-integrated fluid flux. For a scenario of non-dispersive fluid advection through a 1-D column of compositionally homogeneous rock,

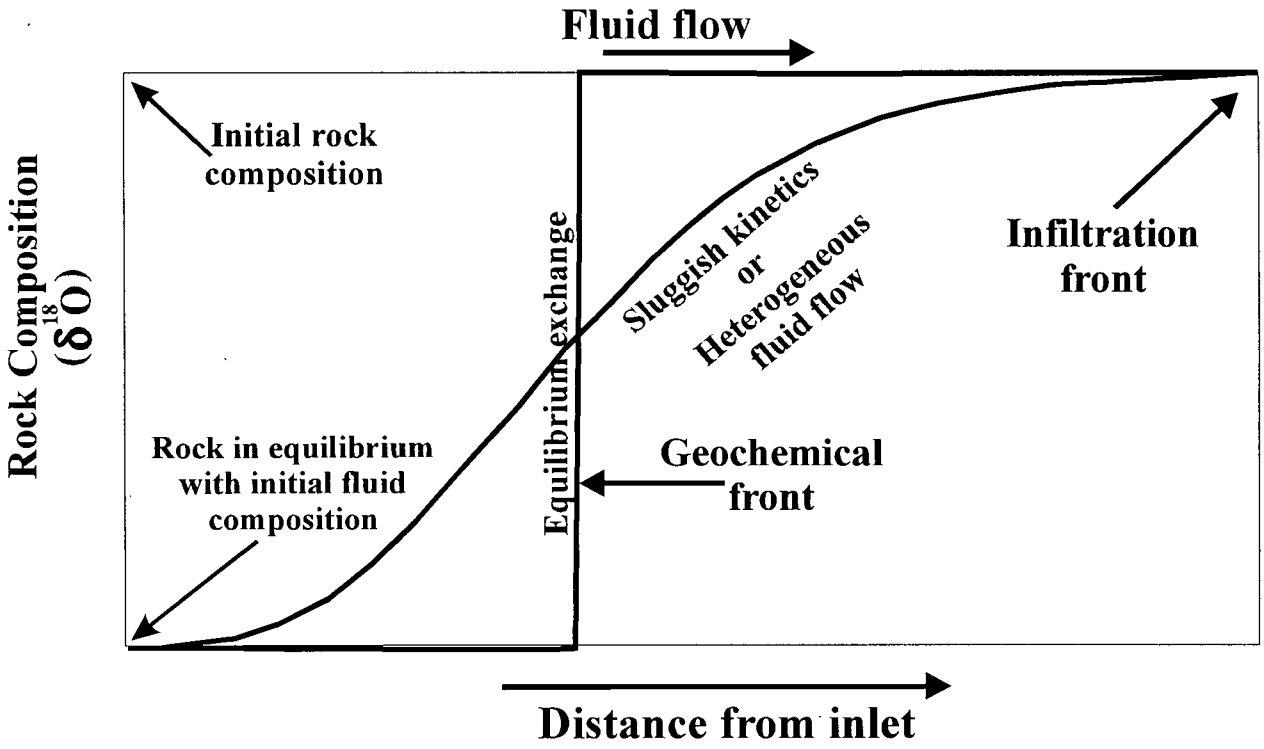

Figure 2.13: Comparison of equilibrium (N_D>>100) versus non-equilibrium (N_D<100) fluid-rock isotope exchange for the infiltration of a low-$\delta^{18}O$ fluid through a homogeneous, isothermal rock volume. Slow kinetics result in a broadened geochemical front (GF), whereas an abrupt geochemical front develops under equilibrium conditions. Isotope compositions to the left of the GF nearer the inlet are fluid buffered, and those to the right are rock buffered.

transport theory dictates that equilibrium exchange between fluid and rock will yield a spatially abrupt geochemical front (GF) across which the $\delta^{18}O_{rock}$ shifts from that in equilibrium with the initial fluid composition to that of the initial rock, or protolith. Under conditions of sluggish reaction kinetics or heterogeneous fluid flow, the GF becomes distended, and the width of the transition zone from fluid to rock-buffered exchange is proportional to the intensity of either of these factors (Figure 2.13). In the case of the Western Ranges, the GF is not abrupt, and equilibrium exchange models are therefore inappropriate for simulating conditions during Mesozoic fluid migration. For two reasons, kinetic disequilibrium between fluid and rock was probably at least partially responsible for the distended GF observed in the transect. Firstly, the temperature of isotope exchange was no greater than 400°C and likely between 300°C and 350°C. The reaction rate constant, κ, is proportional to temperature, and reaction kinetics are therefore inhibited at cooler temperatures typical of the upper crust. In addition, $\delta^{18}O$ values which are systematically lower in veins than wall rocks provide compelling evidence that infiltrating fluid was not in equilibrium with the rocks that it altered. Thus, the magnitude of the difference between wall rock carbonate and vein carbonate signatures, $\Delta^{18}O_{vein\text{-}wall\ rock}$, directly correlates with the extent of kinetic disequilibrium.

2.8.2 Model description

Lassey and Blattner [1988] have devised a 1-D analytical model that imposes kinetic constraints on oxygen isotope transport and exchange by virtue of a non-dimensional term, the Damköhler number (N_D), and is therefore well suited for relatively low temperature conditions.

They derive their solution from two dimensionless equations for mass-balance (1) and kinetic (2) exchange:

$$\partial/\partial\tau\ (\Phi'\delta^{18}O_{water} + \delta^{18}O_{rock}) + \Phi'\ \partial/\partial Z\ \delta^{18}O_{water} = 0 \qquad (1)$$

$$\partial/\partial\tau\ \delta^{18}O_{rock} = N_D(\alpha\delta^{18}O_{water} - \delta^{18}O_{rock} + \Delta) \qquad (2)$$

where τ is dimensionless time since commencement of infiltration (= tq/L; q is the mean longitudinal interstitial (Darcy) velocity; L is the length of infiltrated aquifer); Φ' is the ratio of oxygen in pore-bound fluid to that in rock; Z is the dimensionless position in the aquifer; α represents isotopic fractionation between phases; $\Delta = 10^3\ (\alpha - 1)$; and $N_D = \kappa L/q$.

For a pre-determined aquifer length, the Damköhler number essentially reflects the ratio between the rate constant for ^{18}O exchange between water and rock, κ, and flow rate, q. Therefore, an increasing N_D connotes a closer approach to chemical/isotopic equilibrium. Kinematic dispersion, i.e., heterogeneous fluid flow, is not incorporated into the final solution, but might account for the misfit between model curves and the observed profile.

A FORTRAN program written by G.M. Dipple was used to solve the formulation of *Lassey and Blattner* [1988], which employs an algorithm from *Lassey* [1982] for evaluating the K function in equations 5a and 5b of *Lassey and Blattner* [1988]. In the following simulations, values for time-integrated fluid flux (TIFF) and Damköhler number are varied to obtain a best-fit curve for the distribution of $\delta^{18}O$ in the Western Ranges. The model assumes isothermal fluid flow at 370°C, corresponding to a $\Delta_{calcite\text{-}water}$ of 3.8 ‰ [*O'Neil et al.*, 1969]; initial fluid and rock compositions of 12.2 ‰ ($\approx$ 16.0 $‰_{(calcite)}$ at 370°C) and 21.0 ‰, respectively; permeable porosity of 0.05; and a molar H_2O volume of 25 cm^3 [*Burnham et al.*, 1969]. Varying the porosity to as high as 10 % had no discernable effect on the geometry of the profile.

2.8.3 The pre-Purcell isotopic profile of the Western Ranges

As previously discussed, the main phase of deformation and syn-kinematic vein development in the Dogtooth and Western Ranges pre-dated motion on the Purcell Thrust (PTF) by an indeterminate amount of time. Therefore, an appropriate $\delta^{18}O$ versus distance profile should reflect the tectonic configuration prior to displacement on the PTF. *Kubli and Simony* [1994] have provided the only published cross-section with restored movement on the PTF (Figure 2.14), and it is to this section that data from the Dogtooth and Western Ranges are linked when depicting the most reasonable distribution of $\delta^{18}O$ that immediately followed the proposed syn-D1 alteration event. Distances are measured from a hypothetical fluid inlet located at the contact between the Donald Formation and the lower Chancellor unit where it crosses the trace of the PTF (Figure 2.14(a)). This point was chosen as the most probable inlet for the following reasons:

(1) The $\delta^{18}O$ (calcite) of wall rocks in the Donald Formation are consistent with the low values observed throughout the Dogtooth Range placing it behind, i.e., to the west of, the inlet. In contrast, all rocks above the Donald Formation exhibit comparatively higher compositions suggesting that they lie within the domain affected by the infiltration front.

(2) Based on the hypothesis that fluids were expelled upward and eastward from the locus of deformation in the west, i.e., the Dogtooth Duplex, the restored trace of the PTF represents a reasonable exit point for fluids near the leading edge of the deformation front. The resultant profile, depicted in Figure 2.14(b), shows a 10 km gap between the inlet and Middle Cambrian units that reflects the thickness of the Chancellor Group, which is unexposed in this portion of the Rockies.

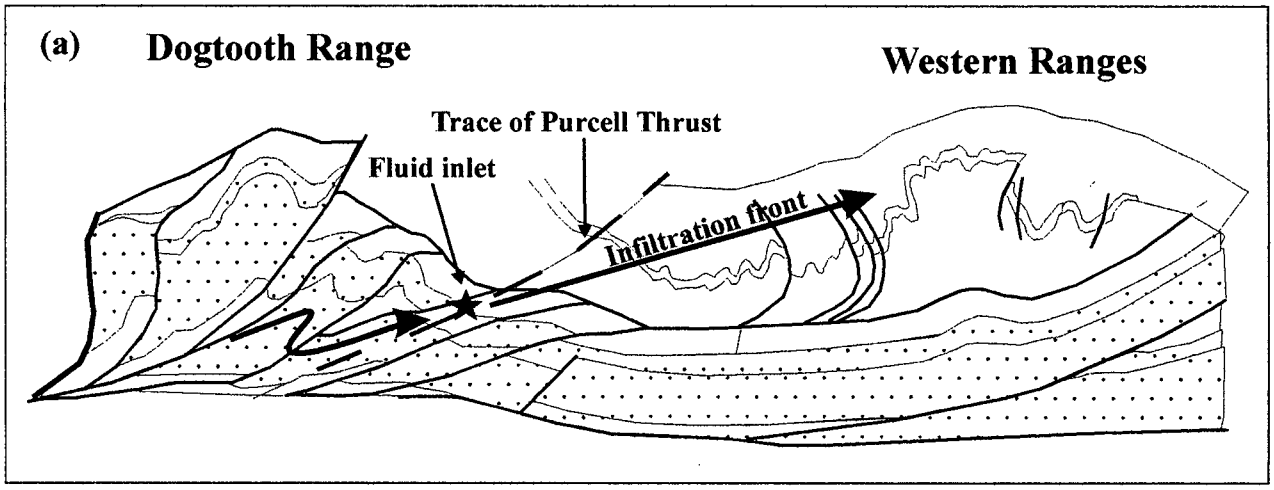

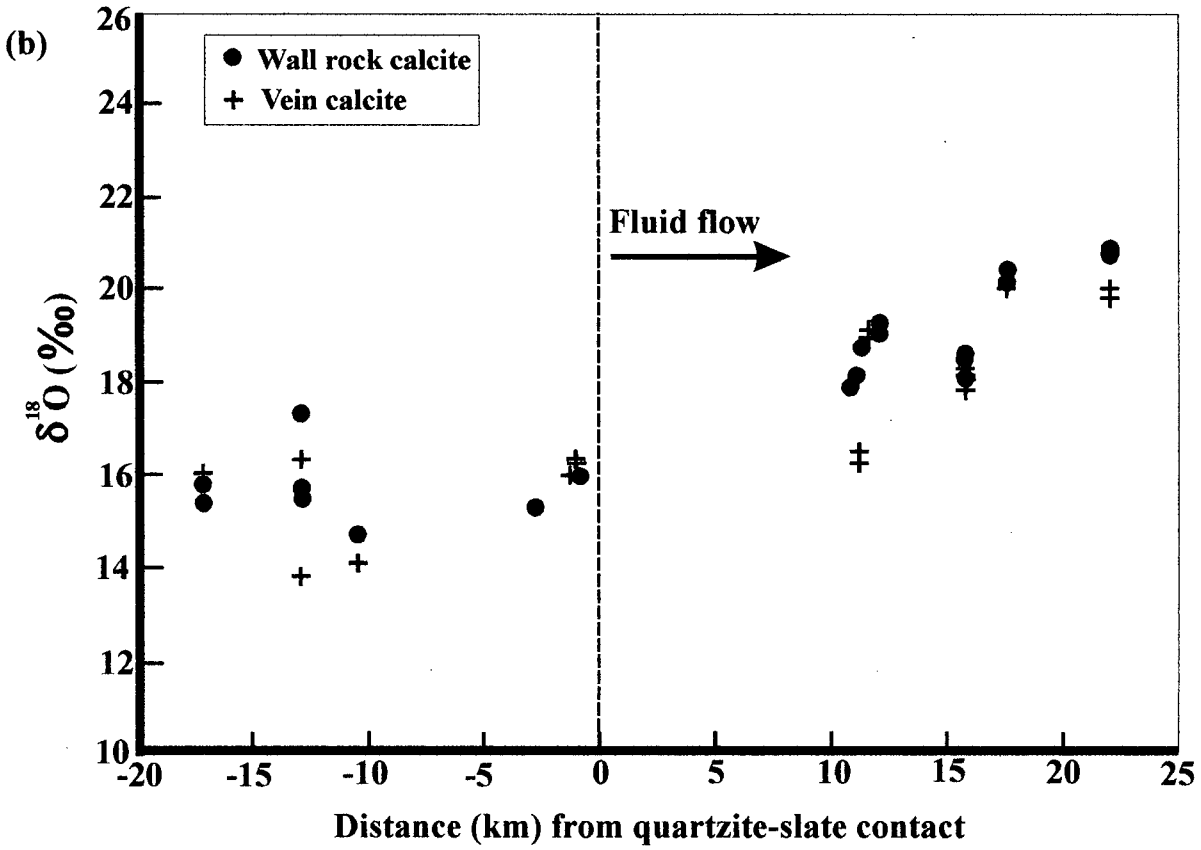

Figure 2.14: (a) Configuration of study area following initial phase of deformation, but prior to displacement on Purcell Thrust. Fluid inlet is chosen as contact between the Donald Formation and Chancellor Group at the trace of the Purcell Thrust. Modified from *Kubli and Simony* [1994]. (b) Distribution of oxygen values allowing for restored motion on the Purcell Thrust.

2.8.4 Modeling results

Increasing the degree of kinetic dispersion (i.e., decreasing the N_D) produces two effects: (1) the geochemical front widens and (2) veins are more depleted with respect to their wall rocks. Thus, a trade-off exists between accommodating the magnitude of vein-wall rock disequilibrium and obtaining a reasonable match for the shape of the GF. To account for this, curves were fit separately to the shape of the rock alteration front (1) and the geometry of the vein profile (2).

Table 2.4: Predicted TIFF and kinetic dispersion for various assumptions

Criteria	Kinetic Constraints	Damköhler number (N_D)	TIFF (mol H_2O/cm^2)
Best-fit curves (rock alteration)	rapid fluid-rock exchange	70	1.3×10^5
	slower fluid-rock exchange	20	1.1×10^5
Best-fit curves (vein, i.e. fluid, composition)	sluggish fluid-rock exchange	1	$5\text{-}8 \times 10^4$
	more rapid fluid-rock exchange	20	$1.1\text{-}1.3 \times 10^5$
Post-Purcell fluid flow (14 km trajectory)	sluggish fluid-rock exchange	2	4×10^4
	more rapid fluid-rock exchange	15	$5\text{-}6 \times 10^4$

TIFF=time-integrated fluid flux

The results of several simulations are listed in Table 2.4 and illustrated in Figure 2.15. For a pre-Purcell Thrust fluid regime, all best-fit solutions correspond to a TIFF between 5×10^4 and 1.3×10^5 mol H_2O/cm^2 ($\cong 1.3 - 3.3 \times 10^6$ cm^3/cm^2). By comparison, *Ferry* [1992] estimated a TIFF of $\sim 4.0 \times 10^2$ mol H_2O/cm^2 for a regional hydrothermal cell within low-grade metamorphic rocks of the Appalachians, and various authors have calculated fluxes between 1.2×10^4 and 2.1×10^6 mol H_2O/cm^2 for ductile fault zones throughout the world [Table 2.5 - *Dipple and Ferry*,1992a; *Bowman et al.*, 1994; *Cartwright et al.*, 1999]. Thus, the volume of fluid necessary to cause the observed alteration falls within the range of values recorded in shear zones throughout the world but well exceeds that calculated for pervasive flow through low-grade metamorphic terranes. Unless uncharacteristically large quantities of fluid were generated

and circulated during greenschist metamorphism in the Rockies, water was probably structurally focussed into zones with a high density of faults and fractures.

Table 2.5: Estimated time-integrated fluid fluxes (TIFF) from various terranes

Study	Locality	TIFF (mol H_2O/cm^2)
Ferry [1992]	Vermont (ankerite metamorphic zone)	4×10^2
Dipple and Ferry [1992a]	Various ductile shear zones	5×10^4 - 2×10^5
Bowman et al. [1994]	Glarus Thrust (mylonite)	1.2 - 2.9×10^4
Cartwright et al. [1999]	Alice Springs Orogen (shear zone)	2.1×10^6
This study	Canadian Rockies (fault and fracture zones)	5×10^4 - 1×10^5

Estimates of kinetic disequilibrium are less well constrained than TIFF, with N_D values that range between 1 and 70 depending on the scenario. A curve with a Damköhler parameter of 20 accommodates most of the data points in Figure 2.15(a). However, the poor fit in Figures 2.15(b) and (c) illustrates that the cause of fluid-rock disequilibrium at each outcrop cannot be strictly attributed to kinetic disequilibrium, and another processes, such as heterogeneous fluid flow (kinematic dispersion), must also be involved. Nevertheless, an N_D of 20 provides one of the best fits for rock-vein disequilibrium and the shape of the rock alteration front and therefore best quantifies the degree of kinetic dispersion within the system. In summary, model simulations suggest that during deformation, the Western Ranges experienced a time-integrated fluid flux of ~1×10^5 mol H_2O/cm^2 and moderately slow kinetics defined by an N_D of ~20. Under conditions of complete fluid-rock equilibrium (N_D=10,000 - not shown) and a TIFF of ~1×10^5 mol H_2O/cm^2 , the geochemical front would have been situated ~12 km from the fluid inlet in the absence of kinetic dispersion or heterogeneous fluid flow.

Finally, to simulate post-Purcell fluid migration, model generated curves were also fit to a $\delta^{18}O$ profile with an x-axis defined by distance across strike from the Purcell Thrust (Figure 2.15(d)). This scenario shortens the infiltration front to < 15 km and consequently diminishes the

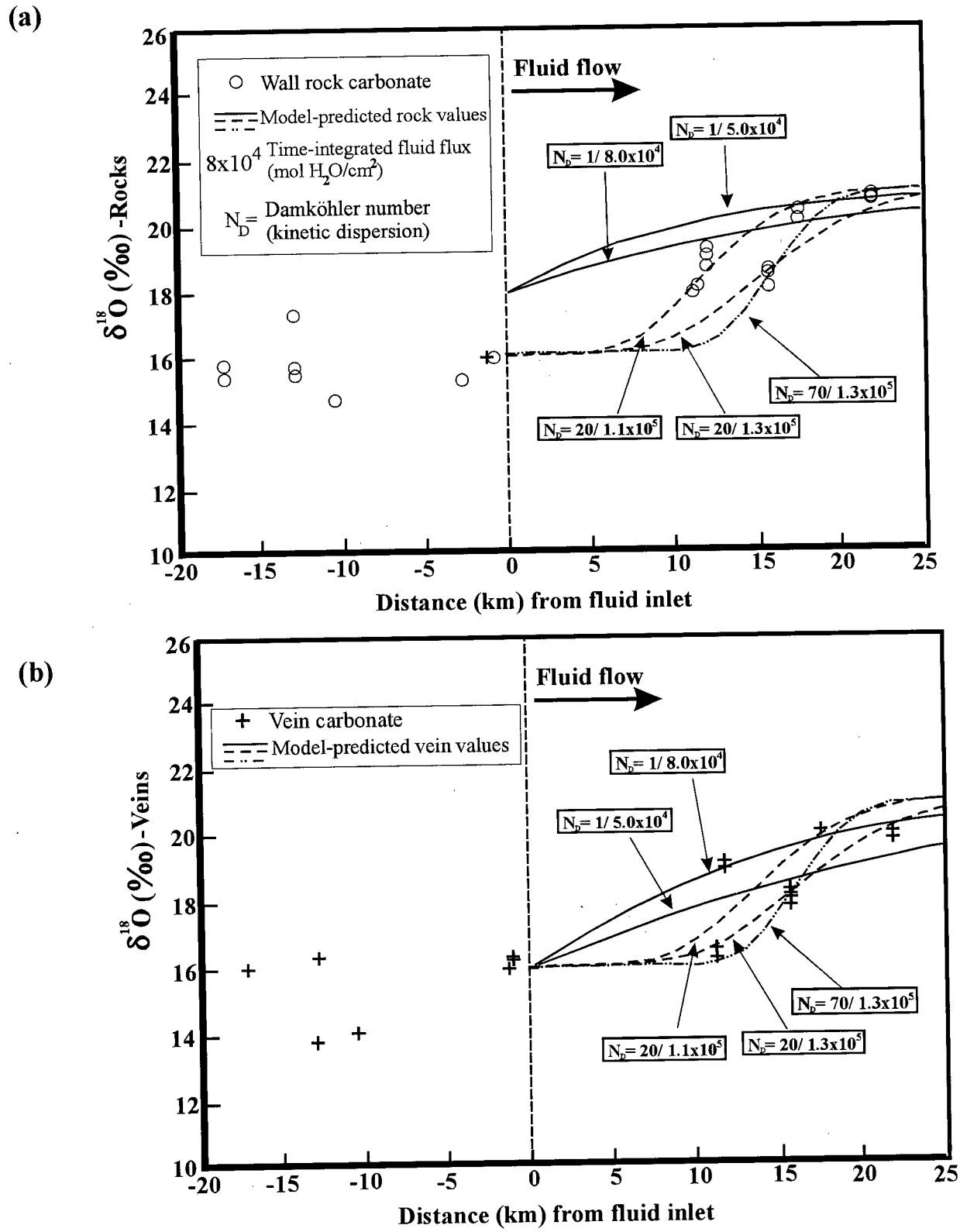

Figure 2.15: Predicted time-integrated fluid fluxes and kinetic dispersion for varying pathlength and assumptions (discussed in text). (a) Predicted rock alteration profiles. Lower Damkohler numbers correspond to higher, i.e. less altered, rock compositions. (b) Predicted vein composition profiles.

(c)

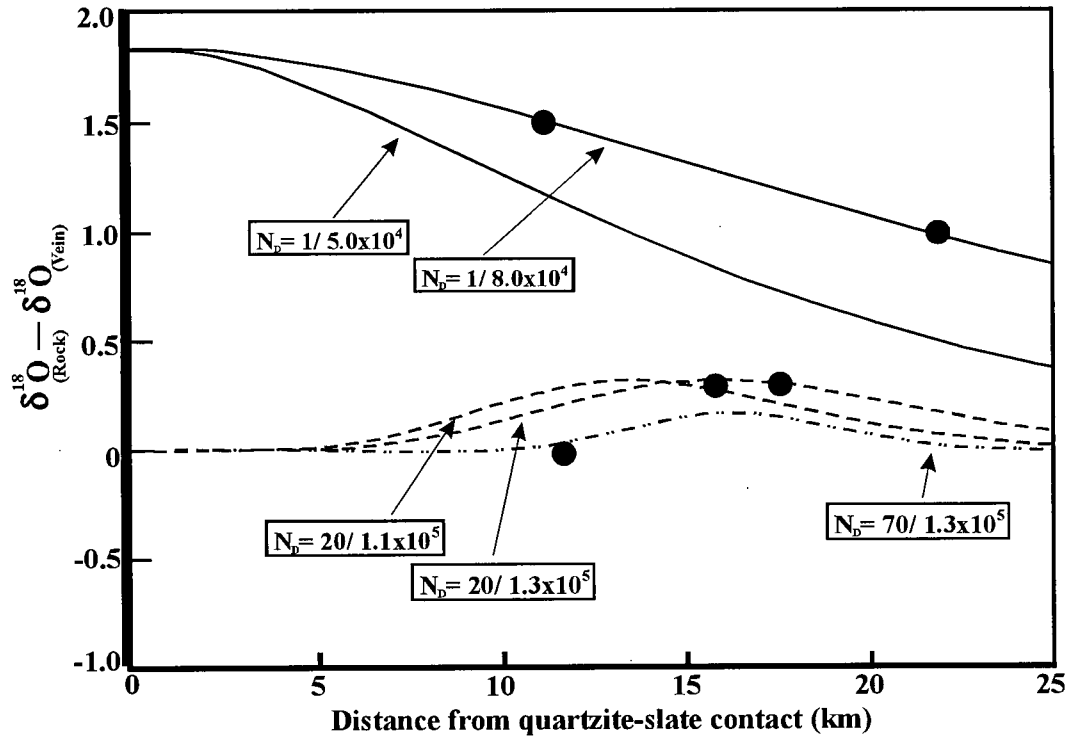

(d)

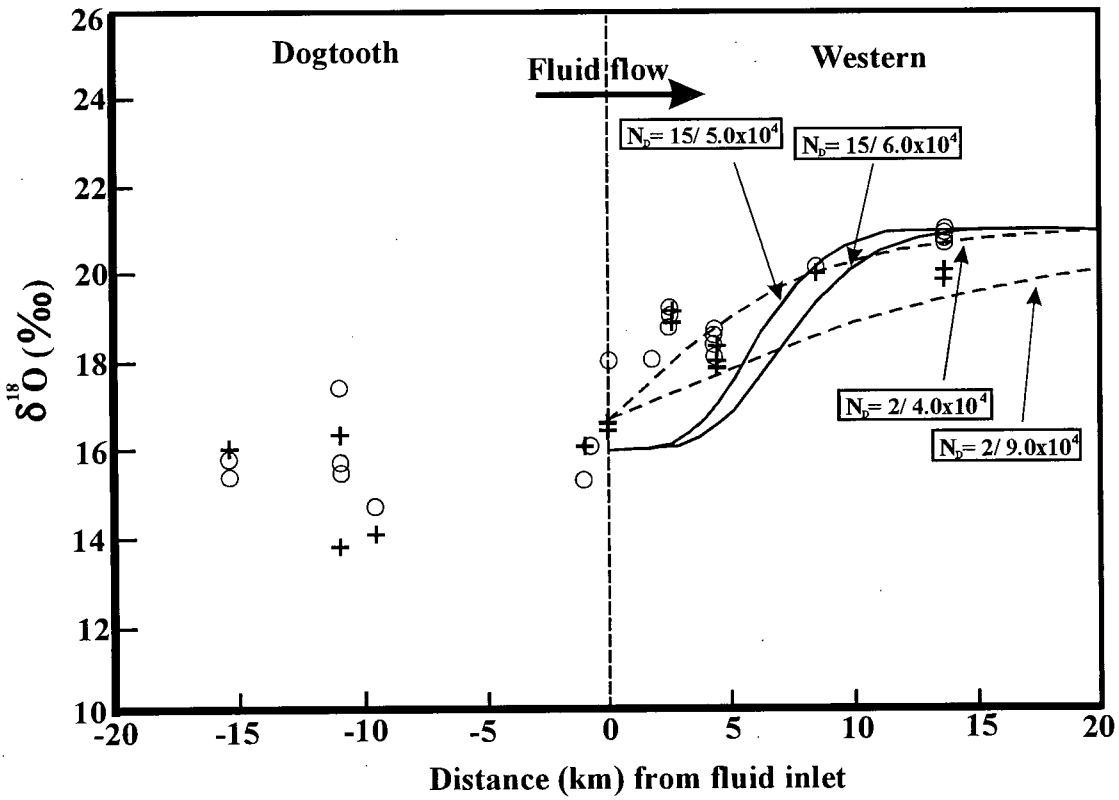

Figure 2.15 (con't): (c) Predicted vein-wall rock disequilibrium that results from kinetic dispersion. No single, model-generated curve can accommodate all the data. Data points represent average vein-wall rock fractionation at each outcrop. (d) Assumption that alteration event occurred after or during the latest stages of displacement on the Purcell Thrust.

estimated TIFF to 4-6 x 10^4 mol H_2O/cm^2. Thus, even for the unlikely scenario that fluid migration occurred shortly before the termination of displacement on the Purcell Thrust, the model still produces TIFF estimates of 10^4-10^5 mol H_2O/cm^2.

2.9 Summary and implications for fluid transport

It is beyond the scope of this study to constrain the exact mechanisms by which fluids were transported across the Western Ranges. Substantial isotope depletions as high as 3.7 ‰ at thrust faults suggest that fault zones experienced slightly greater time-integrated fluid fluxes than fracture networks within thrust sheets. However, three of the four McKay outcrops were within thrust sheets at least 2.2 km across strike from the nearest regional fault, therefore making it unlikely that major thrusts and related fractures were the only principle conduits through which exotic fluids were supplied to these rocks. A spaced, penetrative cleavage is pervasive throughout the Western Ranges, and stylolitization is common even within more competent limestones and dolomites. Numerous studies have emphasized the ability of secondary cleavage to raise rock permeability through volume loss and micro-cracking by an order of magnitude greater than five [e.g., *Etheridge et al.*, 1983; *Cox and Etheridge*, 1989; *Sibson*, 1996]. Others have demonstrated that cleavage planes and stylolites can focus fluids across ≥ 100's of meters [*Bradbury and Woodwell*, 1987; *Rye and Bradbury*, 1988]. Given the extensive evidence for pressure solution, recrystallization, fracturing, and meter-scale faulting at each outcrop, it is a reasonable assumption that deformation and attendant metamorphism actively enhanced permeability and promoted fluid migration throughout the Western Ranges.

Importantly, temporal constraints for this fluid event are based upon cross-cutting relationships between veins, cleavage, and thrust faults. Therefore, without absolute dates for

displacement on the out-of-sequence Purcell Thrust and the regional (S1) fabric that it truncates, I cannot exclude the possibility that the isotopic front evolved during latent tectonism associated with movement on the PTF. The exact cross-sectional configuration during fluid migration, i.e. Figure 2.2 versus Figure 2.12, is ambiguous. Nevertheless, the Purcell Thrust was definitely active no later than the mid-Cretaceous and pre-dates a second phase of transtensional tectonism (D2) [*Kubli and Simony*, 1994]. Thus, the isotopic front described herein must be a feature related to Mesozoic contraction.

To summarize, data from stable isotopes yield several new insights into the nature of fluid-rock interaction across the hinterland-foreland transition in the Dogtooth and Western Ranges:

(1) The anomalously low $\delta^{18}O$ of carbonates and tendency of vein compositions to approach average bulk rock $\delta^{18}O$ at individual outcrops signifies active ≥ meter-scale fluid circulation at outcrops in the Dogtooth Range.

(2) There is no isotopic evidence that fluids were preferentially focussed into fault zones in the Dogtooth Duplex.

(3) The Purcell Thrust Fault delineates a 4.7 ‰ shift towards higher $\delta^{18}O$ values in the east.

(4) Wall rocks in the Western Ranges become gradually enriched in $\delta^{18}O$, and approach more typical values for Late Cambrian-Early Ordivician carbonates with increasing distance eastward from the Purcell Thrust.

(5) Wall rocks in the Western Ranges are homogeneous in composition across ≥ 50 meters.

(6) Syn-kinematic veins in the Western Ranges are systematically depleted relative to their immediate host rock, with the largest depletions occuring within cataclasites from regional thrust faults.

(7) The pattern of wall rock alteration cannot be explained strictly by variations in age or mineral mode at different outcrops. Likewise, mineral mode and thermal and *random (i.e., closed system)* kinetic disequilibrium do not justify vein depletions.

(8) Deformation enhanced fluid migration from low-$\delta^{18}O$ siliciclastic rocks in the Dogtooth Range across ≥ 14 km into the Western Ranges best explains patterns in the composition of veins and wall rocks. During this event, isotopic reaction kinetics were moderately sluggish and time-integrated fluid fluxes were on the order of 10^4-10^5 mol H_2O/cm^2.

(9) Stable isotope and calcite-dolomite thermometry show that veins formed in approximate thermal equilibrium with the wall rocks around them.

Further research in the area should focus upon the link between deformation and wall rock alteration. Relatively pristine outcrops with minimum veining and low cleavage density need to be sampled to test the hypothesis that fluids were channeled within more deformed packages. Also, better constraints need to be placed on the effects of local mineralogy on wall rock composition. Specifically, outcrops with a relatively high volume of siliceous material should be sampled in the east, where alteration is expected to be negligible. If localities high in silica composition are also heavy in ^{18}O, consistent with minimal depletions, the notion of wall rock alteration by isotopic exchange with an externally derived fluid would be further validated.

CHAPTER 3

IMPLICATIONS FROM CARBON AND HYDROGEN ISOTOPES: DOGTOOTH AND WESTERN RANGES

3.1 Introduction

In Chapter 2, oxygen isotope systematics provided ample evidence for both local and large-scale fluid circulation in the western transect. The following two chapters refine our understanding of fluid-rock interactions in the area by introducing three additional methods that are capable of tracking the geochemical effects of syntectonic fluid migration. Here, data from carbon and hydrogen isotopes are interpreted separately.

3.2 Carbon isotopes

3.2.1 The use of carbon isotopes in fluid migration studies

As with $\delta^{18}O$, carbon isotopes can track fluid migration and record the magnitude of fluid-rock interaction in a variety of metamorphic and tectonic settings. *Bradbury and Woodwell* [1987] espoused the use of $\delta^{13}C$ - $\delta^{18}O$ diagrams to calculate minimum fluid-rock ratios as a function of isotopic alteration and to determine fluid X_{CO2} based on the relative shifts between $\delta^{13}C$ and $\delta^{18}O$. Furthermore, the temperature dependence of isotope fractionation between water and carbonates dictates that data from veins formed during gradual heating or cooling will plot along a moderately sloping curve in $\delta^{13}C$ - $\delta^{18}O$ space (Figure 3.1(a)). However, the relatively low mass-ratio of carbon in hydrothermal fluids to that in carbonate rocks, except under conditions of very high X_{CO2}, implies that fluid $\delta^{13}C$ will equilibrate with rocks relatively close to the inlet (compared with $\delta^{18}O$ and δH - Figure 3.1(b)). In other words, large systematic carbon

depletions (> 2 ‰) and correlations between carbon and oxygen signatures are only expected under conditions of high time-integrated fluid fluxes or in systems located near the source of low-$\delta^{13}C$ fluids. Also, the effect of thermal variation on stable isotopes is primarily applicable to environments with exaggerated geothermal gradients, such as skarns and epithermal systems [e.g., *Matsuhisa et al.*, 1985], and is therefore expected to be only a minor factor in this study.

Devolatization reactions that occur during prograde metamorphism are another catalyst for systematic carbon and oxygen depletion in wall rocks. Dehydration associated with the reaction of clay minerals to form muscovite and chlorite was ubiquitous throughout the study area. However, even though phyllites and shales possess 3 - 5 wt % H_2O, the resultant oxygen depletion from dehydration is probably less than 1.0 ‰ [*Valley*, 1986]. Decarbonation in calc-silicates can produce relatively profound changes in $\delta^{13}C$ and, to a lesser degree, $\delta^{18}O$. *Nabelek* [1991] modeled depletions of ~9 ‰ and ~2 ‰ for carbon and oxygen, respectively, at contact aureoles in Utah and Texas. Neither intrusive bodies nor calc-silicate minerals associated with these types of reactions, such as tremolite, wollastonite, and phlogopite, have been documented anywhere within the transect, thus minimizing the role of decarbonation in altering isotope compositions. Finally, thermochemical sulfate reduction, i.e., "the incorporation of carbon derived from the oxidation of hydrocarbons" [*Machel et al.*, 1996], is another mechanism for altering $\delta^{13}C$. Carbon signatures as low as -27 ‰ were documented by *Machel et al.* [1996] in recrystallized calcite from the Western Canada Sedimentary Basin. Graphite is a minor constituent of both the Proterozoic and Cambrian assemblages in this study and might therefore be the source of any dramatic depletions in $\delta^{13}C$.

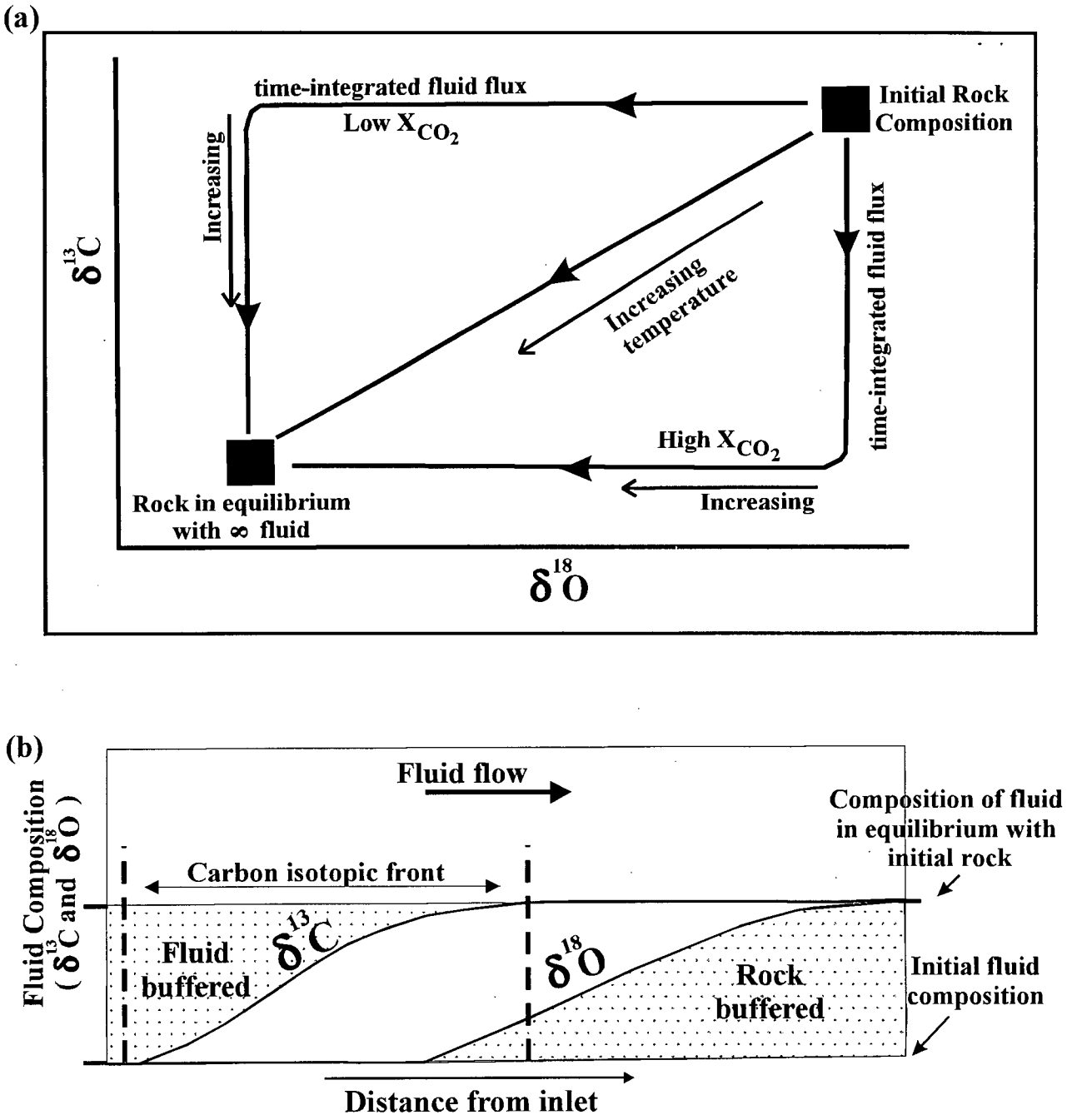

Figure 3.1: (a) Isotope exchange trajectories of carbonate data for both polythermal and isothermal conditions and exchange with a oxygen and carbon depleted fluid (after *Bradbury and Woodwell* [1987]).(b) Schematic of carbon and oxygen alteration fronts across a one-dimensional flow system. Wide distance across fronts based upon assumption that diffusion, dispersion, and/or sluggish reaction kinetics result in disequilibrium between fluid and wall rock. Note that rock buffering of carbon occurs closer to inlet than that of oxygen. Modified from *Bowman et al.* [1994].

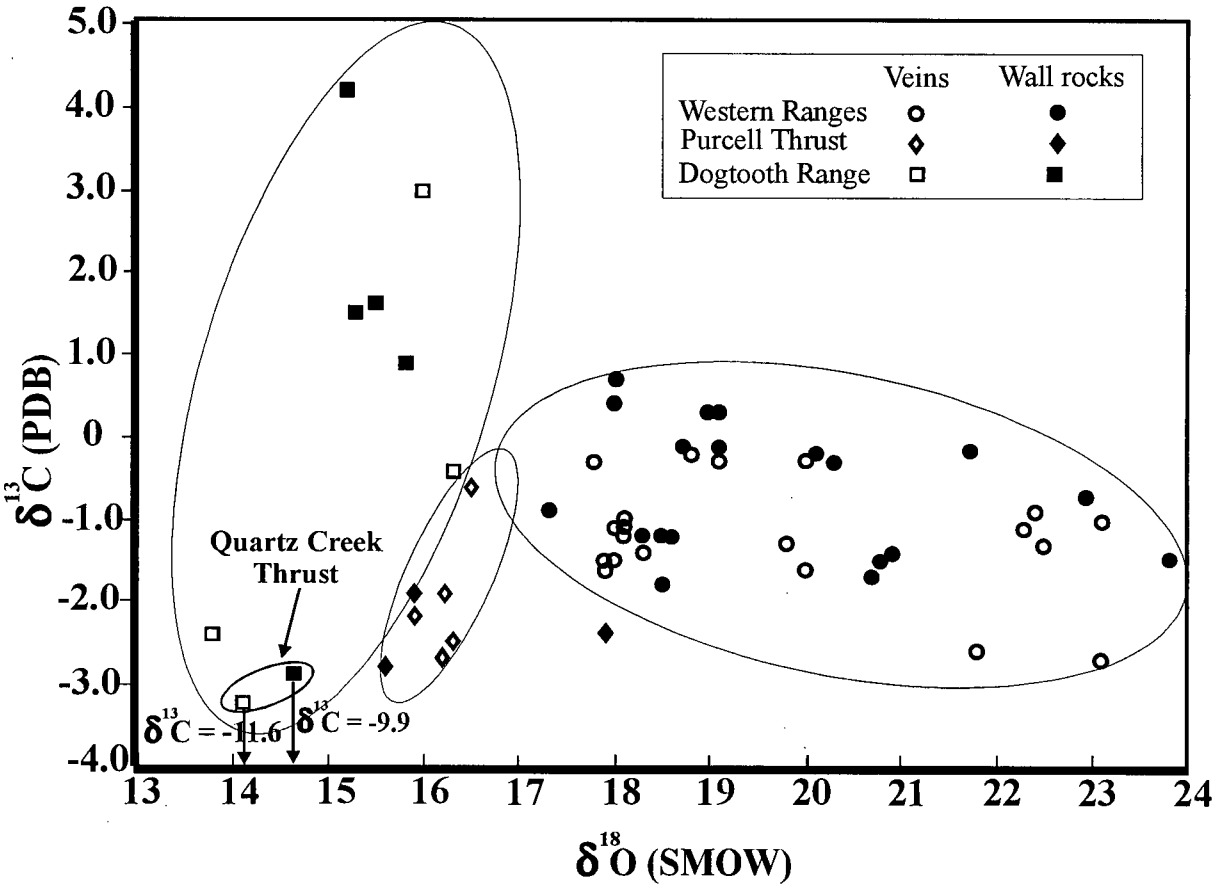

Figure 3.2: Isotopic composition of carbonates in the Dogtooth and Western Ranges. A regional correlation between carbon and oxygen is non-existent in either domain. Proterozoic units in the Dogtooth exhibit large variation in carbon composition with comparatively small changes in oxygen. The inverse relationship hold true for units in the Western Ranges. Rocks and veins from the Purcell Thrust represent the western-most sample locality in the Western Ranges and also exhibit the lowest values, suggesting infiltration by an externally derive, depleted fluid.

3.2.2 Results

Systematic relationships between $\delta^{13}C$ and $\delta^{18}O$ are generally non-existent across the study area and within individual outcrops. However, subtle trends in the fractionation of $\delta^{13}C$ between veins and wall rocks are apparent. The Dogtooth and Western Ranges exhibit contrasting patterns in $\delta^{13}C$, consistent with the hypothesis that they represent two distinct fluid regimes.

Carbon signatures in the Dogtooth Range are heterogeneous and widely distributed between -11.6 ‰ and + 4.2 ‰. Figure 3.2 illustrates the corresponding uniformity in oxygen composition and the lack of a systematic relationship between $\delta^{18}O$ and $\delta^{13}C$. Individual outcrops exhibit no overall correlation between oxygen and carbon, but veins are generally depleted in $\delta^{13}C$ relative to wall rocks (Figure 2.5(a)). At the Quartz Creek Thrust (locality 3 - Figure 2.1), vein calcite exhibits carbon and oxygen depletions of 1.7 ‰ and 0.6 ‰, respectively, relative to wall rocks. These same samples contain anomalously low carbon compositions of -11.6 ‰ and - 9.9 ‰ that are characteristic of fluids derived from oxidized organic material. Also, limestone from the Wiseman Creek Thrust and a fibrous vein from the core of a regional syncline possess atypically high carbon compositions ($\geq$ + 3.0 ‰).

In spite of a gradual shift in $\delta^{18}O$, carbon isotopic signatures are considerably more homogeneous in the Western Ranges, where $\delta^{13}C$ varies between - 2.7 ‰ and + 0.7 ‰. As in the Dogtooth Range, there is no correlation between $\delta^{13}C$ and $\delta^{18}O$, neither across the transect nor within individual outcrops. However, rocks and veins in the footwall of the Purcell Thrust are lower in $\delta^{18}O$ and $\delta^{13}C$ than carbonates farther east and suggest exchange with a depleted fluid (Figure 3.2). Veins are generally enriched in $\delta^{13}C$ relative to surrounding wall rocks (Figure 2.5(b)).

3.2.3 Interpretation of carbon isotopes

The heterogeneity of carbon data from the Dogtooth Range complicates the process of distinguishing distinct fluid events and identifying a protolith signature. *Ghent and O'Neil* [1985] provided insight into the nature of fluid alteration of the Horsethief Creek Group by documenting consistently heavy $\delta^{13}C$ signatures greater than + 3 ‰ and up to + 9.9 ‰. They attributed large variations in the carbon composition of marbles to a complicated history of fluctuating water/rock ratio, temperature, degree of decarbonation, and protolith value. Based on a global trend of anomalously high $\delta^{13}C$ values from Neoproterozoic units, including other correlative packages from the Cordillera [*Wickham and Peters*, 1993], the highest carbon values recorded in this study probably best reflect those of the protolith. Because there is no mineralogical evidence for decarbonation reactions or large temperature fluctuations during vein formation (see section 2.6.3 for geothermometry), the best explanation for the observed scatter in $\delta^{13}C$ is either heterogeneous time-integrated fluid flux across the Dogtooth Range, variable exchange and equilibration with organic material, or a combination thereof. Consistently negative values of $\Delta^{13}C_{\text{(vein-wall rocks)}}$ supports infiltration by an isotopically depleted fluid that was possibly derived from deeper, higher grade meta-sediments.

Comparatively uniform carbon-signatures from the Western Ranges conform to values expected from Paleozoic carbonates [*Montañez et al.*, 2000]. It is noteworthy that wall rocks from the westernmost locality, the Purcell Thrust, exhibit the lowest average $\delta^{13}C$, consistent with the hypothesis that low-$\delta^{18}O$ (and low-$\delta^{13}C$) fluid infiltrated the Western Ranges from higher grade assemblages in the west. If true, then this outcrop represents the tail end of an eastward-propagating carbon isotopic front, and localities east of the Purcell Thrust lie within the

rock-buffered portion of the flow system (Figure 3.1(b)). Because oxygen compositions are systematically altered in the presence of pristine carbon values as discussed in Chapter 2, ^{18}O-depleted fluids must have possessed low X_{CO2} (as in Figure 3.1(a)).

Contradicting the above hypothesis that low-$\delta^{13}C$ fluids penetrated the Western Ranges from the west, values of $\Delta^{13}C_{\text{(vein-wall rock)}}$ are consistently positive and insinuate that vein forming fluids were generally enriched relative to wall rocks (Figure 2.5(b)). Two implications arise from this:

(1) The systematic vein depletions in $\delta^{18}O$ discussed in Chapter 2 are not attributable to H_2O-CO_2 immiscibility within a fluid, as has been suggested in similar studies [*Cartwright et al.*, 1994]. Fractionation of $^{18}O/^{16}O$ and $^{13}C/^{12}C$ between H_2O-HCO_3 and CO_2 demands that ^{18}O and ^{13}C will be preferentially partitioned into CO_2 during phase separation. The removal of CO_2 from water during cooling or a drop in pressure will lower the $\delta^{18}O$ and $\delta^{13}C$ of the remaining fluid [*Cartwright et al.*, 1994]. Consequently, resultant veins can possess oxygen and carbon depletions of a few permil relative to surrounding wall rocks. Coexisting carbon *enrichment* and oxygen depletion in veins from the Western Ranges therefore precludes the possibility that they precipitated from locally derived fluids which had simply exsolved CO_2.

(2) Vein forming fluids might have originated in high-$\delta^{13}C$ sediments from the Horsethief Creek Group. As mentioned above, most processes of isotopic alteration in metamorphic environments involve decreases in $\delta^{13}C$. Thus, the simplest explanation for the observed enrichment in calcite veins is that the fluids from which they formed were derived from a comparatively high-$\delta^{13}C$ reservoir. Based on observations from this study and that of *Ghent and O'Neil* [1985], unaltered protoliths from the Horsethief Creek Group in the Dogtooth Range and localities to the north possess some of the highest carbon signatures in the Canadian Cordillera. Although carbon

fractionation between veins and wall rocks is still relatively small (< +1 ‰), it supports the hypothesis that fluids infiltrated the Western Ranges from deeper sources in the west.

It is difficult to reconcile the observation of carbon enrichment in veins with lower than average $\delta^{13}C$ values from Canyon Creek sediments and veins in the footwall of the Purcell Thrust. One possibility is that the latter population sampled fluid derived from a deeper, more decarbonated reservoir in the Dogtooth Range. Another explanation is that graphite was either more abundant at this locality or exchanged more thoroughly with infiltrating fluid, thereby lowering carbon signatures. Nevertheless, the consistency of positive $\Delta^{13}C_{\text{(vein-wall rock)}}$ values and the slight negative slope of Western Ranges data in Figure 3.2 provide evidence that lower $\delta^{18}O$ outcrops in the west sampled a fluid that was enriched in ^{13}C. At the Purcell Thrust where the data fall off this trend, I suggest that rocks and veins either exchanged with a fluid derived from a deeper, ^{13}C-depleted source or underwent greater isotopic exchange with organic carbon.

In summary, the absence of a strong regional correlation between $\delta^{18}O$ and $\delta^{13}C$ in the Dogtooth and Western Ranges masks the presence of any single, large-scale fluid event across the study area. Large $\delta^{13}C$ fluctuations indicate high variability in the degree of isotopic alteration experienced by units in the Dogtooth Range during regional metamorphism. This is attributable to heterogeneous time-integrated fluid flux and/or exchange with organic carbon. In contrast, the narrow range and typical carbon values observed in the Western Ranges attests to rock-buffering of $\delta^{13}C$ and indicates that if rocks east of the Purcell Thrust were infiltrated by low-$\delta^{13}C$ fluid, it contained low X_{CO2}. Also, consistent carbon enrichment in veins indicates that immiscibility was not responsible for the observed disequilibrium between veins and wall rocks, and lower $\delta^{13}C$ signatures near the Purcell Thrust suggest that this locality was exposed to low-$\delta^{13}C$ fluid that was probably derived from a deeper source in the west.

3.3 Hydrogen isotopes

3.3.1 Analytical Methods

Chlorite and muscovite powders (~ 4 mm^3) were drilled from slabs using diamond impregnated drill bits in a Dremel tool and analyzed for δH at the Queen's University Geochemistry Lab. Coarse grained muscovite in sample 16-3B was first magnetically separated from quartz and dolomite and then hand selected under a binocular microscope. Hydrogen was liberated using the uranium technique outlined in *Bigeleisen et al.* [1952]. Values are expressed in permil relative to VSMOW and were reproducible to 5.0 ‰, as reported by the Queen's University Stable Isotope Laboratory (Kerry Klassen, pers. comm.).

3.3.2 Sample descriptions

Four analyses were obtained from hydrous phases in the Dogtooth and western Main Ranges:

(1) In the Dogtooth Range, a massive, quartz-dolomite vein (16-3B - Type 1 from section 2.4) from the footwall of the Heather Mountain Thrust hosts fibrous muscovite that is absent from the surrounding dolomite and therefore not locally derived. Because the vein is penecontemporaneous with coexisting syntaxial, syn-kinematic dolomite veins, it formed during active tectonism at sufficient P-T conditions to produce muscovite.

(2) Also in the Dogtooth Range, massive chlorite occurs within boudinaged, cleavage-parallel quartz veins (42-5C - Type 2) near the core of the Copperstain Syncline. The chlorite overprints deformed vein quartz and is confined within the vein walls, with the exception of narrow

apopheses that extend outward into parallelism with cleavage. Because these apopheses are folded with cleavage, chloritization must have occurred during tectonism.

(3) Because the chlorite in 42-5C might have precipitated as partially metasomatized segments of host rock, protolith muscovite located ~5 cm from the vein was also analyzed. Even in the case of metasomatism, hydrothermal chlorite is expected to at least partially record the signature of infiltrating fluids.

(4) Near the facies transition between basinal calc-pelites and platform carbonates in the Main Ranges (discussed in Chapter 7), massive chlorite (46-2A) occurs in wavy, cleavage-parallel veins very similar to those in 42-5C. The veins are hosted within slates from the lower Chancellor unit, and some also exhibit a sigmoidal geometry (see Plate 7.1(d)).

3.3.3 δH relationships in hydrothermal chlorite and muscovite

Because hydrogen is partitioned preferentially into the fluid phase, it is one of the stable isotopes that is least susceptible to exchange with wall rocks and therefore most likely to retain the signature of its fluid source. Chlorite and muscovite from three veins and a phyllite yielded δH in the range of -110 ‰ to -62 ‰ (Table 3.1). Assuming a precipitation temperature of 370°C and using fractionation factors established by *Suzuoki et al.* [1976 - muscovite-H_2O] and *Graham et al.* [1984 - chlorite-H_2O], this converts to an δH (H_2O-equivalent) of -76 ‰ to -29 ‰. Of the vein analyses, two chlorite analyses fall well within the field for fluid either derived from metamorphic dewatering or equilibrated with metamorphic rocks (Figure 3.3). The vein muscovite from 16-3B yields a value that is within the compositional range for meteoric fluids near the lower-end of the metamorphic field. The affinity of the two chlorite values to that of the wall rock sample and

metamorphic waters confirms that the fluids which precipitated cleavage-parallel veins in the Dogtooth and Main Ranges were probably locally derived during metamorphism.

Table 3.1: Measured and H_2O-equivalent δH data from four phyllosilicate samples

sample	mineral	location	source	δH	δH (H_2O equivalent)	$\delta^{18}O$ (vein)
42-5C	muscovite	DT	phyllite	-84	-50	18.2 (qtz)
42-5C	chlorite	DT	cleavage-parallel vein	-64	-31	18.2 (qtz)
16-3B	muscovite	DT	fibrous,a-c vein	-110	-76	16.3 (cc)
46-2A	chlorite	MR	cleavage-parallel vein	-62	-29	19.3 (qtz)

DT=Dogtooth Range/MR=Main Ranges/qtz=quartz/cc=calcite
Fractionation factors for mineral-H_2O discussed in text. H_2O-equivalent assumes a closing temperature of 370°C.

In contrast, the 26 ‰ depletion in vein versus metamorphic muscovite from 16-3B demonstrates that low-δH, probably meteoric fluid was at least partially involved in the formation of chaotic fracture networks within a 10 meter thick dolomite bed near the Heather Mountain Thrust. In Figure 3.3, the δH values of phyllosilicates are plotted against the $\delta^{18}O$ of coexisting vein quartz or calcite. If the hydrogen-depleted sample was indeed derived from meteoric fluids, the comparatively enriched $\delta^{18}O$ values reflect an isotopically evolved fluid. In other words, the time-integrated fluid flux experienced by the dolomite must have been low enough for the surrounding wall rock to buffer the oxygen composition of through-flowing fluid. In summary, limited hydrogen isotope data reveal two distinct fluid sources for veins in the Dogtooth and Main Ranges. Two cleavage-parallel (Type 2) veins unequivocally precipitated from metamorphic fluid that lacked any meteoric component. These values are considerably higher than those obtained from fluid inclusions (-60 ‰ to -150 ‰) in similar type veins by *Nesbitt and Muehlenbachs* [1995]. A depleted hydrogen signature from a Type 1 vein indicates

that at least one other vein population sampled low-δH meteoric water. However, the degree of mixing between meteoric and metamorphic fluid within this sample is indeterminate.

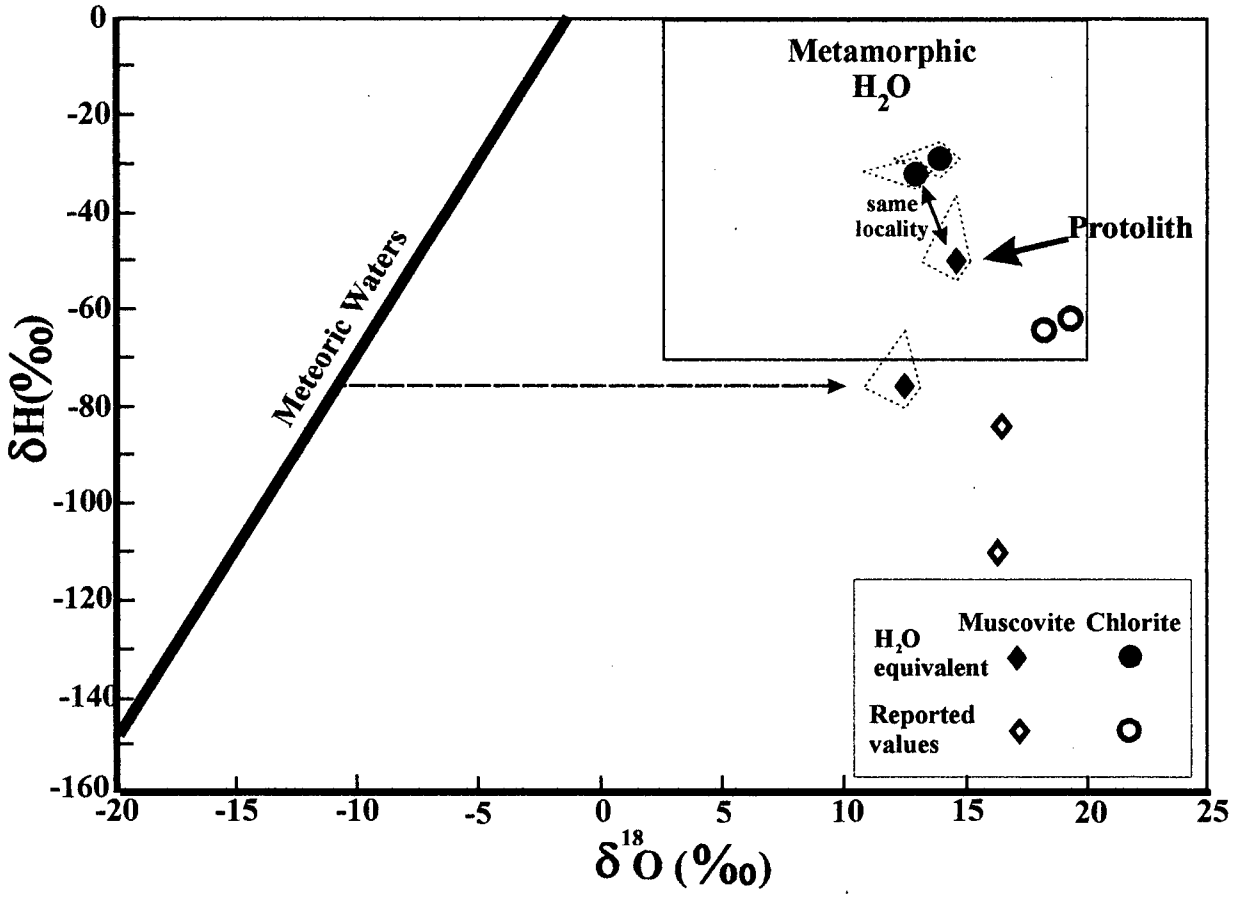

Figure 3.3: Hydrogen composition of chlorite and muscovite plotted against the oxygen composition of coexisting quartz, calcite, or muscovite. Error envelopes represent the uncertainty from mineral-H_2O fractionation factors given a temperature range of 300°C-400°C. Data is plotted at 370°C. The δH of two of the vein samples is consistent with that of muscovite from wall rocks and therefore indicates a metamorphic fluid source. A third vein probably formed from fluids that were at least partly metamorphic in origin. Fractionation factors are taken from: muscovite-H_2O - Suzuoke and Epstein [1976]; chlorite-H_2O - *Graham et al.* [1984]; quartz-H_2O - *Clayton et al.* [1972]; calcite-H_2O - *O'Neil et al.* [1969b]; muscovite-H_2O- *O'Neil and Clayton* [1969a].

CHAPTER 4

CATHODOLUMINESCENCE IN QUARTZ, CALCITE, AND DOLOMITE VEINS FROM THE DOGTOOTH AND WESTERN RANGES

4.1 Introduction

Cathodoluminescence (CL) was used to augment isotope data and provide more detailed microstructural information about smaller scale chemical relationships (mm's - cm's) than those reflected across isotopic traverses (cm's - meters). The purpose of this study was to examine cataclasites, syn-kinematic veins, and a highly strained quartzite under CL in order to: (a) elucidate possible compositional differences between protolith material, dynamically recrystallized matrix, and coexisting veins, (b) identify chemically distinct fluid events that correlate with different types of veins, and (c) distinguish between vein and detrital quartz within rocks that have been deformed by ductile strain. In light of these goals, this chapter emphasizes variations in CL intensity within samples and provides only minimal discussion about implications for the chemical composition of infiltrating fluids. In total, five samples were analyzed, including three dolomite +/- calcite fault breccias, one quartz +/- calcite vein, and a single foliated quartzite from a 10 m wide shear zone. Of these, one was selected from the Dogtooth Range, and four were from the Western Ranges.

4.2 The source and nature of CL in carbonates and quartz

Cathodoluminescence within inorganic solids stems from the radiative decay that follows the excitation of electrons in an atom or ion after bombardment by an electron beam (i.e., cathode ray). When energy from an electron beam is focussed on an insulator such as calcite or dolomite, electrons in the target material absorb the energy and rise to higher, unoccupied energy

levels. Following absorption (or activation), the excited electron cascades back to its ground state along successive energy levels (Figure 4.1(a) - *Marshall*, 1988). The magnitude of emitted energy during this process depends on the gap between each level. Luminescent crystals contain electron gaps that correspond with the energy of visible light, or photons, with a wavelength between 400 nm and 700 nm. For the purposes of this study, the most important causes of luminescence in quartz and carbonates are structural imperfections (i.e., lattice defects) and impurities. Crystal defects generally manifest as linear dislocations during cumulative strain or the presence of atomic vacancies and interstitial atoms during rapid crystallization at high temperatures. Impurities involve the substitution of an ion that is exotic to the standard mineral formula into the crystal lattice. Elements that promote luminescence are "attractors", and those that stifle luminescence by preventing the release of absorbed energy are "quenchers". The relative contribution of structural and chemical factors towards the intensity and color of luminescence differs between carbonates and quartz.

4.2.1 Carbonates

The implications of CL for carbonate diagenesis and trace element chemistry have been extensively researched and are well documented. The primary cause of luminescence in calcite and dolomite is the concentration of attractor ions that substitute for calcium (and magnesium in dolomite). The most important of these is Mn^{2+}, although *Machel et al.* [1991] also observed luminescence in samples that were doped with rare earth elements, such as Sm^{3+}, Tb^{3+}, Dy^{3+}, and Eu^{2+}. Moreover, Fe^{2+} behaves as a quencher, meaning that it absorbs energy, which is transferred from activator ions, and releases it by infrared or other means besides visible light. The intensity of luminescence is therefore usually governed by the ratio of Mn^{2+} to Fe^{2+}. The presence of Mn

generates an orange-red to orange-yellow emission that corresponds with wavelengths between 570 nm and 690 nm and conforms to an average peak around 600 nm in calcite [*Machel et al.*, 1991]. The peak wavelength for dolomite (~640 nm) is consistently longer than that for calcite [*Marshall*, 1988] , and therefore tends towards the orange-red, rather than the orange-yellow portion of the spectrum. *Marshall* [1988] asserts that the two minerals always show contrast under CL. For the most part, crystals that do not luminesce either contain a very low or very high abundance of Mn or Fe, respectively (Figure 4.1(b)). The range of Mn:Fe for which luminescence occurs is fairly broad, and brighter colors signify an increase in Mn:Fe. Thus, CL is most effective as a tool for highlighting chemically and temporally distinct veining and diagenetic events with only limited implications for the absolute abundance of trace elements. Although synthetic samples with high REE concentrations luminesce vividly in green, red, and blue, *Machel et al.* [1991] noted that the effect is drastically subdued in carbonatites and hydrothermal carbonates, possibly because of masking by Mn^{2+}. The observations in this study indicate that Mn^{2+} was the principle attractor in carbonates from the Rockies.

4.2.2 Quartz

Because the abundance of impurities is very small compared with that in carbonates, lattice defects are the most common source of luminescence in quartz. CL zoning has been attributed to variations in Fe, Ti, and Al concentration [*Penniston-Dorland and Cloos*, 1997; *Seyedolali et al.*, 1998] and kinetic effects during crystal growth [*Onasch and Vennemann*, 1995; *Nillni and Soeckhert*, 1996]. Detrital quartz generally luminesces either dull blue or red, and secondary quartz that grows as cement or solution reprecipitation is often non-luminescent

(a)

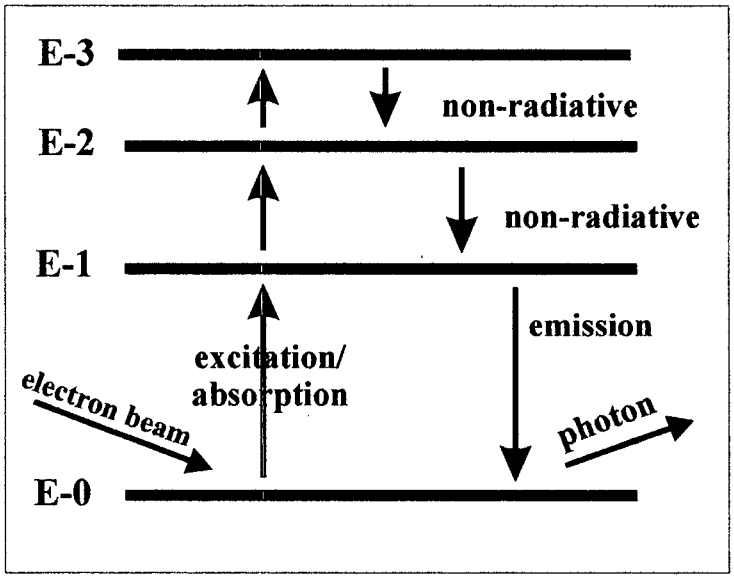

(b)

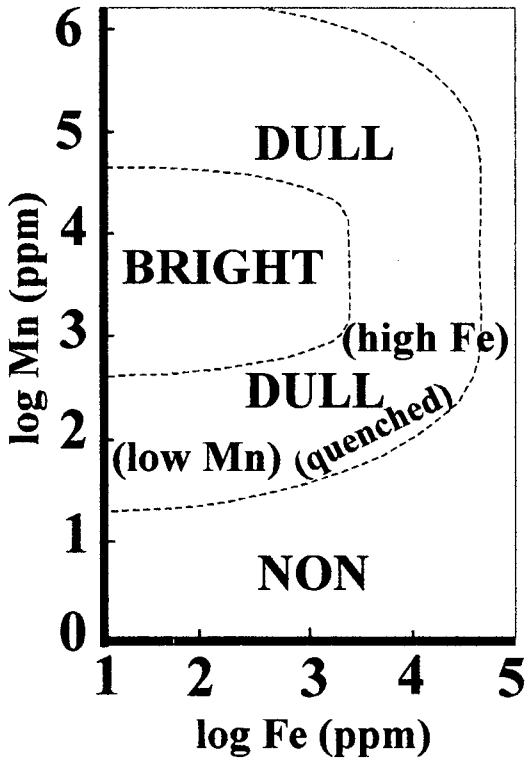

Figure 4.1: (a) Simplified electron path during excitation and emission of photons as cathodoluminescence. Energy absorption following excitation by cathode rays expels electrons from their ground state to higher energy levels. As they cascade back to E-0, discrete energy "packets" of various wavelengths are released as ultraviolet and visible light (after *Machel et al.*, 1991). (b) Fields of luminescence for calcite and dolomite as a function of Fe and Mn content. Iron acts as a quenching ion and manganese as an attractor in most concentrations. For high abundances of Mn, non-visible energy dampens photon emission (after *Machel et al.*, 1991).

[*Sprunt et al.*, 1978; *Marshall*, 1988]. With increasing metamorphism and cumulative strain, quartz color homogenizes under CL and alters to rusty red and blue under greenschist and amphibolite conditions, respectively [*Sprunt et al.*, 1978, *Dietrich and Grant*, 1985]. In a study of low-temperature mylonites, *Shimamoto et al.* [1991] noted that quartz with a high density of dislocations was more likely to luminesce than that which had been dynamically recrystallized from grain boundary migration and other annealing mechanisms. Hence, the intensity of CL in highly strained rocks correlates with the concentration of lattice defects. Diminished CL in recrystallized grains might signify a higher degree of ordering within the new crystal lattice or the reprecipitation of quartz during ductile deformation.

4.3 Equipment and device parameters

This study was performed during the course of a single day in early 2000 at the University of Alberta's Petroleum Geology Laboratory (Hans G. Machel, Dir.). The device consisted of a self-regulating Luminoscope that was attached to an optical polarizing microscope. The electron beam was set to 20 keV at 0.5 mA, except in the case of quartz-bearing samples for which the voltage was increased to 25 keV. All but one observation were obtained at low power magnification (4x) that permitted a field of view of ~ 3 mm.

4.4 Results

In this section, I present the results and interpretations of five CL analyses from different veins and fault related rocks in the northern Purcell and western Rocky Mountains. Equipment limitations prevented photographic exposures of greater than five seconds, and some observations described in the text might not be apparent from the photographs. Because of the

short exposure time and the limitations of optical (versus SEM) CL, non-luminescence in quartz might reflect shortcomings in equipment rather than properties of trace element concentration or lattice configuration. Samples are presented in geographical order from west to east. A complete description of sample localities is available in Appendix A.

43-4A: Quartz Creek Thrust at Dauntless Ridge

Sample 43-4A consists of a foliated quartzite, which is located ~100 m into the footwall of the Quartz Creek Thrust (locality 1 in Figure 2.1) in the Dogtooth Range. It was sampled from a 2 meter wide, southwest striking shear zone that conspicuously cuts massive quartzite of the Hamill Formation. Thin, elongate quartz sub-grains with aspect ratios > 10:1 are kinked and oriented sub-parallel to planar domains of fine-grained muscovite and very fine-grained, dissolved quartz (Plate 4.1). The presence of serrated and embayed grain boundaries signifies that sub-grain rotation and grain boundary migration were both important deformation mechanisms during faulting. The high degree of strain recorded in the sample complicates differentiation between detrital and vein quartz. Specifically, it is impossible to discern whether the high aspect ratios are strictly attributable to dynamic recrystallization of detrital quartz or reflect the initial orientation of stretched vein fibers. Isotopically, the sample is enriched in $\delta^{18}O$ by 1.0 ‰ relative to its undeformed protolith.

Quartz deformed by sub-grain rotation and that annealed by grain boundary migration were non-luminescent. Likewise, larger, more concentric grains that showed undulose extinction and incipient sub-grain development also appeared dark under CL. However, isolated, fractured quartz grains from within the muscovite seams luminesced bright blue and, in some instances,

(a)

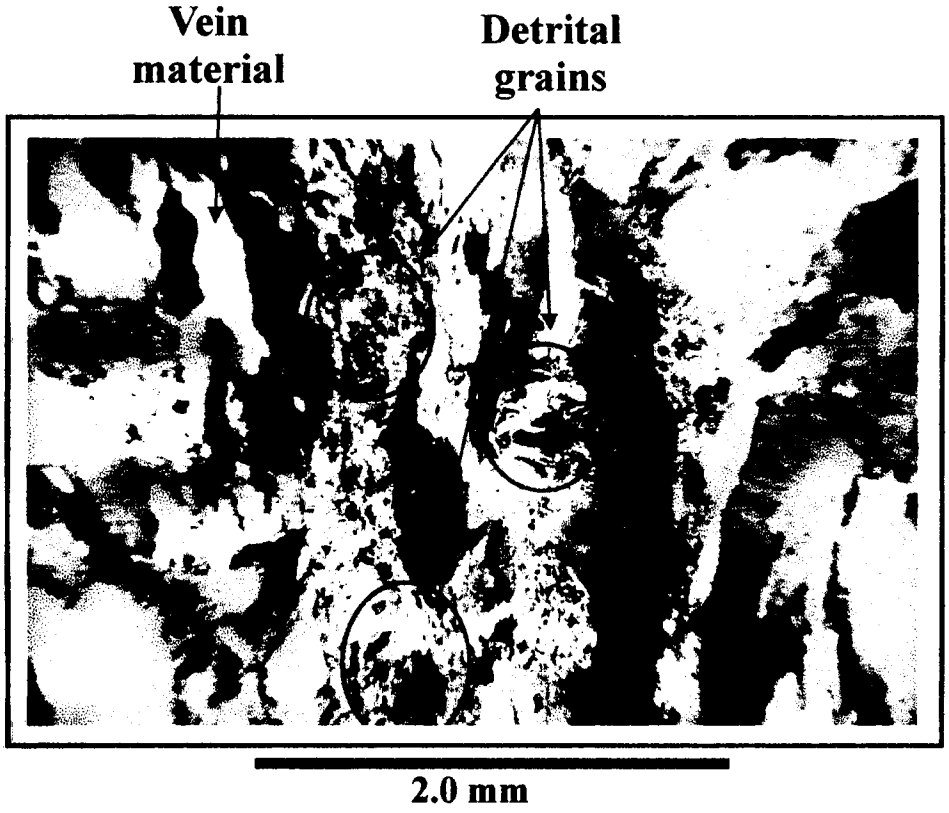

(b)

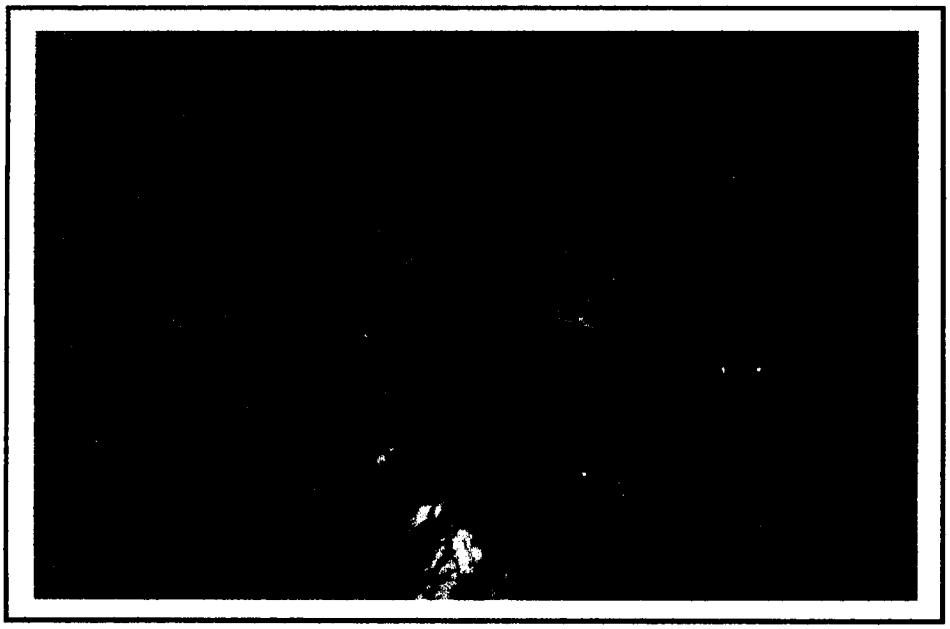

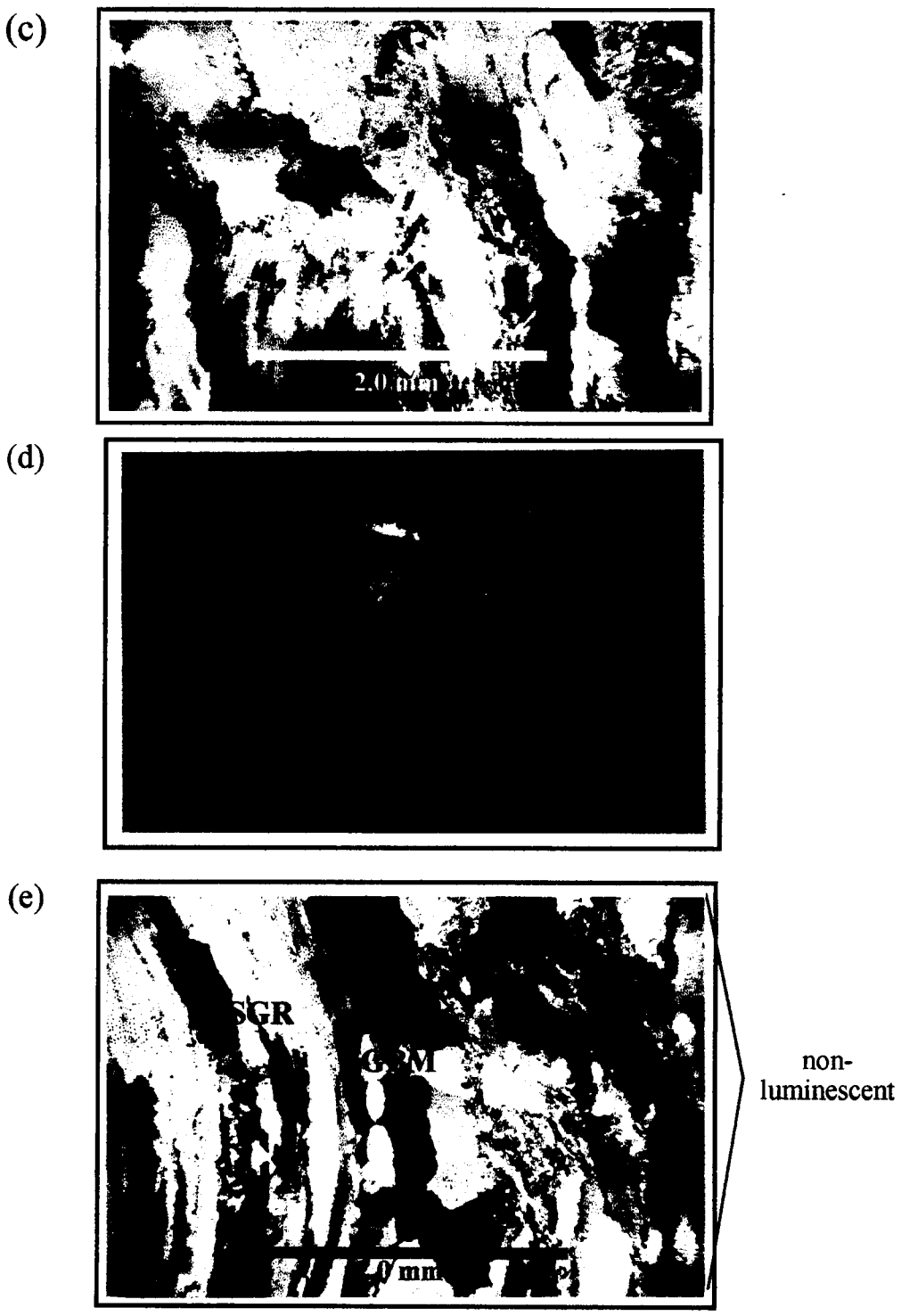

Plate 4.1: Sample 43-4A - Quartz tectonite from Quartz Creek Thrust. (a) - (d) Photomicrographs of sample under cross-polarized light and CL. Detrital quartz luminesces blue and yellow-orange, and deformed vein quartz appears dark under CL. (e) Elongate sub-grains (SGR), grains recrystallized by grain boundary rotation (GBR), and subhedral grains within vein material are non-luminescent.

bronze-yellow. The sharp contrast in CL between the two types of quartz implies that they originated from disparate sources. Because blue quartz generally evolves under amphibolite-grade conditions [*Sprunt et al.*, 1978], the luminescence observed within muscovite seams was probably inherited by detrital material from its source terrane. Although it might have been acquired from ion exchange with a hydrothermal fluid, the lack of zoning makes this unlikely. The yellow color is enigmatic, but probably reflects some type of complex trace element substitution [*G. Goles*, pers. comm.].

The non-luminescence observed within the elongate sub-grains is typical of vein quartz [*Shimamoto et al.*, 1991]. Had the grains evolved from relict detrital quartz, the high density of dislocations would not nullify, but rather homogenize luminescence throughout the strained material [*Dietrich and Grant*, 1985]. It is therefore likely that the high aspect ratios observed in the deformed grains are partially attributable to the original morphology of fibers within crack-seal veins. The small concentration of detrital quartz grains are localized within muscovite domains, which represent narrow conduits for fluids during deformation. The presence of these fluids was probably instrumental in promoting microcracking and pressure solution, as opposed to the plastic strain observed in quartz fibers elsewhere in the sample. Because isotope samples were obtained away from muscovite seams (and therefore detrital grains), the observed enrichment indicates that vein forming fluids were modestly out of equilibrium with their host rocks.

12-2C: Purcell Thrust Fault

Sample 12-2C belongs to a tightly folded, bedding-parallel calcite-quartz vein (Type 1) that was situated ~120 m into the lower plate of the Purcell Thrust (locality 9). Textures vary

from fibrous to blocky, and multiple dark seams define median sutures from which cracks propagated (Plate 4.2). Its oxygen isotope composition is similar to other calcite veins in the outcrop, but depleted by 1.4 ‰ relative to an adjacent wall rock.

Quartz, phyllosilicates, and opaque minerals were non-luminescent throughout the sample. Calcite from the wall rock matrix and the bulk of the vein material luminesce a reddish orange and are indistinguishable from each other under CL. However, a narrow 0.1 – 0.2 mm zone of comparatively bright luminescent calcite forms a halo around portions of the median suture. Although this occurs within blocky calcite where radial growth is expected, the brighter band is congruent with the shape of the suture indicative of crack-seal growth away from the center of the vein. Very fine, yellow luminescent grains are disseminated throughout the vein and probably represent apatite that was also observed under the scanning electron microscope.

Based on inferred similarities in Mn:Fe content between vein material and the adjacent matrix, the bulk of the vein appears to be locally derived; although, the encompassing matrix might also have been recrystallized during fluid infiltration along stylolite networks. The conspicuously bright orange halo around portions of the median suture records a transient pulse of fluid that possessed a higher Mn:Fe ratio. In addition, fibrous and subhedral calcite crystals grew outwards from central sutures and not radially within an open-space fracture.

36-1B: Breccia from unnamed fault (Trans-Canada Highway)

Dolomitic breccia from a bleached, one meter wide fault zone cross-cuts massive dolostones of Ordovician units in the Western Ranges (Plate 4.3-locality 12B). The sample is comprised of pods of undeformed matrix that are surrounded by randomly oriented veinlets and domains of brown, very fine-grained, comminuted dolomite. Narrow (< 1 mm wide) calcite-

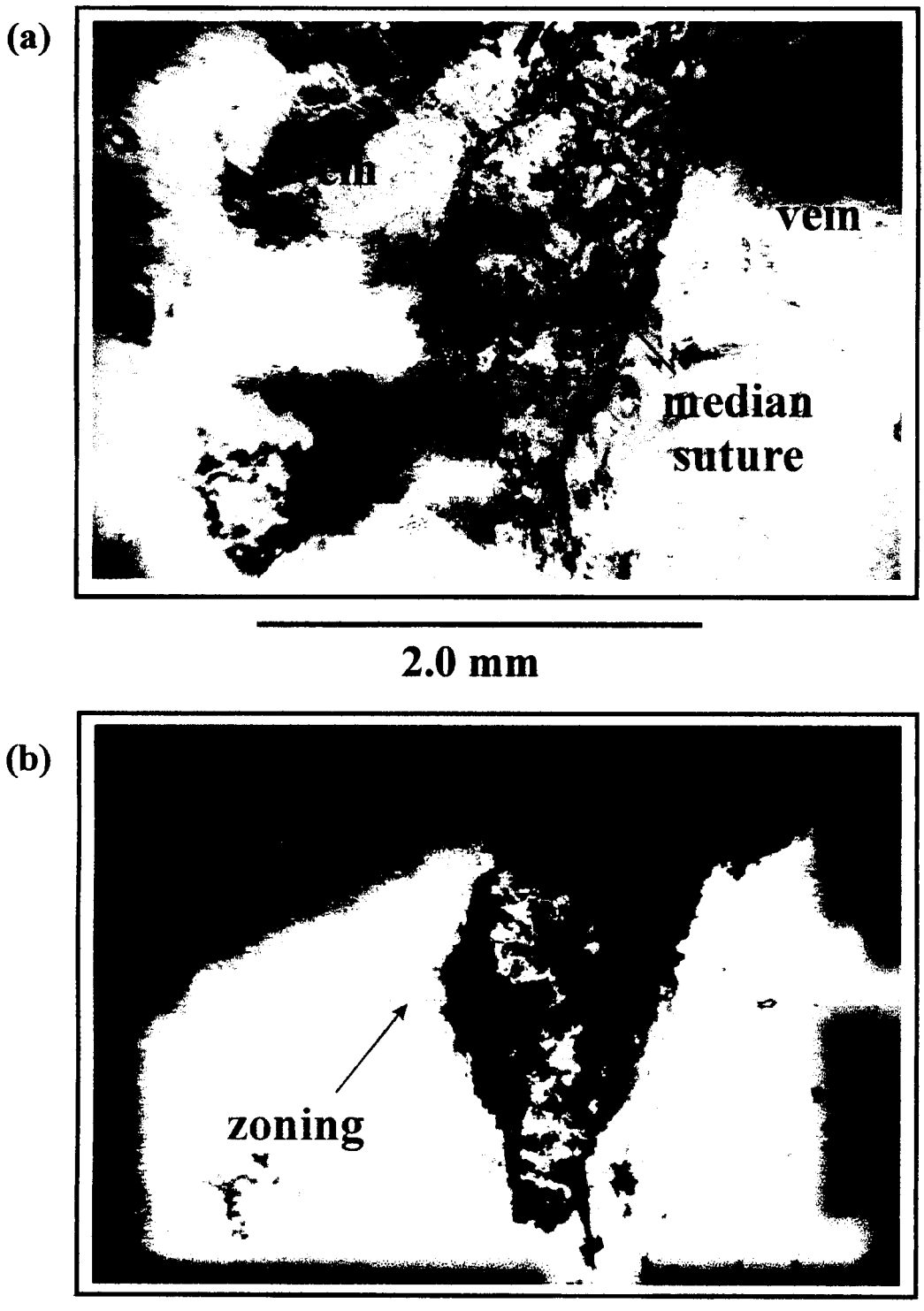

Plate 4.2: Sample 12-2C - Bedding-parallel calcite vein from footwall of Purcell Thrust. Microphotographs under cross-polarized light (a) and CL (b). A narrow zone of brightly luminescent material rims the contact between vein calcite and clay/chlorite laminae.

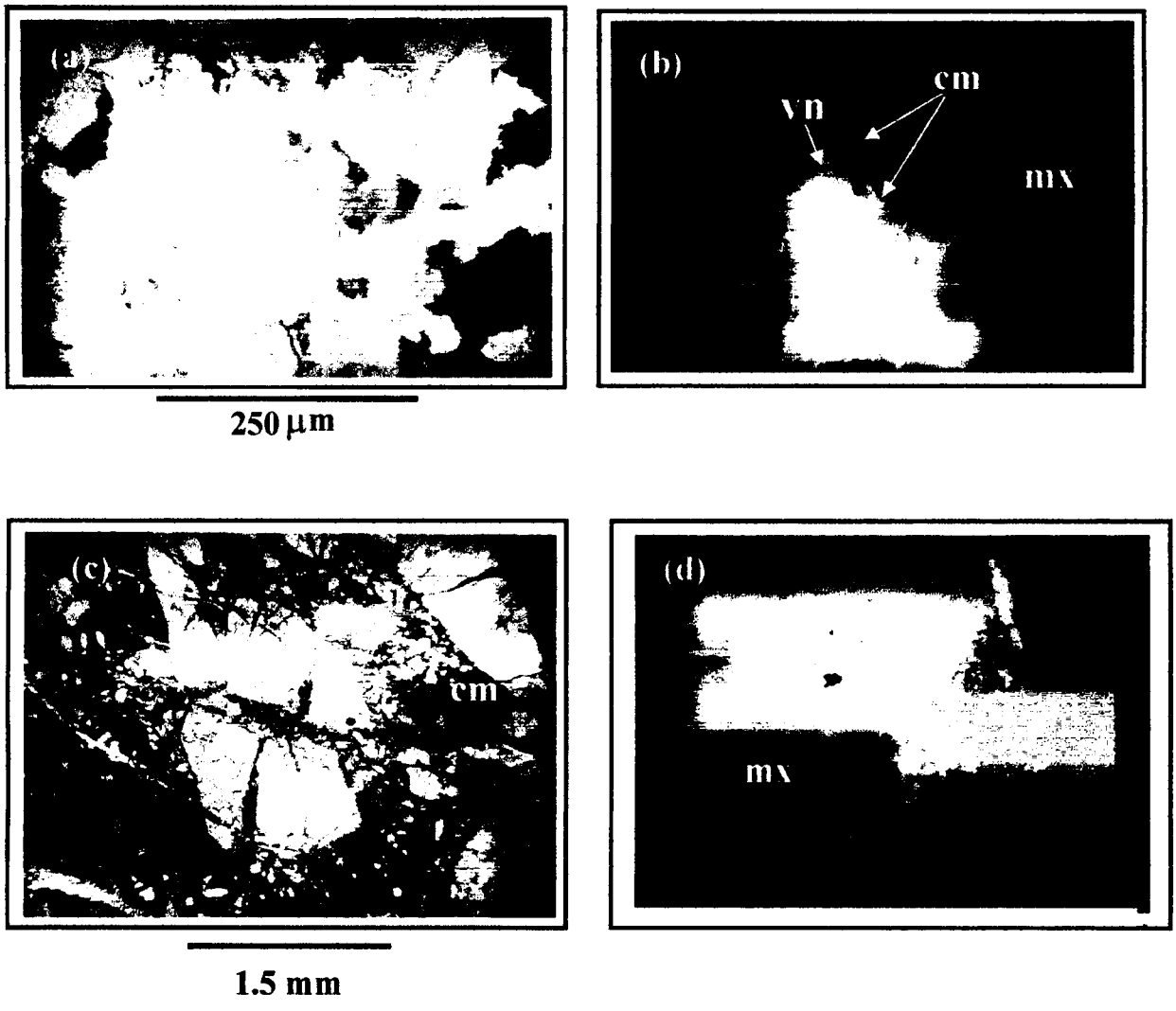

Plate 4.3: Sample 36-1B - Bleached, dolomite fault breccia from unnamed thrust in Western Ranges. Cross-polarized (left) and CL (right) microphotographs from densely veined matrix (mx) and comminuted material (cm). Bright orange veins (vn) are easily differentiated from protolith under CL and are oriented randomly throughout sample. (a) and (b) Grains within zone of reoriented, possibly comminuted material exhibit color variations under CL indicative of varying degrees of fluid interaction. Anomalous, bright yellow veins rim the zone, suggesting that a third, chemically differentiated fluid phase infiltrated the fault during cataclasis. (c) and (d) Pod of protolith material is cross-cut by a dolomite vein and surrounded by comminuted gouge. Vein and gouge luminesce brightly compared with darker red of lesser deformed matrix.

filled veinlets cross-cut all other features. The undeformed breccia luminesces dull red in sharp contrast to the bright orange that highlights numerous cross-cutting veinlets, many of which are not identifiable in plane light. The darker, comminuted material that infills wider fractures also appears much brighter under CL than its coarse grained host. A small population of discontinuous veinlets luminesce bright yellow, indicative of substitution by rare earth elements. Compared with the dolomite veinlets that they cross-cut, calcite veins have a subtle, dull green appearance, although the two are indistinguishable in photomicrographs.

Consistent with observations from stable isotope data, vein dolomite is chemically differentiated from its host matrix and was therefore derived from an external source. Fine-grained and possibly recrystallized gouge also contrasts sharply with undeformed dolomite. Thus, the same fluids that were responsible for producing spider veins were also involved in grain comminution, which likely progressed by a combination of mechanical abrasion and pressure solution. Rare, yellow luminescent veins signify a second, volumetrically minor fluid phase. Internal zoning was observed neither within brecciated material nor individual veinlets.

49-2A: Unnamed Fault at Mt. Moberly

Sample 49-2A was obtained from a diffuse, ~10 m wide zone of dolomitic breccia located 5-20 meters into lower plate dolostone of an overturned thrust fault (locality 12A). Like the breccia discussed above, it consists of undeformed pods of matrix material that are truncated by zones of brecciated dolomite and chaotically oriented veins (Plate 4.4). Narrow calcite veinlets cross-cut and offset all other features. Undeformed matrix luminesces dull red, while cross-cutting dolomite veinlets and darker brecciated material appear bright orange. Calcite veins luminesce yellow-orange. Clusters of primary dolomite grains which are nearly indistinguishable

from secondary dolomite in size and shape are easily identified by their darker appearance under CL. Therefore, brecciated grains underwent varying degrees of exchange with an exotic fluid that possessed a different Mn:Fe ratio than that of the protolith. Grains that were mechanically abraded retained their dull color, while those reduced by pressure solution inherited the bright luminescence exhibited within cross-cutting veinlets. Evidence for chemical zoning is absent within veinlets. Thus, CL indicates that only one fluid event was required for the formation of dolomite veinlets and the grain size reduction of matrix material. Isotope data confirms that the fluid responsible for producing dolomite veins was out of equilibrium with the undeformed wall rock, and also indicates that dolomite and overprinting calcite veins precipitated from compositionally distinct fluids.

29-1D: Unnamed fault at Kicking Horse River

Sample 29-1D was obtained from a 50 cm wide horizon of densely veined fault breccia, which is distinctively hard and resistant compared to surrounding limestone. Numerous mutually cross-cutting calcite veins and stylolites, which are oriented parallel and orthogonal to the main fabric, illustrate multiple fracture events (Plate 4.5-locality 13). Veins vary in width between 0.2 and 5 mm and are composed of blocky or fibrous calcite, dolomite, and trace amounts of very fine grained quartz. Disarticulated fragments of vein material grade into the fine grained matrix, indicative of cycling between brittle and ductile processes during cataclasis. Matrix calcite has undergone intense grain size reduction from 0.4 mm to less than 10 μm, and exhibits a shape preferred orientation parallel to local spaced cleavage.

CL reveals that veins precipitated from at least two chemically distinct fluids that were derived from sources external to the surrounding limestone. The least deformed matrix calcite

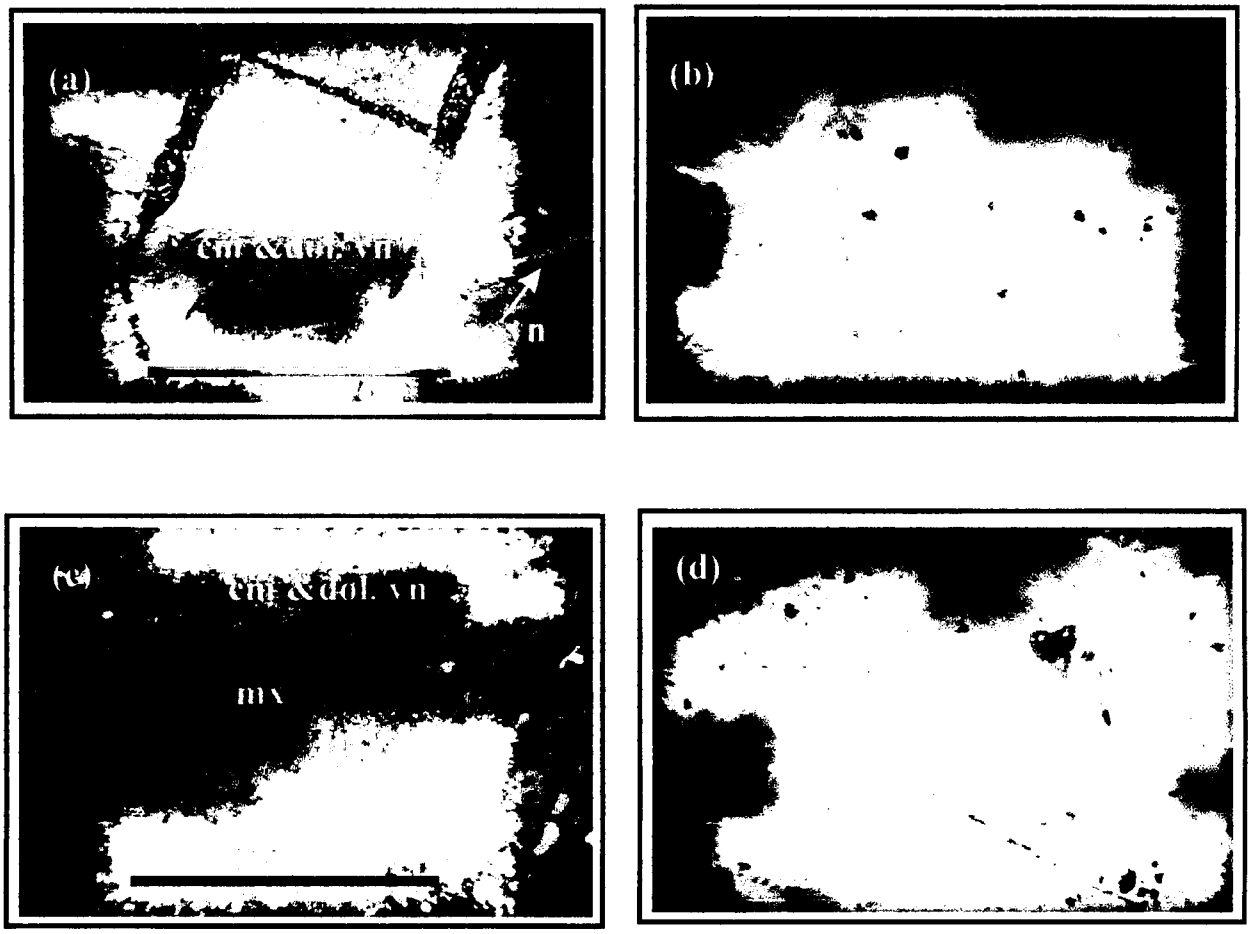

Plate 4.4: Sample 49-2A - Bleached, dolomite breccia from fault at Mt. Moberly. Scale bars = 2 mm. Cross-polar (left) and CL (right) microphotographs. Pods of mildly deformed protolith material (mx) are truncated by dolomite veins (dol vn) and brecciated material (cm), which are in turn cross-cut by calcite veins (cc vn).

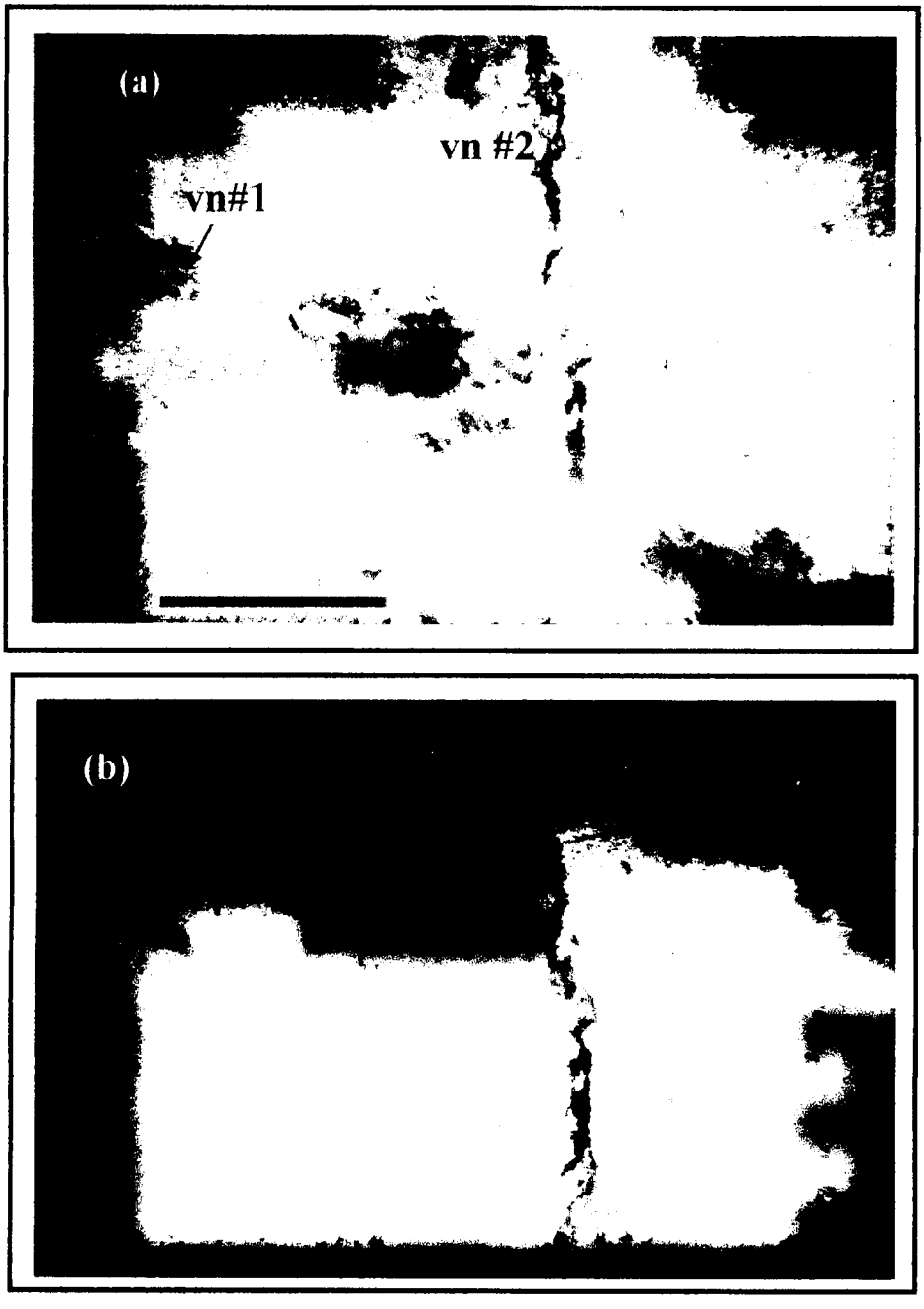

Plate 4.5: Sample 29-1D - Microphotographs of calcite cataclasite from unnamed fault in Western Ranges. Note difference in CL between comminuted matrix (cm) and early and later stage veins. Scale bar is 1.0 mm.

luminesces bright reddish orange with traces of yellow that represent apatite grains. Pods of very fine grained, comminuted calcite also luminesce bright orange, although their intensity is subdued compared with coarser grained calcite. Cleavage-parallel, syntaxial veins appear orange under CL, but are conspicuously duller than matrix material. Blocky veinlets, which cross-cut these at 90° but are themselves truncated by stylolites, exhibit dull red, low intensity CL. A larger, ~ 4 mm wide vein is rimmed at each margin by dark material, but cored by brightly luminescent calcite similar to that in the protolith.

In contrast to previously discussed samples of breccia, this example reflects infiltration by fluids probably bearing a lower Mn:Fe ratio (i.e., darker luminescing) than that possessed by the wall rock. Subtle color variations between the protolith and comminuted material demonstrates the contribution of fluids, probably by pressure solution, to grain size reduction during cataclasis. Two vein sets precipitated from chemically distinct fluids, which had at least partially sampled a reservoir exotic to local wall rocks. A final pulse of locally sourced fluid is represented by a blocky, cross-cutting vein that luminesces similar to matrix calcite. The same vein exhibits growth zoning at its contact with the host matrix. As in the prior two samples, both veins and brecciated matrix show modest depletions in $\delta^{18}O$ relative to the undeformed protolith.

4.5 Summary

Observations of quartz under optical CL only resulted in minor success, due to the limited capabilities of the Luminoscope. However, blue luminescent detrital grains were easily distinguishable from non-luminescent, deformed vein fibers within a tectonite from the Quartz Creek Thrust. Carbonates from the Western Ranges exhibited a wide range of colors from dull red to bright orange and yellow and therefore contain variable concentrations of Mn, Fe, and rare

earth elements. Isolated evidence of growth zoning in veins was present in only two samples, which showed crystal growth orthogonal to a median suture and a lens of brecciated calcite. The CL properties of veins in cataclasites from the Western Ranges suggest that chemically distinct fluids infiltrated fault zones during as many as three pulses, and some fluids were siphoned from sources exotic to the surrounding lime/dolostone matrix. Finally, color contrasts between minimally deformed protolith and comminuted breccia indicate that these same exotic fluids were partially responsible for grain size reduction, probably by pressure solution, during cataclasis. These observations are consistent with $\delta^{18}O$ data that demonstrate different values for veins, brecciated matrix, and undeformed protolith.

CHAPTER 5

STABLE ISOTOPE SYSTEMATICS IN THE WESTERN MAIN RANGES

5.1 Introduction

Oxygen and carbon isotope data from wall rocks, syn-kinematic veins, and thrust faults in the western Main Ranges elucidate fluid regimes east of the Porcupine Creek Anticlinorium and present a basis for comparison with similar rock types in the Western Ranges. In total, 33 analyses, including 14 wall rocks and 19 veins, were obtained from five localities in the vicinity of Field, BC within Yoho National Park (Figures 5.1 and 5.2). The outcrops are spread across ~5 km of strike and contained within 75 km^2. Most occur within the Middle Cambrian Chancellor Group and correlative platform carbonates to the east. The primary objectives for this portion of the transect were to: (i) compare whole rock compositions with typical, unaltered signatures from carbonate rocks of similar age; (ii) compare isotope values between veins and wall rocks to assess the importance of structurally controlled infiltration of exotic fluids; and (iii) compare and contrast data in the Main Ranges with that from the Western Ranges. Previous geochemical work in the region includes the extensive study of fluid regimes in the southern Canadian Cordillera by *Nesbitt and Muehlenbachs* [1994, 1995] and *Yao and Demicco's* [1997] investigation of a dolomite front within the platform carbonate succession. Neither of these addressed vein-wall rock relationships at the centimeter to meter scale and their implication for fluid transport during Mesozoic deformation.

5.2 Regional geology and sample localities

The western Main Ranges comprise the northeastern limb of the Porcupine Creek Anticlinorium (PCA), a prominant fan structure that plunges gently southeastward and extends more than 250 km along strike [*Lickorish*, 1993]. Bedding, cleavage, faults, and folds are steeply overturned on both flanks of the PCA, although to a greater degree in the southwest. As in the Western Ranges, faults in the western Main Ranges accommodate only a minor amount of shortening, with strain mainly partitioned into spaced cleavage, centimeter-scale crenulations, and broad folds [*Cook*, 1975]. With increasing distance east of the core of the PCA and throughout most of the study area, bedding is predominantly homoclinal and dips towards the southwest.

Balkwill [1969] interpreted the Main Ranges as a vast thrust sheet that was carried passively eastward by the Simpson Pass Thrust, which cuts through Proterozoic strata of the Miette Group. Progressive contraction resulted in minor thrust faulting, the formation of steep, slaty cleavage, parasatic folding, and the subsequent tightening and overturning of structural fabrics. Observations of deeper horizons in the north convinced *Lickorish* [1993] that deformation in the PCA gradually shifted from south to north and progressed above a series of detachments that tranferred strain to deeper levels in the crust. In this manner, deformation propagated farther eastward towards the foreland, and *Lickorish* [1993] postulated that the basal detachment at the latitude of this study is situated near the lower contact between the slate-dominated Chancellor Group and quartzite of the Gog Group (Figure 5.2).

Based on restored cross-sections from the Dogtooth and Western Ranges, *Kubli and Simony* [1994] speculate that the Martin Creek Thrust, which crops out in the Main Ranges, might represent such a detachment. They also propose that the Martin Creek Thrust is the most

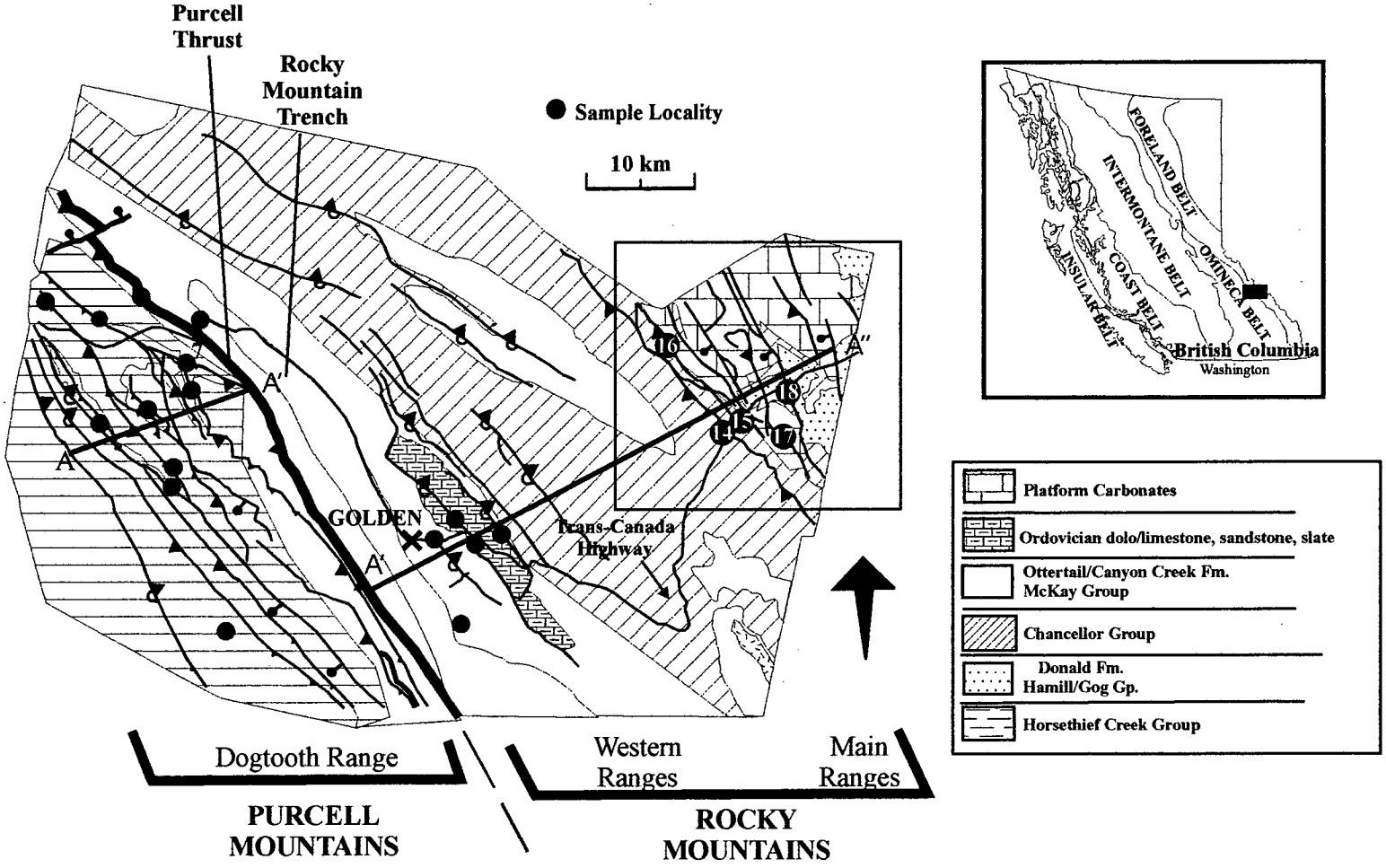

Figure 5.1: Regional map of study area, including sample locations denoted by solid circles. Numbers correspond to localities referenced in text. Modified from *Price and Simony* [1971].

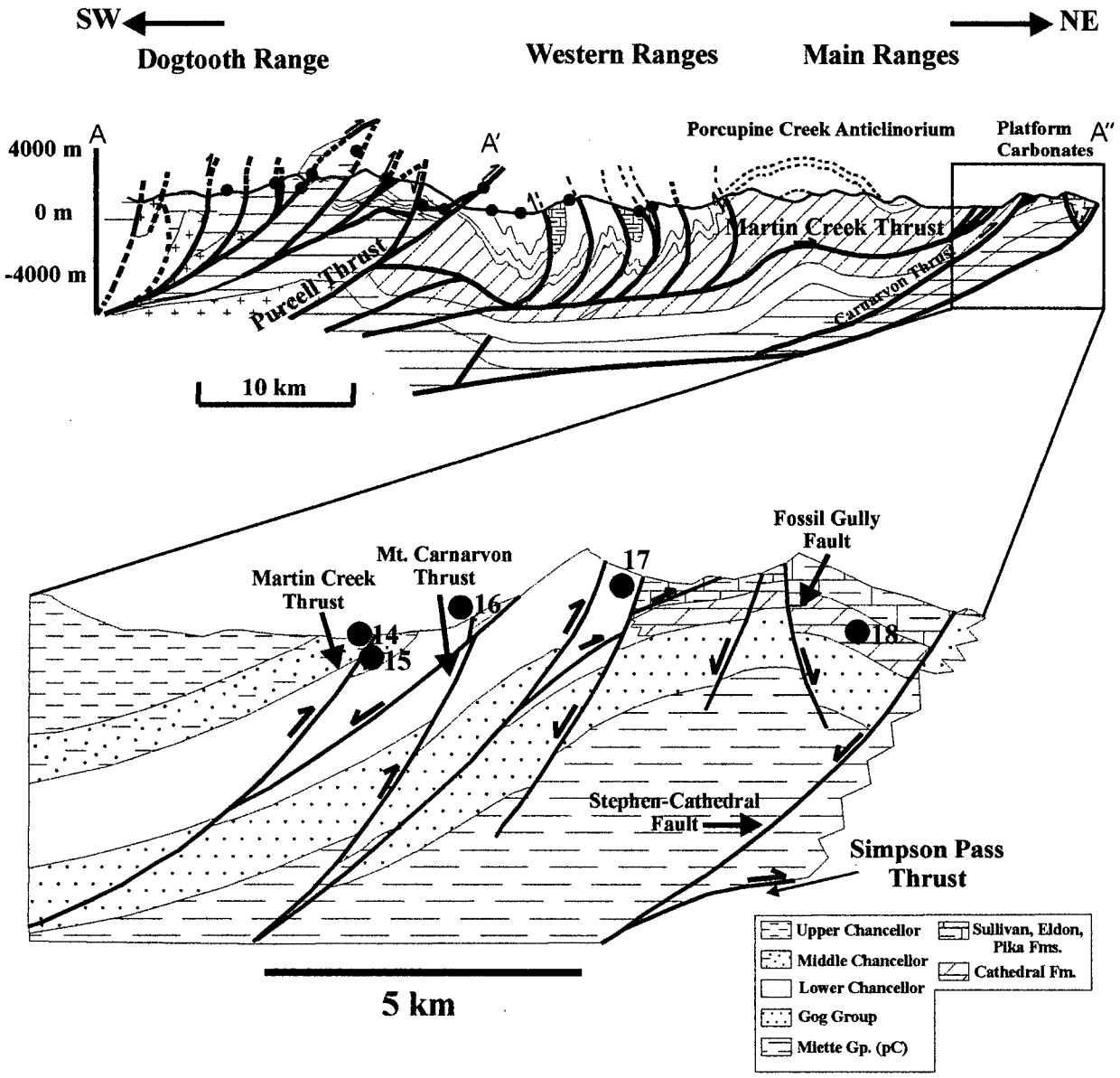

Figure 5.2: Simplified cross-section of the northern Purcell and western Rocky Mountains. Modified from *Kubli* [1990], *Kubli and Simony* [1994], *Price and Simony* [1971], *Balkwill* [1969], and *Cook* [1975]. Detail of eastern transect after *Cook* [1975].

likely candidate for the eroded roof thrust of the Dogtooth Duplex. Because of its structural significance, I sampled veins and wall rocks at and immediately adjacent to the Martin Creek Thrust at two localities (14 and 15 in Figure 5.1). Apparent offset along the fault in the area of sampling is on the order of 100's of meters. However, *Cook* [1975] argued that the true magnitude of reverse slip was probably closer to the 6 km observed north of the transect, but has been masked by subsequent normal displacement. The Mt. Carnarvon Thrust cuts up-section through Cambrian strata in the footwall of the Martin Creek Thrust and represents the only other regionally extensive reverse fault in the study area. It exhibits minor displacement (<1000 m) and is either a splay off the Martin Creek Thrust or a separate, parallel detachment that penetrates the Gog quartzite at depth [*Cook*, 1975]. A laminated, thrust-parallel quartz-calcite vein was sampled along the south ridge of Mt. Carnarvon (16) at the fault contact.

Sampling at two other localities (17 and 18) focussed on the facies change between basinal slates of the Chancellor Group and their correlative platform units with the goal of identifying possible fluid channeling either parallel or transverse to the contact. Isotope analyses were conducted on distinct generations of veins located within massive dolomite at the Monarch Mine, a Mississippi Valley - type (MVT) deposit (18). *Yao and Demicco* [1997] and *Nesbitt and Muehlenbachs* [1995] concluded that the Pb-Zn ore body and the dolomite itself precipitated during large-scale fluid transport that occurred prior to Mesozoic tectonism and possibly as early as Silurian-Devonian time. However, pervasive tension gashes near the mine indicate that at least one vein set formed during contraction-related folding or shearing and was not contemporaeneous with the earlier, structurally passive flow event (see section 5.3 for detailed vein descriptions).

Most samples were hosted within the Lower and Middle Chancellor formations (mC – uC), which comprise approximately 1900 meters of section [*Stewart*, 1989] and unconformably overlie the quartzite-dominated Gog Group (Figure 5.3). The Gog Group is a laterally extensive assemblage that is correlative and lithologically similar to the Lower Cambrian Hamill Group in the Dogtooth Range to the west. The Chancellor Group, which has been eroded in the Dogtooth Range and is unexposed in the Western Ranges, represents a voluminous isotopic reservoir in the western Main Ranges. Deposited in a submarine fan-carbonate ramp setting, the Lower and Middle Chancellor are the fine-grained, basinal equivalent of seven units that formed within a passive carbonate platform. In general, the Chancellor is a heterogeneous assemblage of massive, terrigenous mudstone with a variably calcareous matrix; argillaceous limestone; ribbon ("flaggy") limestone and dolomite; interbedded, nodular limestone; and laminated shale [*Stewart*, 1989]. Where sampled, metapelites contain at least 50 % calcite matrix with laminations defined by variable concentrations of muscovite and calcite. Cleavage is pervasive and defined by parallel grains of muscovite and chlorite, elongate calcite, and graphite seams or occurs as a spaced fracture cleavage in more competent, micritic horizons.

Compared with the Upper Cambrian McKay Group discussed in Chapter 2, the remobilization of calcite and quartz is more conspicous in Chancellor rocks and manifested as prominant stylolite networks that are lined with phyllosilicates and elongate quartz grains, and quartz-filled pressure shadows that exhibit both face- and displacement-controlled crystal growth [*Passchier and Trouw*, 1996, p. 145]. *Gardner et al.* [1976] used mesoscopic strain markers to estimate a 20 % volume decrease in slate, limestone, and veins from the upper Chancellor during cleavage and stylolite development. Fluid flow, at least at the cm-scale, was likely an important catalyst for mass transport during bulk shortening.

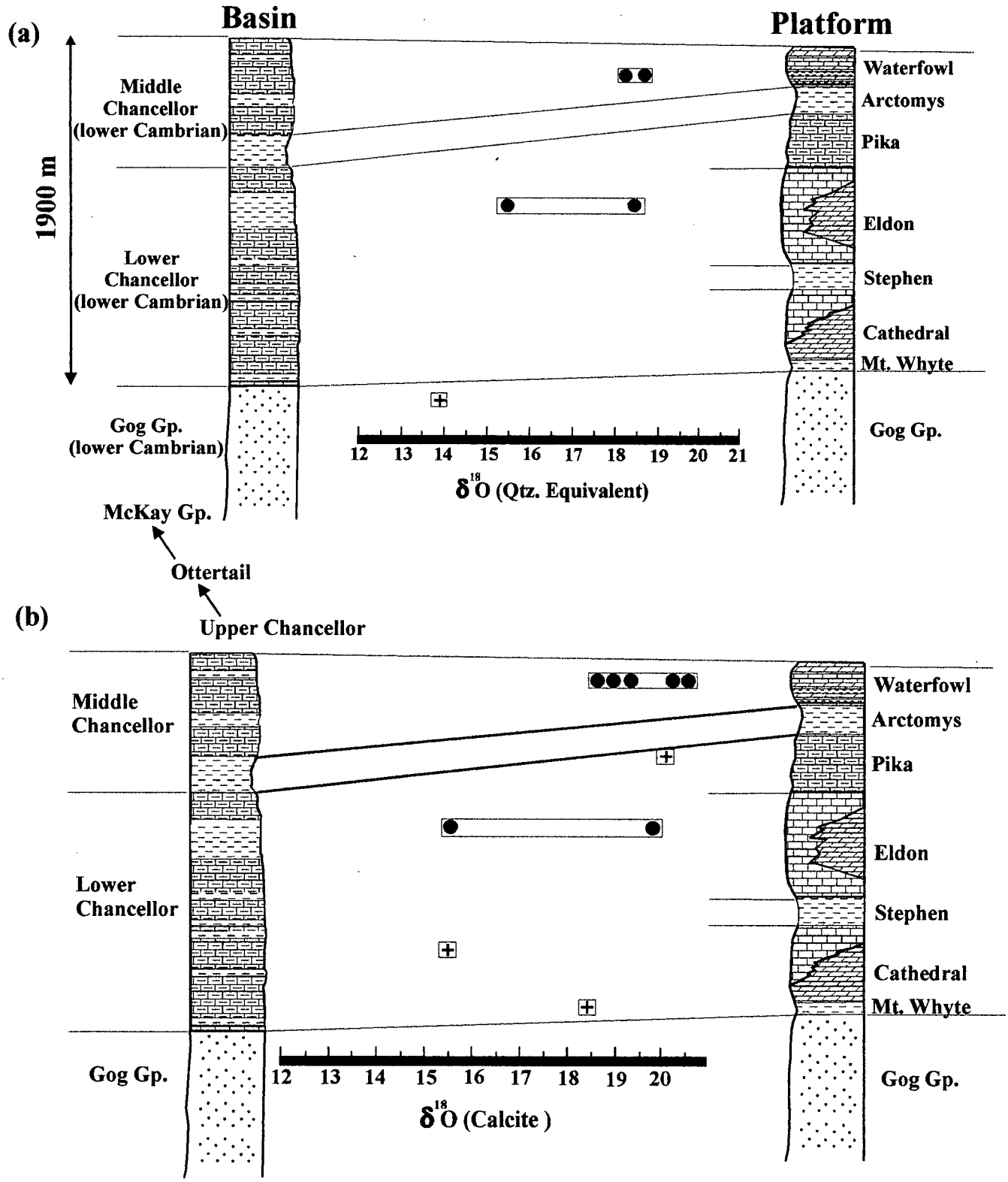

Figure 5.3: Distribution of wall rock $\delta^{18}O$ by statigraphic unit. + = platform units and ● = basinal units. (a) and (b) illustrate silicate and carbonate compositions, respectively. Note asystematic relationship between age and composition. Section modified from *Cook* [1975].

Based on P-T estimates for the Hamill (≈ Gog) Group [*Kubli*, 1990], Chancellor units were buried to depths no greater than ten kilometers. Metamorphism in the western Main Ranges did not exceed the chlorite grade of the greenschist facies. *Gardner* [1977] also noted that the presence of the quartz-calcite-paragonite assemblage suggests that "CO_2 was a significant component of the gas phase during metamorphism".

5.3 The geometry and timing of veins

Syn-tectonic veins vary widely in their geometry and texture and testify to fluctuations in local principle stress orientations and the rheology of host rocks. Compared with the Western Ranges, zones of relatively high vein density (> 5 % outcrop area) are less common in the Main Ranges and tend to concentrate near regional thrust faults, at outcrops with numerous meter-scale faults, or in areas where cleavage has been broadly folded and disturbed. Within most sample localities, wall rocks are generally homogeneous in their composition and hence rheology. However, different types of anisotropy that clearly affected the geometry and dilation direction of veins, in order of significance, include: cleavage planes, fault planes, fold hinges, and bedding contacts in massive carbonates. Veins are composed of calcite ± quartz ± dolomite ± chlorite ± pyrite. Five distinct generations of syn-kinematic veins were observed and are presented below (Plate 5.1). In addition, a coarse grained, idiomorphic, and presumably pre-tectonic quartz vein that was taken from the ore zone of the Monarch Mine and analyzed for $\delta^{18}O$ and $\delta^{13}C$ is briefy described.

Type 1: Pyrite pressure shadows

Quartz-filled strain fringes commonly mantle euhedral (45-3B and 31-2D), framboidal (25-2M), and smeared (25-2D) pyrite crystals within calcareous slates. They extend as far as 1

cm from the host grain and are frequently connected to stylolites, which probably functioned as conduits that supplied silica-rich fluids to the dilation site. They are more commonly elliptical than sigmoidal in shape, and therefore exhibit minimal non-coaxial shear strain based on the criteria of *Passchier and Trouw* [1996, p.145]. Their relative timing is ambiguous with respect to neighboring veins. However, the wide radius (~ 1 cm) and substantial curvature within a cleavage-parallel, symmetrical fringe (25-2M) that formed around a framboid testifies that some formed during progressive shear strain along cleavage planes.

Type 2: Sigmoidal tension gashes

These were documented in a faulted outcrop of middle Chancellor micrite and calcareous slate near the trace of the Martin Creek Thrust (15) and in massive dolomite from the Cathedral Formation at Monarch Mine (18). At the Chancellor outcrop, 1 - 8 cm wide calcite + quartz ± pyrite veins developed in the immediate hanging wall of meter-scale, northeast verging thrust faults. At the fault contact, they are congruent with the overturned limbs of surrounding drag folds and sheared into parallelism with fault-bounding veins. Many Type 2 veins incorporate angular wall rock fragments and possess a blocky texture. Their truncation by fault-bounding veins and spatial association with thrust faults suggests that they formed during the initiation of faulting, perhaps in conjunction with fold propagation in the hanging wall.

At the Monarch Mine, Type 2 veins are 0.2 - 3 cm wide and consist of quartz + dolomite (Plate 5.1(a)). They are offset by bedding-parallel veins and shallow slip planes between dolomite beds and consistently exhibit a dextral, top to the northwest sense of shear (i.e. oblique to northeast-vergent thrusts in the area) . Texturally, they possess coarse grained (up to 8 mm in diameter), subhedral crystals with grain diameter decreasing to 0.4 mm near the margins,

indicating slower crystal growth towards the core of the vein. Because they record displacement that is oblique to the regional strain field, and their host dolomite is broadly folded about a NE-SW axis, these veins probably precipitated during an early stage of tectonism, perhaps with the intiation of megascopic folding (e.g., *Ramsay and Huber*, 1987, p. 431).

Type 3: Bedding-parallel veins

In faintly foliated micritic rocks of the middle Chancellor unit, 5 mm wide calcite ± quartz veins form low amplitude (~ 5 mm) ptygmatic folds (Plate 5.1(b)). Veins are rimmed by a 2 mm wide zone of intense dissolution, which is represented by dense, cleavage-parallel graphite seams that are most abundant within fold hinges. Calcite is fibrous, orthogonal to vein walls, and truncated along median sutures that are filled with opaque minerals (possibly graphite) and typical of crack-seal veins. Although Type 3 veins have been offset and dissolved along dissolution seams, small apophesies branch off from the core vein into parallelism with clevage. Vein material therefore continued to precipitate after the initiation of cleavage.

At the Monarch Mine, rare bedding-parallel veins are planar, up to 3 cm wide, and filled with dolomite and quartz. They develop between thick (~ 1-2 m) dolomite beds and probably precipitated in conjunction with elevated pore fluid pressure along bedding contacts. In thin section, dolomite is variably fibrous and blocky and oriented both parallel and perpendicular to vein walls. Furthermore, opaque dissolution seams are oriented at random angles to calcite and lined with fine-grained quartz. Vein quartz is subhedral and exhibits minimal strain, but contains numerous dolomite-filled fractures. Type 3 veins at this outcrop therefore underwent a complex dilational history that involved at least two fluid events.

Type 4: Cleavage-parallel veins

These were the most common vein type observed in the western Main Ranges and were documented at most sample localities. They are subdivided into boudinaged and chlorite-bearing veins. Variably distended calcite + quartz veins are up to 25 cm wide and exhibit an increase in thickness by as much as 500 % from neck to boudin. They are usually vertical and cross-cut horizontal stylolites and fold hinges. The thicker segments of some veins are faintly sigmoidal. This suggests that they formed during protracted shear along fracture cleavage, and "boudins", in some instances, are dilational jogs along slip planes. In other veins, quartz and calcite fibers are orthogonal to the vein wall in boudins and parallel to cleavage in necks, indicative of a two-stage dilational history with extension in opposite directions (see *Gardner's* [1977] description of similar veins in the Blaeberry Creek area). In sample 25-2J, spectacular 0.5 mm wide, antitaxial quartz + muscovite veinlets propagate off the core vein at an oblique angle and signify a later, syn-tectonic phase of silica infiltration (Plate 5.1(e)).

Conspicuous, ~ 2.5 m thick zones of green, crenulated phyllite in the lower Chancellor unit (17) host a high concentration of quartz + calcite ± chlorite veins. Veins which are oriented parallel to cleavage, cross-cut cleavage, and form en echelon arrays are often interconnected and in some cases posses slickensides that record shearing with the host rock (Plate 5.1(d)). They range between < 1 cm and 13 cm wide and occupy sequences in which cleavage is broadly folded. Their resemblance to the chlorite bearing veins from chloritized zones in the Dogtooth Range is noteworthy (see Section 2.2). All minerals have a blocky texture with a distinct lack of texural zoning. Massive chlorite is probably metasomatized fragments of wall rock that have been entrained within the vein. The unusual mineralogy and sigmoidal geometry of some veins indicates formation under non-coaxial shear that was localized within a narrow zone.

Connectivity between cleavage-parallel and cross-cutting sigmoidal veins illustrates that local shear stress and fabric anisotropy were competing factors in determining vein geometry.

Type 5: Fault-parallel veins

These cross-cut all other vein types and represent the most recent phase of syn-kinematic fluid infiltration. Where they coincide with the contact of meter-scale reverse faults, Type 5 veins are up to 8 cm wide and consist of quartz and calcite (Plate 5.1(f) and (g)). Texturally, they are generally blocky with coarse grained ($\geq$ 4 mm) material that exhibits moderate strain evident as incipient sub-grain rotation at contacts between quartz grains. At their margins, they radiate into the surrounding wall rock along cleavage planes and form fibrous, antitaxial veinlets that are interspersed with domains of muscovite and graphite.

At the Martin Creek Thrust on Mt. Burgess (14), an extensive quartz + calcite ± prehnite vein (31-2E) delineates the contact between siliceous phyllite and micrite of the lower and middle Chancellor units, respectively. The vein varies in width between 12 and 24 cm and anastomoses across and sub-parallel to the local foliation (145/78 SW). Over its strike length of at least 100 m, it splinters into smaller veinlets that cross-cut cleavage. It is a mosaic of entrained wall rock fragments, plastically deformed anhedral quartz, and fractured, overprinting calcite. Quartz grains are coarse ($\geq$ 3 mm) and possesses elongate sub-grains and deformation lamellae oriented parallel to cleavage. Host rock fragments are rimmed and internally replaced with prehnite, probably formed as a reaction halo between vein forming fluids and wall rock slate. Despite the poor exposure of distinct, fault-related fabrics, I propose a syn-kinematic evolution for this vein based upon the relatively intense intragranular strain that it possesses, its coincidence with cleavage, and its association with veinlets that cross-cut cleavage.

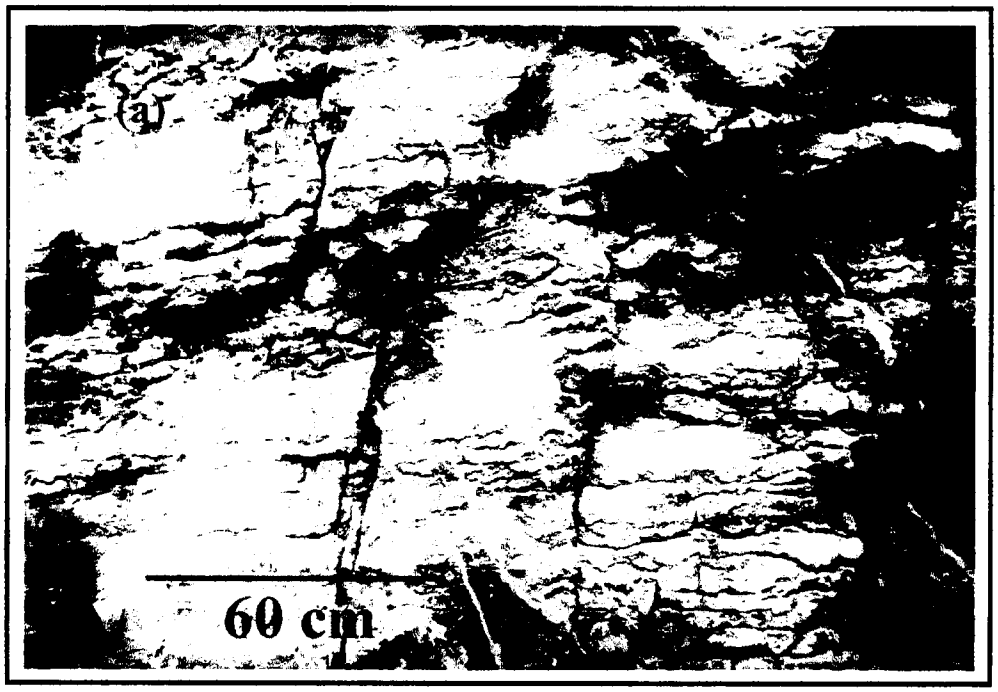

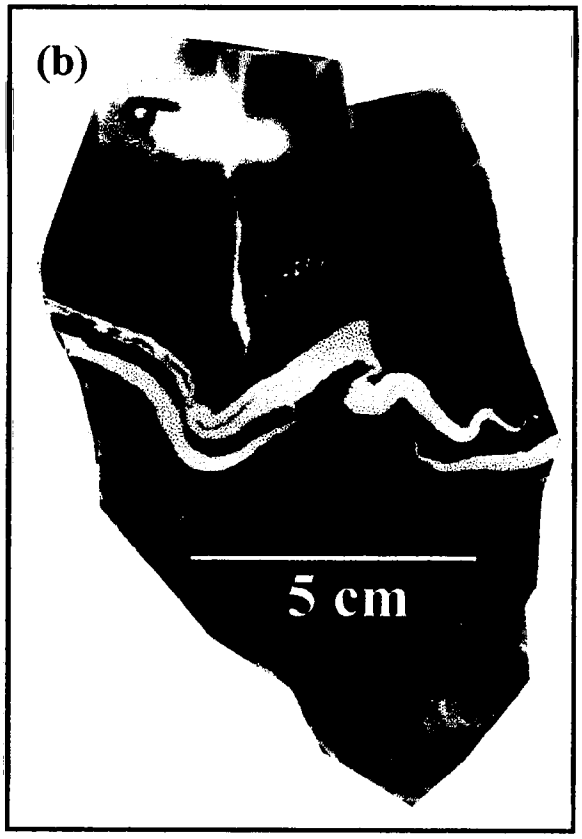

Plate 5.1 : Typical vein morphologies and textures in the Main Ranges. (a) Type 2 - Quartz-dolomite tension gashes (38-2C) in the Cathedral Formation near the Monarch Mine. (b) Type 3 - Bedding-parallel vein (25-2A) from the middle Chancellor unit. Limbs of vein are truncated by dissolution seams.

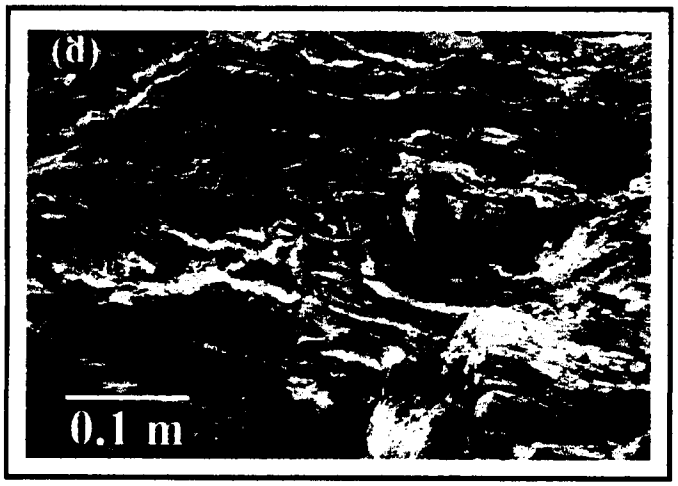

Plate 5.1 (con't): (c) Type 4 - Cleavage-parallel veins that are localized within folded slates of the middle Chancellor unit. (d) Type 4 - Folded, cleavage-parallel veins near the facies transition between lower Chancellor phyllite and the Eldon limestone (46-2A). Veins are composed of quartz, calcite, and chlorite. (e) Antitaxial quartz veinlet that extends from a distended, cleavage-parallel vein (25-2J). The veinlet is oriented oblique to bedding and fabric.

Plate 5.1 (con't): (f) Type 5 - Fault-parallel quartz-calcite vein at local thrust fault in the middle Chancellor unit (44-4B). Note absence of veins within footwall and hanging wall. (G) Photomicrograph (cross-nicols) of a laminated, fault parallel vein at the Carnarvon Thrust (45-2B). Quartz fibers are kinked and show evidence of sub-grain rotation. Calcite is blocky and replaced with quartz.

Ore zone vein

A single quartz + dolomite vein was collected from a shaft entrance at the Monarch Mine. The shaft itself was inaccessible but possessed a high vein density (≤ 90 %), and possibly formed part of the ore-matrix breccia associated with solution collapse and related fracturing [e.g., *Leach and Sangster*, 1993]. The sampled vein is ~ 3 cm wide and belongs to a chaotically oriented array of fractures that bound the main breccia zone. It is primarily composed of euhedral quartz crystals that are up to 5 mm in diameter and exhibits very minor intragranular strain as orthogonal microfractures and sweeping extinction. Vein dolomite is subhedral, sparsely twinned, and in apparent textural equilibrium with the quartz. These textures, which are unique among veins sampled at the outcrop and within the study area, attest to a comparatively slow rate of crystallization within an open fracture.

5.4 Results of stable isotope analysis

5.4.1 Analytical methods and reporting of data

The analytical and sampling techniques for rocks in the Main Ranges are identical to those described in Chapter 2. All powders were analyzed at the Queen's University Geochemistry Lab. Of 33 oxygen analyses, 16 were performed on silicates and the remaining 17 on carbonates. Most of the silicate analyses were taken from samples of vein quartz, with only four from fine grained pelites. The same methodology used to calculate the uncertainty involved in normalizing whole rock values to those of quartz in Chapter 2 yielded a maximum uncertainty of ± 0.7 ‰ (31-2B). Only two samples exhibited uncertainties that were above ± 0.5 ‰ (Table 5.1). Again, the designation "qtz. equivalent" is attached to values that have been normalized to quartz. Results are tabulated in Appendix A.

Table 5.1: Predicted uncertainties for converting whole rock $\delta^{18}O$ into quartz equivalent values.

Sample	Mineral Mode (+/- permil)	Temperature (+/- permil)	Fractionation Factor (+/- permil)
31-2D-WR	0.2	**0.6**	<0.1
31-2B-WR	**0.7**	0.4	**0.4**
25-3A-WR	0.4	0.1	<0.1
47-1A-WR	0.3	0.1	0.1

Each column shows uncertainties associated with three separate input variables. In most cases, mineral mode was visually estimated (see section 2.5.2 for details). Temperatures were varied between 300°C and 400°C, and fractionation factors from *Zheng* [1993] are compared with those from *Clayton and Kieffer* [1991; quartz-albite], *Wenner and Taylor* [1971;quartz-chlorite], and *Chacko et al.* [1996; quartz-muscovite].

5.4.2 Distribution of wall rock $\delta^{18}O$

Compared with signatures in the Dogtooth and Western Ranges, the oxygen composition of wall rocks in the Main Ranges is heterogeneous both within and across outcrops. Furthermore, no correlation exists between wall rock $\delta^{18}O$ and stratigraphic or structural horizon. Calcareous slate and micrite from the lower and middle Chancellor units possess carbonate signatures that range from 15.6 ‰ to 20.7 ‰ with an average composition of 19.2 ‰ (Table 5.2). Only three carbonates were analyzed from the equivalent platform succession, but these also reflect a wide variance in $\delta^{18}O$: 15.5 ‰, 18.5 ‰, and 20.1 ‰. The low value was obtained from a secondary dolomite in the Cathedral formation (18) and therefore signifies anomalously low $\delta^{18}O$, dolomitizing fluids that pre-dated Mesozoic contraction. Figure 5.3 demonstrates no correlation between stratigraphic horizon (i.e. age) and oxygen signature, and Figure 5.4 illustrates no systematic change with lateral distance across structural strike. This inconsistency in oxygen values is evident across relatively local (10's of meters) as well as regional scales. Five wall rocks obtained from a 100 m wide outcrop in the middle Chancellor unit (15) vary from 19.0 ‰ to 20.6 ‰ (Figure 5.5). By comparison, the maximum spread between any two samples at an

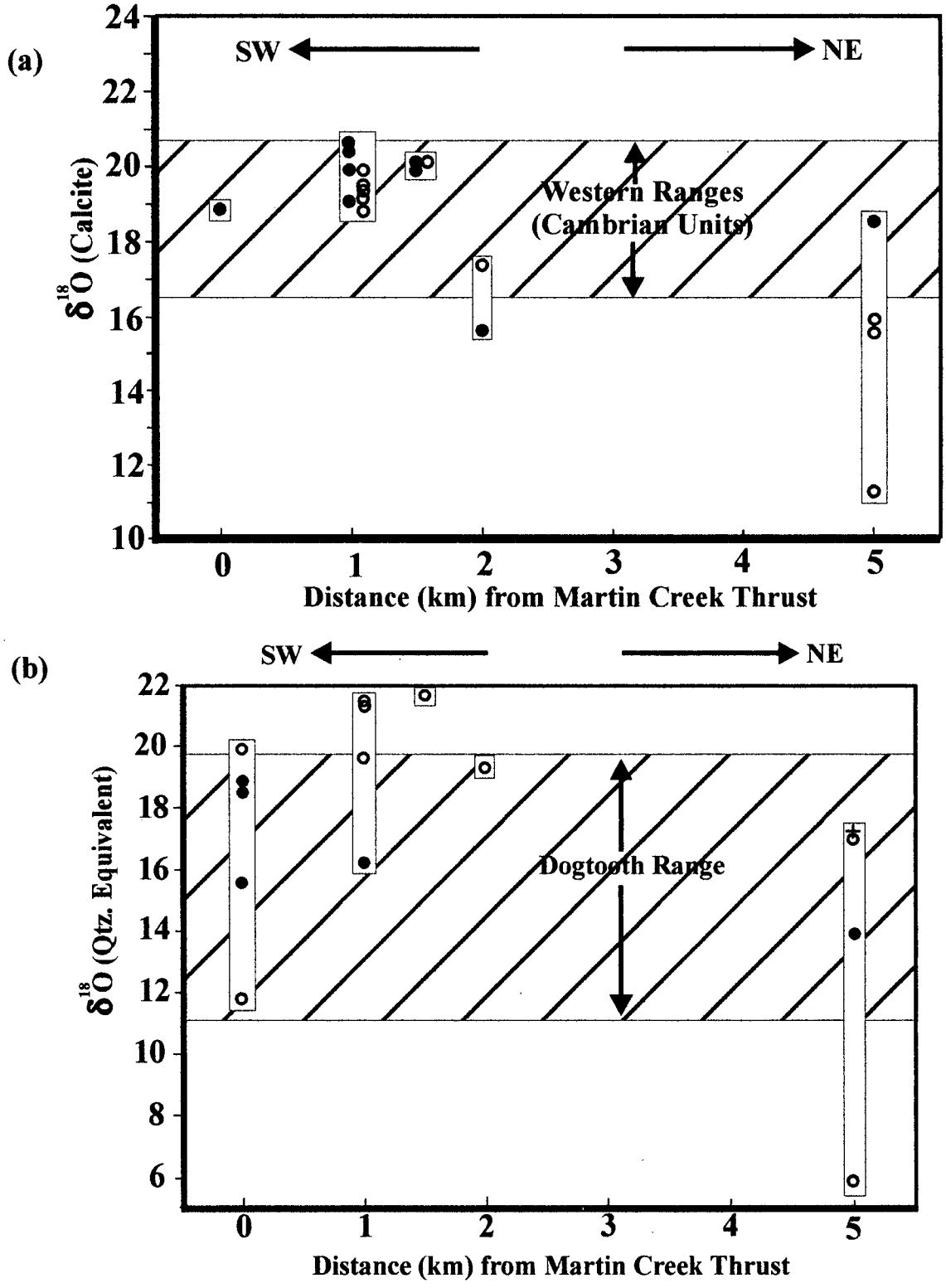

Figure 5.4: Lateral distribution of oxygen isotope compositions in the western Main Ranges. Distance is measured perpendicular across strike from the Martin Creek Thrust. (a) and (b) illustrate carbonate and silicate values, respectively. Closed and open circles depict wall rocks and veins, respectively. Cross represents quartz vein from the ore zone at Monarch Mine. Note wide compositional variation within and between outcrops.

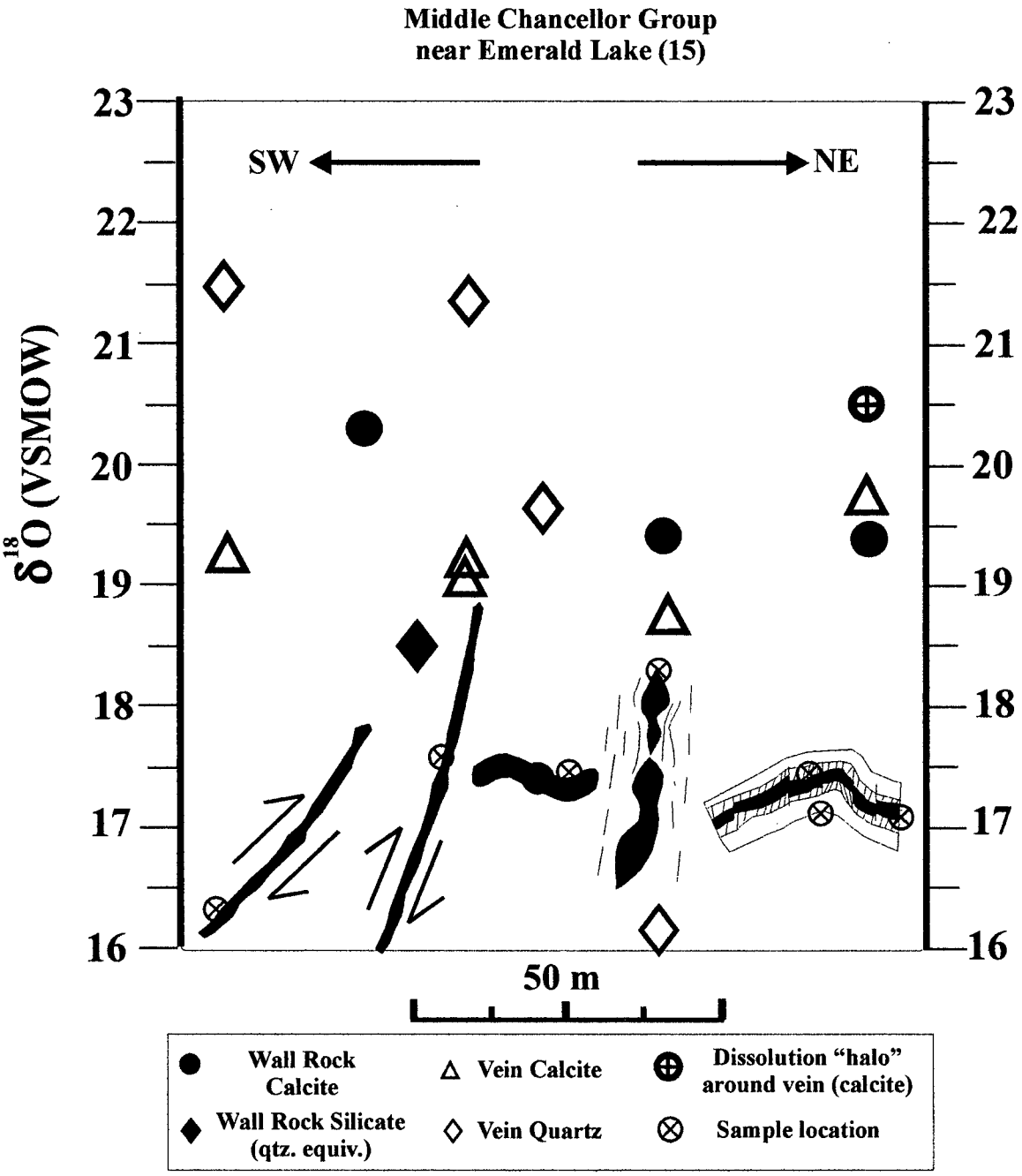

Figure 5.5: Isotope signatures at locality #15. Outcrop coincides with approximate trace of Martin Creek Thrust and consists of multiple generations of veins and several meter-displacement reverse faults. Note consistency in oxygen composition of vein calcite compared with scattered quartz compositions.

individual outcrop in the Western Ranges was only 0.6 ‰ and generally less than 0.4 ‰. Though only four whole rock silica values were measured from Chancellor slates, they are mutually consistent and possess an average $\delta^{18}O$ of 17.8 ‰ (qtz. equivalent). Three of these fall within the range 18.3 ‰ - 18.8 ‰ (qtz. equivalent) with a low value of 15.5 ‰ (qtz. equivalent) (Figure 5.3a). Compared with similar rock types from the Proterozoic package in the Dogtooth Range, siliceous pelites from the Main Ranges are heavier on average by 2.4 ‰. Because Horsethief Creek and Chancellor strata have a similar provenance [*Stewart*, 1989; *Kubli*, 1990], silica enrichment in the east more likely reflects isotopic exchange with higher-$\delta^{18}O$ carbonates than a change in sediment source.

Table 5.2: Average $\delta^{18}O$ (SMOW) of wall rocks and veins in the Main Ranges.

MAIN RANGES **lower and middle Chancellor Formations**				
	whole rock (‰)	**quartz equivalent (‰)**	**range (‰)**	**n**
wall rock carbonates	19.2 +/- 1.6		15.6-20.7	8
vein calcite	**19.1 +/- 1.0**		**17.3-20.3**	**6**
wall rock silicates	15.8 +/- 2.8	17.8 +/- 1.5	15.8-18.8 (qtz)	4
vein quartz	**18.8 +/- 3.4**		**11.8-21.7**	**8**
Platform rocks				
	whole rock (‰)	**quartz equivalent (‰)**	**range**	**n**
wall rock carbonates	18 +/- 2.3		15.5 - 20.1	3
vein calcite	**13.6 +/- 3.3**		**11.2-15.9**	**2**
wall rock silicate	13.1	13.9		1
vein quartz	**11.4 +/- 7.8**		**5.9-16.9**	**2**

Uncertainty defined as 1σ of population.

5.4.3 Veins and vein-wall rock relationships

Vein signatures depict a complicated history of both open and closed-system fluid migration and differ from those in the Western Ranges in that they are neither systematically enriched nor depleted with respect to neighboring wall rocks. In some veins, quartz and calcite

clearly precipitated in isotopic disequilibrium with one another suggesting that the two phases were derived from distinct reservoirs and/or crystallized at different temperatures. As in the Dogtooth and Western Ranges, vein morphology does not correlate with isotopic composition.

Calcite from veins hosted by metapelites from the Chancellor Group exhibits consistent oxygen compositions between 17.3 ‰ and 20.3 ‰ and averages 19.1 ‰ (Table 5.2). Vein quartz is more variable with signatures that range between 11.8 ‰ and 21.7 ‰ and average 18.8 ‰. Two veins that were sampled from the Cathedral Formation across the facies transition are substantially lighter in $\delta^{18}O$ with values as low as 5.9 ‰ and 11.2 ‰ for quartz and calcite, respectively. A ~100 m wide, locally faulted package of middle Chancellor slate and micrite best illustrates the contrast between compositional trends in quartz and calcite (Figure 5.5). The signature of calcite from three distinct vein types (3, 4, and 5) fluctuates by only 0.5 ‰, whereas quartz shows significant variance in $\delta^{18}O$ by as much as 5.3 ‰. The lowest value was obtained from a distended, cleavage-parallel vein (25-2J). Because the same vein exhibits a $\Delta^{18}O_{(calcite-quartz)} > 0$, the two phases are not in isotopic equilibrium. In contrast, quartz from two later-stage, fault-parallel veins is comparatively enriched in oxygen and in equlibrium with coexisting calcite at ~ 350°C (see section 5.4.5). The only quartz that exhibits an isotopic affinity with nearby siliceous slate was that from a pressure shadow. Thus, calcite-saturated fluids had been largely buffered by wall rocks, but oscillating values in vein quartz reflect complex hydrodynamics, disparate fluid sources, and/or diverse time-integrated fluid flux for silica-saturated fluid.

Comparisons between the composition of veins and their host rocks in Figure 5.6 show a non-systematic relationship for quartz, whereas vein calcite is usually lighter in both $\delta^{18}O$ and $\delta^{13}C$. The even distribution of vein quartz on either side of equilibrium either reflects multiple fluid regimes that incorporate isotopically distinct silica components or background variation in

the composition of wall rock silicates. Limited silicate data from metapelites complicates assessment of the latter possibility. However, three of the four samples are between 18 ‰ and 19 ‰, thus suggesting that wall rocks are fairly consistent in oxygen composition (as opposed to meta-pelites in the Dogtooth Range, for example). Furthermore, observations of large isotopic fluctuations in vein quartz from individual outcrops, such as the one in Figure 5.5, agree with the assertion that large variations in vein quartz are primarily the result of disparate fluid sources and not buffering by compositionally diverse wall rocks.

Modest, but fairly consistent calcite depletion indicates that fluids were systematically out of equilibrium with wall rocks in both $\delta^{18}O$ and $\delta^{13}C$. A similar, more exaggerated pattern was observed in the Western Ranges, although it is noteworthy that veins to the west were usually enriched in $\delta^{13}C$. No correlation exists between vein type and the sign and magnitude of $\Delta^{18}O_{\text{vein-wall rock}}$ (Figure 5.7). There is also only limited evidence for the channeling of exotic fluids exclusively into fault zones. Veins associated with the Carnarvon Thrust (15) and local thrust faults exhibit quartz enrichment and small depletions in calcite. A large depletion of 6.7 ‰ does occur within a cleavage/fault-parallel vein at the Martin Creek Thrust (31-2E; locality 14). The fact that another vein located 1 meter away is equilibrated with surrounding slates implies that either ^{18}O -depleted fluid was focussed into a relatively narrow fault zone or fluid-rock exchange around the fault was highly erratic. In later discussion, I suggest that proximity to extensional faults was a factor in supplying anomalously low-$\delta^{18}O$ fluids to the fault zone, as well as to another locality that exhibits intense oxygen depletions.

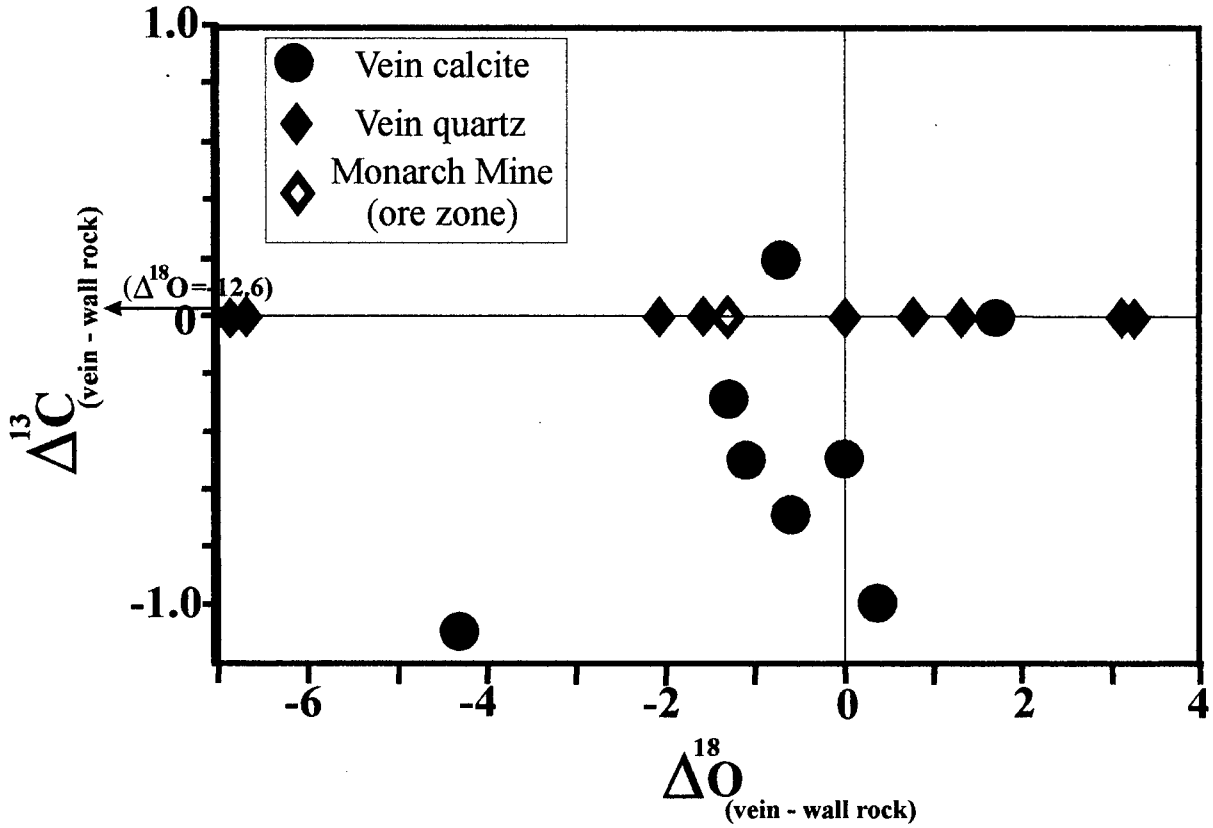

Figure 5.6: Relationship between vein and wall rock composition. Vein carbonate is compared with nearest wall rock carbonate and vein quartz with the nearest wall rock silica (quartz equivalent). Note wide distribution in quartz compared with general oxygen and carbon depletions in calcite and dolomite.

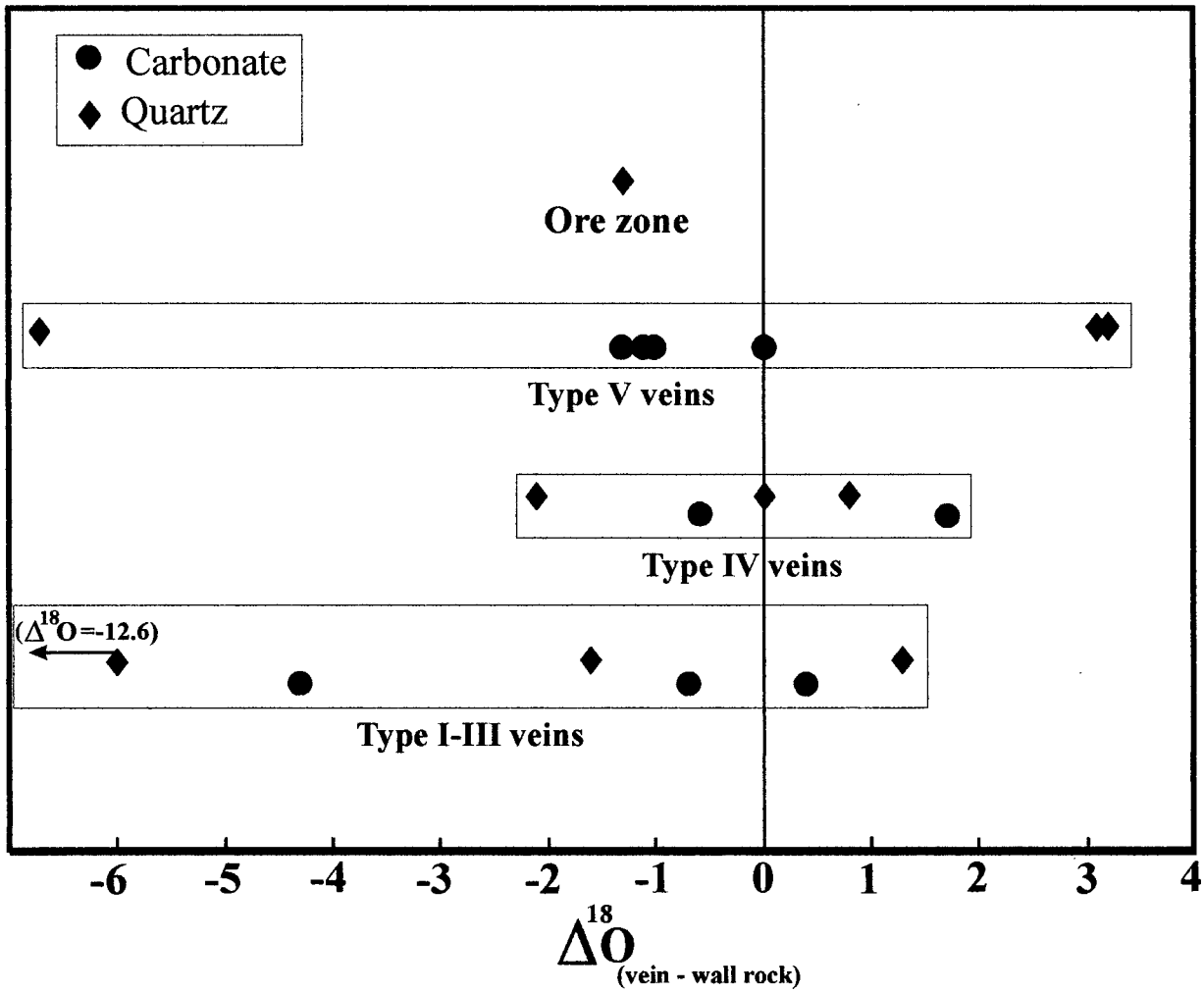

Figure 5.7: Oxygen fractionation between vein and wall rock by vein type. Relative enrichments and depletions appear impervious to timing of vein formation.

5.4.4 Trends in carbon isotope composition

The $\delta^{13}C$ of wall rocks and veins corresponds to a narrow range between -2.4 ‰ and +0.1 ‰, and all values are typical of Cambrian sediments [*Montañez et al.*, 2000]. In general, veins tend to be slightly lighter than wall rocks with two samples, both from the Monarch Mine locality, that exhibit depletions greater than -0.8 ‰ (Figure 5.6). Figure 5.8 shows that data do not conform to a simple pattern in $\delta^{13}C$-$\delta^{18}O$ space, although subtle trends are apparent in samples from locality 15 near the trace of the Martin Creek Thrust. This outcrop exhibits a positive correlation between $\delta^{13}C$ and $\delta^{18}O$ with veins generally possessing lighter compositions than host rocks. The shape of the array also resembles the curves described in Figure 3.1, which correspond to wall rock exchange with a fluid of relatively low X_{CO2}. The disequilibrium in $\delta^{18}O$ and $\delta^{13}C$ between initial calcite from the wall rocks and that in equilibrium with the intial fluid composition is 1.8 ‰ and 0.7 ‰, respectively. Granted, the extent of alteration is very minor, especially compared with data from the Pyrenees [*Rye and Bradbury*, 1988] for which oxygen and carbon signatures are displaced by as much as 10 ‰ and 2 ‰, respectively. However, it does provide one line of evidence for the migration of a low-X_{CO2} fluid across a distance $\geq$ 100 m.

At an outcrop near the facies transition between platform and basinal carbonates (17), veins and wall rocks show depletions of $\sim$ 5 ‰ in oxygen and $\sim$ 2 ‰ in carbon compared with "pristine" signatures from Chancellor slates (Figure 5.8). Time-integrated fluid fluxes were therefore high enough to override the buffering effect of wall rocks at some localities. However, without further data that shows a continuous regional correlation between $\delta^{18}O$ and $\delta^{13}C$, there is insufficient evidence to support the existence of a single, large-scale fluid cell across the Main Ranges. Sporadic depletions of variable magnitude across the study area support highly heterogeneous fluid channeling and isotope exchange with wall rocks. The lack of continuity in

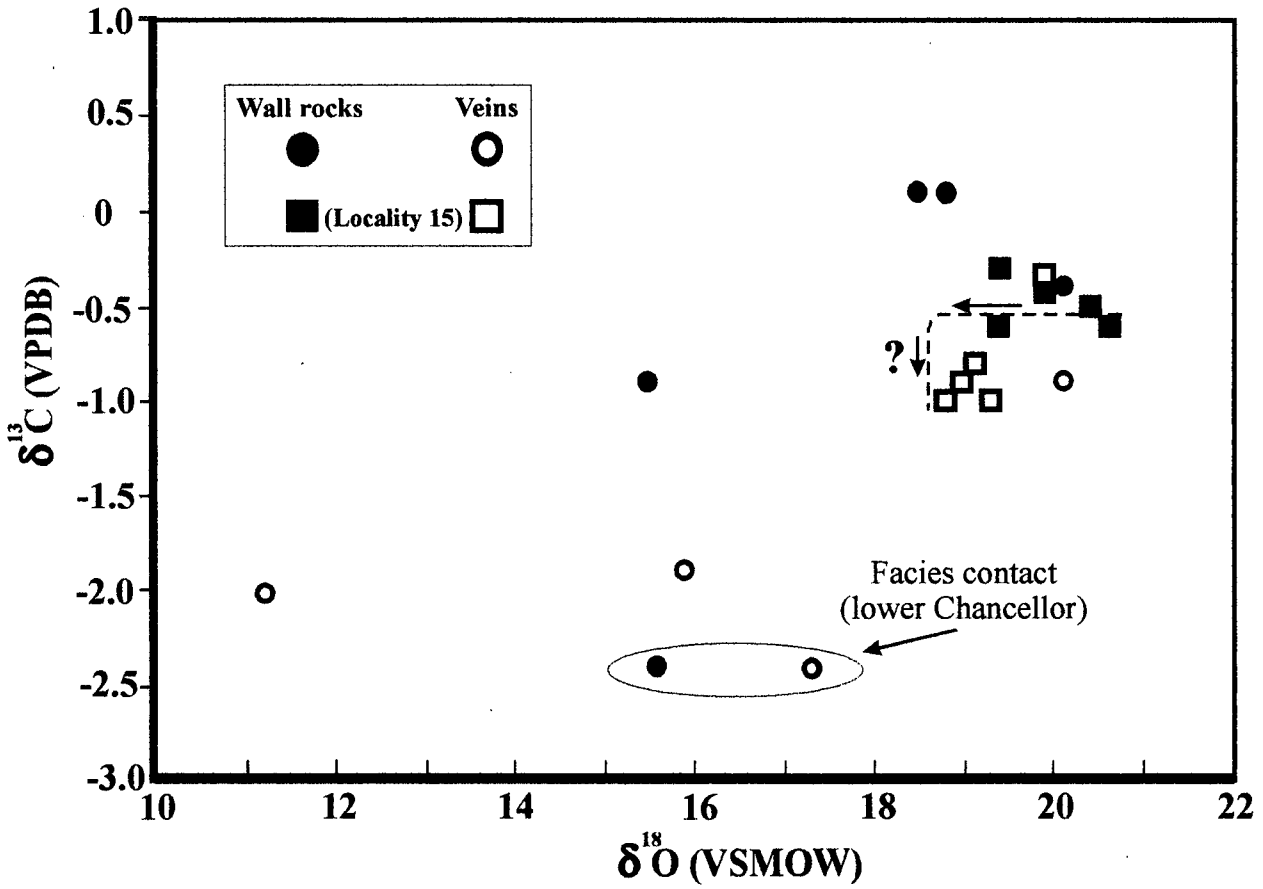

Figure 5.8: Distribution of carbonates in the western Main Ranges. Carbon-oxygen exchange trajectory is well illustrated in values from locality #15 (also depicted in Figure 5.5). Otherwise, distinct correlations between oxygen and carbon are unapparent.

$\delta^{13}C$ and $\delta^{18}O$ data between outcrops suggests either that each locality sampled fluids that were derived from a unique source or time-integrated fluid fluxes were highly variable between outcrops.

5.4.5 Stable isotope thermometry of vein material

Stable isotope thermometry was applied to coexisting quartz and calcite using fractionation factors formulated by *Sharp and Kirschner* [1994]. Only three veins yielded reasonable temperatures of 342°C, 355°C, and 387°C. These included two fault-parallel veins (25-3D; 44-4A) and a cleavage-parallel, chlorite bearing vein within the lower Chancellor (46-2A). The results are compatible with those from the Western and Dogtooth Ranges and lie within the range of wall rock temperatures from Chancellor slates that were estimated by *Gardner* [1977] (Figure 2.8). This provides further evidence that veins are indeed syn-kinematic and formed under conditions of maximum metamorphism. Laminated veins from the Carnarvon Thrust (Type 5) and Monarch Mine (Type 3) gave temperatures greater than 450°C indicating that quartz and calcite either precipitated in disequilibrium or were not co-precipitated.

5.5 Discussion

5.5.1 Interpretation of wall rock $\delta^{18}O$

Many carbonates from the Main Ranges exhibit lower than expected oxygen compositions. This trend in carbonate depletions is similar to, albeit less systematic than that in the Dogtooth and Western Ranges. Based on the compilation of global carbonate data presented in *Veizer and Hoefs* [1976] and *Veizer* [1983], the $\delta^{18}O$ of Cambrian limestones is generally at or above 21.0 ‰ (see section 2.7.2 for further discussion). Consistent with this, *Kirschner and*

Kennedy [in press] documented an average signature of ~21 ‰ from undeformed limestones of the Eldon formation, the platform equivalent of the lower Chancellor unit, in the hanging wall of the McConnell Thrust. *Woodwell* [1985] also recorded wall rock values above 21 ‰ from the Eldon near the McConnell thrust contact. These factors provide evidence that wall rock compositions lighter than 20 ‰, which account for more than half the data in the Main Ranges, have been lowered as a result of exchange with comparatively low-$\delta^{18}O$ fluids. That is, fluctuations in $\delta^{18}O$(calcite) are not an artifact of diagenesis, but representative of heterogeneous alteration under conditions of variable time-integrated fluid flux. I exclude data from the Monarch Mine in this discussion, because the low $\delta^{18}O$ values observed in the Cathedral formation might record pre-Mesozoic dolomitization. Observations from the Western and Dogtooth Ranges have shown that pervasive quartz and other silicates within calcareous sediments can diminish calcite signatures by centimeter to meter-scale homogenization during diffusion and/or advection-assisted exchange. However, two of the lowest signatures from the Chancellor Group, 15.6 ‰ (46-1A) and 18.8 ‰ (31-3C), were obtained from units with less than 10 % vol. silicate minerals, and mineralogically similar calcareous sediments at the outcrop in Figure 5.5 exhibit isotopic differences of 1.4 ‰. It follows that the low-$\delta^{18}O$ fluids responsible for altering some of the wall rocks were derived from sources external to individual outcrops.

5.5.2 Interpretation of vein $\delta^{18}O$ and implications for fluid migration

Veins in the Main Ranges depict a complicated paleohydrology that involved multiple episodes of open and closed-system fluid migration during deformation. Any proposed scenario must reconcile (a) anomalously low oxygen compositions within some veins, (b) widespread variability in quartz $\delta^{18}O$, and (c) modest, but systematic depletions in $\delta^{18}O$ and $\delta^{13}C$ within vein

calcite. Unfortunately, the broad resolution of sampling in this portion of the study and the unsystematic nature of the results stifle the development of an all-encompassing hydrodynamic model for the western Main Ranges. However, there is sufficient evidence to support the presence of at least two distinct fluid events, one of which involved the ingress of isotopically pristine, meteoric fluid into units buried 8-10 km below the surface.

Two veins yielded the lowest oxygen compositions observed anywhere in the transect. Highly strained quartz from an extensive fault/cleavage-parallel vein at the Martin Creek Thrust possessed a $\delta^{18}O$ of 11.8 ‰ (31-2E), and a sigmoidal tension gash from the Cathedral Formation near the facies transition recorded compositions of 5.9 ‰ and 11.2 ‰ (38-2C) for quartz and dolomite, respectively. Assuming a temperature for quartz precipitation of 300°C - 400°C, the composition of the fluids from which the veins formed was +4.9 ‰ to +7.7 ‰ and -1.0 ‰ to +1.8 ‰ [*Matsuhisa et al.*, 1979]. Both of these plot within the compositional range for surface-derived fluids (~ -40 ‰ - +10 ‰; *Hoefs* [1997]), but the fault-parallel vein also overlaps with low-end values for metamorphic waters (+3 ‰ to +20 ‰; *Shepphard* [1986]). Within the study area, protoliths are rarely below 13.0 ‰, and extremely low-$\delta^{18}O$ igneous rocks are absent. Thus, the possibility that these veins precipitated from ascending metamorphic fluids that were derived from deeper siliciclastic units is unlikely.

For the following reasons, I propose that surface-derived fluids gained access to deep-seated dilation zones by way of reversed pressure gradients along Mesozoic extensional faults. The focussing of surface-derived fluid into veins appears to have been a very localized phenomenon exclusive to zones proximal to normal faults. Both veins are located less than 1000 m from extensive normal faults that accommodated between 240 m and 900 m of displacement [*Cook*, 1975]. Importantly, the low-$\delta^{18}O$ tension gashes documented at the Monarch Mine are

situated within a small graben that is bounded by the Fossil Gulley and Stephen-Cathedral normal faults (Figure 5.9). In addition, the Martin Creek Thrust possesses a normal fault in its footwall with which it possibly merges at depth. Because similar striking normal faults in the Main Ranges show evidence for a later compressional phase and are truncated by the Simpson Pass Thrust, *Cook* [1975] concluded that extension occurred in conjunction with regional contraction. Thus, extensional faults represent the most probable conduits for siphoning meteoric fluids into contraction-related faults and fracture zones.

Most veins are compositionally similar to adjacent wall rocks and indicate that the fluids from which they precipitated were largely rock-buffered regardless of their relative timing (Figure 5.6). However, systematic $\delta^{13}C$ and $\delta^{18}O$ depletions in vein calcite and comparatively large variations in the composition of vein quartz reflect heterogeneity in fluid composition, which might represent variable time-integrated fluid fluxes. Depletions in vein calcite are consistent with the conclusion that wall rock carbonates have been altered to lower values following exchange with a low-$\delta^{18}O$, probably metamorphic fluid. Interestingly, the lowest calcite signatures in the Chancellor Group (15.6 ‰ and 17.3 ‰) were observed within a phyllite and cleavage-parallel vein situated within 1 meter of the facies transition, where cleavage has been broadly folded and veins and wall rocks are chloritized. The fact that these also coincide with a belt of complex folding [*Cook*, 1975] raises the possibility that low-$\delta^{18}O$ metamorphic fluid was structurally channeled through axial planes and related fracture networks.

By virtue of comparatively low oxygen compositions (i.e. $\Delta^{18}O_{(quartz\text{-}calcite)} < 0$), the quartz in some veins is clearly out of isotopic equilibrium with local calcite (e.g., a pyrite pressure shadow (25-2M), a cleavage-parallel vein (25-2J), and a bedding-parallel vein (38-2G)). For example, a distended, cleavage-parallel vein at locality 15 (Figure 5.5) exhibits a $\delta^{18}O$ (quartz) of

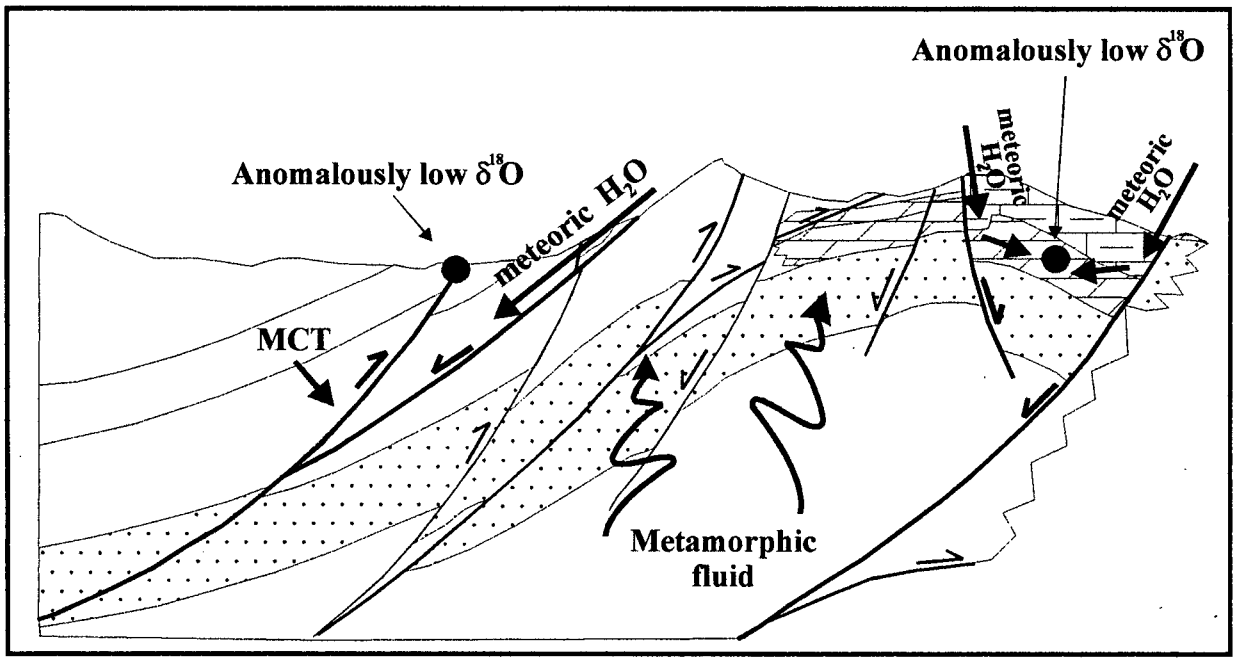

Figure 5.9: Proposed scenario for vein depletions and altered wall rock signatures. Meteoric water is focussed along Mesozoic normal faults and channeled into fracture zones and reverse fault zones. Advection of metamorphic fluid derived from deeper, probably siliciclastic horizons drives systematic calcite depletion in veins and wall rocks. MCT = Martin Creek Thrust.

16.2 ‰ and is depleted relative to all other veins and wall rocks at the outcrop. Here, the time-integrated fluid flux was high enough to prevent buffering of dissolved silica by wall rock carbonates. In fault-parallel veins from the same locality, quartz compositions are elevated with respect to wall rock silicate and equilibrated with calcite. This either signifies very low time-integrated fluid fluxes and/or localized fluid circulation across less than 100 meters. Vein forming silica was therefore derived from multiple sources, at least one of which was external to the outcrop. The relationship of these disparate quartz values to the infiltration of metamorphic and surface-derived fluids proposed above is enigmatic. However, it is notable that younger, fault-parallel veins within at least two outcrops exhibit the most evolved, i.e., highest, quartz signatures. This indicates that open-system advection was primarily operative during cleavage development, while later-stage faults incorporated locally derived fluids that were isotopically buffered with respect to local calcite.

5.6 Conclusions

Isotope systematics in the western Main Ranges depict a convoluted syn-tectonic fluid history that involved infiltration from at least two distinct sources:

(1) Extreme oxygen depletions in two veins imply that meteoric fluid accessed fault and fracture zones probably by way of nearby extensional faults that were active during compression.

(2) Sporadic departures from typical Cambrian signatures in the $\delta^{18}O$ (calcite) of wall rocks and systematic $\delta^{18}O$ and $\delta^{13}C$ depletions in calcite veins suggest that low-$\delta^{18}O$, probably metamorphic, fluids infiltrated outcrops within a highly heterogeneous flow regime. Based on the absence of a strong regional correlation between $\delta^{18}O$ and $\delta^{13}C$, rock and vein alteration cannot be ascribed to a single, large-scale fluid cell.

(3) Isotopic fluctuations in quartz veins within and between outcrops reflect variability in time-integrated fluid fluxes and disperate silica sources. This variation cannot be explained by local shifts in wall rock $\delta^{18}O$ alone.

Further sampling is needed to better constrain these fluid events with respect to timing and mechanisms. Specifically, veins directly related to normal faults should be analyzed to test the hypothesis that extensional faulting is responsible for channeling meteoric fluids into deep-seated dilation zones. Also, heterogeneity in the composition of vein quartz and wall rocks can be addressed by aggressive sampling of multiple vein generations within well exposed, highly fractured outcrops like the one at locality 15. By detailing the sources of low-$\delta^{18}O$, vein-forming fluids, robust constraints can be placed on the time-integrated fluid flux that was active during distinct veining events.

CHAPTER 6

CONCLUSIONS

Stable isotope data reveal that several fluid regimes operated at multiple scales during Mesozoic tectonism in the Dogtooth, Western, and Main Ranges. In the Dogtooth Range, wide variation in the oxygen and carbon signatures of wall rocks and veins, systematic oxygen depletion in carbonates, and δH values with a metamorphic affinity support the circulation of metamorphic fluids across a scale of at least meters, but probably 100's of meters, under conditions of heterogeneous time-integrated fluid flux. A single low-δH signature suggests that some vein forming fluids were at least partially derived from meteoric water. General vein-rock equilibrium at fault zones indicates that fluids were not exclusively chaneled into regional detachment structures.

Carbonate data in the Western Ranges outline a ~15 - ~25 km long isotopic alteration front that propogated eastward and upward away from the Dogtooth Range, consistent with the expulsion of low-X_{CO2}, Dogtooth-derived fluids into the foreland. Modest but systematic oxygen depletions in veins demonstrate that fluids were not in equilibrium with the surrounding wall rocks. These observations agree with model-derived estimates for a time-integrated fluid flux of 3×10^4 - 1×10^5 mol H_2O/cm^2 under conditions of relatively sluggish kinetics (i.e. $N_D = 20$). Increased oxygen depletion in cataclasites and densely veined outcrops attest to the structural focussing of fluids into fault and fracture zones. Observations from cathodoluminescence also show that faults hosted fluids that were chemically exotic to the surrounding wall rocks.

In the Main Ranges, large variations in isotope composition are indicative of a complex fluid regime that involved heterogeneous fluid-rock interaction within individual outcrops and

the influx of isotopically exotic fluids from at least two distinct sources. Extremely low $\delta^{18}O$ values within some veins demonstrate that meteoric fluids descended to depths of ~ 8-10 km probably by way of proximal syn-contractional normal faults. Elsewhere, sporadically low oxygen and carbon values in quartz and calcite, in conjunction with a metamorphic δH signature, suggest that metamorphic fluids migrated across at least 100's of meters during tectonism and probably originated in deeper, low-$\delta^{18}O$ siliciclastics.

Oxygen isotope and calcite-dolomite solvus thermometry on veins throughout the study area reflect precipitation temperatures of 260°C - 387°C, which indicates that they were in general thermal equilibrium with the surrounding wall rocks. Finally, the overall lack of a correlation between vein type and the magnitude of depletion or enrichment indicates that both closed and open system fluid circulation occurred throughout the duration of tectonism and were not temporally restricted to specific veining events.

These results provide further evidence that major orogenic events are capable of producing large, km-scale fluid cells that not only leave their geochemical imprint on fault zones and veins, but also register as alteration fronts within wall rocks. Combined structural and stable isotopic studies that neglect wall rock compositions or fail to capitalize on regional isotopic shifts risk overlooking subtle trends that record large flow events. This study also emphasizes the difficulty in deciphering distinct fluid regimes under conditions where highly heterogeneous time-integrated fluid fluxes prevailed, leaving large variations in isotopic signatures. In such situations, detailed sampling at approximately centimeter intervals across outcrops is the best strategy for studying terranes with complex fluid histories. Finally, the above conclusions carry implications for similar orogenic belts, where siliciclastic-dominated domains have been structurally juxtaposed against large carbonate sequences.

REFERENCES

Anovitz, L.M. and Essene, E. J., Phase equilibria in the system $CaCO_3$-$MgCO_3$-$FeCO_3$, Journal of Petrology, 28, 389-414, 1987.

Balkwill, H.R., Structural geology, Lower Kicking Horse River region, Rocky Mountains, British Columbia, Bulletin of Canadian Petroleum Geology, 20, 608-633, 1972.

Balkwill, Hugh Robert, Structural Analysis of the Western Ranges, Rocky Mountains, near Golden, British Columbia, Ph.D thesis, University of Texas at Austin, 1969.

Berman, R.G., Internally-consistent thermodynamic data for minerals in the system Na_2O-K_2O-CaO-MgO-FeO-Fe_2O_3-Al_2O_3-SiO_2-TiO_2-H_2O-CO_2, Journal of Petrology, 29, 2445-2552, 1988.

Bickle, M.J. and McKenzie, D., The transport of heat and matter by fluids during metamorphism, Contributions to Mineralogy and Petrology, 95, 384-392, 1987.

Bigeleisen, J., Pearlman, M.L., and Prosser, H.C., Conversion of hydrogenic materials to hydrogen for isotopic analysis, Anal. Chem., 24, 1356-1357, 1952.

Bowman, John R., Willett, Sean D., and Cook, Stephen J., Oxygen isotopic transport and exchange during fluid flow: one-dimensional models and applications, American Journal of Science, 294, 1-55, 1994.

Bradbury, Harry J. and Woodwell, Grant R., Ancient fluid flow within foreland terrains, in Fluid Flow in Sedimentary Basins and Aquifers, Geological Society Special Publication, 34, edited by Jeremy C. Goff and B.P.J. Williams, pp. 87-102, Geological Society of London, 1987.

Brady, John B., The role of volatiles in the thermal history of metamorphic terranes, Journal of Petrology, 29, 1187-1213, 1988.

Burkhard, Martin and Kerrich, Robert, Fluid regimes in the deformation of the Helvetic nappes, Switzerland, as inferred from stable isotope data, Contributions to Mineralogy and Petrology, 99, 416-429, 1988.

Burnham, C. Wayne, Holloway, John R., and Davis, Nicholas F., Thermodynamic properties of water to 1000°C and 10,000 bars, GSA Special Paper 132, 1969.

Cartwright, I. and Buick, I.S., The flow of surface-derived fluids through Alice Springs age middle-crustal ductile shear zones, Reynolds Range, central Australia, Journal of Metamorphic Geology, 17, 397-414, 1999.

Cartwright, I., Power, W.L., Oliver, N.H.S., Valenta, R.K., and Mclatchie, G.S., Fluid migration and vein formation during deformation and greenschist facies metamorphism at Ormiston Gorge, central Australia, Journal of Metamorphic Geology, 12, 373-386, 1994.

Chacko, T., Xiangsheng, H., Mayeda, T.K., Clayton, R.N. & Goldsmith, J.R., Oxygen isotope fractionations in muscovite, phlogopite, and rutile,.Geochimica et Cosmochimica Acta, 60, 2597-2608, 1996.

Chatterton, Brian D. and Ludvigsen, Rolf, Upper Steptoean (upper Cambrian) trilobites from the McKay Group of southeastern British Columbia, Canada. Journal of Paleontology, Suppl, 72, p. 43, 1998.

Clayton, R.N. & Keiffer, S.W., Oxygen isotopic thermometer calibrations, in Stable Isotope Geochemistry: A tribute to Samuel Epstein, The Geochemical Society, Special Publication No.3, edited by H.P. Taylor, J.R. O'Neil, and I.R. Kaplan, pp. 3-10, 1991.

Clayton, Robert N. and Mayeda, Toshiko, K., The use of bromine pentafluoride in the extraction of oxygen from oxides and silicates for isotopic analysis, Geochimica et Cosmochimica Acta, 27, 43-52, 1963.

Clayton, R.N., O'Neil, J.R., and Mayeda, T.K., Oxygen isotope exchange between quartz and water, Journal of Geophysical Research, 77, 3057-3067, 1972.

Cook, D.G., Structural style influenced by lithofacies, Rocky Mountain Main Ranges, Alberta British Columbia, Geological Survey of Canada, Bulletin No. 233, 1975.

Cox, S .F. and Etheridge, M.A., Coupled grain-scale dilatancy and mass transfer during deformation at high fluid pressures: examples from Mount Lyell, Tasmania, Journal of Structural Geology, 11, 147-162. 1989.

Dean, W.T., Lower Ordivician trilobites from the uppermost McKay Group at its type section, Southeastern British Columbia, in Contributions to Canadian Paleontology, Geological Survey of Canada, Bulletin 379, pp. 1-15, 1988.

Dietrich, Dorothee and Grant, Paul R., Cathodoluminescence petrography of syntectonic quartz fibres, Journal of Structural Geology, 7, 541-553, 1985.

Dipple, Gregory M. and Ferry, John M., Metasomatism and fluid flow in ductile fault zones, Contributions to Mineralogy and Petrology, 112, 149-164, 1992.

Dipple, Gregory M. and Ferry, John M., Fluid flow and stable isotopic alteration in rocks at elevated temperatures with applications to metamorphism, Geochemica et Cosmochimica Acta, 56, 3539-3550, 1992.

Etheridge, M.A., Wall, V.J., and Cox, S.F., High fluid pressures during regional metamorphism and deformation: implications for mass transport and deformation mechanisms, Journal of Geophysical Research, 89, 4344-4358, 1984.

Ferry, John M., Regional metamorphism of the Waits River Formation, Eastern Vermont: Delineation of a new type of giant metamorphic hydrothermal system, Journal of Petrology, 33, 45-94, 1992.

Fisher, Donald M. and Brantley, Susan L., Models of quartz overgrowth and vein formation: deformation and episodic fluid flow in an ancient subduction zone, Journal of Geophysical Research, 97, 20,043-20,061, 1992.

Gabrielse, H. and Campbell, R.B., Upper Proterozoic Assemblages, in Geology of the Cordilleran Orogen, Geology of Canada, No. 4, edited by H. Gabrielse and C.J. Yorath, pp. 125-150, Geological Survey of Canada, Ottawa, 1992.

Gabrielse, H. and Yorath, C.J., Introduction, in Geology of the Cordilleran Orogen in Canada, Geology of Canada, No. 4, edited by H. Gabrielse and C.J. Yorath, pp. 3-11, Geological Survey of Canada, Ottawa, 1992.

Gardner, Douglas A.C., Structural Geology and Metamorphism of Calcareous Lower Paleozoic Slates, Blaeberry River-Reburn Creek Area, near Golden, British Columbia, Ph.D. thesis, Queen's University, Kingston, 1977.

Gardner, D.A.C., Price, R.A., and Carmichael, D.M., The petrology and structural fabric of some Paleozoic calcareous pelites in the Porcupine Creek Anticlinorium near Golden, British Columbia, in Geological Survey of Canada, Paper 76-1A, pp. 137-140, 1976.

Ghent, Edward D. and O'Neil, James R., Late Precambrian marbles of unusual carbon-isotope composition, southeastern British Columbia, Canadian Journal of Earth Science, 22, 324-329, 1985.

Graham, C.M., Atkinson, J. and Harmon, R.S. Hydrogen isotope fractionation in the system chlorite-water in NERC 6th Progress Report of Research 1981-1984, NERC Publication Series D, No. 25, p. 139, 1984.

Gray, David R., Gregory, Robert T., and Durney, David W., Rock-buffered fluid-rock interaction in quartz rich turbidite sequences, Eastern Australia, Journal of Geophysical Research, 96, 19,681-19,704, 1991.

Gregory, Robert T. and Criss, Robert E., Isotopic exchange in open and closed systems, in Stable Isotopes in High Temperature Geological Processes, Reviews in Mineralogy, Vol. 16, edited by J.W. Valley, H.P. Taylor, Jr., and J.R. O'Neil, pp. 91-127, Mineralogical Society of America, 1986.

Hoefs, Jochen., Stable Isotope Geochemistry. Springer Press, New York, 1997.

Kirschner, David L. and Kennedy, Lori A., Limited syntectonic fluid flow in carbonate-hosted thrust faults of the Front Ranges, Canadian Rockies, inferred from stable isotope data and structures, Journal of Geophysical Research, in press.

Koons, P.O. and Craw, D., Evolution of fluid driving forces and composition within collisional Orogens, Geophysical Research Letters, 18, 935-938, 1991.

Kubli, Thomas E., Geology of the Dogtooth Range, northern Purcell Mountains, British Columbia, Ph.D. thesis, University of Calgary, Calgary, 1990.

Kubli, Thomas and Simony, Philip S.,The Dogtooth Duplex, a model for the structural development of the northern Purcell Mountains, Canadian Journal of Earth Sciences, 31, 1672-1686, 1994.

Kubli, Thomas E. and Simony, Philip S., The Dogtooth High, northern Purcell Mountains, British Columbia, Bulletin of Canadian Petroleum Geology, 40, 36-51, 1992.

Lassey, Keith R., On the computation of certain integrals containing the modified Bessel function $I_0(\xi)$, Mathematics of Computation, 39, 625-637, 1982.

Lassey, Keith R. and Blattner, Peter, Kinetically controlled oxygen isotope exchange between fluid and rock in one-dimensional advective flow, Geochimica et Cosmochimica Acta, 52, 2169-2175, 1988.

Leach, D.L. and Sangster, D.F., Mississippi Valley-type lead-zinc deposits, in Mineral Deposit Modeling: Geological Association of Canada Special Paper 40, edited by R.V. Kirkham, W.D. Sinclair, R.I. Thorpe, and J.M. Duke, pp. 289-314, 1993.

Lee, Young-Joon, Wiltschko, David L., Grossman, Ethan L., Morse, John W., and Lamb, William M., Sequential vein growth with fault displacement: An example from the Austin Chalk Formation, Texas, Journal of Geophysical Research, 102, 22,611-22,628, 1997.

Lickorish, W.H., Structural development of the Porcupine Creek Anticlinorium, Western Main Ranges, Rocky Mountain, British Columbia, Journal of Structural Geology, 15, 477-489, 1993.

Machel, H.G., Cavell, P.A., and Patey, K.S., Isotopic evidence for carbonate cementation and recrystallization, and for tectonic expulsion of fluids into the Western Canada Sedimentary Basin, Geological Society of America Bulletin,108, 1108-1119, 1996.

Machel, Hans G., Mason, Roger, A., Mariano, Anthony N., and Mucci, Alfonso, Causes and emission of luminescence in Calcite and Dolomite in Luminescence Microscopy: Quantitative and Qualitative Analysis, edited by Charles E. Barker and Otto C. Kopp, Society of Economic and Petroleum Geologists, pp. 9-25, 1991.

Marquer, D. and Burkhard, M., Fluid Circulation, progressive deformation and mass-transfer processes in the upper crust: the example of basement-cover relationships in the External Crystalline Massifs, Switzerland, Journal of Structural Geology, 14, 1047-1057, 1992.

Marshall, D.J., Cathodoluminescence of Geologic Materials, Unwin Hyman, Boston, 1988.

Matsuhisa, Y., Goldsmith, J.R. and Clayton, R.N., Oxygen isotopic fractionation in the system quartz-albite-anothite-water, Geochimica Cosmochimica et Acta, 43, 1131-1140, 1979.

Matsuhisa, Y., Morishita, Y., and Sato, T., Oxygen and carbon isotope variations in gold-bearing hydrothermal veins in the Kushikino mining area, southern Kyushu, Japan, Economic Geology, 80, 283-293, 1985.

McCaig, Andrew W., Deep fluid circulation in fault zones, Geology, 16, 867-870, 1988.

McCrea, J.M., On the isotope chemistry of carbonates and a paleotemperature scale, Journal of Chemical Physics, 18, 849-857, 1950.

Montañez, Isabel P., Osleger, David A., Banner, Jay L., Mack, Larry E., and Musgrove, MaryLynn, Evolution of the Sr and C isotope composition of Cambrian oceans, GSA Today, 10, 2000.

Nabelek, Peter I., Stable isotope monitors in Contact Metamorphism, Mineralogical Society of America, Reviews in Mineralogy, 26, edited by Derrill M. Kerrick, pp. 395-435, 1991.

Nesbitt, Bruce E. and Muehlenbachs, Karlis, Paleo-hydrology of late Proterozoic units of southeastern Canadian Cordillera, American Journal of Science, 297, 359-392 ,1997.

Nesbitt, Bruce E. and Muehlenbachs, Karlis, Geochemistry of syntectonic, crustal fluid regimes along the Lithoprobe Southern Canadian Cordillera Transect, Canadian Journal of Earth Sciences, 32, 1699-1719, 1995.

Nesbitt, Bruce E. and Muehlenbachs, Karlis, Paleohydrology of the Canadian Rockies and origins of brines, Pb-Zn deposits and dolomitization in the Western Canada Sedimentary Basin, Geology, 22, 243-246, 1994.

Nillni, Adriana M. and Stoeckhert, Bernhard, Cathodoluminescence and microthermometry in hydrothermal quartz, Cerro Vanguardia Deposit; Santa Cruz Province, Argentina in XIII Congreso Geologico Argentino; III Congreso de Exploracion de Hidro Carburos. Actas del Congreso Geologico Argentino.13, Vol. III, pp. 181-188, 1996.

O'Neil, J.R. and Taylor, H.P., Jr., Oxygen isotope equilibrium between muscovite and water, Journal of Geophysical Research, 74, 6012-6022, 1969.

O'Neil, J.R., Clayton, R.N., and Mayeda, T.K., Oxygen isotope fractionation in divalent metal carbonates, Journal of Chemical Physics, 51, 5547-5558, 1969.

Oliver, Jack, Fluids expelled tectonically from orogenic belts: Their role in hydrocarbon migration and other geologic phenomena, Geology, 14, 99-102, 1986.

Oliver, N.H.S., Review and classification of structural controls on fluid flow during regional metamorphism, Journal of Metamorphic Petrology, 14, 477-492, 1996.

Onasch, Charles M. and Vennemann, Torsten W., Disequilibrium partitioning of oxygen isotopes associated with sector zoning in quartz, Geology, 23, 1103-1106, 1995.

Passchier, C.W. and Trouw, R.A.J., Microtectonics, Springer Press, New York, 1996.

Penniston-Dorland, Sarah C. and Cloos, Mark, Scanned Cathodoluminescence of quartz and interpretation of textures in quartz-sulphide veins in the Grasberg Igneous Complex, a porphyry copper ore district in Abstracts with Programs, GSA Annual Meeting, A-61, 1997.

Price, R.A.. and Simony, P, Geology of the Lake Louise-Golden Area (map), Alberta Society of Petroleum Geologists, 1971.

Ramsay, John G. and Huber, Martin I., The Techniques of Modern Structural Geology. Volume 2: Folds and Fractures, Academic Press Limited, London, 1983.

Rumble, D., Stable isotope fractionation during metamorphic devolatilization reactions in Characterization of Metamorphism through Mineral Equilibria, Reviews in Mineralogy, Volume 10, edited by J.M. Ferry, pp. 327-353, 1982.

Rye, Danny M. and Bradbury, Harry J., Fluid flow in the crust: An example from a Pyrenean thrust ramp, American Journal of Science, 288, 197-235, 1988.

Seyedolali, Abbas, Reed, Mark, Rusk, Brian, and Goles, Godon G., Dissolution and healing fabrics of vein quartz in the Butte, Montana porphyry copper deposit revealed by cathodoluminescence, in Abstracts with Programs, GSA Annual Meeting, A-370, 1998.

Sharp, Z.D. and Kirschner, D.L., Quartz-calcite oxygen isotope thermometry: A calibration based on natural isotopic variations, Geochimica et Cosmochimica Acta, 58, 4491-4501,1994.

Sheppard, S.M.F., Characterization and isotope variations in natural waters in Stable Isotopes, in High Temperature Geological Processes, Reviews in Mineralogy, Volume 16, edited by J.W. Valley, H.P. Taylor, Jr., and J.R. O'Neil, Mineralogical Society of America, pp. 165-183. 1986.

Shimamoto, Toshihiko, Kanaori, Yuji, and Asai, Ken-ichi, Cathodoluminescence observations on low-temperature mylonites: potential for detection of solution-precipitation microstructures, Journal of Structural Geology, 13, 967-973, 1991.

Sibson, Richard H., Structural permeability of fluid-driven fault-fracture meshes, Journal of Structural Geology, 18, 1031-1042. 1996.

Simony, P.S. and Wind, G., Structure of the Dogtooth Range and adjacent portions of the Rocky Mountain Trench in Structure of the Southern Canadian Cordillera; Geological Association of Canada, Special Paper No. 6, edited by J.O. Wheeler, pp. 41-51, 1970.

Sprunt, Eve S., Dengler, Lori A., and Sloan, Doris, Effects of metamorphism on quartz cathodoluminescence, Geology, 6, 305-308, 1978.

Stewart, W.D., A preliminary report on the stratigraphy and sedimentology of the lower and middle Chancellor Formation (Middle to Upper Cambrian) in the zone of facies transition, Rocky Mountain Main Ranges, southeastern British Columbia in Current Research, Part D, Geological Survey of Canada, Paper 89-1D, pp. 61-68, 1989.

Suzuoki, T. and Epstein, S., Hydrogen isotope fractionation between OH-bearing minerals and water, Geochemica Cosmochimica Acta, 40, 1229-1240, 1976.

Valenta, R.K., Vein Geometry in the Hilton area, Mount Isa, Queensland: implications for fluid behavior during deformation, Tectonophysics, 158, 191-207, 1989.

Valley, John W., Stable isotope geochemistry of metamorphic rocks, in Stable Isotopes in High Temperature Geological Processes, Reviews in Mineralogy, Vol. 16, edited by J.W. Valley, H.P. Taylor, Jr., and J.R. O'Neil, pp. 445-489, Mineralogical Society of America, 1986.

van der Velden, Arie J. and Cook, Frederick A., Structure and tectonic development of the southern Rocky Mountain Trench. Tectonics, 15, 517-544, 1996.

Veizer, Jan, Trace elements and isotopes in sedimentary carbonates, in Carbonates: Mineralogy and Chemistry, Reviews in Mineralogy, No. 11, edited by Richard J. Reeder, pp. 265-299, Mineralogy Society of America, Washington, D.C., 1983.

Veizier, Jan and Hoefs, Jochen, The nature of O^{18}/O^{16} and C^{13}/C^{12} secular trends in sedimentary carbonate rocks, Geochimica et Cosmochimica Acta, 40, 1387-1395, 1976.

Waldron, Helen M. and Sandiford, Michael, Deformation volume and cleavage development in metasedimentary rocks from the Ballarat slate belt, Journal of Structural Geology, 10, 53-62, 1988.

Wenner, D.B. & Taylor, H.P. Jr., Temperatures of serpentinization of ultramafic rocks based on O^{18}/O^{16} fractionation between coexisting serpentine and magnetite, Contributions to Mineralogy and Petrololgy, 32, 165-185, 1971.

Wickham, Stephen M. and Peters Mark T., High $\delta^{13}C$ Neoproterozoic carbonate rocks in western North America, Geology, 21, 165-168, 1993.

Woodwell, Grant R., Fluid Migration in an overthrust sequence of the Canadian Cordillera, Ph.D. thesis, Yale University, New Haven, 1985.

Yao, Qinjun and Demicco, Robert V., Dolomitization of the Cambrian carbonate platform, southern Canadian Rocky Mountains: Dolomite front geometry, fluid inclusion geochemistry, isotopic signature, and hydrogeologic modeling studies, American Journal of Science, 297, 892-938, 1997.

Yao, Qinjun and Demicco, Robert V., Paleoflow patterns of dolomitizing fluids and paleohydrogeology of the southern Canandian Rocky Mountains: Evidence from dolomite geometry and numerical modeling, Geology, 23, 791-794, 1995.

Zheng, Yong-Fei, Calculation of oxygen isotope fractionation in anhydrous silicate minerals, Geochimica et Cosmochimica Acta, 57, 1079-1091, 1993.

Zheng, Yong-Fei, Calculation of oxygen isotope fractionation in hydroxyl-bearing silicates, Earth and Planetary Science Letters, 120, 247-263, 1993.

APPENDIX A

EXPANDED OVERVIEW OF FIELD AND ISOTOPIC STUDIES FOR 1998-1999 FIELD SEASONS (INCLUDING OUTCROP DESCRIPTIONS AND MAPS)

Overview of field and isotopic studies for 1998-1999 field seasons

TABLE OF CONTENTS

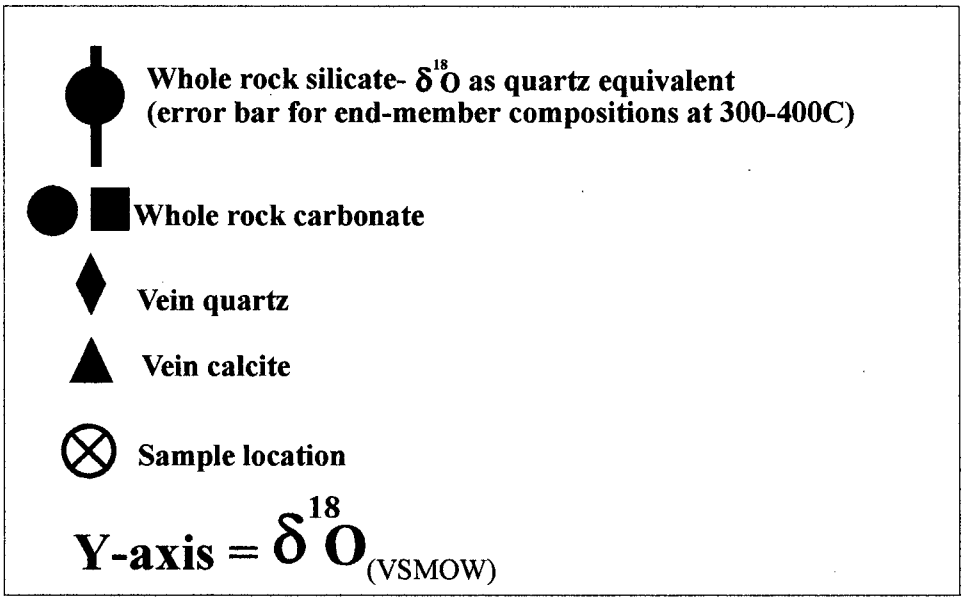
Whole rock silicate- $\delta^{18}O$ as quartz equivalent
(error bar for end-member compositions at 300-400C)
Whole rock carbonate
Vein quartz
Vein calcite
Sample location
Y-axis = $\delta^{18}O_{(VSMOW)}$

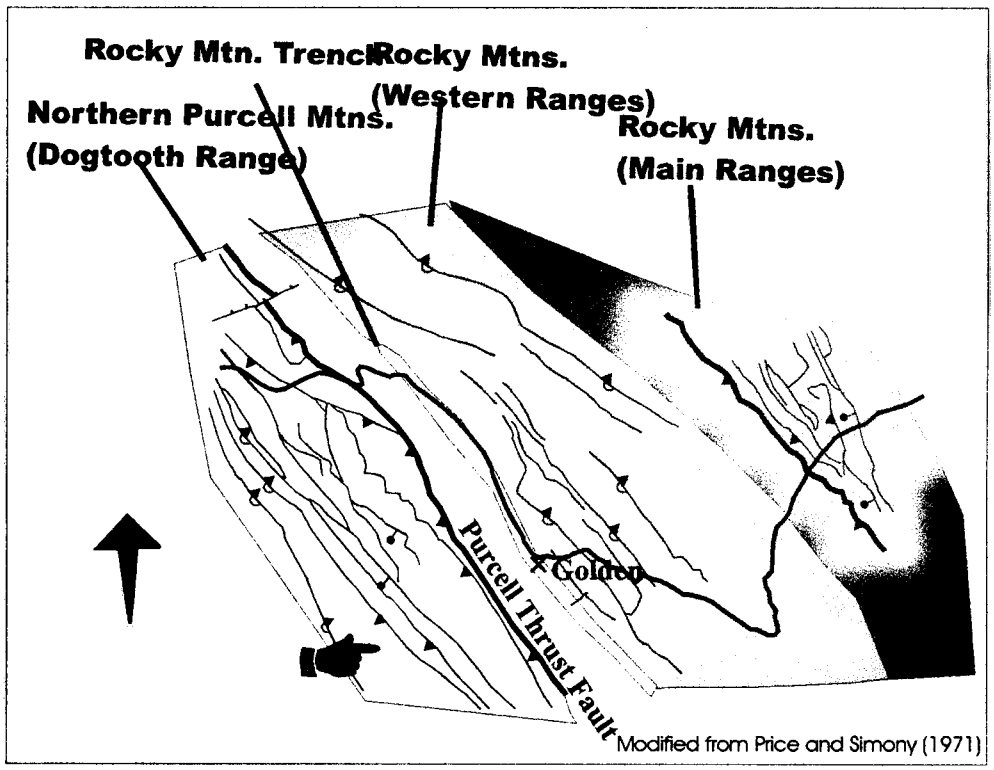
Rocky Mtn. Trench
Rocky Mtns.
(Western Ranges)
Northern Purcell Mtns.
(Dogtooth Range)
Rocky Mtns.
(Main Ranges)
Golden
Purcell Thrust Fault
Modified from Price and Simony (1971)

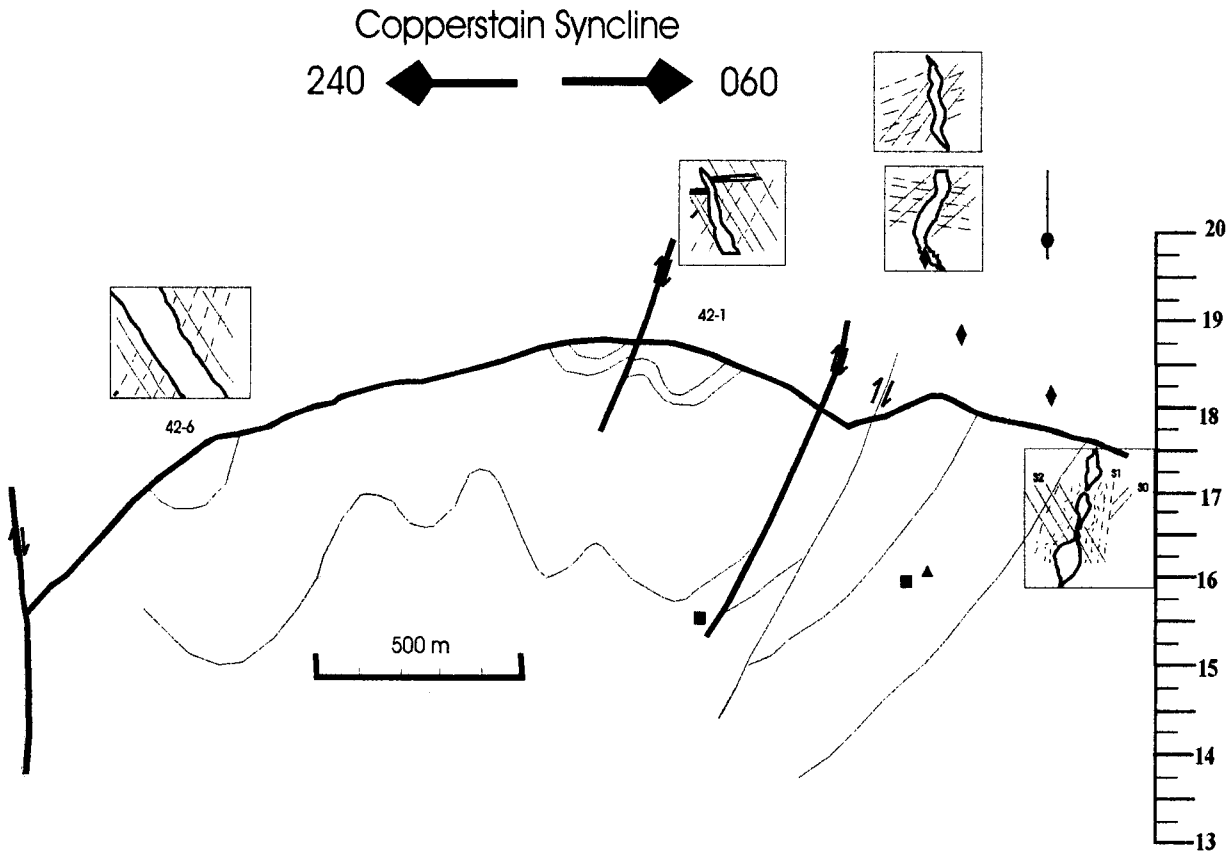
Copperstain Syncline
240
060
42-6
42-1
500 m
20
19
18
17
16
15
14
13

Copperstain Syncline (Day 42)

The westernmost extent of the study area straddles the eastern ridge of Copperstain Mountain along the Copperstain syncline, an upright fold with wavelength > 4.5 km within the footwall of the Grizzly Creek Thrust. The 350 m long traverse crosses carbonate (pChc(ca)) and slate (pChc(sl)) units of the Horsethief Creek Group across the fold's eastern limb. Mean foliation (S1) across the transect is 330/85 NE, and the fold axis, estimated from intersection lineations, is 08/168 SE.

Dark gray, laminated slates interbedded with 0.5-1 m thick beds of limestone are the dominant lithology throughout the lower pChc(ca). Veining within very fissile, less competent slates and phyllites is sparse to non-existent. Although minor thrust faults offset slates within the core of the syncline, veins in the pChc(ca) localize within more competent limestone and siltstone units and are probably linked to non-coaxial shear associated with parasitic folding. Composition of calcareous slates is approximately 45% calcite, 45% chlorite, and 10% quartz with minor occurrences of pyrite and siderite porphyroblasts.

Limestones contain 3-6 mm wide mode I quartz-calcite tension gashes that cross-cut en echelon vein arrays. Folded siltstones and calcareous slates host 4-5 cm wide sigmoidal veins composed of quartz, calcite, and secondary chlorite. Tension gashes are sub-parallel to the a-c plane (i.e. opening direction parallel to fold axis), and sigmoidal, fold-related veins are oriented parallel to hko. Quartz fibers possess core and mantle structures at grain boundaries and are oriented 30° to vein walls (see conjugate shear and extension veins *in Beach*, 1975). Perpendicular to these are cross-cutting, planar calcite veinlets, which are restricted to within the boundaries of the sigmoidal vein and angled approximately 60° to the vein wall (42-4a).

The calcite component diminishes within greenish gray muscovite-quartz phyllites from the upper pChc(sl). Thin sections reveal dense, continuous networks of dissolution seams accounting for up to 40% of the rock volume, and <0.2 mm quartz clasts within microlithons are pervasively flattened and truncated from pressure solution. Quartz grains also exhibit significant crystallographic preferred orientation resulting from plastic deformation by dislocation glide. These units, like the fissile slates above them, are largely unaffected by veining. However, a conspicuous 75 m wide zone of broadly crenulated phyllite contains pervasively boudinaged, S1 sub-parallel quartz veins. Bedding across the outcrop is homoclinal, and an incipient secondary foliation is oriented 335/57 NE. The orientation and restricted occurrence of this fabric in the Copperstain area are consistent with a spaced foliation (S1') possibly linked to the overturning of folds and S1 during movement on the Quartz Creek Thrust (*Kubli,* 1990). Disturbed cleavage zones surround some of the veins where the foliation is isoclinally folded about multiple fold axes. Broad folds with wavelengths of about 30 cm are superimposed upon mm-scale asymmetric crenulations. In thin section, these crenulations reflect a well-developed S2 fabric, interpreted as an artifact of post-metamorphic regional transtension (*Kubli,* 1990).

Average thickness of vein boudins and necks are approximately 8 and 1 cm respectively, and veins are variably affected by folding of S1. Vein quartz is blocky and demonstrates sweeping extinction and internal sub-grain development. Secondary, massive chlorite restricted to zones within vein walls has replaced between 20 and 50% of the vein material. Sub-mm chlorite apophesies extending outward from the vein material merge into parallelism with S1 and are subsequently folded. Because bedding is oblique to the principle foliation, it is

unlikely that parallelism between the veins and S1 resulted from transposition of pre-existing vein sets. This and the concordance of replacement chlorite with S1 demands that quartz vein emplacement (and subsequent chloritization) occurred synchronously with cleavage development. Formation of veins parallel to S1 (i.e. perpendicular to σ_1) is possible only if pore fluid pressure increases during a sudden decrease in differential stress, a scenario specific to conditions following post-rupture stress relaxation at neighboring faults (*Valenta*, 1989). Subsequent distension parallel to S1 results from pure shear during progressive cleavage development (*Ramsay and Huber,* 1983a).

Isotope Results

Oxygen isotopes were analyzed from three veins (two sigmoidal and one S1-parallel) and two wall rocks (one calcareous siltstone and one phyllite).

Sample	42-#	$\delta^{18}O$(measured)	$\delta^{18}O$ (qtz)	$\delta^{13}C$	δH	Temp.
Limestone	1A	15.4	16.3	1.5		
siltstone	4C	15.8	16.8	0.9		
sigmoidal vein qtz	**4A**	***19.7***	***19.7***		-84(musc);-64(chl	***210°(S&K);70***
sigmoidal vein cc	**4A**	***16.0***	***17.0***	***3.0***		
sigmoidal vein qtz	**4B**	***18.9***	***18.9***			
phyllite	5B	16.5	19.9			
cleavage parallel vein	**5C**	**18.2**	**18.2**			

S&K=Sharp and Kirshner (1994);Z=Zheng (1993)

Although vein quartz in the Copperstain syncline is in isotopic disequilibrium with the surrounding matrix, it falls within the wide range of wall rock compositions. Quartz from sigmoidal veins is compositionally enriched relative to the host rock by 2.9 and 2.1 ‰, while overprinting vein calcite is buffered by the surrounding siltstone. Calcite-dolomite geothermometry indicates that maximum temperatures in the Dogtooth reached 360-375° (*Kubli,* 1990). Because the main phase of deformation would likely coincide with maximum depth of burial, low emplacement temperatures of 200° or less are probably not the cause of such large fractionations between vein quartz and calcite (*Sharp and Kirshner,* 1994*; Zheng,* 1993). Enrichment in silica more likely resulted from either outcrop-scale equilibration with host rock compositions or down temperature fluid migration (up-structural section) during local folding and faulting.

Distended cleavage parallel veins are depleted by 1.7 ‰ relative to adjacent phyllite. This discrepancy demonstrates infiltration of fluids that have not fully exchanged with surrounding rocks. However, the vein signature is intermediate between that of nearby wall rocks (16.8-19.9 ‰(qtz)). Isotopically distinct vein sets might then reflect a single fluid cell that is buffered by rocks across a minimum of 200 m.

Main points

- vein are generally excluded from fissile slates
- veins form during fold-related simple shear and utilize anisotropy along cleavage planes
- veining and secondary chloritization was synchronous with cleavage formation
- secondary calcite is buffered by surrounding carbonate
- veins are out of equilibrium with immediate host rocks, but homogenized over 200 m

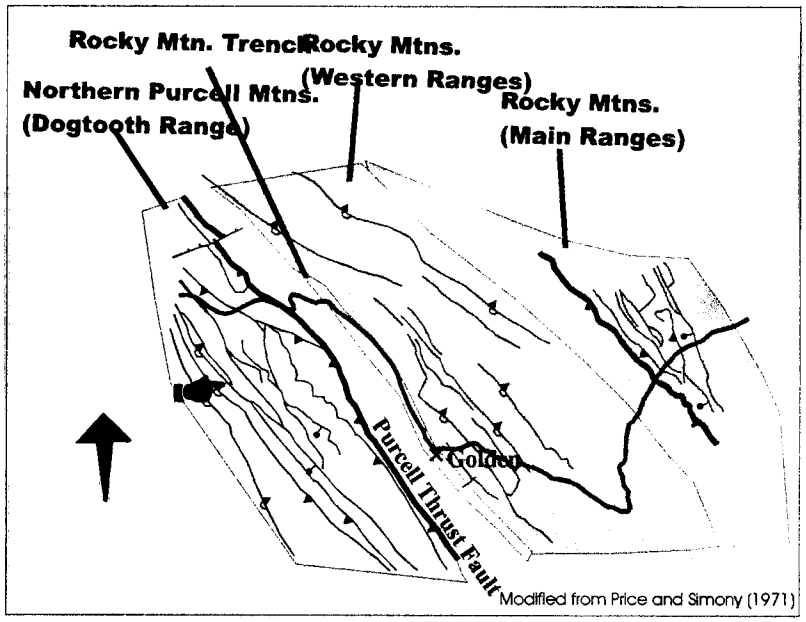

Heather Mountain Thrust at Quartz Creek

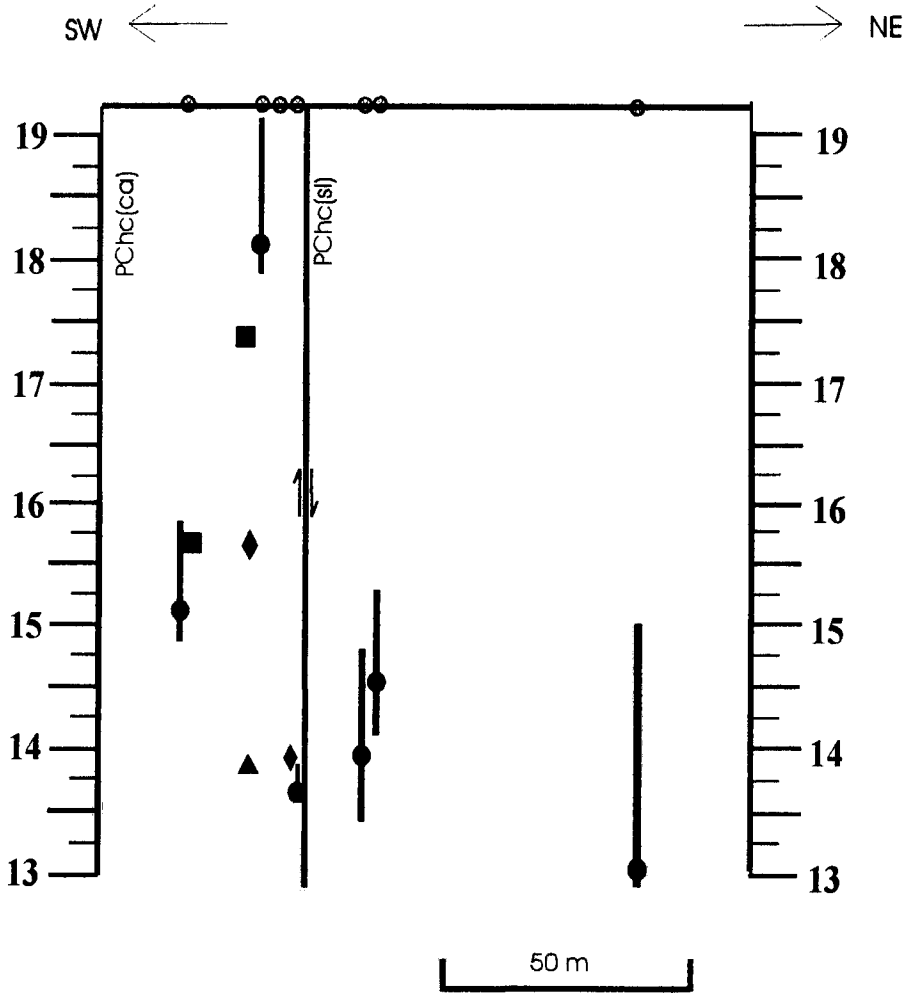

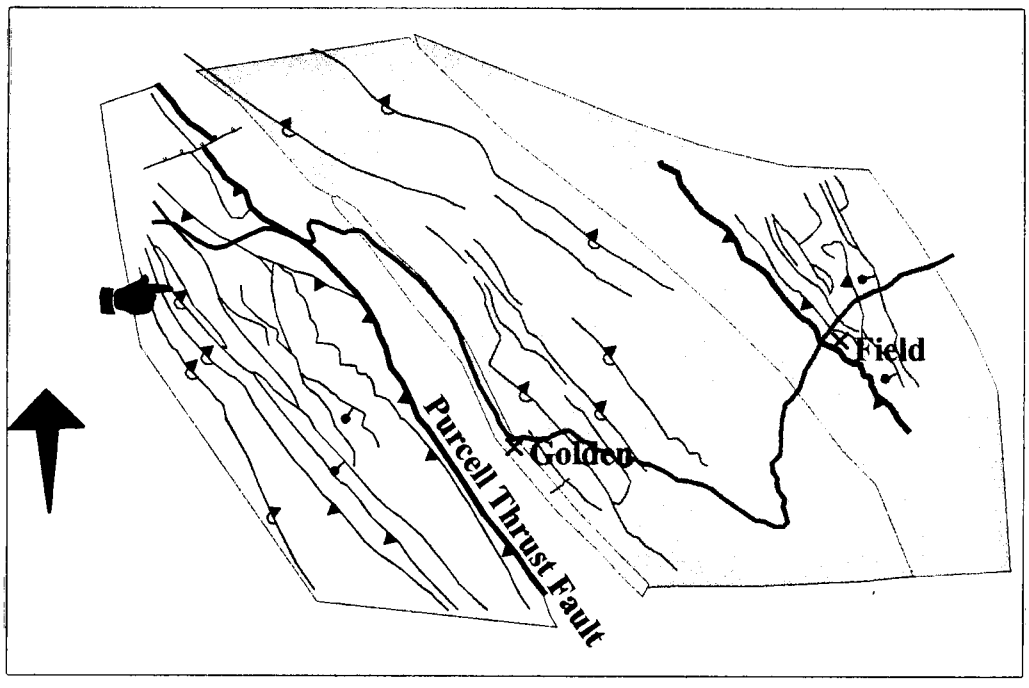

Heather Mtn. and Prairie Hills Thrusts at Heather Mountain

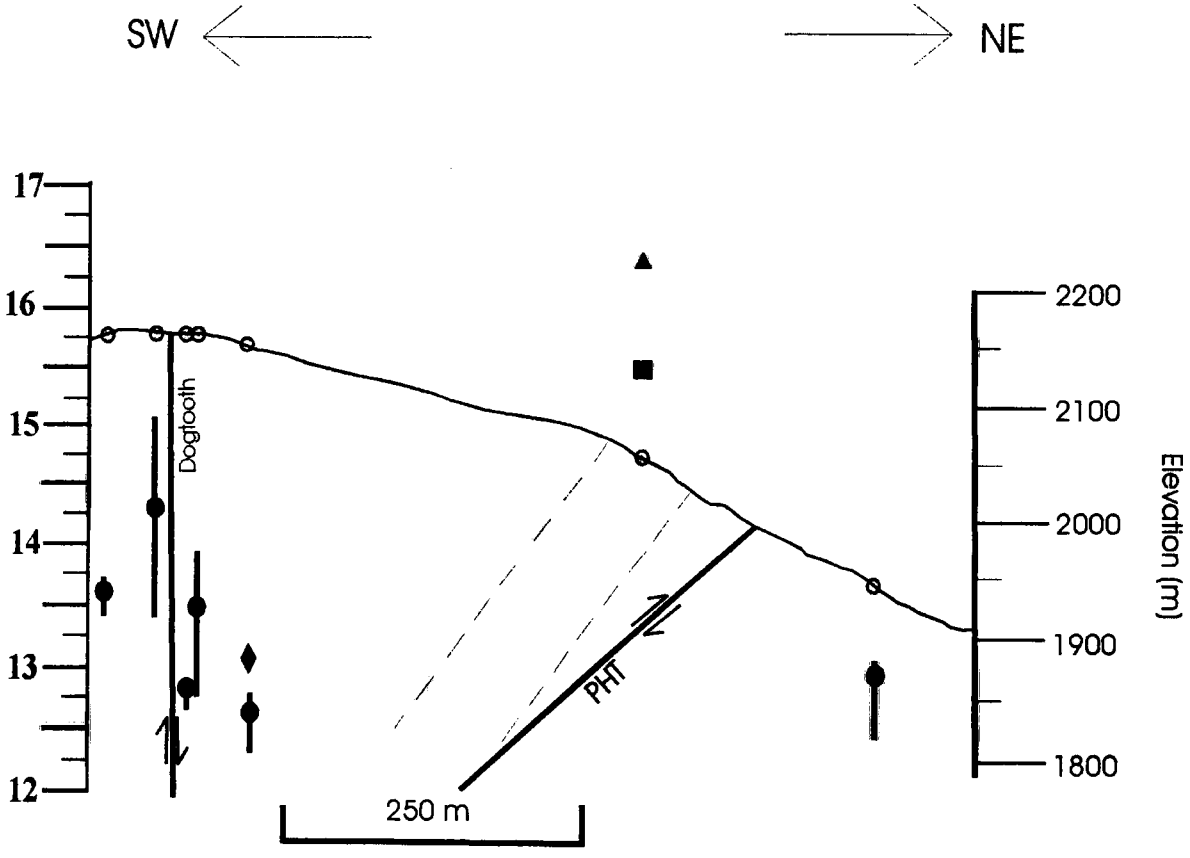

Heather Mountain Thrust and Prairie Hills Thrust (Days 16 and 17)

The Heather Mountain Thrust (HMT), formerly the Dogtooth Thrust, signifies the easternmost occurrence of lower Cambrian units in the Dogtooth Range. It is a steeply dipping detachment, overturned to the northeast, that juxtaposes sequences of the Horsethief Creek Group (pChc) with those of the Hamill Group (Ch). Because the Quartz Creek Thrust (QCT) accommodates much of the strain north of Grizzly Creek, displacement on the HMT reaches a maximum of only 500 m (*Kubli and Simony,* 1994). The Prairie Hills Thrust (PHT), an earlier fault that outcrops 300 m into the footwall of the HMT, accounts for at least 1800 m of displacement. Samples were collected along 300-500 m transects at two localities 8.5 km apart. The southern locale is a ridge to the west of Quartz Creek, where dolomitized slates, sandstones, and dolomites of pChc(ca) are emplaced upon argillites and muscovite-chlorite phyllites of pChc(sl). At the northern exposure near Heather Mountain, recessive muscovite-quartz phyllites and quartz sandstone of pChc(ca) are thrust against upper Hamill quartzite. The faults are poorly exposed, limiting sampling accuracy to 5-20 m. Exposures lack evidence of strain localization from cataclasis and ductile fabric development, and fault contacts were inferred from stratigraphic discontinuities. This insinuates that rupture was either limited to a very narrow (<1 m) contact between incompetent Proterozoic phyllites and rigid Hamill quartzites, or that transport was broadly distributed throughout a brittle damage zone (>20 m), the evidence for which being diffuse veining within the quartzites and massive carbonates.

Cleavage

Steep, northeast dipping cleavage at both localities is defined within slates by dense networks of hematized and/or oxidized pressure solution seams (3c,3d,2b) that truncate clasts of quartz and dolomite. Pressure shadows and rotation of 0.1-0.75 mm clasts indicates pervasive non-coaxial shear along foliation planes. Fabric within more competent dolomite, grit, and quartzite is rare and represented by sinuous, discontinuous <100 μm wide muscovite seams (2b). Narrow, 15 cm wide shear zones occur within muscovite schists from pChc(sl). The zones are conspicuous, due to the presence of blocky, intensely strained quartz veins with thorough sub-grain development. Chlorite overprints vein margins and fills quartz microcracks (16-3g,h).

Slate hosted veins

Strain partitioning by pressure solution and ductile processes results in limited vein development within slates. With the exception of shear zones mentioned above, only rare occurrences of veinlets parallel and sub-perpendicular to S1 are observed within both hanging wall and footwall slates. Approximately 7 m into the hanging wall, anastomosing 1 mm wide quartz veinlets are folded at mm-scale about S1(16-2d). Vein quartz is polygonal and blocky with minimal internal strain, and portions of the veinlets are rimmed or internally replaced by fibrous chlorite along dissolution seams. Mutual cross-cutting and offset of vein material by S1 in conjunction with the absence of internal deformation within the quartz is consistent with vein formation being contemporaneous with cleavage development.

Dolomite and quartzite hosted veins

Veining within Horsethief Creek dolomites and Hamill quartzites is sporadic and exhibits no clear correlation with proximity to fault zones. Vein orientations are sub-parallel to the a-c/b-c planes, indicating a geometric relationship between veins and the regional fold axis. Dilation might result from fracturing linked to flexural slip on m-scale folds. Quartzite hosted veins are 8-10 cm wide and consist of >5 mm grains of milky quartz, sub-mm grains of entrained plagioclase, and lenses of fibrous muscovite. Sub grains are pervasive, and deformation lamellae are oriented perpendicular to vein walls (17-2i). Isolated systems of en echelon vein arrays were also observed >100 m into the footwall. The high angle between tension gash and shear zone boundary is evidence for negative dilation during local shearing (*Ramsay and Huber,* 1983a). Also notable is a small, 20 cm wide shear zone within a grit unit adjacent to the HMT. Relict sedimentary textures are absent, and quartz has passively recrystallized, either because of fluid infiltration or overgrowth in silica oversaturated pore fluid. Core and mantle structures and sub-grain rotation are evident, but not pervasive, in larger quartz grains. The size contrast between these coarse (4 mm) grains and the matrix suggests that a veining or diffuse fluidization event introduced secondary quartz into the system that underwent subsequent ductile strain. Secondary dolomite overprints relict plagioclase, but is in apparent equilibrium with the coarser grained "vein quartz". Thus, fluidization within some units might manifest as pervasive replacement of matrix minerals as well as fracture filling veins.

Dolomite beds are riddled with brittle fractures and accompanying fibrous, quartz-calcite-dolomite-muscovite bearing veins (17-3e;16-3b). The veins do not cross bedding contacts with siliceous units and exhibit multiple orientations that are consistent with a prolonged dilation history in an evolving local stress field. Minor curvature of quartz and calcite fibers illustrates both syntaxial and antitaxial morphologies. All phases appear to be in textural equilibrium. Despite consisting of >95 % carbonate, veins are multi-phased indicative of fluid infiltration from an external source.

Isotope Results

Oxygen isotope analyses included fourteen whole rock and five vein samples from both localities. Two dolomites were sampled: a 0.2 m thick bed 10 m into the hanging wall of the HMT and a 75 m thick package approximately 50 m into the hanging wall of the PHT.

		Sample	d18O (measured)	d18O(qtz)	d13C	dH	Temp.
QUARTZ CREEK	**Hanging Wall**	calcareous slate(17-3C)	10.8	15.1			
		s/a-calcite	15.6	16.6	-2.8		
	<20 m from fault	phyllite(17-3D)	13.7	18.1			
		dolomite(17-3E)	17.3	18.4	-0.9		
		fibrous calcite(17-3E)	***13.8***	***14.8***	***-2.4***		***400°(S&***
		fibrous quartz(17-3E)	***15.7***	***15.7***			***200°(Z)***
		recrystallized s-s(shear zone)(17-3F)	***13.6***	***13.8***			***260°-35 (cc-dol)***
		silicified material(17-3F)	***13.9***	***13.9***			
	Footwall	***altered chlorite phyllite(shear zone)(17-3G)***	***9.5***	***14***			
		altered chlorite phyllite(17-3H)	***9.3***	***14.5***			
		chlorite phyllite(17-3K)	10.2	14.2			
HEATHER MTN.	Hanging Wall	grit(16-2B)	13.4	13.6			
	7 m from fault	phyllite(16-2D)	10	14.3			
	Footwall	quartzite(16-2E)	12.5	12.8			
		dissolved quartzite(16-2G)	11.1	13.5			
		dissolved quartzite(16-2I)	11.9	12.6			
		planar, a-c vein(16-2I)	***13.1***	***13.1***			
	<100 m into PHT hanging wall	dolomite(16-3B)	15.5	16.5	1.6		
		fibrous vein cc(16-3B)	***16.3***	***17.3***	***-0.4***		
		fibrous vein muscovite(16-3B)				***-110(musc)***	
	footwall PHT	quartzite(16-1A)	12.3	12.9			

Isotopic disequilibrium of fault rocks and veins relative to their hosts within 20 m of the HMT and PHT was not observed. Oxygen isotope compositions from grits and phyllites within the pChc(ca) unit in the HMT hanging wall exhibit a wide spread of values between 13.6 and 18.4 ‰ (qtz). Footwall phyllites from pChc(sl) possess $\delta^{18}O$ signatures that are uniform (14-14.5 ‰(qtz)), in contrast to their diverse mineralogy. Hamill quartzites from within the HMT and PHT footwall are lithologically, and therefore compositionally homogeneous with signatures between 12.6 and 13.5 ‰(qtz). Although recystallized and dolomitized sandstone (17-3F) from a shear zone near the DTF is depleted by 4.3 ‰ with respect to adjacent phyllites, its composition is consistent with that of a similar, unsheared unit at the northern locality, suggesting that the discrepancy reflects lithologic variations rather than infiltration of isotopically exotic fluids. Thus, an increasing quartz component coincides with diminished $\delta^{18}O$ values in pChc(ca).

Only in one dolomite sample were veins out of equilibrium with the protolith. Approximately 20 m into the DTF hanging wall, a 20 cm thick dolomite bed hosts antitaxial quartz and calcite which are depleted relative to their host by 2.6 and 3.5 ‰, respectively (17-3E). Although the possibility exists that progressive fracturing of the dolomite promoted bedding parallel flow of a lower $\delta^{18}O$ fluid, a simpler explanation would be cross-bed, outcrop scale circulation of fluids that had exchanged with depleted quartz rich units such as those noted above. In such an instance, vein compositions would reflect "average" signatures of units throughout the circulation system (see *Gray et al.,* 1991). Migration of fluids at the scale of >10's of meters is thus inferred.

Because siliceous phyllites and sandstones are lithologically dominant over a surrounding radius of at least 40 m, such a low vein calcite signature is significant. Under such circumstances, fluid-rock ratios would have to be low enough to promote isotopic exchange between H_2CO_3 (the carbonate bearing species at high temperatures) and silicate minerals. The link between this local fluid cell and the growth of fracture networks around the fault zone is ambiguous. It is notable that vein calcite from within a densely fractured, much wider (75 m) dolomite bed over 50 m into the hanging wall of the shows no evidence of exchange between vein forming fluids and the surrounding quartzites, which have signatures up to 4.4 ‰ lower than that of the dolomite. Either the significant thickness of the bed promotes rock buffering of circulating fluids, or distance from the fault zone disallows the creation of a through going fracture network.

Both vein calcite samples show respective $\delta^{13}C$ depletions of 1.5 and 2.0 ‰. In each instance, fluids had not yet equilibrated with the surrounding rock. In the case of a low X_{CO2} fluid, carbon is expected to isotopically homogenize with rock compositions prior to oxygen equilibration. Perhaps the above depletions reflect a flow path through a high volume of siliceous units, allowing fluids to partially retain their initial $\delta^{13}C$ signature.

Based on hydrogen isotope fractionation between muscovite and H_2O, a single analysis of syn-kinematic muscovite within a fibrous vein equates with a δD signature of -70 ‰ for water. Determination of a fluid source is ambiguous, because this value is consistent with compositions of both meteoric water and water derived from metamorphic devolatization reactions.

Main points

- fault zone poorly defined
- no spatial or isotopic correlation between veins and fault zone
- shear zones in upper and lower plate defined by local fabric, thick veins, chloritization
- wide variance in wall rock $\delta^{18}O$
- fluid flowing through 20 cm wide dolomite bed exchanged with silicates and carbonate units i.e. isotopic homogenization of fluids

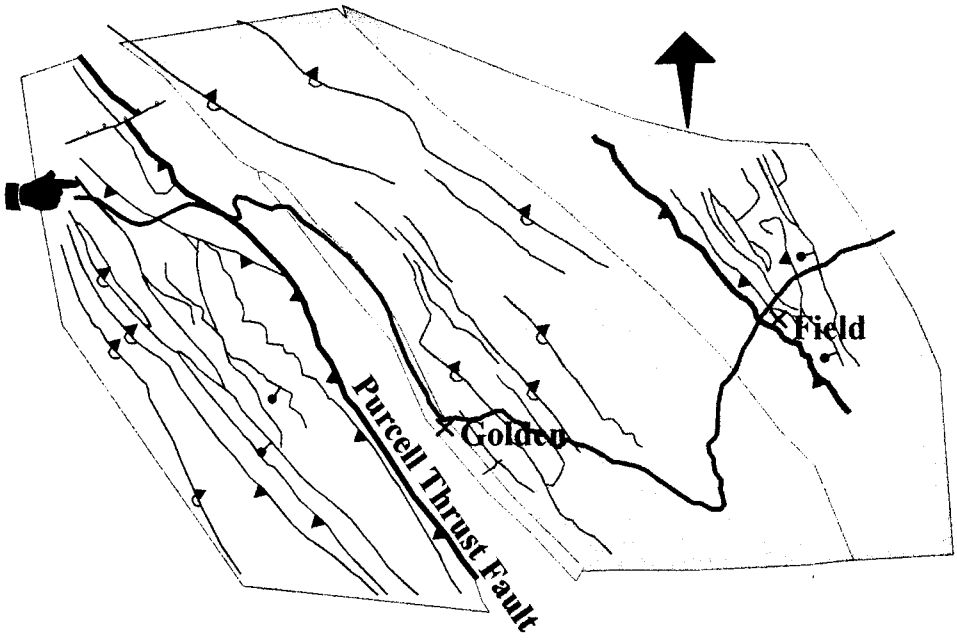

Quartz Creek Fault at Kinbasket Lake

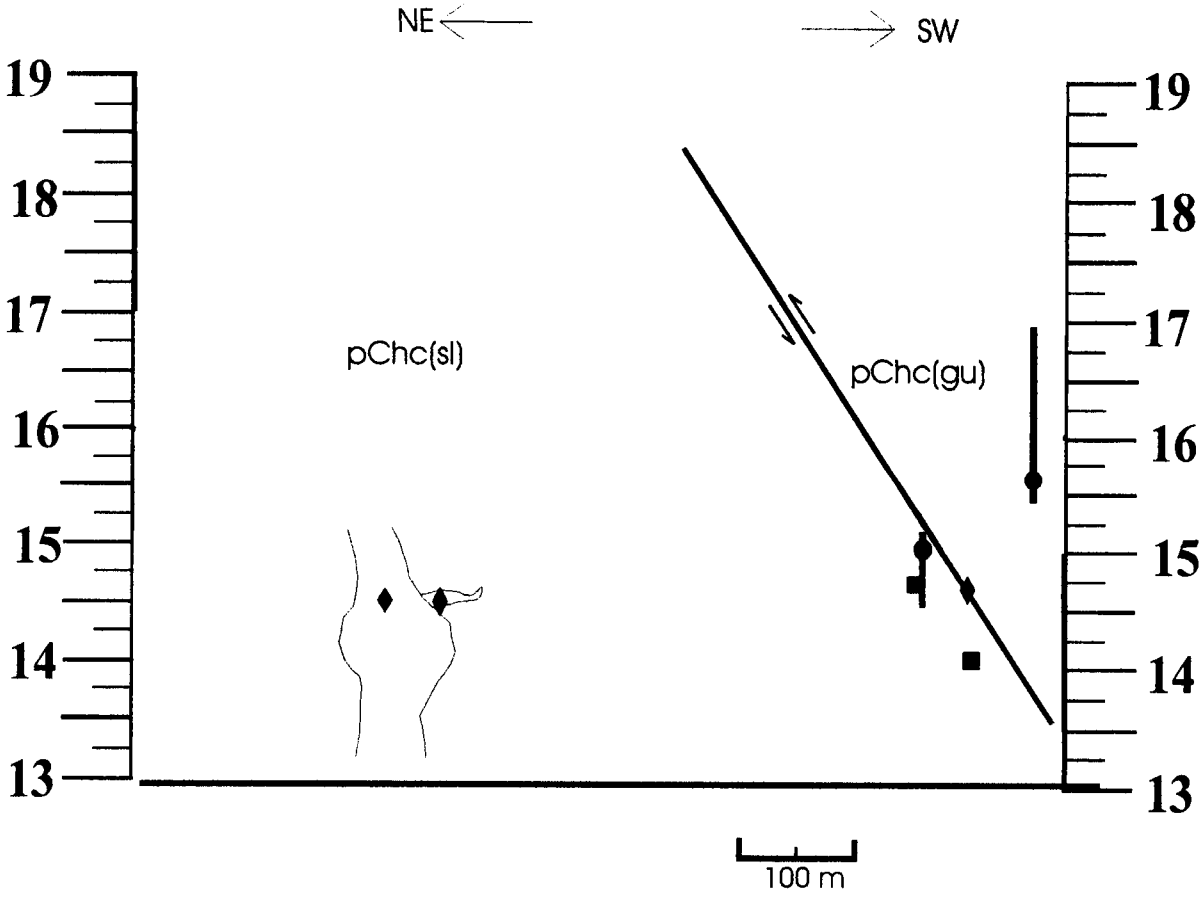

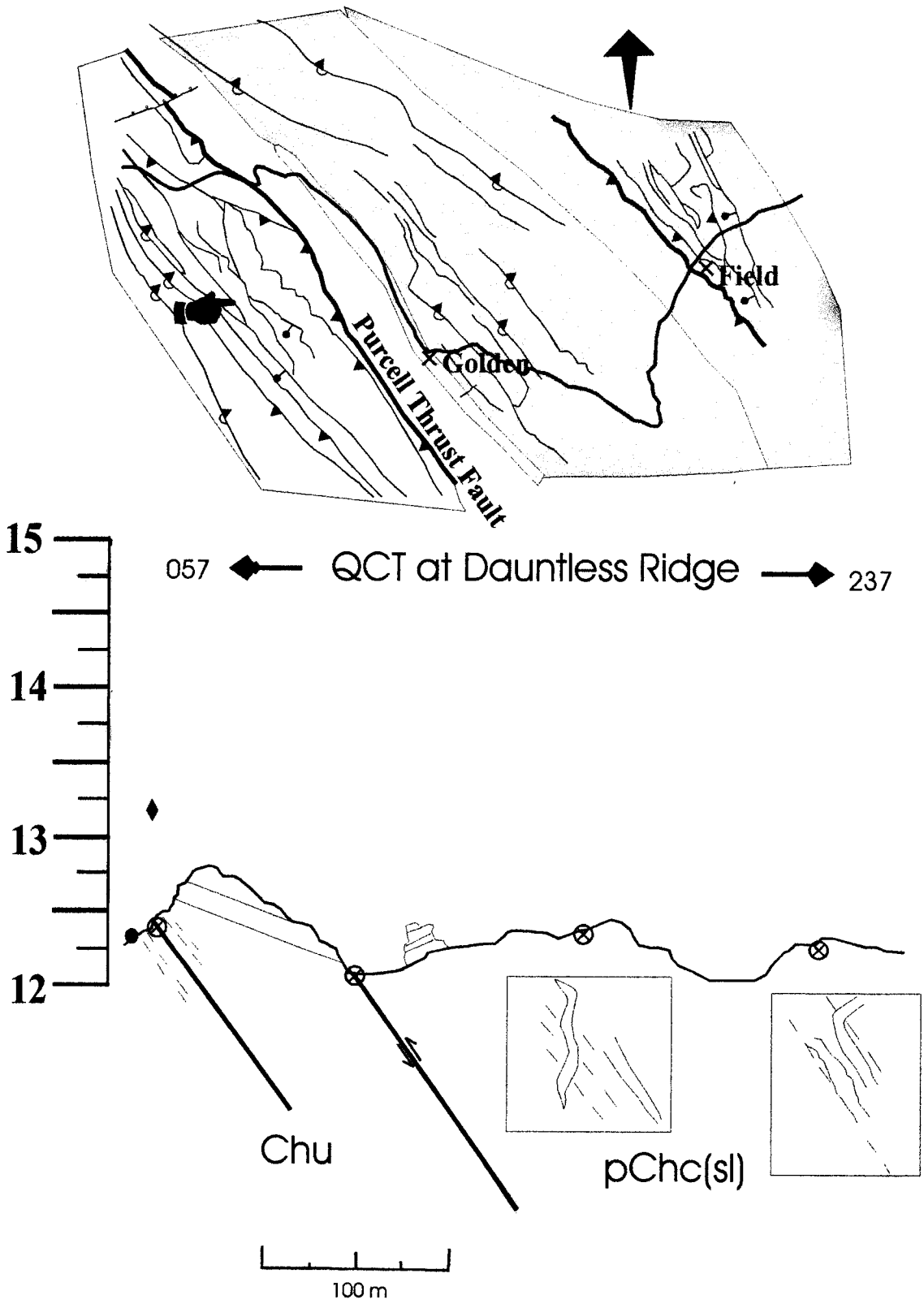
Field
Golden
Purcell Thrust Fault
15
14
13
12
057
QCT at Dauntless Ridge
237
Chu
pChc(sl)
100 m

Quartz Creek Thrust (Days 34 and 43)

Throughout much of its strike length, the QCT places recessive slates and grits of pChc(gu) upon similar type strata within pChc(sl). Despite limited outcrop in the Quartz Creek valley, the fault contact is exposed at two localities. A railroad cut along Beaver Creek north of Highway 1 exposes about 250 m of outcrop on either side of the fault zone, and 20 km to the south, continuous outcrop along a ridge east of Dauntless Mountain reveals the thrust contact between Chu and pChc(sl). However, pervasive weathering of slates and poorly exposed fault features preclude comprehensive isotopic analysis at the southern locality. Displacement on the QCT is estimated at 3-5 km, and its linkage with the Dogtooth Thrust to the south indicates a prolonged slip history for the fault (*Kubli and Simony*, 1994). Movement on the QCT following cessation of the Heather Mountain Thrust probably resulted in the overturning of structures observed in the western Dogtooth Range (*Kubli*, 1990).

Beaver Creek

At Beaver Creek, folds, quartz veins, minor faults, and the QCT are closely associated. The QCT is delineated by a 10 m wide gully that separates foliated quartzite and muscovite-quartz schist in the hanging wall from graphitic slates and muscovite schist of the footwall. Although fault related fabrics related to cataclasis or ductile shear were not observed at the mesoscopic scale, intensification of veining and secondary silicification of wall rock phyllites within 5 m on either side of the gully attest to the focussing of fluids along the fault zone during rupture. The principal foliation (S1) in the gully walls is steep but broadly folded constraining latest motion on the QCT to post cleavage development. Penetrative cleavage throughout the hanging wall and footwall exhibits a mean orientation of 149/64 SW, consistent with that of the fault.

Hanging Wall

Strain in hanging wall phyllites is accommodated by pressure solution cleavage and NW-plunging isoclinal folds overturned to the NE. Approximately 50 m from the fault, foliated sandstone beds approximately 30 cm wide are separated by thin layers of phyllite. Microlithons 5mm wide highlight spaced cleavage with characteristic refraction between units of differing rheology. In contrast to the sparse veining in the phyllites, sandstones host uniform, evenly spaced en echelon quartz veins 0.5-2 cm wide and 1.5 m long. Most are distinctly planar, uniform in orientation (40° angle with cleavage) and are spatially restricted to 0.75 m thick beds (i.e. not overstepping). However, veins of the same size and orientation that extend across bedding contacts exhibit a "ladder" morphology indicative of either folding or sequential vein growth during slip on cleavage planes. Larger, 15 cm thick veins also cross contacts, and suggest that the mechanical process resulting in vein formation occurred at multiple scales. The coexistence of planar, cross-cutting veins and those which are apparently folded or offset along S1 brackets the timing of vein formation as syn-kinematic with respect to cleavage.

Fault zone

Although the QCT itself is not well exposed, a unique population of S1-parallel quartz veins and microstructures within the surrounding quartzite expose a zone of intense strain localization and possible fluid

flow. Veins are typically 1-5 cm wide and discontinuous, possessing an arrhythmic pinch and swell morphology (34-2b,c). Vein quartz is blocky and substantially deformed by sub-grain rotation. A dense network of microcracks, some replaced with calcite and muscovite, align sub-perpendicular to the surrounding foliation. Irregular, sub-mm seams run parallel to the surrounding cleavage. The seams consist of muscovite with grains of quartz, plagioclase, and calcite entrained within them. The presence of *protolith* minerals indicates that these are thin veneers of wall rock that represent a plane of weakness on which fracturing initiated and *not a zone of secondary pressure solution (*i.e. post-vein*)*. Because the lenses bear a resemblance to unevenly spaced cleavage planes within adjacent wall rock, I believe vein forming fractures initiated after S1 development in the quartzite. This, and the degree of internal strain demonstrated within the vein quartz requires that infiltration occurred following S1 initiation but before cessation of compressional stress.

Pervasive dynamic recrystallization throughout surrounding quartzite results in well defined shape preferred orientation among quartz grains that defines a foliation sub-parallel to the fault plane. Larger (> 1 mm) grains are mantled by sub-grains and are consistently rotated, creating pressure shadows infilled with very fine grained quartz and muscovite. The shear sense defined by the lensoidal shape of larger grains varies throughout samples. Discontinuous muscovite seams that rim larger grains of quartz are sub-parallel to the surrounding fabric. However, soma mica seams and isolated lenses of recrystallized quartz grains are oriented transversely across the main foliation at a constant angle, indicative of an incipient C-fabric (34-2a). Plagioclase accounting for less than 5 % of the sample is largely unaffected by sub-grain rotation and grain boundary migration observed in quartz. Widespread truncation of feldspar boundaries by mica seams is evidence that pressure solution is a main mechanism of strain accommodation in plagioclase. Because dolomite grains replace quartz but are truncated by pressure solution seams, infiltration of carbonate bearing fluids into the host rock occurred *before or during tectonism.*

Footwall

Footwall splay faults sub-parallel to the regional foliation and QCT are evident through the extent of exposure (≅ 400 m NE of QCT). Fault zones are typically 1-20 m wide and are highlighted by moist, black, heavily weathered slate due to groundwater seepage. Apparent drag folds in S1 adjacent to some splay faults show that latest displacement occurred after cleavage development. The orientation of these indicates top to the northeast and therefore reverse displacement, thus constraining faulting and associated veining to Mesozoic in age. Despite the presence of multiple generations and morphologies of veins, the majority of them precipitate immediately adjacent to and within fault zones. All veins have been subjected to ductile and/or brittle deformation and were therefore emplaced during ongoing strain within the fault zone.

The earliest are 1-6 cm wide, quartz filled, and sub-parallel to S1. These have subsequently been folded with the foliation, presumably during faulting. Similar but later stage quartz veins are also S1-sub-parallel but are offset across foliation planes. Their thickness is widely variable and they connect with or are folded into veins perpendicular to cleavage. Randomly oriented segments of wall rock phyllite are entrained within them, and they have a discontinuous, fractured quality consummate with slip and rotation of the surrounding fabric.

The latest, but most prominent, footwall veins are boudinaged, S1-parallel, and composed of quartz and dolomite (34-3b). They are located 350 m into the footwall and propagate at the contact between foliated quartzite and the weathered fault rock discussed above. They vary in width between 4 and 15 cm and cross-cut an en echelon array of sigmoidal quartz veins (3c). Because they post-date local shear zones but are themselves distended, timing of emplacement is constrained as syn-kinematic. Microscopically, quartz has undergone rampant dynamic crystallization evident as elongate grains parallel to foliation and serrated grain boundaries. Localized domains of quartz traverse across the main foliation and reflect an incipient C-fabric. Veining in the footwall is therefore related to numerous splay faults and manifests as multiple generations of fluid events during non-coaxial (and possibly coaxial) shear. The association between veins both parallel and oblique to S1 indicates that ambient differential stresses varied in magnitude and perhaps orientation during deformation. Evidence of extension both perpendicular and parallel to S1 exemplifies this phenomenon.

Dauntless Ridge

Lack of vein material and pervasive alteration at the QCT contact along Dauntless Mountain ridge precluded sampling for isotopic analysis. Vein styles further into the hanging wall slates of pChc(sl) include fibrous, sigmoidal quartz-carbonate veins indicative of fold related shear within more competent beds as well as cleavage parallel veins (*see* Copperstain syncline). Buttressing of the relatively incompetent slate unit against quartzite in the Hamill Group results in minimal strain partitioning in the footwall. However, approximately 100 m from the QCT, an anomalous, through-going shear zone penetrates the quartzite creating a 1 m thick foliated zone. The zone is distinguished by a foliation defined by elongate quartz grains and muscovite domains in sharp contrast with the massive quartz-feldspar sandstone in the surrounding package. The foliation dips steeply NW and forms an angle of about 90° with the regional fabric. Because of this discrepancy, the shear zone probably does not represent a splay off the QCT. Instead, it is more likely a local fault that accommodates strain during megascopic, flexural slip folding within the 500 m thick sequence of quartzite.

Microstructures display quartz sub-grains that are 3 mm in length and oriented sub-parallel with the foliation. Small segments of healed ribbon quartz are oblique to the local fabric, and aspect ratios within the surrounding quartz exceed 10:1. The more elongate grains are kinked and form discontinuous folds with amplitudes of 2 mm. It is ambiguous whether these features represent ongoing strain of the protolith or complete replacement by vein material and subsequent deformation. However, the degree of quartz elongation and lack of plagioclase typical in the protolith indicate that quartz within the shear zone is secondary. The kinked nature might therefore reflect simple shear within vein fibers that have subsequently been distended parallel to the shear zone. If true, the extension direction during vein propagation was sub-perpendicular to S1, with simple shear occurring parallel to the fabric. High pore fluid pressures are the probable cause of brittle dilation normal to S1 during initial stress build-up. The discontinuity of fibers throughout thin sections suggests *multiple*, small scale veining episodes preceeded intense, plastic deformation during non-coaxial strain across the shear zone. The high density of vein material within the shear zone indicates that fluid channeling might have been crucial in localizing fracture and dislocation climb during deformation.

Isotope Results

At Beaver Creek, oxygen isotopes were analyzed from two wall rocks and three veins. One sample of quartzite protolith and another from the footwall shear zone were analyzed from Dauntless Ridge.

		Sample	$\delta^{18}O$ (measured)	$\delta^{18}O$(qtz)	$\delta^{13}C$
Kinbasket Lake	Hanging Wall	muscovite phyllite (34-1C)	12.2	15.7	
	Fault	***S1-parallel vein***(34-2B)	***14.7***	***14.7***	
	Fault	**s/a-median suture-cc**	**14.1**	**15.1**	**-11.6**
	Footwall	foliated qtzite(34-2A)	14.2	15	
		s/a	14.7	15.7	-9.9
		distended, S1-parallel vein (34-3B)	***14.5***	***14.5***	
		cross-cut, sigmoidal vein (34-3C)	***14.5***	***14.5***	
Dauntless Ridge	Footwall	Hamill Quartzite(43-4B)	12.5	12.5	
	Shear Zone	***foliated qtz-musc vein*** (43-4A)	***13.1***	***13.5***	

There is no evidence from the oxygen isotope data to suggest that fluids originating from an exotic reservoir advected across km's and channeled along the Quartz Creek Thrust and its coexisting splay faults. Even though each vein reflects a distinct fluidization event, fluids present during ongoing tectonism were compositionally uniform and therefore derived from a common source. The observed fractionation between veins and foliated quartzite at Kinbasket Lake (0.2 - 0.5 ‰) falls within the calculated uncertainty from estimation of temperatures of formation and host rock composition. Quartz veins are depleted relative to the hanging wall phyllite by at least 0.9 ‰ after accounting for uncertainty. Fluid communication across the QCT from the upper into the lower plate (>90 m) was therefore either non-existent or occurred at very low time-integrated fluid fluxes. Vein forming silica either derived from adjacent footwall sandstone and was precipitated under closed-system conditions, or diffusive mass transfer permitted homogenization of veins and wall rock during protracted ductile strain (see *Kirschner et al.* , 1995b). Because veins with different degrees of internal deformation have similar isotopic signatures, the former scenario is more likely.

The shear zone at Dauntless Ridge is enriched by 1.0 ‰ relative to its undeformed protolith. Due to the paucity of data, the possibility that this fractionation might reflect variations in wall rock composition cannot be ruled out. Perhaps the enrichment observed in the veins is an artifact of down-temperature fluid migration from a deeper source. However, it is reasonable to conclude that the fluids focussed into the shear zone were in near isotopic equilibrium with the surrounding package, and did not retain the oxygen composition of their distal reservoirs (i.e. meteoric, connate, or metamorphic).

Main points:

- association between faults and veining
- veins at both localities and muscovite-quartz schists (at Kinbasket Lake) have undergone intense plastic deformation

- at Dauntless Ridge, shear zone in footwall quartzite perhaps reflects multiple brittle veining events followed by ductile, simple shear
- no evidence of infiltration of meteoric, connate, or metamorphic fluids (or very low fluid-flux)
- despite different vein styles and timing of formation, compositions are uniform and buffered by host quartzite (at both localities)
- no evidence of exchange between hanging wall phyllites (>90m from QCT) and syn-kinematic veins at fault and in HW; therefore, no fluid coupling across the QCT

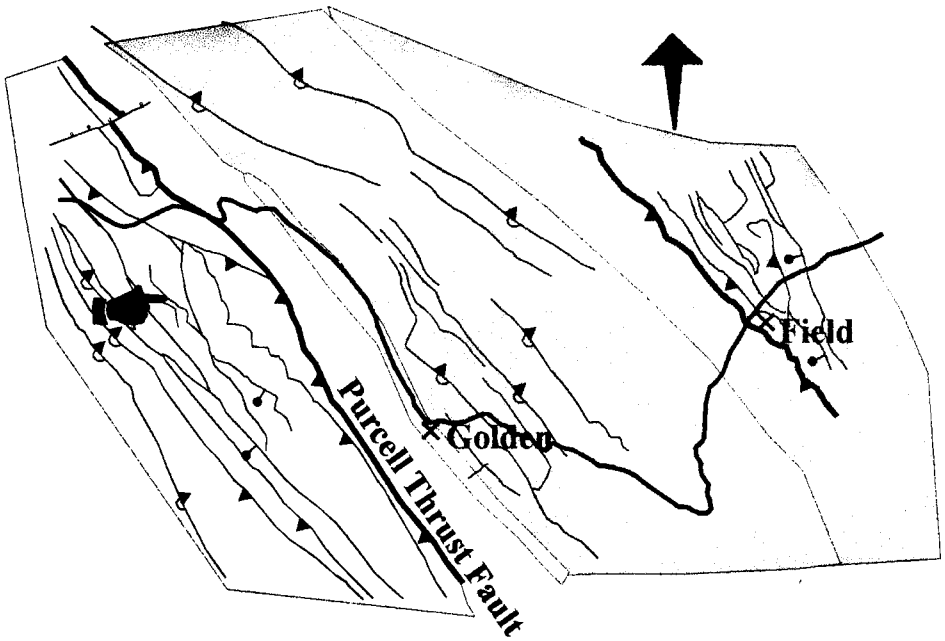

SW ← Unnamed Fault at Quartz Creek → NE

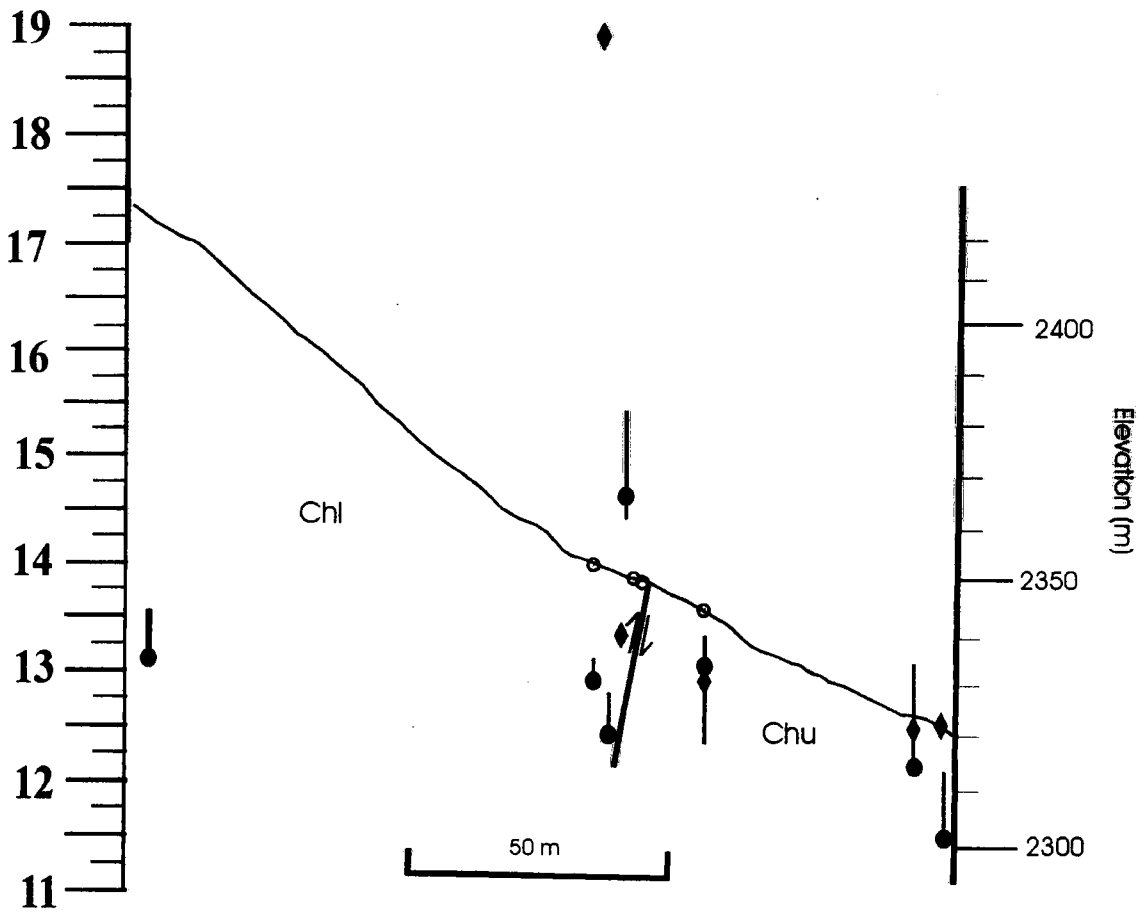

Unnamed Fault east of Quartz Creek (Day 18)

A series of northwest trending thrust faults are exposed along ridges south of Fish Lake and east of Quartz Creek in the north-central Dogtooth Range. They are possibly part of system of splays off the Quartz Creek Thrust that transfer motion onto the Wall Thrust, which first appears near the southern termination of the Fish Lake Syncline (*Kubli*, 1990). The fault I examined places lower Hamill quartzite and slate upon similar strata in the upper Hamill, and therefore has minor displacement of less than 350 m. Because of the similarities in footwall and hanging wall strata, coupled with the absence of fault related fabrics and a distinct fracture zone, I relied upon map interpretations and an abrupt discontinuity in bedding orientation to constrain the location of UF. Sampling accuracy with respect to the exact fault location was therefore limited to within 50 m.

Hanging wall alteration zone

Although massive quartzite units dominate both sides of the fault contact, a 100 m wide sequence of orange, oxidized dolomite interbedded with green phyllite outcrops 100 m into the hanging wall. Muddier horizons within the dolomite possess a spaced foliation defined by moderately SW-dipping chloritized horizons(18-2J). Massive quartz veins > 15 cm wide are abundant in the unit, but exhibit no preferred orientation. Adjacent quartzite is substantially more deformed than its protolith. Whereas typical Chl comprises sub-rounded quartz grains with point contacts suggestive of relict sedimentary textures(18-2E), quartzite proximal to this "alteration " zone has undergone pressure solution such that muscovite oriented parallel to the regional foliation rims all grain boundaries (18-2G). Solution transfer in quartz grains leads to elongation parallel to S1 and aspect ratios of 2:1. Lenses of very fine grained quartz (< 20 μm) define zones of reprecipitation of silica derived from adjacent grain boundaries. Interspersed horizons of > 50 % muscovite entrain angular, 0.5 mm wide quartz grains, and represent domains of intense pressure solution. Within bleached quartzite units are planar, discontinuous seams of lime green clay minerals indicative of hydrothermal alteration(18-2K). Despite the pervasive imprint of fluid migration throughout these rocks, constraints on timing of the event are ambiguous. Internal strain within quartz grains and a SW dipping foliation present in alteration minerals imply a pre to syn-tectonic origin for the veins. Unfortunately, no clear linkage to nearby faulting can be deduced.

Veins

Vein density does not increase with proximity to the fault zone and there is no evidence of brecciation or strain localization anywhere at the fault contact. Numerous slicks on bedding surfaces likely result from flexural shear during mesoscopic folding. Veins are composed of quartz and are generally isolated, cross-cutting the regional foliation (110/87 SW). Some 1-3 cm wide veins appear to infiltrate irregular, jogged fractures that dip moderately to the northwest. Their orientation with respect to cleavage suggests parallelism with hko and formation during folding (*Price*, 1967). In thin section, most veins are fibrous indicating dilation perpendicular to vein walls. Those that are NW dipping have undergone subsequent pressure solution and rampant replacment by muscovite at grain contacts, implying that veining preceded the cessation of tectonism.

Veins sub-parallel to S1 are rare and usually less than 2 cm wide(3b). Discontinuous median surfaces within these are filled with chlorite, and fibers reflect dilation normal to S1 and therefore parallel to σ_1. This phenomenon can arise from a sudden decrease in effective stress in conjunction with heightened pore fluid pressure (*Valenta*, 1989). Nearest the vein wall, fibers have undergone dynamic grain size reduction from 100 to 20 μm. The new subgrains realign parallel to the foliation in the surrounding muscovite slate and demonstrate that tectonism and deformation continued following vein formation.

Footwall alteration zone

Further evidence of syn-kinematic fluid flow occurs within a 3 m wide sequence of green, foliated quartzite 50 m into the footwall. Numerous 3 cm wide veins dip moderately to the northwest, sub-parallel with bedding, and have also been broadly folded. Quartz grains in the host rock are angular due to solution transfer, and muscovite rims all grain boundaries. This interconnected network of muscovite "seams" is the result of high permeability within the well sorted host rock that permitted pervasive dissolution and reprecipitation of silica. Two types of veins are apparent. Coarse grained (>5 mm), fibrous quartz veins exhibit dilation normal to wall rock contact with no shear component(3e). The quartz is riddled with deformation lamellae aligned parallel to the dilation direction, and core and mantle structures are evident in very fine grains (< 10 μm) along most grain boundaries. Parallelism between strain lamellae and vein fibers reveals that fluctuations in the orientation of the regional stress field did not affect strain patterns at that locality. That is, ongoing stress resulted in a progression from brittle fracture and crack-seal events to ductile process that produced strain lamellae.

Dissolution seams filled with fibrous muscovite and chlorite and blocky hematite penetrate similarly oriented ribbon veins (3d). The seams are anastomosing, densely distributed, and parallel to S1. Vein quartz is strongly deformed and kinked, forming elongate grains parallel to S1. Microfabrics resemble those observed in a quartzite hosted shear zone at the Quartz Creek Thrust (43-4a). Serrated grain boundaries and intense undulose extinction attest to the high degree of ductile strain to which the vein material has been exposed following brittle rupture. The high aspect ratio might partly be due to an initially fibrous texture caused during succesive crack opening events parallel to S1. However, the chlorite-muscovite seams are not median sutures from a crack-seal mechanism. Instead they represent zones of ongoing dissolution and precipitation following vein formation.

Isotope Results

Seven wall rocks and four veins along a 150 m transect were analyzed for oxygen isotopes.

	Sample	18-#	$\delta^{18}O$(wr)	$\delta^{18}O$(qtz)
Hanging wall	bleached, foliated quartzite	2G	12.9	13.1
Fault zone	protolith quartzite	2E	12.7	12.9
	coarse grained, fibrous vein	***2E***	***18.8***	***18.8***
	protolith quartzite	2A	12.3	12.5
	muscovite slate	3B	10.5	14.7
	fibrous, S1-parallel vein	***3B***	***13.4***	***13.4***
Footwall	quartzite(intense pressure sol'n)	3C	11.8	13.2
	fibrous, a-c vein	***3C***	***12.9***	***12.9***
	deformed, crack-seal vein	***3D***	***12.5***	***12.5***
	foliated, bleached quartzite	3E	11.1	11.5
	strained, fibrous vein	***3E***	***12.7***	***12.7***

For the most part, fractionations between veins and host rocks are low, between -1.3 and 1.2 ‰, and reveal no systematic trend. With one exception, vein quartz has a narrow range of compositions between 12.5 and 13.4 ‰. Host rock quartzite exhibits similar values over a slightly broader range of 11.5 - 13.2 (qtz)‰. A single sample of slate from near the fault possesses a signature of 14.7 (qtz)‰, the highest observed within a host rock. The maximum depleted value, taken from an antitaxial vein (18-3B) occurring within a 50 cm wide slate bed, has a $\delta^{18}O$ composition comparable to that of the neighboring quartzite. Fluids from which vein quartz precipitated were therefore isotopically buffered by the dominant quartzite package. However, the slate hosted vein has a slightly higher $\delta^{18}O$ than most of the other quartz veins, suggesting that modest exchange between advecting fluids and the immediate host did occur. Most importantly, the uniformity of vein compositions relative to host rocks is evidence that fluid migration was not restricted to individual units, but flowed across bedding contacts between slate and quartzite.

A stark departure from this story is the anomalous 5.9 ‰ enrichment observed in an otherwise typical a-c vein in the hanging wall. It hosts the highest $\delta^{18}O$ (18.8 ‰) of any siliciclastic hosted vein for the entire study area. Temperature effects due to ascending fluids alone cannot explain such an extreme enrichment. The simplest explanation for the fluid source is neighboring carbonates. The nearest carbonate package is that discussed above, which is at least 90 m farther into the hanging wall. Slates with $\delta^{18}O$ above 18 ‰ were observed across Quartz Creek near the Heather Mountain Thrust and the Copperstain Syncline. However, it is unlikely that slates occupying less than 5 % of the host rock volume would exert such an influence on locally derived fluids. Without more geochemical constraints, the source of such enriched fluids is ambiguous. It is clear, however, that they originated from a reservoir at least 90 m away from the vein, and experienced little or no isotopic exchange with the surrounding quartzite. In conclusion, most of the syn-kinematic veins from the UF exhibit signatures expected from a closed system in which fluids are isotopically buffered by quartzites and slates along the transect. However, an anomalous $\delta^{18}O$ indicates that open system advection of fluids from a rock dominated reservoir outside of the sampling area was active at some stage during either folding or faulting.

Main Points:

- textural, mineralogical evidence of a pre-syn tectonic hydrothermal event proximal to the fault
- no clear association of veins with faulting
- veins are fibrous, but have undergone subsequent pressure solution or dynamic recrystallization during protracted tectonism
- host rock quartzite has undergone varying degrees of pressure solution and diffusive mass transfer
- rock-dominated, closed-system fluid regime during tectonism
- evidence of fluid exchange between both quartzite and slate, and therefore cross-bed flow
- evidence for open-system regime, whereby enriched fluids advect from a rock-dominated reservoir at least 90 m away

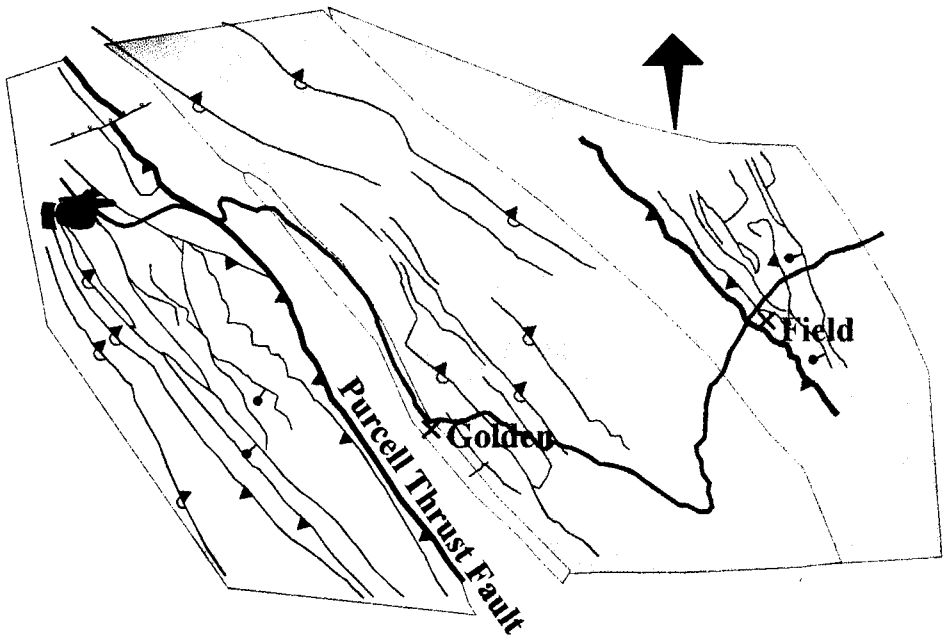

Wiseman Creek Fault at Kinbasket Lake

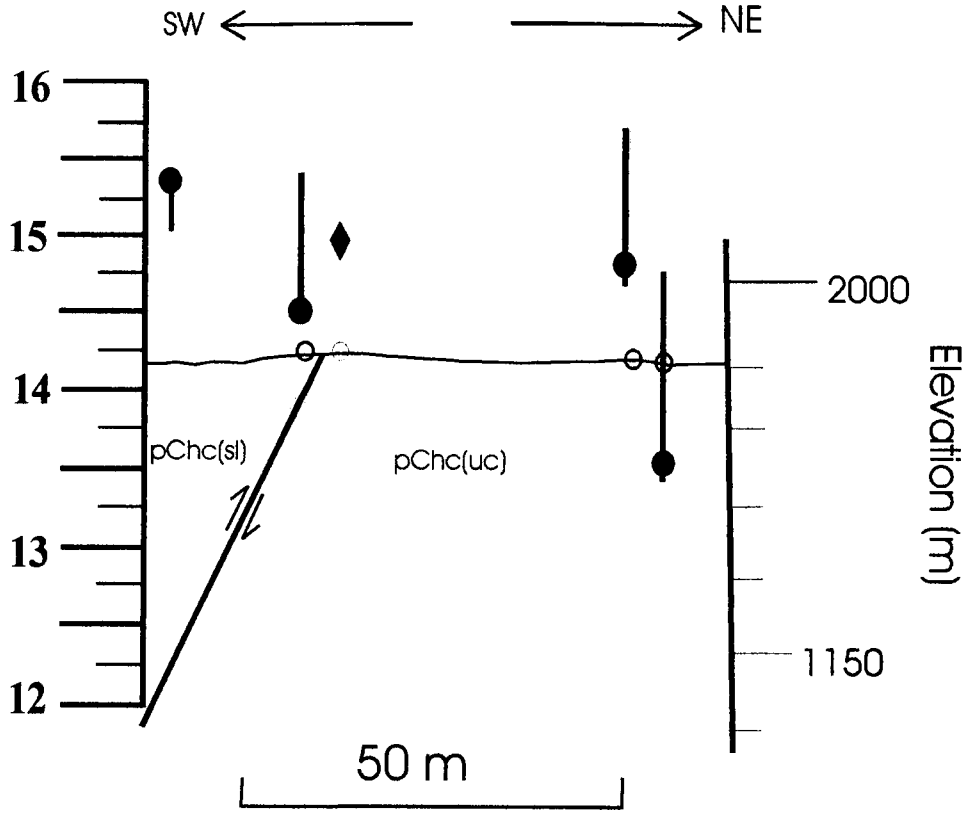

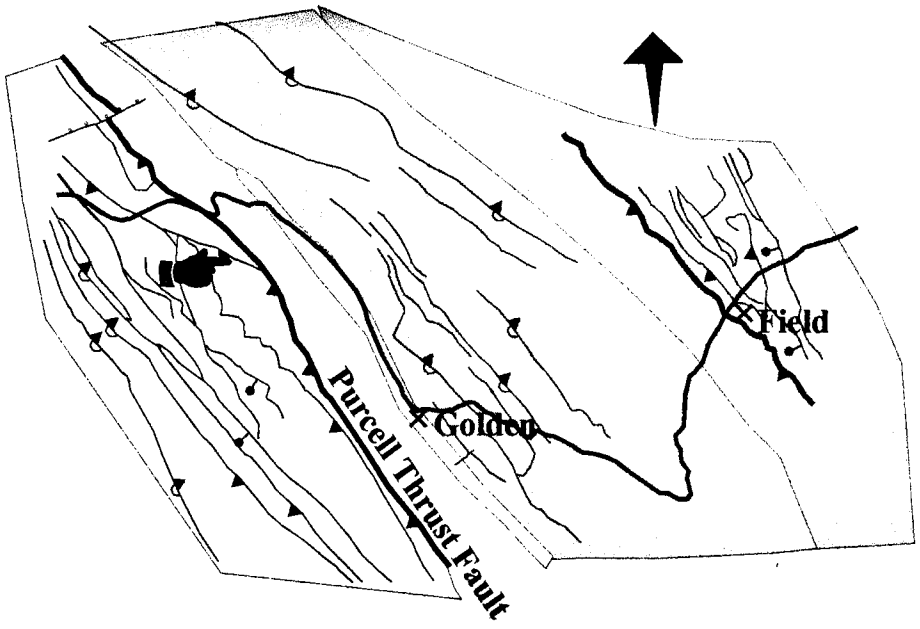

Wiseman Creek Fault at Oldman Creek

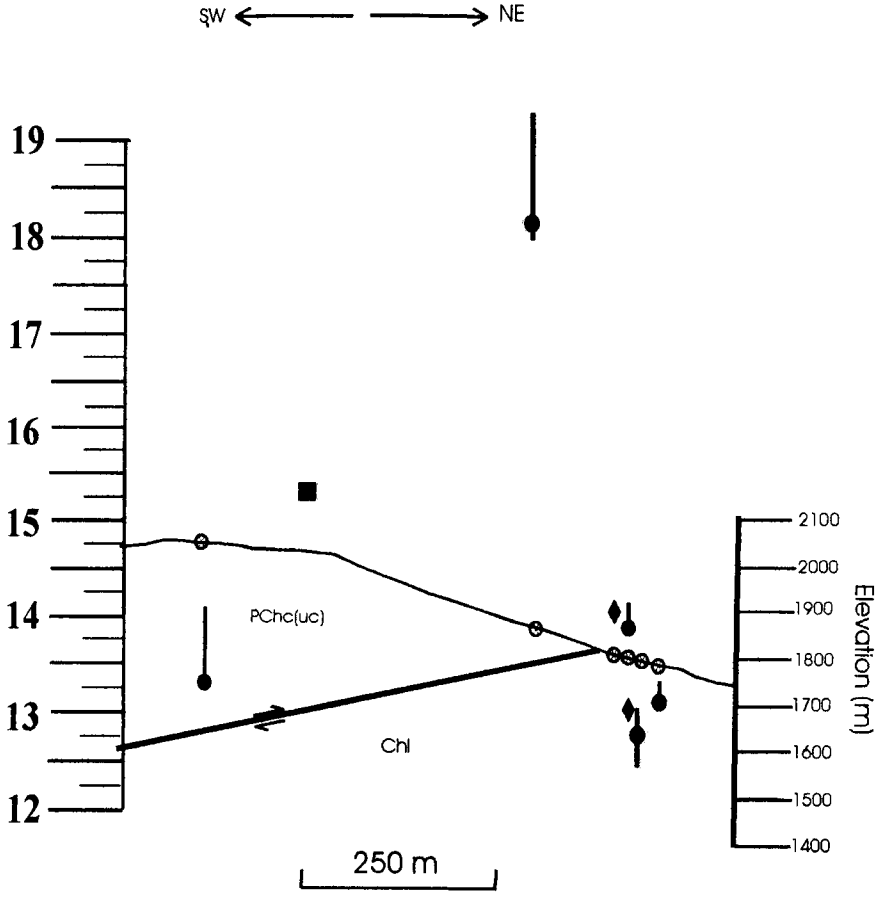

WISEMAN CREEK THRUST (Days 9,13, and 14)

The Wiseman Creek Thrust is the easternmost and therefore the youngest major fault in the Dogtooth Range. Displacement on the WCT is 1800-2350 m (*Kubli and Simony*, 1994), and Kubli (1990) hypothesizes that it represents the sole detachment for the Dogtooth Duplex. Exposure of the fault contact is evident where incompetent slate and siltstone of the Horsethief Creek Group (pChc(uc&sl)) are thrust against coarser grained grit and quartzite from the Hamill Group (Chl) and pChc(uc). Samples were collected from two localities separated by 10.5 km. North of the Trans-Canada Highway near Kinbasket Lake, recessive, fissile slates from pChc(sl) are juxtaposed against ridge forming foliated sandstones of pChc(uc). Further south near Oldman Creek, laminated grits and slates of pChc(uc) are thrust against a prominent package of Chl quartzite so densely veined that primary quartz grains have been entirely overprinted.

Kinbasket Lake

At the northern locality, a sharp competency contrast between upper and lower plate rocks permits precise estimation of the fault contact. The transect traverses 75 m across strike and crosses gradations in deformation intensity with proximity to the WCT. Grey, fissile slates comprise the immediate upper plate and are only exposed in roadcuts along the logging roads. Isolated beds of schist composed of quartz, muscovite, calcite, and siderite outcrop 20 m into the hanging wall(3a). Subangular quartz and plagioclase grains 0.5-1 mm in diameter are supported by a matrix of very fine grained quartz (<0.1 mm). Quartz and feldspar grains with maximum internal strain exhibit sweeping extinction indicating that dislocation creep impacted hanging wall only to a minor degree. Most of the strain was accommodated by pressure solution of coarse grained clasts as illustrated by muscovite seams that truncate quartz and feldspar grains. The seams define a spaced cleavage distributed across 3 mm intervals and parallel to the S1 (308/84 NE). Muscovite crystallizes along quartz microcracks and occupies isolated lenses within microlithons. The fine grained quartz matrix accounts for 50 % of the rock and lacks a shape or crystallographic preferred orientation associated with dynamic recrystallization. Instead, it precipitated during solution transfer from silica dissolved at stressed grain contacts and flowed into to pore spaces with lower normal stresses. Fluids are therefore a major factor in promoting solution mass transfer as the dominant deformation mechanism in hanging wall schist. These observations are consistent with the scarcity of veins found in the hanging wall. Low activation energy in incompetent phases within slates precluded brittle fracturing. In the sandstone protolith, high pore connectivity enhanced permeability thus preventing the escalation of pore fluid pressures necessary for vein formation.

Deformation intensity and style varies along strike of the fault contact. At one location, well sorted, medium grained quartzite has been replaced by a tectonized, very fine grained quartz-muscovite schist(14-2a). The schist delineates the footwall contact of the fault, but is laterally discontinuous over a distance of meters as it grades into undeformed quartzite. Fabric is defined by discontinuous but parallel domains of muscovite that comprise about 5 % of the sample volume. Microstructures exhibit a cycling of brittle and ductile processes during deformation. Relict coarse grains 0.25-0.75 mm in diameter have undergone mechanical rotation and intense grain size reduction to produce a matrix composed of grains smaller than 10 μm. The matrix quartz has

both a shape and crystallographic preferred orientation. Mutually parallel lenses of quartz and muscovite oriented oblique to the main foliation suggest an incipient C-fabric that indicates top down shear. Insertion of the lambda plate reveals veinlets approximately 100 μm wide that are mutually cross-cutting with S1. Subsequent plastic strain has diminished grain size to that equivalent with the matrix. However, CPO within vein material is oriented antithetic to the S-surface, distinguishing it from the surrounding matrix. The foliation is oriented 295/69 NE, which is consistent with S1, but contrasts sharply with the orientation of the WCT (≈136/64 SW (*Kubli*, 1990)). Thus, tectonism that promoted grain size reduction in the form of solution transfer and dynamic recrystallization preceded motion on the WCT. Slickensides on the surface plunge towards 025°, consistent with the direction of transport expected on the WCT. Veins were not observed anywhere near the sample.

Elsewhere at the fault contact, strain localization is not as evident. Fine grained grits within 50 m into the footwall have a well developed cleavage defined by muscovite domains that truncate quartz and feldspar clasts. Aside from modest undulose extinction within quartz, most evidence suggests that strain is partitioned by a mechanism of dissolution and transfer of silica out of the system. Planar, milky quartz-filled veins oriented sub-parallel to S1 might represent nearby sinks for the dissolved silica.

Oldman Creek

Sampling south of Highway 1 focussed along a 500 m transect across strike of the WCT. The fault contact is constrained to within 50 m based upon the last occurrences of upper plate grits and lower plate quartzite. Penetrative cleavage was observed in hanging wall slate and foliated sandstone. The mean foliation is oriented135/19 SW, consistent with the WCT, and intersection lineations reflect a regional fold axis plunging shallowly SE. Intensely strained tectonites such as those described above were not observed anywhere near the fault zone. However, immediately adjacent to the fault contact, bulk replacement of footwall quartzite with vein material demonstrates that a significant volume of fluid utilized the WCT contact either during or after fault movement. A gradation from high to low vein density away from the contact supports a correlation between faulting and fluid advection. Quartzite within 3 m of the fault consists of massive, white vein material that overprints all relict sedimentary textures in the rock(13-4a). The vein quartz is unique to that observed anywhere else in this study for two reasons. First, the coarser grained material (0.25-0.5 mm) that accounts for 30 % of the sample is remarkably undeformed. Grain contacts are polygonal with no evidence of pressure solution, and dislocations from intragranular strain are minimal to nonexistent. Crystals are euhedral and therefore do not retain any signature of crack-seal or other kinematic processes. In addition, the surrounding fine grained quartz matrix (<10 μm) exhibits no systematic geometric relationship with the coarser grains. That is, pods of coarser grains seem to be randomly distributed with no geometric evidence for multiple, overprinting veining events. The fine grained quartz is subhedral and does not have CPO. Therefore, the fluid event leading to bulk replacement of the protolith was either:

1) a syn- or post-contractional fluid phase that resulted from pervasive veining associated with stress relaxation on the fault, or

2) a focussing of large volumes of fluids enhancing syn-tectonic mass transfer to the degree that either most detrital quartz was dissolved at point contacts and transported over cm's into low pressure sinks (fine grained quartz) (see *Etheridge et al.*, 1984) or detrital quartz was simply overprinted in the presence of a silica oversaturated fluid.

However, the second condition does not explain the absence of muscovite, an abundant mineral in other affected packages.

A resolution to the above quandary is gleaned from microtextures in "intermediate" quartzite that outcrops 3-12 m from the WCT(4b). Three distinct quartz domains outline a progression of events that lead to the bulk replacement discussed above. Rounded grains with muscovite haloes signify relict quartz clasts similar to those in the unaffected protolith. Cross-cutting, randomly oriented veinlets are 4 mm wide and infilled with coarsely crystalline (0.5-3 mm), euhedral quartz. Many of these veinlets are rimmed by very fine grained, subhedral quartz similar to that discussed above. Similar quartz also infills numerous intragranular fractures. The fine grained quartz reflects an initial fracture event that results in infiltration and rapid crystallization. Small scale, heterogeneous stress gradients controlled by grain contacts are responsible for the random orientation of veinlets and intragranular fractures. Subsequent rupture within veins promoted further advection of fluids and precipitation of the second, coarse grained phase. A size gradation between the fine and coarse grained domains might suggest a *common* infiltration event. If this is the case, fine grained quartz precipitated where numerous nucleation sites were available and the size differentiation therefore represents a kinetic effect. Nevertheless, a bimodal grain size distribution is characteristic of larger fractures, whereas, mm-scale intra- and intergranular fractures contain very fine grained quartz. Nebulous terminations for many veinlets imply that although fracturing created the pressure gradient necessary to siphon fluid from the surrounding rock, infiltrating fluid utilized connected pore space in addition to dilatant sites for quartz precipitation. These observations support hypothesis (1) above. That is, the fine grained quartz in 13-4a has precipitated from multiple phases of cracking and rapid quenching due to elevated fluid temperature relative to the host rock.

At distances more than 12 m from the WCT, veining within the quartzite is minimal, and relict sedimentary textures are dominant. In the hanging wall veining intensity does not increase with proximity to the fault. However, a 3 m wide outcrop approximately 50 m into the hanging wall exhibits folded and disturbed cleavage in conjunction with pervasive veining and quartz replacement of immature sandstones. Unfortunately, the isolation of this outcrop, together with severe weathering preclude a well constrained structural interpretation and isotopic analysis.

Isotope Results

Eight wall rocks and five rocks from the fault zone were submitted for oxygen isotopic analysis.

		Sample	#	$\delta^{18}O$ (measured)	$\delta^{18}O$ (qtz)
Kinbaske Lake	Hanging Wall	muscovite phyllite	14-3A	14.9	15.3
	Fault	***foliated quartzite***	***14-2A***	***14.9***	***14.9***
	Footwall	foliated grit	14-4C	12.8	14.5
		grit	14-4A	13.8	14.8
		grit	14-1F	11.9	13.5

		Sample	#	$\delta^{18}O$ (wr)	$\delta^{18}O$ (qtz)	$\delta^{13}C$
Oldman Creek	Hanging	sandstone	9-2E	13.2	13.4	
		Limestone	9-1D	15.2	16.2	4.2
		calcareous slat	13-1A	15.1	18.2	
	Fault	***massive vein***	***13-4A***	***14.1***	***14.1***	
		quartzite matrix	13-4B	13.9	13.9	
		qtz veinlet	***13-4B***	***13.1***	***13.1***	
		quartzite	13-4C	12.2	12.8	
	Footwall	quartzite	8-2	13.2	13.2	
		quartzite	48-5A	14.7	14.7	

Despite strong variations in deformation style and intensity between the two localities, isotopic systematics are mutually consistent. The tectonite and vein quartz from the fault zone are compositionally similar to the undeformed protolith. Importantly, there are no large isotopic depletions that accompany veining and dynamic recrystallization, and therefore no evidence for open system circulation of fluids. At Kinbasket Lake, footwall $\delta^{18}O$ values fall between 13.5 and 14.8 ‰, compared with 14.9 ‰ from a quartzite schist at the WCT contact. Protolith quartzite near Oldman Creek exhibits a wide spread in $\delta^{18}O$, between 12.2 and 14.7 ‰. Vein material from the fault zone has signatures of 13.1-14.1 ‰. The high-end wall rock value of 14.7 ‰ is from 48-5A, which was collected more than 1 km along strike and approximately 200 m down section from the other samples. The sample is anomalously enriched by 1-2 ‰ relative to other samples of Hamill quartzite. If this value is disregarded, both samples nearest the fault have compositions slightly enriched (0.1-1.4 ‰) relative to their protolith. Similar observations were made above from the Hamill hosted shear zone and veins at the Quartz Creek Thrust and Unnamed Fault.

The similarity between upper plate and lower plate $\delta^{18}O$ precludes conclusions about fluid communication across the WCT. Isotope data was not obtained at a scale small enough to explain minor (< 1 ‰) differences between protolith and veins. Thus, it is possible that slight enrichments in fault rocks arise from > 30 m circulation and exchange of fluids between the upper and lower plate such that the composition of vein forming fluids reflect an average between high end hanging wall and low end footwall values. However, the emergent pattern of enrichment observed in all Hamill hosted veins and tectonites in the study area might be the

result of quartz precipitation of ascending fluids flowing down a temperature gradient. If true, then pressure gradients caused by repeated fracturing siphoned fluids from deeper sources. It is also noteworthy that the coarse crystalline vein in 13-4B has $\delta^{18}O$ 1.0 ‰ less than that of the fine grained quartz vein matrix from 13-4A. The difference can be attitributed to lower temperatures of crystallization in the fine grained veins (higher $\Delta^{18}O_{H2O\text{-}qtz}$) or separate fluid sources.

Major points:

- pervasive pressure solution and reprecipitation of quartz(and feldspar) demonstrates role of fluid channeling in deformation of coarser grained siliciclastic units
- varied styles of deformation along strike of the WCT
- Kinbasket Lake: mutually offsetting veinlets and muscovite fabric with intense grain size reduction at WCT imply cycling of brittle and ductile processes during deformation
- Oldman Creek: vein intensity in footwall increases with proximity to fault-immediate fault contact delineated by quartzite that was entirely overprinted by successive generations of mm-scale veins
- no isotopic evidence for open system fluid circulation
- enrichments in fault rocks relative to protolith is consistent with all other Hamill hosted shear zones
- might reflect down-T fluid flow or fluid communication between higher $\delta^{18}O$ hanging wall and footwall

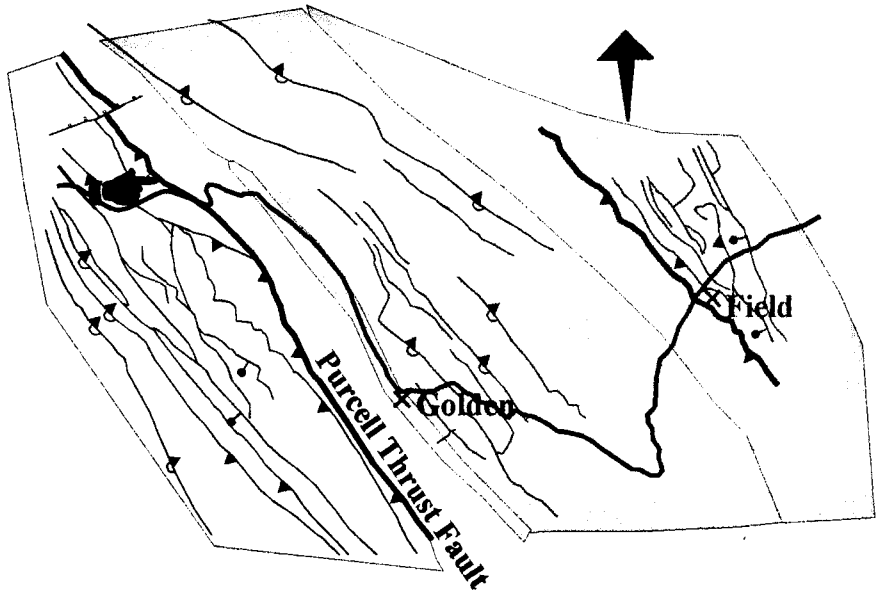
Field
Golden
Purcell Thrust Fault

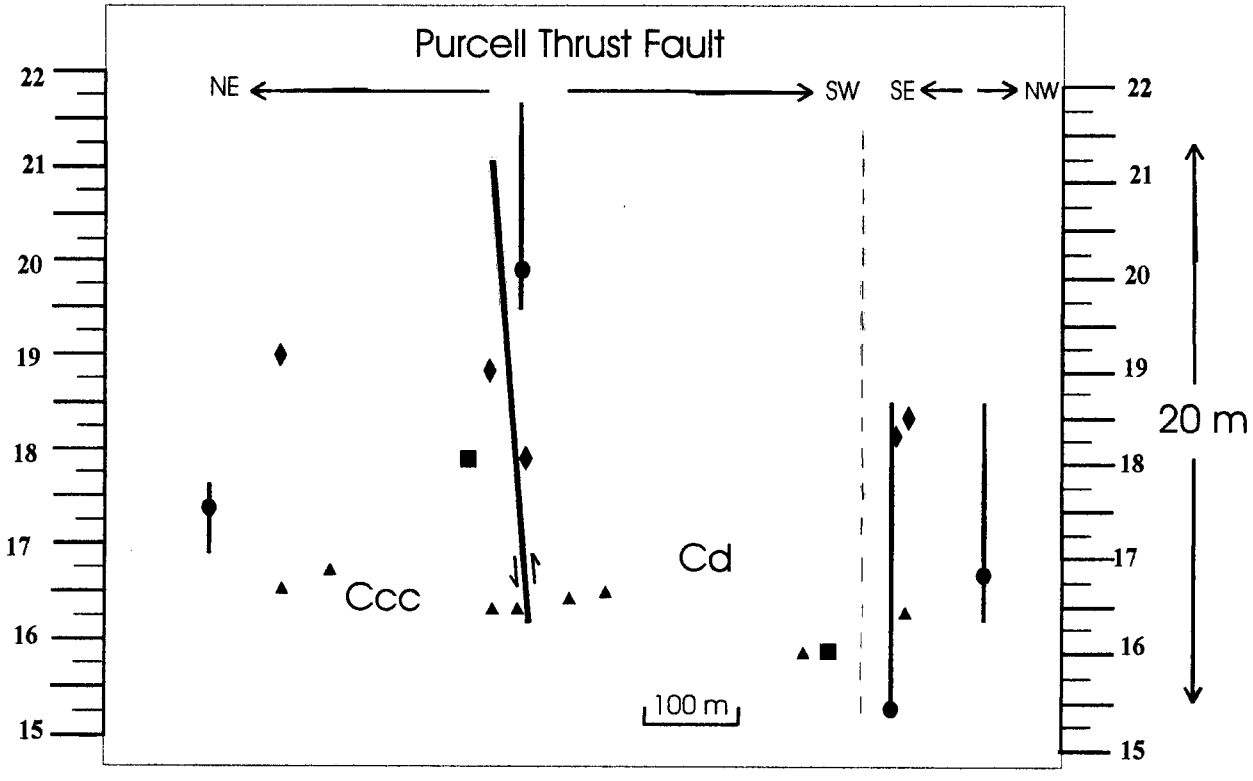
Purcell Thrust Fault
NE
SW
SE
NW
22
21
20
19
18
17
16
15
Ccc
Cd
100 m
20 m

Purcell Thrust Fault (Days 10-11-12-34-35)

The Purcell Thrust is one of the most regionally significant structures in the study area. It delineates the eastern boundary of the Purcell Anticlinorium and juxtaposes lower Cambrian siliciclastic units in its hanging wall against middle Cambrian calcareous slates and argillites. It also represents an important compositional divide, separating low $\delta^{18}O$ siliciclastics and carbonates from higher $\delta^{18}O$ calcareous slates, limestones, and argillites. Because it cross-cuts thrust faults, folds, and S1 cleavage in the Dogtooth and Western Ranges, the PTF is described as an out-of-sequence fault with 10 km displacement (*Simony and Wind*, 1970). Homogenization between syn-D1 veins in the upper and lower plates would therefore insinuate that D1 fabrics observed at the outcrop are synchronous with movement on the PTF.

Samples were taken from a railroad cut near the Trans-Canada highway, the only known outcrop of the PTF in the Dogtooth Range. Here, siltstone and slate from the Donald Fm.(Cdo) are placed upon fissile slate, phyllite, and interbedded limestone from the Canyon Creek Fm.(Ccc). The transect crosses 600 m and includes diverse styles of deformation and veining that affect disparate rock types. The PTF is expressed as a 15 m wide zone of intensely weathered, wet black slate that grossly defines a contact between competent calcareous siltstone in its upper plate and calcareous slate in its footwall. Consistent with Balkwill's (1969) observation, cleavage is consistent in orientation on either side of the fault (145/84 SW), but varies between three distinct modes throughout the outcrop. Graphitic slates and siltstones >200 m into the hanging wall exhibit a foliation that dips moderately to the northeast (325/59), consistent with that expected in the eastern Dogtooth Range. Isolated faults on both sides of the PTF comprise steeply SW-dipping fabrics (119/75), and the most common orientation for S1, 134/46 SW, parallels that of the PTF.

Veins

Numerous vein morphologies across the outcrop reflect rheological contrasts, as well as changing strain gradients associated with progressive folding and shear zone development. Cross-cutting relationships between different vein types and structures are complex, and, in some cases, ambiguous.

I) The earliest observed veins are 3 mm wide en echelon, calcite filled tension gashes that occupy graphitic slate in the hanging wall and 10 cm thick micrite beds in the upper and lower plates (35-1A,11-4C). Veins cross-cut S1, but are themselves offset along dissolution seams running slightly oblique to the foliation indicating emplacement during foliation development. They are fibrous and perpendicular to S1, indicative of mode I propagation under tensile stresses. A 10 μm rim of fibrous quartz and internal translation of fibers documents antitaxial growth in a non-coaxial stress field. A discontinuous graphite seam that encases portions of the vein records volume loss of matrix and vein material parallel to the vein (normal to σ_1) during simple shear.

II) Calcite (+/- quartz) filled, S0-parallel crack-seal, "ribbon" veins approximately 2-4 cm in width and 5 cm to 1 m long occupy both calcareous slate and graphitic argillite attesting to the regional circulation of carbonate bearing fluids through hanging wall and footwall (12-3C,35-1A). Veins are often compressed into cm amplitude, isoclinal folds, some of which have undergone volume loss during dissolution along axial planar cleavage planes and stylolites. Because they cross cut type I veins above, timing is constrained as synchronous with S1 development. A consistent association between ribbon veins and laminated units suggests that permeability anisotropy promoted elevated pore fluid pressure ($> \sigma_3 + T$) and consequent rupture at contacts between mm-scale laminae during sub-horizontal compression. Apatite is abundant within some of the veins, and blocky calcite reflects open space filling by vein forming fluids. Kinked and offset (mode III) twins and subhedral, undeformed quartz illustrate strain partitioning into the calcite. Chlorite, very fine grained quartz,

and muscovite comprise sub-mm internal domains (or median sutures) within the vein. These sutures exhibit a crenulation (S2) cleavage defined by opaque (graphite?) seams.

III) Sub-planar, 0.5-1 cm wide, calcite-quartz filled tension gashes occupy 0.5 m thick calc-siltstone beds 200 m into the hanging wall(34-4a;10-4b). The gashes are mutually parallel, cross-cut bedding contacts, and contain slickensides on their surfaces. Their timing relative to S1 and other veins is unclear, but formation likely occurred during the latest stages of folding.

IV) Planar, S1-parallel calcite-quartz ribbon veins (12-2b) cross-cut and coexist with S0-parallel type II veins. They are sporadically truncated (or pinch out) at fold hinges where volume loss through pressure solution has occurred. Discontinuous, anastomosing dissolution seams (or median sutures) are sub-parallel with S1. Veins contain both blocky grains, and elongate crystals of quartz and calcite oriented parallel to foliation. Irregular grain boundaries indicate a crack-seal origin for the elongate minerals (see *Cox and Etheridge*, 1983) with extension parallel to S1. Intragranular strain resembles that within type II veins, and isolated lenses of elongate quartz (fibrous?) quartz are partially overprinted by latent calcite mineralization.

V) Cleavage-parallel 1-5 cm wide quartz-calcite veins first outcrop approximately 200 m into the footwall and continue sporadically through the extent of the outcrop (12-3a-c). Carbonate hosted veins appear wider and more blocky than those within phyllite. Isoclinal folds within some of these indicate transposition into parallelism with S1, and boudinage illustrates S1 parallel extension following formation. Cross-cutting relationships with other vein types are unapparent, but the varying degrees of deformation recorded by these indicates formation during early and late phases of S1 development.

VI) Blocky and fibrous ribbon veins define fault contacts, including that of the PTF, throughout the outcrop (11-2a;35-4a,b;10-5a). At the PTF, a 3 m long ribbon vein defines the contact between weathered, black slate and muscovite phyllite. It is noteworthy that veining density does not increase on either side of the fault, and that the fault cross-cuts the main foliation (125/65 SW). Calcite and quartz are euhedral and show only moderate internal strain. Grain size is proportional to distance between dissolution seams (or median sutures). Calcite exhibits mode II-III twinning. Seams host muscovite, chlorite, and very fine grained quartz (as in type II and IV veins), and a crenulation cleavage is locally evident. However, the chaotic orientation of the seams implies that they are not a secondary, cross-cutting fabric, but a median suture instead. This observation and the modest intragranular strain are consistent with vein formation post-dating foliation development. A typical crack-seal vein (10-5a) hosted by calc-siltstone lines a splay fault 300 m into the hanging wall. Drag folds at the fault suggest reverse-slip displacement. Fibrous quartz and calcite exhibit intense intragranular strain as calcite twins are pervasively kinked (mode IV), and deformation lamellae and incipient sub-grains within the quartz align parallel to the grain boundary. Quartz grains appear highly corroded and overprinted by a latent pulse of carbonate rich fluid.

VII) Numerous tapered, calcite-quartz veinlets are S1-sub-parallel and occupy phyllites 300 m into the footwall (12-7d). They offset cleavage-parallel (type V) veins and are oriented 133/50 SW, 20° from S1. Some are broadly folded about cleavage planes implying formation contemporaneous with S1-development, but post-dating veins of type I-V. Morphologically similar veins were observed by Beach and Jack (1982) in the French Alps.

Isotope Results

Seventeen isotope analyses from five wall rocks and eight veins were obtained from the PTF.

	Sample	$\delta^{18}O$ (measured)	$\delta^{18}O$(qtz)	$\delta^{13}C$	Distance from fault	Temperature
Hanging Wall	argillite(11-1B)	14.7	16.3		400 m	
	local fault-slate(10-5C)	13.8	15.4		300 m	
	type VI vein(10-5C)	***18.1***	***18.1***			
	type VI fibrous vein(10-5A)	***18.3***	***18.3***			***355°(S&K);165***
	type VI fibrous vein(cc)(11-4C)	***16.2***		***-1.9***		
	type I vein(cc)(34-5A)	***16.2***		***-2.7***	100 m	
	Calcareous siltstone(34-4A)	16.0		-1.9		
	Tension gashes(34-4A)	***16.0***		***-2.2***		
	type I vein(cc)(34-1A)	***16.3***		***-2.5***	50 m	
	muscovite-graphite phyllite(34-5C)	15.6	19.8		<1 m	
FAULT	***type VI vein(34-5A)***	***18***	***18***		0 m	420°;210°
	type VI vein(cc)(34-5A)	***16.2***		***-2.7***		
	same vein-continuation(34-5B)	***18.7***	***18.7***			***315°;140°***
	same vein (cc)(34-5B)	***16.2***		***-2.7***		
Footwall	calcareous slate(34-6B)	17.9		-2.4	1 m	
	type II vein(12-2C)	***16.5***		***-0.6***	200 m	
	local fault-type VI vein(35-3B)	***19***	***19***		250 m	315°;140°
	s/a (calcite)(35-3B)	***16.5***		***-0.6***		
	slate(12-3C)	15.7	17.4		330 m	

Despite a wide variance in wall rock signature and vein morphology across the outcrop, vein compositions are distinctly uniform. Wall rock $\delta^{18}O$ signatures fall between 15.4 and 18.9 ‰ (13.8-17.9 ‰(wr)), compared with vein compositions of 17.2-19 ‰ (16.2-19 ‰(wr)). This trend is particularly conspicuous in the hanging wall, where disparate vein types possess a narrow range of oxygen compositions (17.2-18.1 ‰) that are enriched by 1.8 - 2.9 ‰ relative to the surrounding siliciclastic rocks (15.4-16.3 ‰).

The degree of homogenization in vein composition throughout the 600 m transect is enigmatic considering the alleged timing of formation for most of the veins. With the exception of those observed at the PTF contact and perhaps other type VI veins from local splays, most veins are contemporaneous with S1 and thus pre-date the PTF. However, homogenization across the outcrop implies fluid communication between the hanging wall and footwall, each of which has a distinctive lithology and $\delta^{18}O$ composition. Because this pattern is observed in quartz as well as calcite, isotopic resetting from latent exchange is not likely. Lack of absolute timing constraints for S1 and the PTF precludes a definitive resolution to the quandary.

The ribbon vein sampled at the PTF contact exhibits the lowest observed vein quartz composition in the outcrop. It is depleted by 0.9-1.8 ‰ relative to surrounding wall rocks and 0.7 ‰ with respect to the blocky vein with which it merges 1 m away. Isotopic composition of vein quartz decreases with proximity to the PTF. Thus, channeling of silica bearing fluids partially derived from an exotic source likely occurred during displacement on the PTF. However, this pattern is not apparent in vein calcite, which is remarkably consistent

in composition throughout the outcrop. Any hypothesis for the nature of fluid flow at and around the PTF must explain three observations: a) outcrop scale homogenization in vein quartz and calcite b) vein quartz depletion proximal to PTF.

I propose that two fluid regimes operated simultaneously during D1 and motion on PTF. Fluid circulation over a scale of at least 600 m effected homogenization of vein compositions. The main foliation therefore continued to develop after the juxtaposition of Donald siltstones and slates against higher $\delta^{18}O$ calcareous slates from Ccc or underlying Cch, i.e. movement of the PTF. Furthermore, infiltration of externally derived fluid along the PTF resulted in the observed depletion of quartz proximal to the fault contact. The same event introduced a depleted carbonate species to the outcrop.

Two distinct $\delta^{13}C$ populations reflect either different fluid sources or a single evolving fluid regime. The lower $\delta^{13}C$ (-2.7 ‰) might represent the more evolved fluid phase because it more closely resembles that of the host rock carbonate. However, the two samples with elevated carbon compositions (35-3b and 12-2c) formed during two chronologically distinct events: 1) early bedding-parallel crack-seal propagation and 2) late-stage faulting and blocky vein formation. Although the duration of time that separated these two events is ambiguous, other veins with low $\delta^{13}C$ must have formed during that hiatus. It is therefore more likely that differences in carbon composition either arise from different sources of advecting fluids or from different exchange paths from source to sink.

Based on these geochemical and structural observations, folding, active slip on S1 planes, and associated fluctuations in the ambient stress field probably occurred during displacement on the PTF. If true, this allows for juxtaposition of Ccc with Cdo during formation of all observed vein types and a resultant cross-fault fluid circulation cell.

Main Points

- PTF and local faults host crack-seal and ribbon veins at contact
- no correlation between vein density and proximity to fault
- seven distinct vein morphologies reflect ambient stress field and influence of rheological anisotropy
- apparent isotopic homogenization throughout chronologically and morphologically distinct vein types on both sides of the PTF is enigmatic (i.e. fluids are apparently buffered by both hanging wall and footwall despite their lack of juxtaposition until late-stage deformation).
- $\delta^{18}O$ of vein quartz is increasingly depleted with proximity to the PTF
- $\delta^{18}O$ of vein calcite is consistent throughout outcrop, and is depleted by 1.7 ‰ relative to the only apparent source of wall rock carbonate. Suggestive of partially exotic fluid source.
- infiltration of partially exotic fluid at PTF and subsequent exchange with wall rocks throughout outcrop: higher silica content at outcrop means lower fluid-mineral ratio for silica than calcite.
- two distinct $\delta^{13}C$ populations result from different exchange paths from source to sink

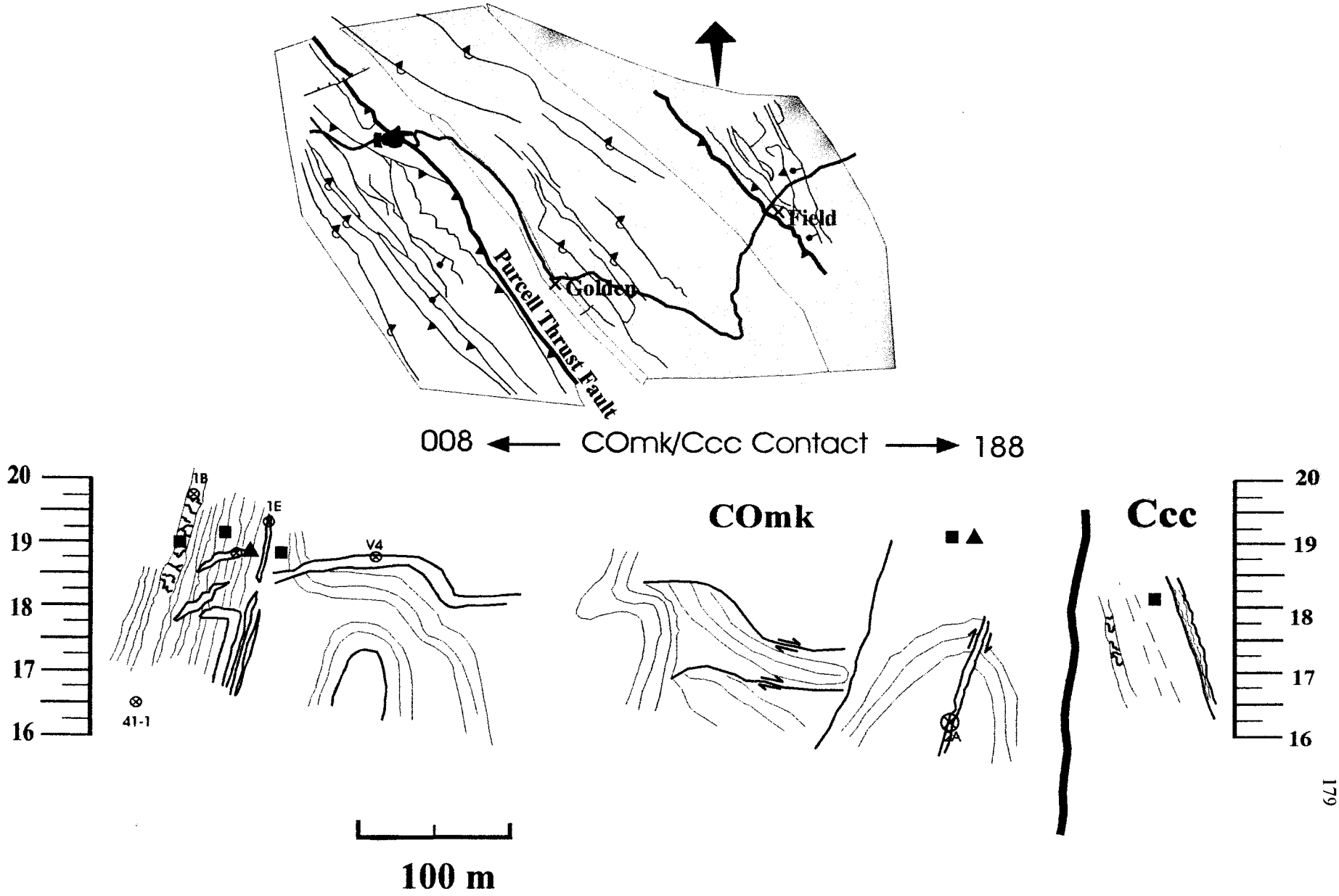
Field
Golden
Purcell Thrust Fault
008
COmk/Ccc Contact
188
20
19
18
17
16
1B
1E
V4
41-1
COmk
Ccc
100 m

COmk near contact with Ccc at Trans-Canada Hwy.(Day 41)

Samples were collected along a 150 m long transect located 45 m east of the contact between the McKay and Canyon Creek Group. Reasons for targeting the outcrop are two-fold. First, variations in the geometry and orientation of calcite veins illustrate a clear correlation with rheological contrasts and strain partitioning in the surrounding host rock. Pervasive fracturing in different rock types is coincident with progressive cleavage development, transposition of bedding, and consummate brittle faulting along fold limbs and within axial planes of megascopic folds. Furthermore, the contact between Ccc and COmk represents a subtle, but well delineated change from dominantly siliciclastic argillites and phyllites to more calcareous slate and limestone (*Balkwill*,1969). Stable isotope analysis is an opportunity to test whether compositional variations and progressive strain correlate with geochemical transitions, or if the presence of a pervasive fluid phase during contraction homogenized the effect of local differences in lithology and deformation enhanced fluid flow.

Beds of sparry limestone 60-80 cm thick occupy 5-10 % of the outcrop and are transposed into parallelism with cleavage (298/81 NE). Veins are plentiful and replace 10 - 30 % of the limestone(41-1a,b). They are restricted within bedding and cross-cut layering at high angles (70-90°), typical of mode I fractures. Much of the limestone has been replaced with domains of white, sparry calcite that forms irregularly shaped veins indicative of pervasive dissolution and reprecipitation within a fluid phase. Timing of this event with respect to tectonism is ambiguous.

Brown calcareous siltstone accounts for 75 % of the outcrop and hosts 0.5-6 cm wide calcite veins that cross cut bedding (and cleavage) at high angles typical of mode I fractures(41-1c). However, the veins are also broadly folded across bedding contacts suggesting formation following the main transposition of bedding, but prior to cessation of tectonism. Very fissile, calcareous slates represent 15 % of the outcrop and host thin, fibrous calcite veins oriented parallel to the foliation(41-1d,e). Although most of these are planar, some connect with the cross-bedding veins mentioned above. Because they exhibit opposing dilation directions, synchronous formation of these two vein types is unlikely. It is more realistic that one vein tip formed a surface from which the other propagated during a change in the ambient stress field.

A local fault with m-scale displacement bisects a tight, SW-vergent fold along its axial plane. The surface shows reverse displacement reflecting a transfer of strain from ductile folding to brittle shear. A resistant vein of coarse, crystalline calcite defines the fault contact (41-2a). Straight fibers 2.5 mm long bound the vein, but coarser subhedral calcite occupies the bulk of the vein indicating initial crack-seal opening followed by infilling of an open fracture. Mild intragranular strain is accommodated by mode I-II twin development. It appears that initial slip triggered systematic crack-seal opening, but subsequent strain softening initiated chaotic fracturing and infilling, similar to that observed within limestone beds discussed above.

Isotope Results

Two wall rocks and one vein were analyzed for isotopic composition.

	Sample	41-#	d18O (measured	d13C
	Slate	1D	18.8	-0.1
	Calc. silstone	1C	19.2	-0.1
	cross-cut/fold. vein	1C	18.9	-0.2
	limestone	1B	19	0.3
FAULT	sparry limestone	2A	19.1	0.3
	Blocky vein	***2A***	***19.1***	***-0.3***
	Calc slate	3C	18.1	0.4

The limited data available contain no evidence for open system fluid migration or exchange with the surrounding rock package. The fault bounding vein and neighboring limestone have identical $\delta^{18}O$ compositions, and it appears that vein material originated as locally dissolved calcite. Another possibility is that recrystallization of sparry limestone occurred during deformation, and the measured wall rock signature does not accurately reflect that of the protolith. Perhaps the observed 0.6 ‰ $\delta^{13}C$ depletion in vein calcite relative to wall rock implies that carbon had not fully exchanged between an externally derived fluid and the local carbonate. Isotope data from calcite within more siliceous, less permeable units is necessary to test the above hypothesis.

Main points

- three distinct vein types reflect gradations in competency
- faulting along axial plane evolves from overtightening of megascopic fold
- fault vein formed within closed isotopic system-identical composition to surrounding limestone

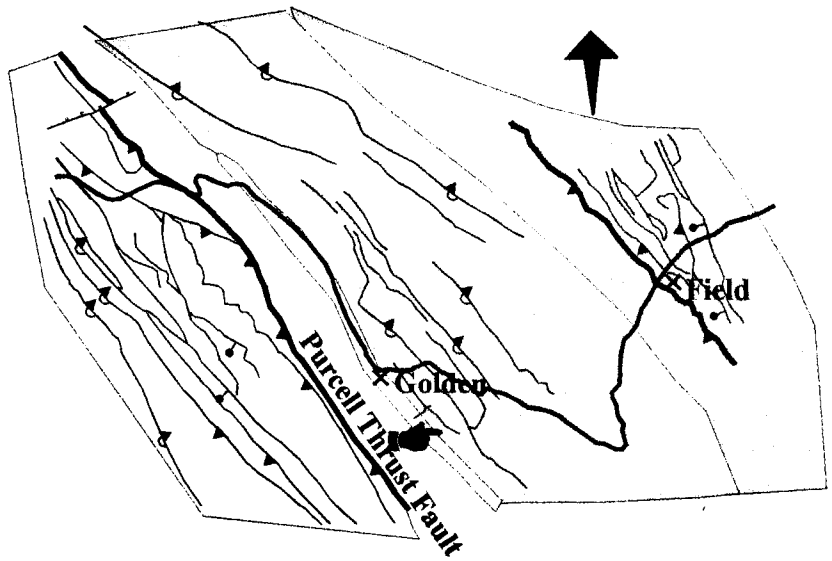
Field
Golden
Purcell Thrust Fault

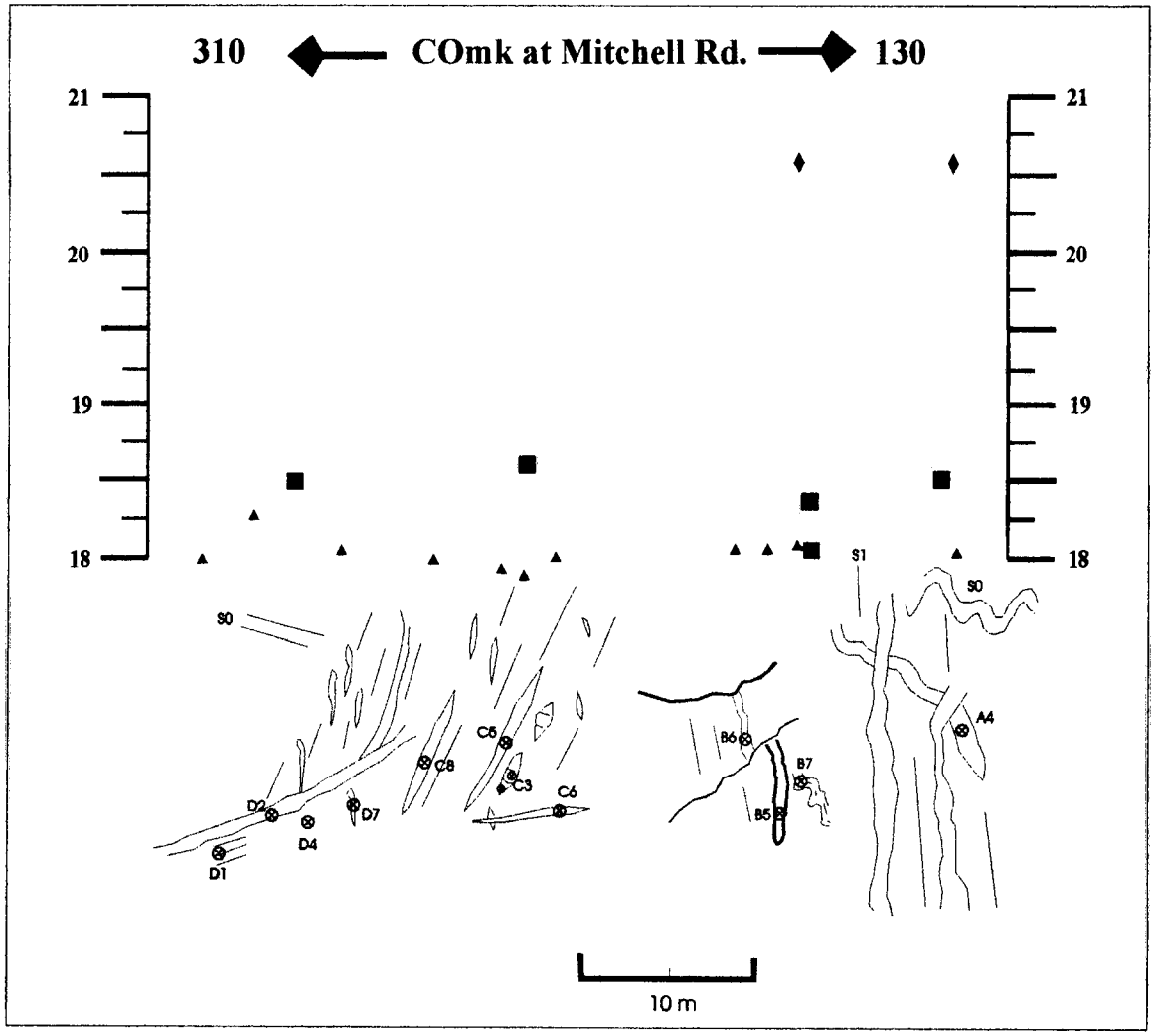
310
COmk at Mitchell Rd.
130
21
20
19
18
S0
S1
C5
C8
C3
C6
D2
D7
D4
D1
B6
B7
B5
A4
10 m

COmk at Mitchell Rd.(Days 20 and 21)*

Samples from the McKay group (undifferentiated) were collected at a roadcut along Highway 95 south of Golden about 200 m east of the Columbia River and more than 2.5 km from the nearest regional fault. The outcrop is located near the core of the RMT synclinorium and was selected due to the high density of veins and small faults that exhibit excellent cross-cutting relationships. Lithologic variations across the exposure are more subtle than those noted at the McKay/Canyon Creek Group contact discussed above, and no obvious correlation between rock type and vein morphology is apparent.

Wall Rocks

Calcareous slates are interbedded with massive, nodular micrite beds that serve as the only marker of bedding/cleavage relationships. Four rock types are distinguished in thin-section.

i) Calcareous slate occupies most (>60 %) of the outcrop and is composed of domains of elongate calcite (~ 30 %), muscovite preferentially oriented parallel to cleavage (~ 40 %), and continuous dissolution seams filled with chlorite and illite(?)(~30 %)(D4). Dissolution seams and muscovite domains define both S1 and an S2 crenulation oriented approximately 20° to the main foliation.
ii) Calcareous slate composed of subhedral calcite grains (~ 50%), oriented muscovite (~ 40%), and very fine grained quartz (10-15 %)(C7).
iii) Massive micrite consists of 90-95 % calcite grains, most of which are < 40 μm in size (A2). Irregular grain boundaries in coarser calcite (> 120 μm) show evidence of incipient pressure solution suggesting that the rock has undergone pervasive grain size reduction. Very fine grained quartz in interspersed throughout the sample (5-10 % vol.) as are local, discontinuous dissolution seams parallel to S1.
iv) Nodules consist entirely of massive, very fine grained calcite (<20 μm)(C3).

Veins

Six distinct vein types were observed throughout the outcrop.

I) Groups of micrite nodules cored by light gray material represent relict fold limbs after volume loss in hinge zones during cm-scale folding of narrow limestone layers. Individual nodules are aligned parallel to S1. The gray cores are rectangular and imbricated, indicating non-coaxial shear along cleavage planes. Dense networks of dissolution seams occupy the surrounding darker material. Some host sparry calcite tension fractures aligned perpendicular to the long axis of the nodule.

II) Milky, 6 cm wide calcite-quartz veins are folded about S1 with an amplitude of 0.5 m(20-2a/A4). Thickening and truncation of the hinges at the foliation illustrates a volume transfer and loss during folding. Type II veins are oblique to bedding and are not as tightly folded as S0, indicating that formation post-dates initiation of folding. They are rimmed by multiple seams of opaque minerals, and internal fabrics document a complex dilational history. Lenses of elongate, fibrous calcite grains are variably oriented, and are in contact with euhedral grains. Subhedral quartz grains overprint the blocky calcite and angular clasts of wall rock are entrained within. Intragranular strain is moderate to non-existent in both phases. The vein therefore records a prolonged history of cyclical crack-seal dilation and open fracture filling within a transient stress field. Lack of intragranular deformation implies that strain was primarily accommodated by ongoing brittle fracture under conditions of elevated pore fluid pressure.

III) Fibrous, 30 μm wide calcite veinlets proximal and sub-perpendicular to type II veins document purely tensile fracture during folding(A4). They perhaps reflect spatial incompatibility and consequent rupture within an incompetent matrix that surrounds a folded rigid body (i.e. the type II vein).

IV) Crack-seal veins 1 cm wide form minor accordion folds with limbs parallel and perpendicular to cleavage(B7,B2,D7?/20-5a)). Some are offset along cleavage planes (21-1a) as a result of either volume loss or shearing. Also, when parallel to S1, they lose their median suture and appear blocky. A similar phenomenon was documented in type II veins at the PTF. Their temporal relationship with type II veins above cannot be constrained. Internally, calcite fibers with high aspect ratios are separated by thin domains of either insoluble material or very fine grained quartz. Fibers are aligned parallel with the vein wall and are likewise folded. In some cases, fibers are disturbed across hinge zones and appear rotated into parallelism with the axial surface. Euhedral quartz that overprints and is in turn cross-cut by calcite attests to multiple phases of fluid infiltration during vein formation.

V) Variably straight and boudinaged cleavage-parallel veins cross-cut all of the above vein types(B5/20-4a). They are 3-7 cm wide and are numerous within well defined zones of the exposure. Calcite is dominant and precipitates as euhedral crystals. Finer grained quartz fills microcracks and occasionally overprints calcite reflecting infiltration of latent, silica oversaturated fluids. Wavy, discontinuous dissolution seams filled with muscovite, quartz, and insoluble material occasionally truncate vein material.

VI) Fault bounding veins 5-9 cm wide localize along northeast dipping faults(20-7a/D2). Drag folds indicate reverse, top to the southwest displacement. The faults offset cleavage and all of the above vein types making this the latest recorded fluid event. Micro-textures belie three distinct fluid events. Coarse grained calcite is euhedral and exhibits offsetting and kinked twins characteristic of mode III-IV structures (*Passchier and Trouw*, 1996). Subhedral, medium grained quartz overprints this early phase and has undergone variably severe deformation as evidenced by sub-grain development and intense undulose extinction. A final pulse of calcite overprints the quartz and occupies healed microfractures. The intragranular strain observed in type VI veins is the most intense of any observed at the exposure.

Isotope Results

Eighteen isotope analyses were obtained from four wall rocks and twelve veins.

*isotope samples collected by G.M. Dipple and N.H.S. Oliver

Sample	$\delta^{18}O$ (measured)	$\delta^{13}C$	Temperature
A3/micrite(iii)	18.5	-1.2	
A4/type II vein	***18.0***	***-1.1***	***305°(S&K);135°(Z)***
s/a(quartz)	***20.6***		
B1/micrite(iii)	18.0	0.7	
B4/micrite(iii)	18.3	-1.2	
B7/type IV vein	***18.1***	***-1.0***	***330°(S&K);150°(Z)***
s/a(quartz)	***20.5***		
B5/type V vein	***18.1***	***-1.2***	
B6/type V vein	***18.1***	***-1.2***	
C3/micrite(iii)	18.6	-1.2	
C3/type I nodule	***17.8***	***-0.3***	
C5/type V vein	***17.9***	***-1.5***	
C8/type V vein	***17.9***	***-1.6***	
C6/type VI vein	***18.0***	***-1.5***	
D4/slate(i)	18.5	-1.8	
D7/type III vein	***18.1***	***-1.1***	
D1/type VI vein	***18.0***	***-1.1***	
D2/type VI vein	***18.3***	***-1.4***	

Despite diverse vein geometry across the exposure, the oxygen isotopic data exhibit the greatest degree of homogenization observed anywhere in the study area. Wall rock compositions range from 18.0 to 18.5 ‰ with vein calcite showing slightly lower signatures between 17.8 and 18.3 ‰. There is no apparent correlation between age or vein type and isotope signature.

However, modest but consistent depletions in the $\delta^{18}O$ of vein calcite relative to neighboring wall rocks persist throughout the outcrop. Wall rock sample 96MRB1 is the only data point that falls off this trend, with an uncharacteristically low $\delta^{18}O$ of 18.0 ‰. An anomalously high $\delta^{13}C$ within the same sample suggests that perhaps it was subject to a higher time integrated fluid flux than surrounding rocks. Disregarding sample B1, vein-host rock fractionations range from -0.2 to -0.8 ‰. The largest and possibly most illustrative discrepancy is within micrite nodules, between the light gray core and darker halo. The dark halo, which is dense with dissolution seams, can be interpreted as a site of net volume loss and a source for dissolved carbonate. Its $\delta^{18}O$, the highest observed at Mitchell Road, either resembles that of the protolith or implies preferential removal of ^{16}O during pressure solution.

Conversely, the massive, light gray core represents a depositional sink for dissolved carbonate and will thus register the infiltration of any isotopically exotic fluid into the system. Indeed, sample 96MRC3 possesses the lowest recorded $\delta^{18}O$ (17.8 ‰) and one of the highest $\delta^{13}C$ compositions (-0.3 ‰). One can calculate the degree of isotope disequilibrium between fluid and wall rock if the total volume loss within the darker haloes from pressure solution can be accurately estimated. Widespread homogenization within veins at Mitchell Road

reflects pervasive exchange with surrounding wall rocks. However, modest depletions show that time integrated fluid flux was sufficiently high that the circulating fluid and surrounding rock package had not yet reached equilibrium.

Main points

- subtle variations in wall rock lithology-no correlation between vein geometry and lithology
- six distinct generations of veins
- most veins contain euhedral calcite (i.e. infilling of open space fractures) and multiple generations of quartz and calcite
- generally low intragranular strain within vein quartz and calcite
- homogenization of vein $\delta^{18}O$ implies pervasive exchange with wall rocks
- consistent vein depletion relative to wall rock suggest kinetic disequilibrium with wall rocks
- "large" fractionation within nodule records infiltration of isotopically depleted fluid

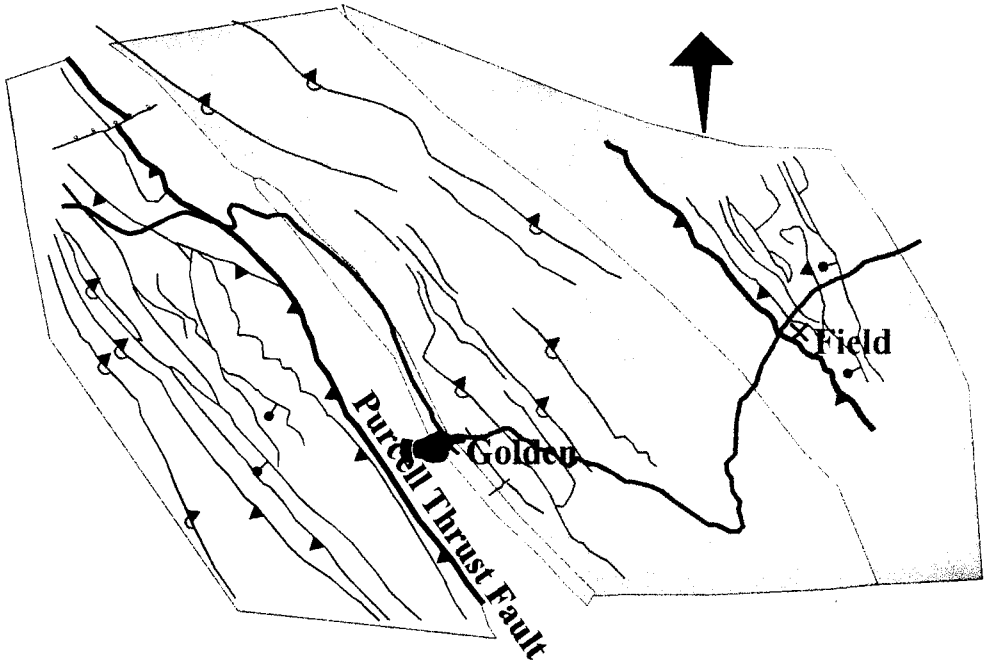
Field
Golden
Purcell Thrust Fault

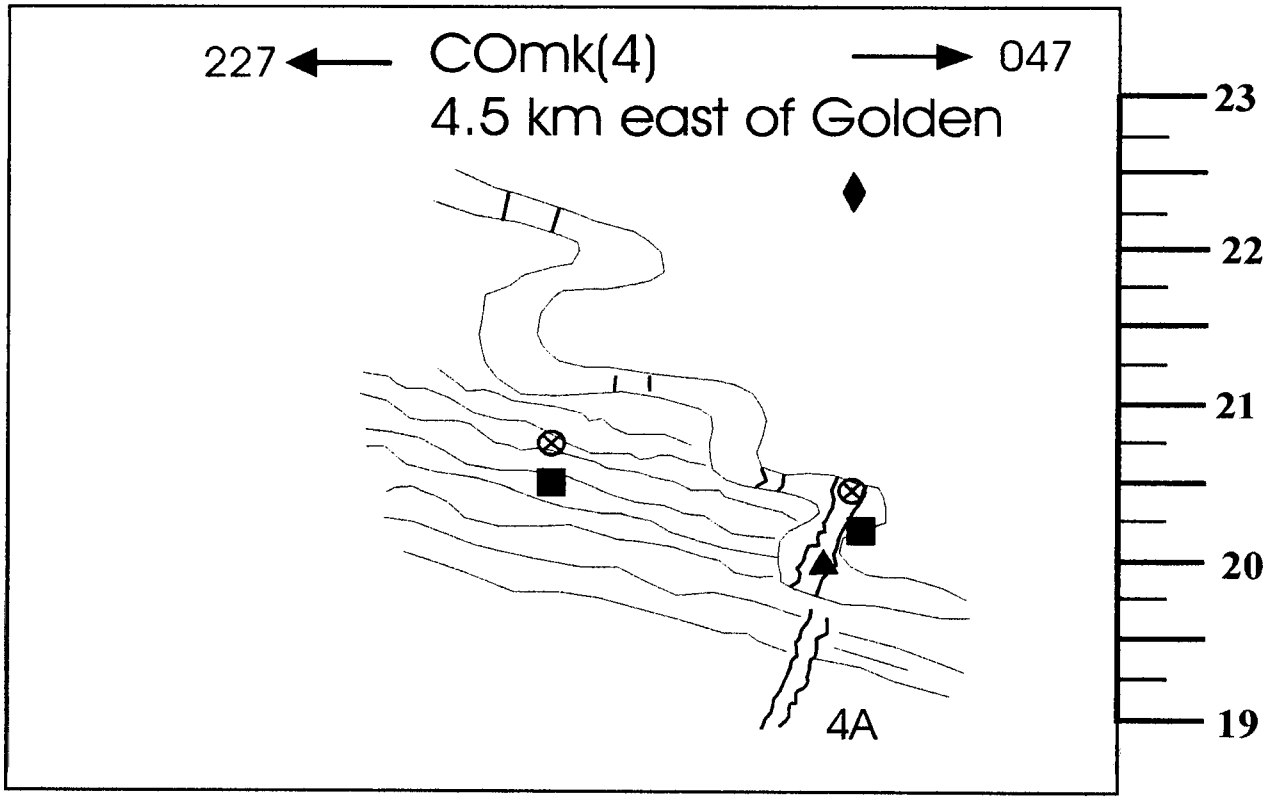
227
COmk(4)
047
4.5 km east of Golden
4A
23
22
21
20
19

COmk 4.5 km east of Golden, BC (Day 41)

Rocks were studied from an exposure of the McKay group (unit 4) along Highway 1. The outcrop is composed of 85-95 % nodular, calcareous slate(41-4b). Limestone beds 5-10 cm thick form distinctive recumbent, isoclinal folds that verge towards the southwest, typical of overturned structures on the southwest flank of the PCA. Tensile, mode I style quartz-calcite veins have replaced ~30 % of the limestone and are oriented perpendicular to bedding(41-4a). The veins are restricted to the limestone and bisect fold hinges, implying formation after or during the latest phases of deformation. Small concentrations of 0.5 cm thick veins offset cleavage within the slate. Vein calcite is coarse grained (>2.5 mm) and subhedral with polygonal grain boundaries. Quartz is substantially smaller (<0.5 mm) and also subhedral. Both phases are in textural equilibrium and evidence very minor intragranular strain (mode II twinning-sweeping extinction). Wall rock calcite is finer grained and possesses kinked twins that terminate within grains (mode III-IV), thereby showing a higher degree of strain than the vein material. Very fine grained quartz (<0.1 mm) occupies 30-40 % of the host rock.

Isotope Results

Four isotope analyses were performed on one vein and two wall rock samples.

Sample	41-#	$\delta^{18}O$ (measured)	$\delta^{13}C$	Temperature
Calc slate	4B	20.4	-0.3	
limestone	4A	20.1	-0.2	
mode I vein	***4A***	***20***	***-0.3***	**340°(S&K);155°(Z)**
s/a(quartz)	***4A***	***22.3***		

Both isotopic systems within vein calcite exhibit full equilibration with the surrounding limestone (within the range of analytical uncertainty). There is no evidence for influx of fluid exotic to the system during vein formation. Veins probably acted as a sink for carbonate and silica dissolved during pressure solution in the surrounding slates within a closed system.

Main points

- mode I veins - brittle fractures - propagate at limestone beds and either formed after or during the waning stages of deformation
- similar $\delta^{18}O$ and $\delta^{13}C$ between limestone and slate
- identical $\delta^{18}O$ and $\delta^{13}C$ between vein and limestone means closed-system fluid regime and veins probably were sink for material dissolved within surrounding slates

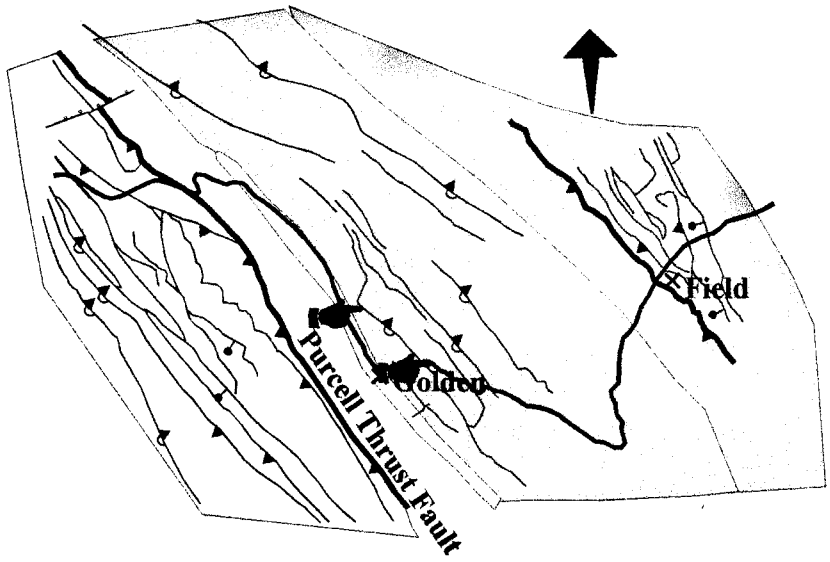

OTF fault at Mt. Moberly and Trans-Canada

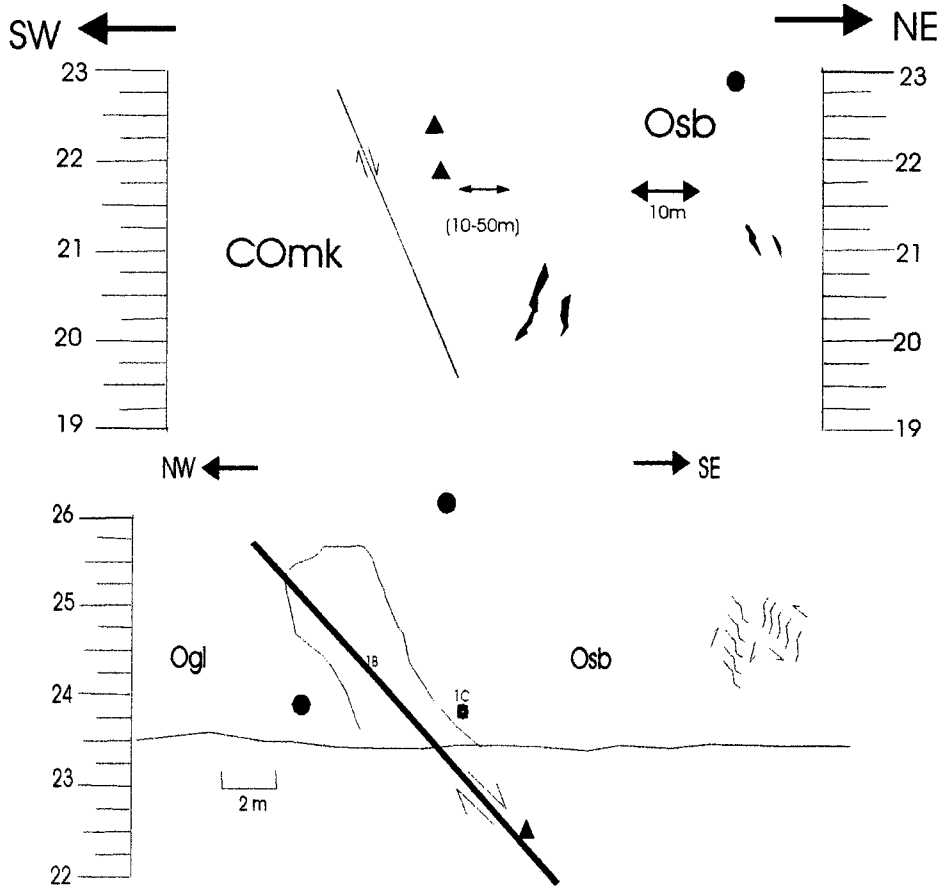

Overturned fault at Mt. Moberly and Trans-Canada Hwy. (49;36)

Samples were collected at a steeply dipping, southwest overturned thrust fault (OTF) that is representative of structures in the southwest limb of the Porcupine Creek Anticlinorium. The OTF is one of a series of faults in the area with minor displacement (500-1500 m), which have been overturned during latest northeast translation on a regional decollement at depth (*Balkwill*, 1972; *Kubli and Simony*, 1994). Along the Trans-Canada Highway, massive limestone and dolomite from the Glenogle Formation (Ogl) is thrust upon massive dolomite in the Beaverfoot Formation (Osb). The OTF contact is exposed as an abrupt zone of highly weathered, incompetent material bounded on either side by densely veined cataclasite(36-1B). Subhedral dolomite grains ~0.5 mm in diameter occur within vein/breccia bounded domains that comprise 60-70 % of the cataclasite. Ductile strain in dolomite grains is minimal, as documented by mode I twinning. Calcite filled veinlets 25 μm wide cross-cut and offset these domains and often terminate at zones of brecciated dolomite within a matrix of insoluble material. In the breccia zone, grain size has been reduced by an order of magnitude to 30 μm in diameter.

Samples were also retrieved from an outcrop at Mt. Moberly where rocks from the McKay group are thrust upon Osb. Like the breccia discussed above, this sample consists of relatively undeformed domains of subhedral dolomite truncated by chaotically oriented narrow veinlets. However, most of the veins and breccia are filled with very fine grained dolomite (<10μm)(i.e. minimal calcite) and there is proportionally less insoluble material along grain boundaries. Dolomite rhombs, ~ 20 μm in diameter, overprint undeformed detrital quartz and chert clasts. Although the thrust contact is poorly exposed, en echelon tension gashes record the presence of active tectonism, and I therefore propose that sample 49-2A does indeed record a fault fabric as opposed to solution collapse features. There is no evidence from the literature that the regional dolomitization event that affected much of the Rocky Mountain foreland prior to Mesozoic deformation had an impact on units this far west (*Yao and Demicco*, 1995; *Nesbitt and Muehlenbachs*, 1994).

Isotope Results

Ten isotopic analyses were obtained from two wall rock and two breccia samples.

	Sample	#	$\delta^{18}O$(wr)	$\delta^{13}C$	Temperature
Trans-Canada Highway	wall rock(calcite)	36-1B	26.2	-0.7	
	breccia/matrix(cc)	***36-1B***	***25.1***	***-0.6***	
	s/a(dolomite)	***36-1B***	***24.1***	***-0.4***	***Cc and dolomite out of thermal equilibrium***
	breccia/veinlets(cc)	***36-1B***	***22.5***	***-1.3***	
	s/a(dolomite)	***36-1B***	***22.3***	***-1.1***	
Mt. Moberly	wall rock(dolomite)	49-1A	22.9	-0.7	
	breccia/matrix(cc)	***49-2A***	***23.1***	***-1***	***Cc and dolomite out of thermal equilibrium***
	s/a(dolomite)	***49-2A***	***22.4***	***-0.9***	
	breccia/veinlets(cc)	***49-2A***	***23.1***	***-2.7***	
	s/a(dolomite)	***49-2A***	***21.8***	***-2.6***	

Isotope data from the OTF exhibit a greater spread within a single sample of breccia than that observed over 100's of meters at other outcrops west of the Purcell Thrust. Samples from within mm's of each other show changes of up to 2.6 ‰ indicating wide fluctuations in either fluid flux or composition. At Highway 1, fractionation between breccia calcite and the protolith range from -1.1 to -3.7 ‰ with maximum depletion occurring in the vein material. Vein dolomite is similarly depleted compared to matrix material revealing that secondary dolomite also precipitated from an externally derived fluid. Negative dolomite-calcite fractionations demand that the phases either did not precipitate in thermal equilibrium or they formed from compositionally distinct fluids. Vein $\delta^{13}C$ is also distinct from that of the matrix, exhibiting a depletion of 0.6 ‰.

At Mt. Moberly, breccia calcite, a phase that is exotic to the system, is unexpectedly equilibrated with the protolith. Compared with the breccia from Highway 1, dolomite demonstrates similar, but more subdued, depletions in matrix and vein compositions of 0.5 and 1.1 ‰, respectively. Also, like the southern outcrop there is a significant ^{13}C fractionation of -1.9 ‰ between vein and host rock.

The increasing trend in $\delta^{18}O$ from veinlet to matrix to protolith records increasing degrees of ^{18}O exchange between fluid and rock. Alteration of relict dolomite domains (matrix) signifies the presence of a comparatively large volume of isotopically exotic fluid within the fault zone during cataclasis. That $\delta^{13}C$ depletions are not recorded in the matrix material only reflects the resistance of carbonate rocks to diffusive mass transfer of ^{13}C within a water dominated fluid phase. The disequilibrium between calcite and dolomite is enigmatic, but probably results from fluctuating thermal conditions during faulting rather than infiltration of compositionally distinct fluid phases.

Main points

- 1-10 m wide breccia zone delineates fault contact
- significant $\delta^{18}O$ and $\delta^{13}C$ depletions in veins and matrix from breccia relative to host rock

- alteration of undeformed, relict dolomite domains in breccia attests to the infiltration of significant volume of isotopically exotic fluid into fault zone
- isotopic disequilibrium between calcite and dolomite records thermal fluctuations during faulting (?)

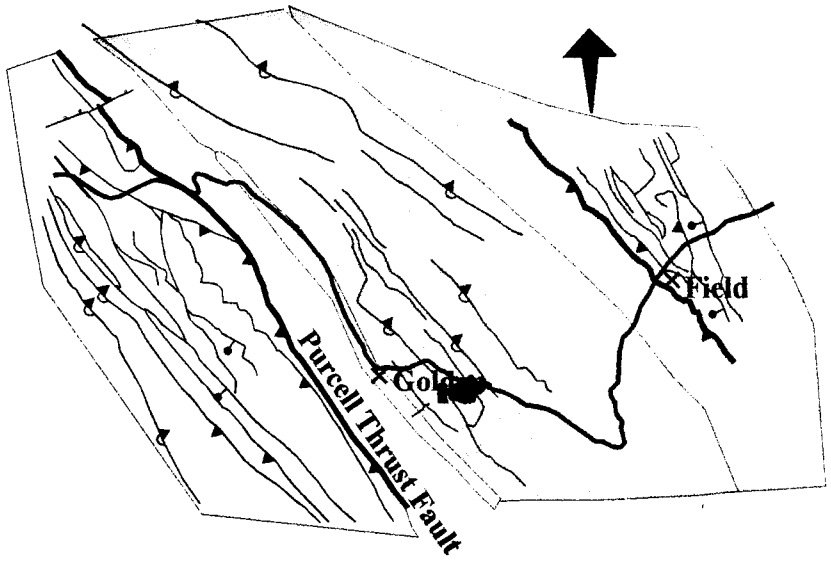

Overturned Thrust Fault at Kicking Horse River

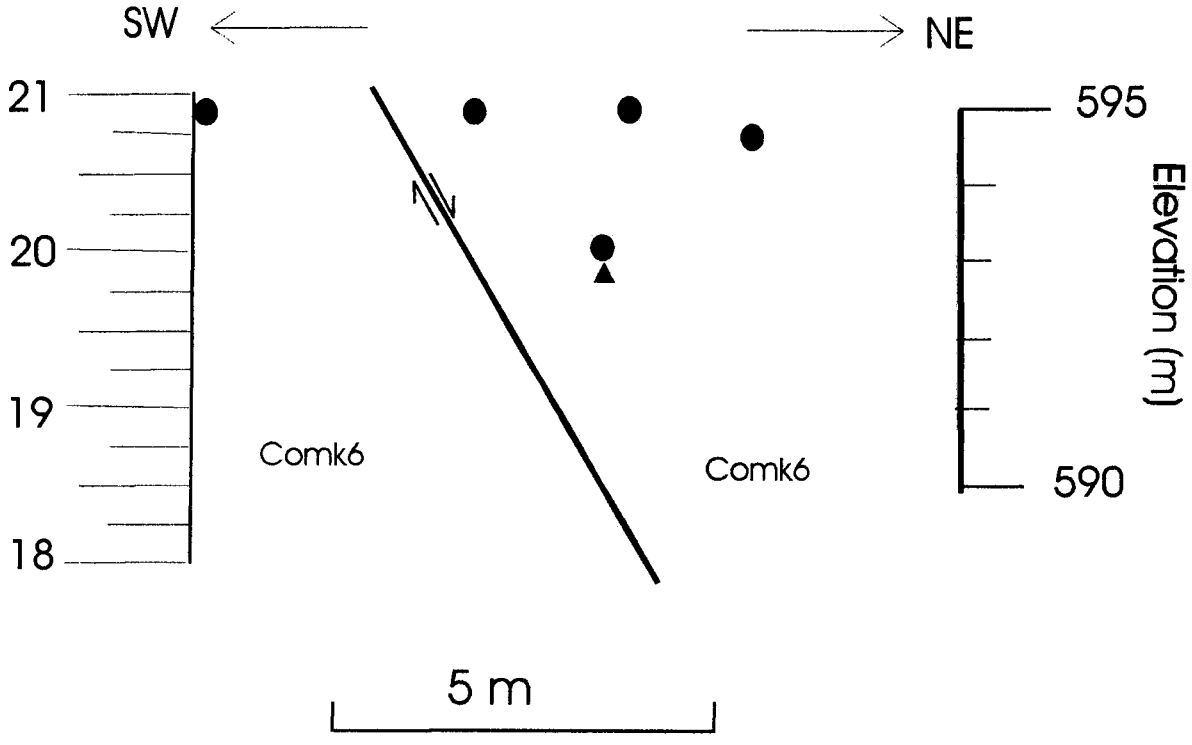

Overturned fault at Kicking Horse River (Day 29)

Samples were collected along a 10 m transect across a well exposed overturned thrust fault (KHF) in a cliff face on the Kicking Horse River. Displacement is approximately 750 m (GSC cross-section) and, at the level of exposure, occurs entirely within the McKay group (unit 6). The fault is steeply overturned to the southwest but retains its flat-ramp-flat geometry from initial translation. Like the OTF discussed above, the KHF belongs to the system of overturned thrusts that splay from a basal detachment in lower Cambrian strata west of the PCA (*Balkwill*, 1972).

A 50 cm wide horizon of folded and interleaved shale and densely veined breccia designate a damage zone along which most of the strain is localized. The breccia is distinctively hard and resistant compared to surrounding limestone (29-1d). Numerous mutually cross-cutting calcite veins and stylolites at different scales are parallel and orthogonal to the main fabric illustrating multiple fluid events. Matrix calcite has undergone *intense grain size reduction* from 0.4 mm to less than 10 μm, and exhibits a strong shape preferred orientation parallel to S1. Twinning within the few relict coarser grains is moderate, suggesting that solution transfer (Coble Creep) was the dominant mechanism of recrystallization. However, dislocation and Coble creep might have acted in tandem to cause the dramatic reduction in grain size.

Fine grained, detrital quartz is localized in stylolites and, to a lesser degree, in the recrystallized matrix. It occupies only 2-5 % of the sample, shows mild internal strain, and was apparently insoluble given local P-T conditions. Stylolites are typically oriented parallel to the local fabric and fault plane (325/70 NE), but in some instances form as stepovers across S1-parallel veinlets. Here they offset the veinlets by ~5 mm, highlighting significant volume loss during pressure solution. Veins vary in width between 0.2 and 5 mm and are composed of proportionally sized calcite grains 0.1-3 mm in diameter. The grains are blocky and euhedral and in textural equilibrium with trace amounts of very fine grained quartz. Disarticulated fragments of vein material grade into the fine grained matrix, indicative of cycling between brittle and ductile processes during cataclasis.

Surrounding limestone has a composition that varies from 5-10 % to less than 1 % quartz (29-1h). Stylolites parallel to the main fabric are present in all lithologies. However, rocks with a more slaty appearance tend to have more discontinuous stylolite arrays. These also possess calcite with a shape preferred orientation and a smaller constituent of quartz.

Isotope Results

Four wall rocks and two samples from the damage zone were selected for isotopic analysis.

	Sample	29-#	$\delta^{18}O$ (measured)	$\delta^{13}C$
Hanging Wall	limestone/5 m	1H	20.8	-1.5
	limestone/30 cm	1A	20.8	-1.7
FAULT	***breccia/matrix***	***1D***	***20***	***-1.6***
	breccia/veinlet	***1D***	***19.8***	***-1.3***
Footwall	limestone/1 m	1G	20.9	-1.4
	limestone/3 m	1G	20.7	-1.7

Oxygen and carbon isotope compositions at KHF fall within a narrow range of values (+/- 0.5 ‰) indicative of a predominantly rock buffered system. Wall rock limestone, regardless of subtle textural variations, is completely homogenized within the range of analytical uncertainty. However, a modest but well constrained $\delta^{18}O$ depletion of 0.8 and 1.0 ‰ within breccia matrix and vein material, respectively, is consistent with the influx of unequilibrated fluid into the fault zone during cataclasis. Isotopic discordance between dynamically(?) recrystallized matrix material and its protolith confirms the contribution of fluids to enhanced ductility. Carbon compositions exhibit no such changes at the fault zone, demonstrating the higher susceptibility of carbon species to rock buffering during fluid migration through limestone.

Main points

- well defined, ~50 cm thick cataclasite within fissile slate demarcates fault zone
- cross-cutting stylolites and veins, intense grain size reduction within the matrix, and detached vein segments that grade into the matrix illustrate the importance of both brittle and ductile processes during deformation
- small, but well constrained, oxygen depletion in the breccia records infiltration of unequilibrated fluids into fault zone during cataclasis

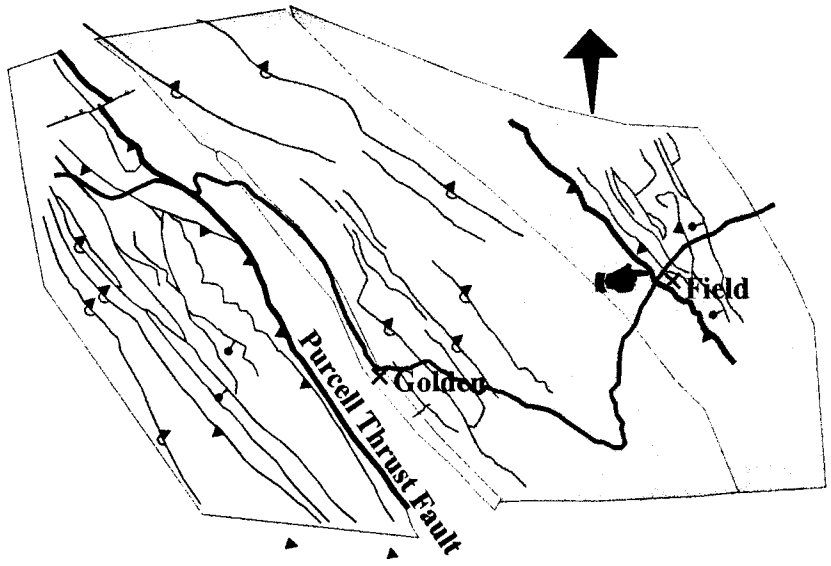

Martin Creek Thrust at Mount Burgess

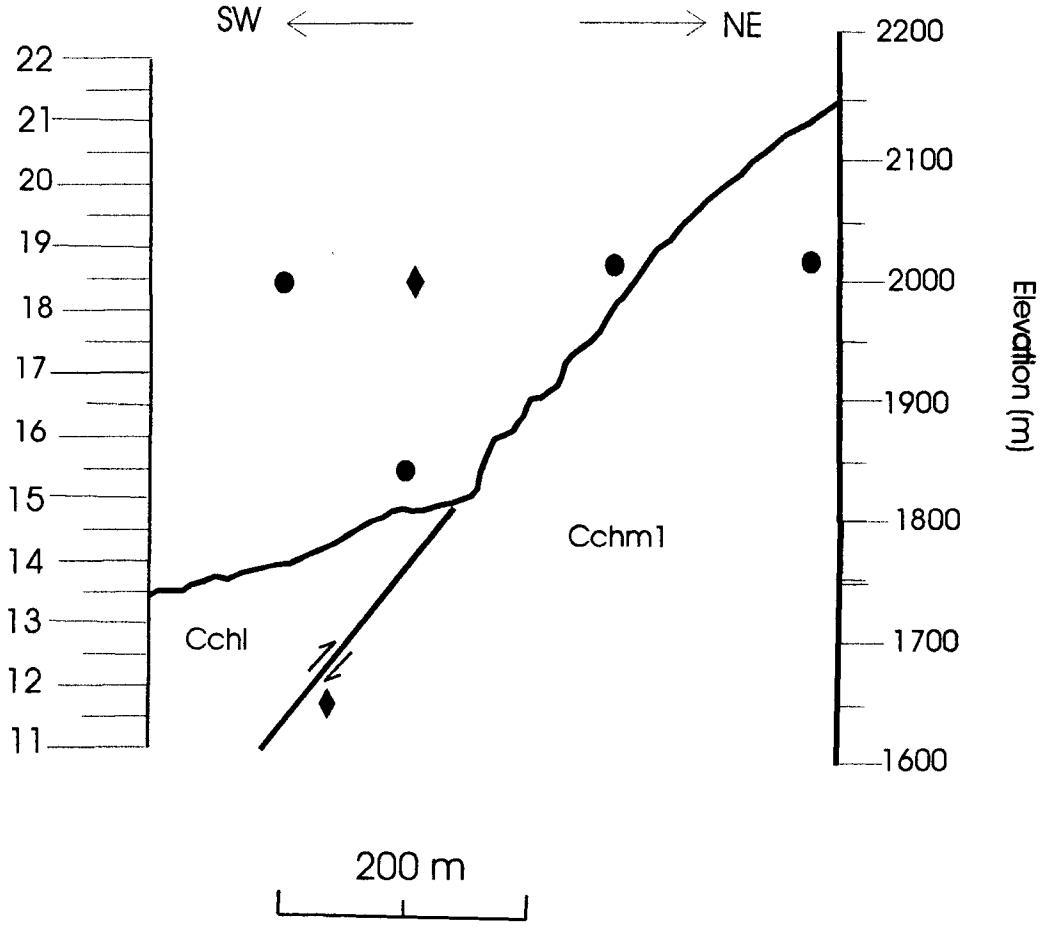

Martin Creek Thrust at Mt. Burgess (Day 31)

Samples were collected along a 400 m traverse across the Martin Creek Thrust where it crosses the southwest flank of Mt. Burgess near Field, BC. With a strike length of more than 30 km, the Martin Creek Thrust is the most prominent fault in the Main Ranges and might represent the continuation of the roof thrust to the Dogtooth Duplex as it extends through middle Cambrian slates (*Kubli and Simony*, 1994). Displacement on the MCT increases from 300 m in the SE to 6 km near Mt. Keays in the NW (*Cook*, 1975). At the sampling locality, separation is on the order of 100's of meters, but initial offset of a greater magnitude is probably occluded by latent normal slip (*Cook*, 1975). The MCT thrusts muscovite-chlorite slates from the lower Chancellor formation (Cchl) against calcareous slate, micrite, and flaggy dolomite of the middle Chancellor formation (Cchm).

The exact fault contact is difficult to identify due to erosion. However, a blocky quartz-calcite vein, unique in size and extent, that coincides with the contact between siliceous slates and calcareous units is designated as the fault zone. The vein is sub-parallel to S1 (145/78 SW), up to 24 cm wide, and has a strike length greater than 100 m (31-2E). It splinters into smaller veinlets that cross-cut cleavage and is proximal to smaller, but similarly oriented veins. In thin section, the core vein is a mosaic of entrained fragments of wall rock slate, plastically deformed, anhedral quartz, and overprinting calcite. Host rock fragments are rimmed and internally replaced by prehnite, which possibly formed from reaction between vein forming fluids and clay minerals. Quartz grains are greater than 3 mm in diameter and contain elongate sub-grains and deformation lamellae oriented parallel to S1, as well as numerous primary fluid inclusions. Calcite occupies quartz microcracks and overprints all other phases, but is also intensely fractured and weathered. Because data on the orientation of nearby bedding was unobtainable, it is possible that the core vein is a pretectonic feature subsequently transposed into parallelism with cleavage. However, its coincidence with the fault contact suggests otherwise. A neighboring, S1-parallel vein (31-2B) also exhibits a 0.5 mm wide prehnite fringe at the vein-slate contact.

During prolonged contraction, chemically distinct fluids infilled fractures yielding multiple phases and varied textures. Syn-kinematic fluid flow is recorded by mutually cross-cutting cleavage parallel and orthogonal quartz-calcite veins within footwall micrite(31-3C). Ribbon quartz documents stretching parallel to S1, and overprinting calcite shows intense intragranular strain in the form of kinked, mode IV twinning.

Isotope Results

Four wall rocks and two veins were sampled for isotopic analysis.

	Sample	31-#	$\delta^{18}O$ (measured)	$\delta^{18}O$ (qtz)	$\delta^{13}C$
Hanging Wall	slate(25 m)	2D	14.1	18.5	
	slate(10 m)	2B	12.8	15.5	
	S1-parallel vn	***2B***	***18.5***	***18.5***	
FAULT	***core vein***	***2E***	***11.8***	***11.8***	
Footwall	calcareous slate(50m)	2G	18.8	18.8	
	micrite (300 m)	3C	18.8	19.8	0.1

Conclusions regarding the nature of syn-kinematic fluid flow at MCT are ambiguous. Considering the diverse mineral phases (quartz-calcite-chlorite-muscovite) analyzed, the data yield fairly consistent oxygen compositions for wall rocks across the upper and lower plate. Three of the four wall rocks, each analyzed for a different phase, range between 18.5 and 19.8 ‰(qtz). The lower composition from the fourth sample (15.5 ‰ (qtz)) might be an artifact of errors from estimation of mineral fractions. Otherwise, the depletion might record fluid channeling along cleavage planes during faulting. However, the elevated $\delta^{18}O$ composition (18.5 ‰) of an S1-parallel vein immediately adjacent to that sample makes this latter interpretation unlikely. The 6.7 ‰ discrepancy between two very similar veins near the fault zone is enigmatic. While a vein from the immediate hanging wall is equilibrated with its host rocks, the core vein at the fault contact shows one of the largest depletions and lowest signatures observed anywhere in this study. Such a low $\delta^{18}O$ reflects infiltration of fluids exotic to the system, which have experienced very little exchange with surrounding wall rocks. Based on the intense intragranular strain observed in vein quartz, dilation and consequent meteoric influx during later stages of uplift and relaxation is unlikely. However, because of our inability to measure local bedding at the fault, we cannot exclude the possibility that the vein is pre-tectonic and underwent later transposition into parallelism with cleavage. Without further detailed sampling, the results are ambiguous.

Main Points

- fault contact defined by uncharacteristically thick quartz-calcite-prehnite vein
- vein might be pre-tectonic, later transposed into parallelism with S1
- wall rocks in footwall and hanging wall have consistent $\delta^{18}O$ despite lithological differences
- hanging wall vein is equilibrated with host rocks, but core vein shows substantial depletion commiserate with open-system fluid circulation
- ambiguous timing of vein formation means ambiguous implications for fault related fluid flow

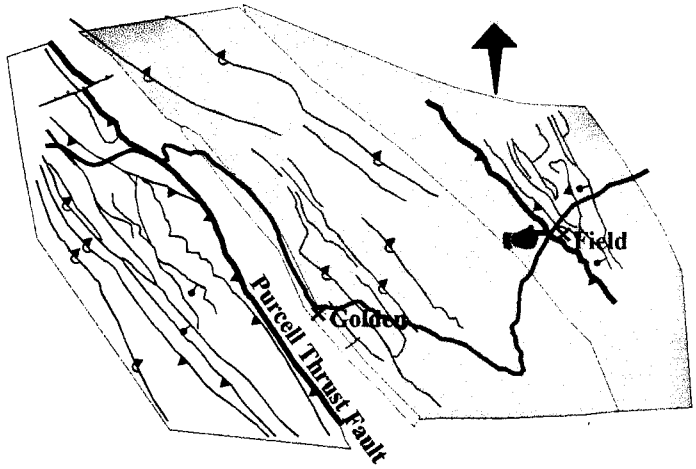

Ccm near Emerald Lake

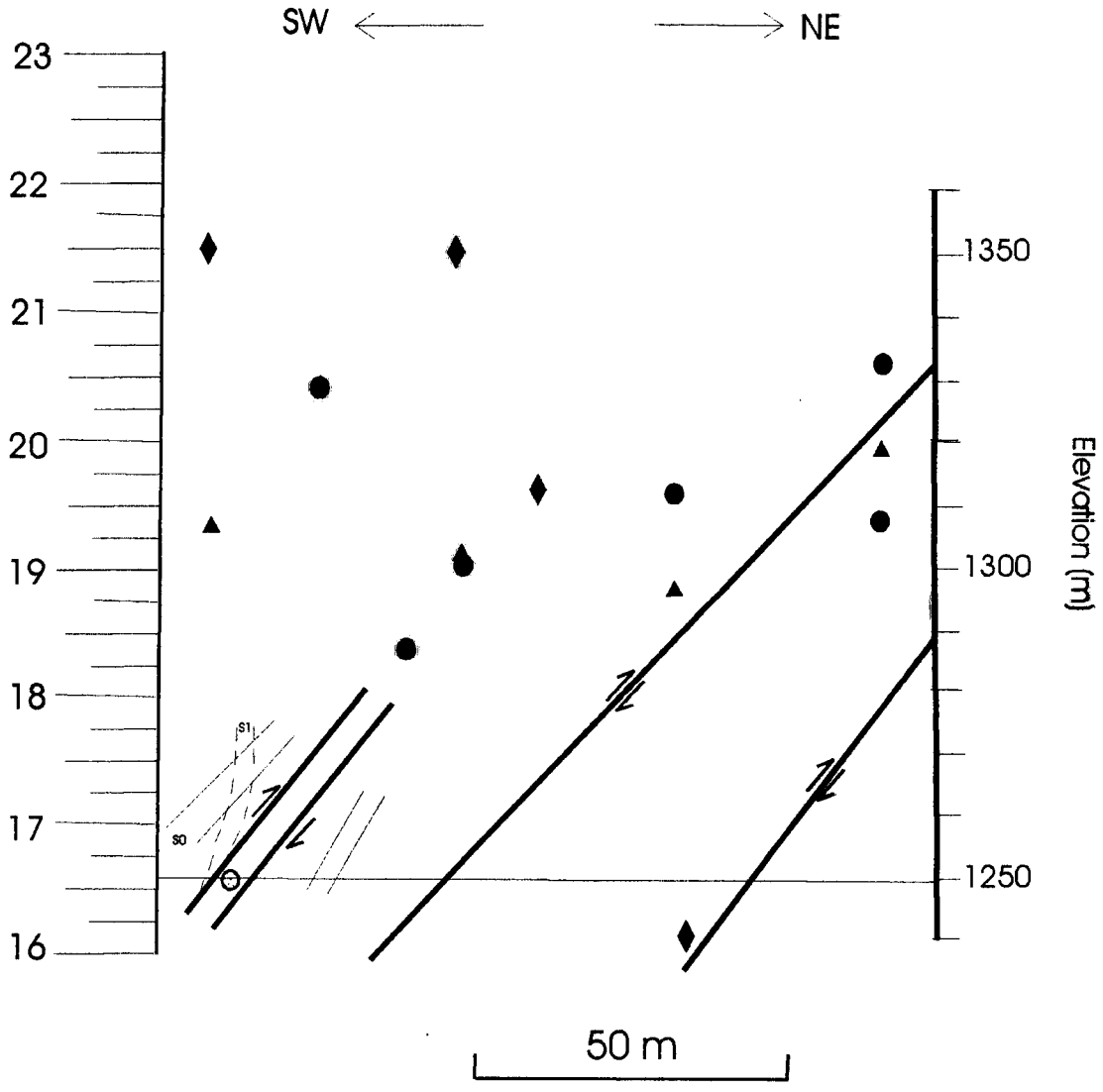

Cchm roadcut at Field, BC (Days 25 and 44)

A series of well exposed calcareous and siliceous slates in a roadcut along the Emerald Lake road were analyzed. We selected the outcrop for study because:

a) it serves as a superb illustration of localized strain accommodation within thrust sheets by a continuum of structural fabrics related to m-scale faulting, brittle fracture (i.e. veining), and folding.
b) multiple, cross-cutting veining events are well exposed
c) the location coincides with the approximate trace of the Martin Creek Thrust.

The outcrop is punctuated by several northeast and northwest vergent reverse faults with visible offset on the order of meters. In some instances, vein density and style vary dramatically on either side of the fault implying that the surface functioned as a conduit or barrier to fluid flow, and/or acted as a discontinuity in the ambient stress field between footwall and hanging wall. Drag folding of spaced and fracture cleavage documents reverse displacement. Small folds with amplitudes of ~30 cm frequently form in the immediate footwall of local faults, with the hanging wall exhibiting homoclinal bedding oriented slightly oblique to the fault surface.

Veins

Tension gashes, and bedding and fault parallel veins occur in close association with the thrusts, while cleavage parallel veins seem to form through progressive folding and foliation development within incompetent units. Six distinct categories of veins are evident at the outcrop.

I) Quartz-calcite filled extension fissures are confined to 10 cm thick micrite beds (see *Ramsay and Huber*, 1987(b)). The gashes are oriented in a fan around the fold axis implying formation prior to folding.

II) Fibrous, quartz filled framboids mantle pyrite porphyroblasts and record episodes of non-coaxial shear.

III) Bedding parallel, crack-seal veins are hosted by faintly foliated micrite. They are ~ 0.5 cm wide and filled with calcite(25-2a). They possess multiple median sutures filled with graphite and form ptygmatic folds. The vein material is rimmed by a 2 mm zone of intense dissolution recorded by dense, S1-parallel graphite seams with seam density the highest in the core of folds. Offset and truncation of vein material along cleavage reflects substantial volume loss following S1 formation. However, sub-mm apophesies branching into parallelism with S1 suggest that veining, seam development, and folding were synchronous.

IV) Sigmoidal tension gashes <1 - 5 cm wide cross-cut bedding and cleavage and merge with fault-parallel veins (25-2c-e). They tend to be proximal to faults where cleavage is folded and probably formed during localized ductile shear prior to rupture.

V) Variably boudinaged, cleavage parallel veins are present throughout the outcrop. They are composed of quartz and calcite and have thicknesses that range between 5 and 25 cm from neck to boudin (25-2j). Type V veins cross-cut folds and are sometimes diffracted across bedding contacts because of competency contrasts. The host rock is generally poorly cleaved, very fine grained (<20 μm) micrite composed of a minor amount (28 %) of quartz. Grains along the vein boundary are fibrous with blocky material filling the vein core. Quartz and calcite fibers are orthogonal to the vein wall in boudins and parallel to cleavage in vein necks indicating a two-stage dilation history. Similar veins and microfabrics have been documented in Chancellor units to the north (*Gardner*, 1977). Very thin, 0.5 mm antitaxial veinlets filled with quartz and muscovite splay off the core vein at an angle oblique to the foliation and represent latent influx of silica oversaturated fluid.

VI) Quartz-calcite veins that line fault surfaces exhibit both crack-seal and blocky morphologies (25-3c,d) They possess one or more median surfaces filled with opaque minerals and post date all other veins. Vein material is coarse grained (> 4mm) and contains very minor intragranular strain in the form of mode II twins(calcite) and

sweeping extinction (quartz). Type VI veins grade into wall rock that has been recrystallized with antitaxial calcite and quartz veinlets. The veinlets are interlayered with mm-scale lenses of muscovite and graphite that are sporadically oblique to cleavage. Curved calcite and quartz fibers are oriented antithetic to the surrounding muscovite consistent with dilation during sinistral shear.

Isotope Results

Thirteen isotopic analyses were performed on six wall rock and five vein samples.

Sample	#	$\delta^{18}O$ (measured)	$\delta^{18}O$(qtz)	$\delta^{13}C$	Temperature
micrite	25-2A	19.4		-0.6	
dissolution zone	25-2A	20.6		-0.6	
type III vein	***25-2A***	***19.9***		***-0.4***	
calcareous slate (30% qtz)	25-2J	19.4		-0.3	
type V vein	***25-2J***	***18.8***		***-1***	
s/a (quartz)	***25-2J***	***16.2***			***Out of thermal equilib***
type II framboid	***25-2M***	***19.6***			
secondary calcite in wall rock	25-3D	19		-0.9	
type VI vein	***25-3D***	***21.4***			***310°C(S&K)***
s/a	***25-3D***	***19.1***		***-0.8***	
calcareous slate (40% qtz)		17.5	18.3		
micrite		20.4		-0.5	
type VI vein		***19.3***		***-1***	***355°(S&K);165°(Z)***
s/a (quartz)		***21.5***			

Vein calcite across the transect is grossly homogenized with respect to calcite within the host rock. The range of oxygen compositions from vein carbonate (18.8-19.9 ‰) is slightly depleted but for the most part inclusive within that for wall rock calcite (19-20.6 ‰). Minor depletions in veins relative to their immediate host rock result from fluid-rock equilibration over the scale of the outcrop (> 100 m). The compositional relationship between a bedding parallel vein (20-2a), its dissolution halo, and the surrounding micrite confirms that mass transfer must occur at scales greater than cm's. If volume were conserved during solution transfer between wall rock and vein, the micrite $\delta^{18}O$ would reflect the average composition of the vein and dissolution halo. However, both are enriched relative to the protolith thus requiring infiltration of an enriched fluid into the system.

Vein quartz exhibits a much wider spread (16.2-21.5 ‰) and therefore must precipitate from multiple fluid regimes. A single silicate analysis from a quartz rich protolith yields an intermediate value of 18.3 ‰(quartz equivalent). Fault parallel veins are heaviest in ^{18}O suggesting that during this latest stage of tectonism, fluid fluxes were low enough that silica compositions were buffered by the surrounding carbonates. The pyrite framboid has a $\delta^{18}O$ nearest that of the host rock quartz, consistent with the hypothesis that pressure shadows are filled with locally dissolved material transported over mm's-cm's (*Passchier and Trouw*, 1996). Most enigmatic is the substantially depleted composition of quartz from a distended, S1-parallel vein. This is especially perplexing in light of the apparent textural equilibrium between vein quartz and calcite. Assuming

that both phases precipitated from a common fluid, the fluid flux must have been sufficiently high to preclude equilibrium between silica and wall rock quartz, but low enough for host rock calcite to buffer the carbonate species. Regardless, open system fluid circulation was operative during an intermediate stage of tectonism.

Main Points

- local faults are structural discontinuities that divide different vein domains
- six distinct syn-kinematic vein types, some of which appear mutually exclusive
- $\delta^{18}O$ of vein calcite reflects homogenization over 100 m
- relationship between micrite, vein, and dissolution halo illustrates that mass transfer occurred over scales greater than cm's.
- $\delta^{18}O$ of vein quartz reflects three distinct fluid regimes
- S1-parallel veins formed during open system fluid regime

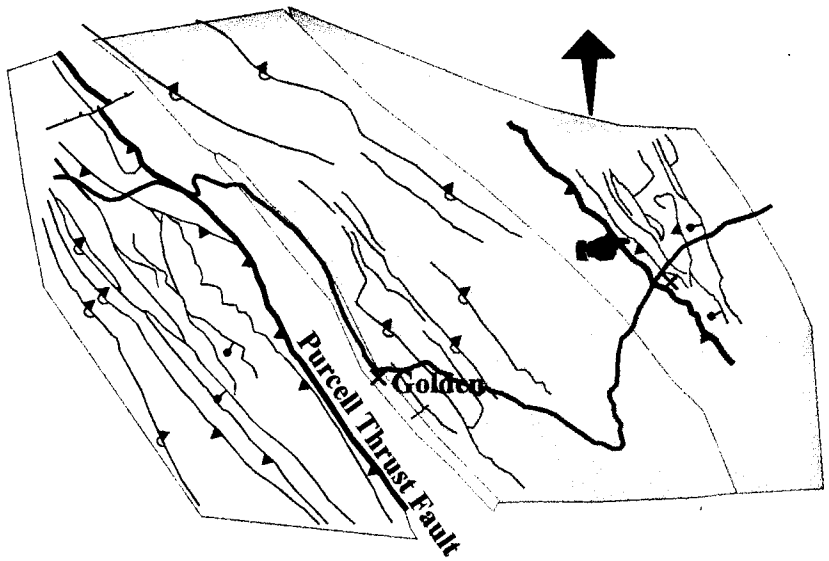
Purcell Thrust Fault
Golden

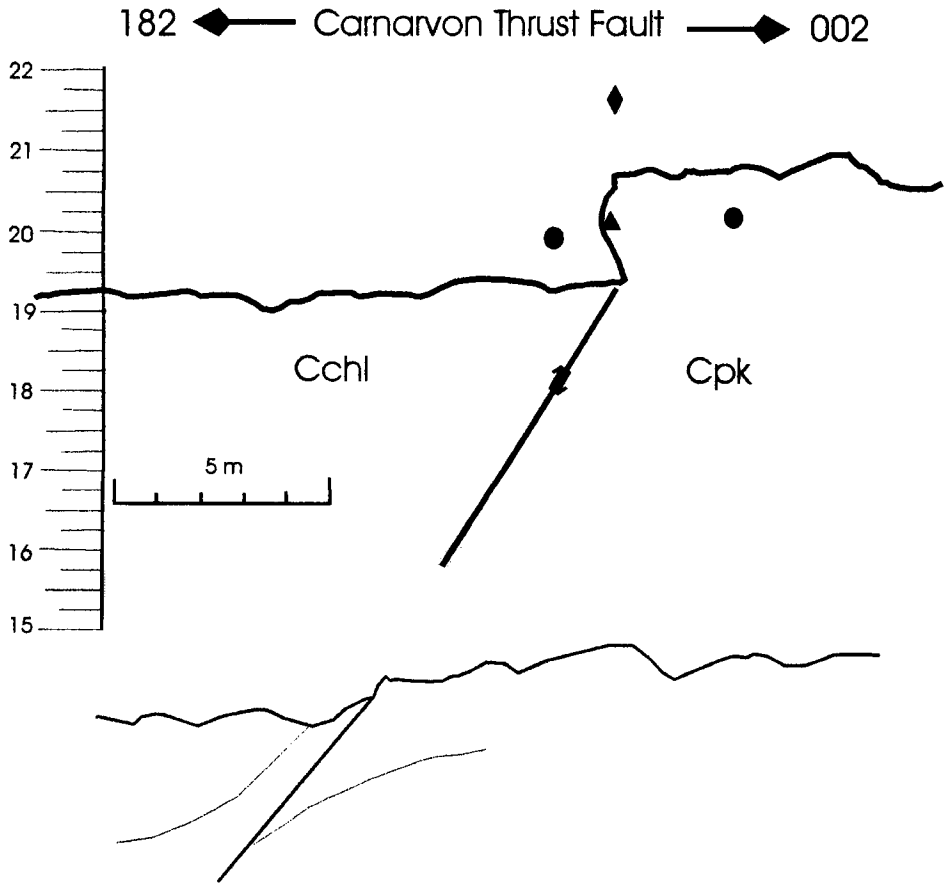
182
Carnarvon Thrust Fault
002
22
21
20
19
18
17
16
15
Cchl
Cpk
5 m

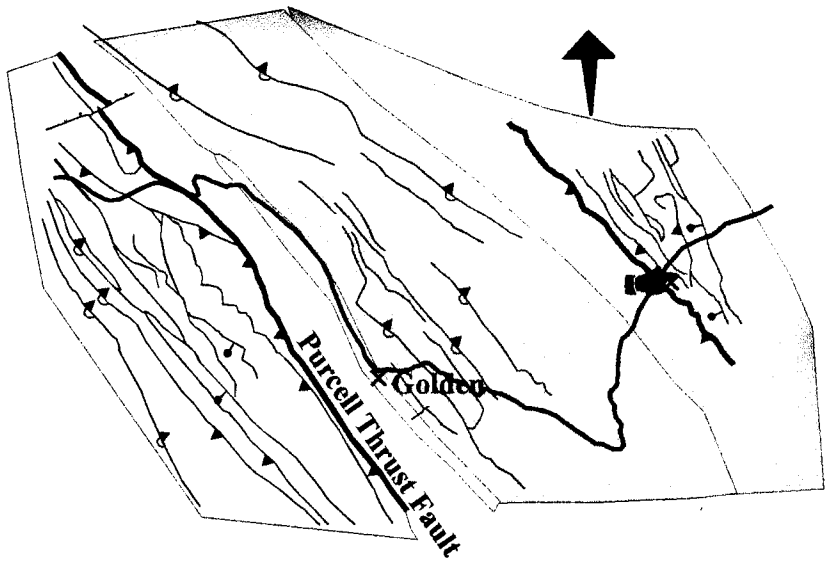

050 ← Cchl/Cel Contact → 230

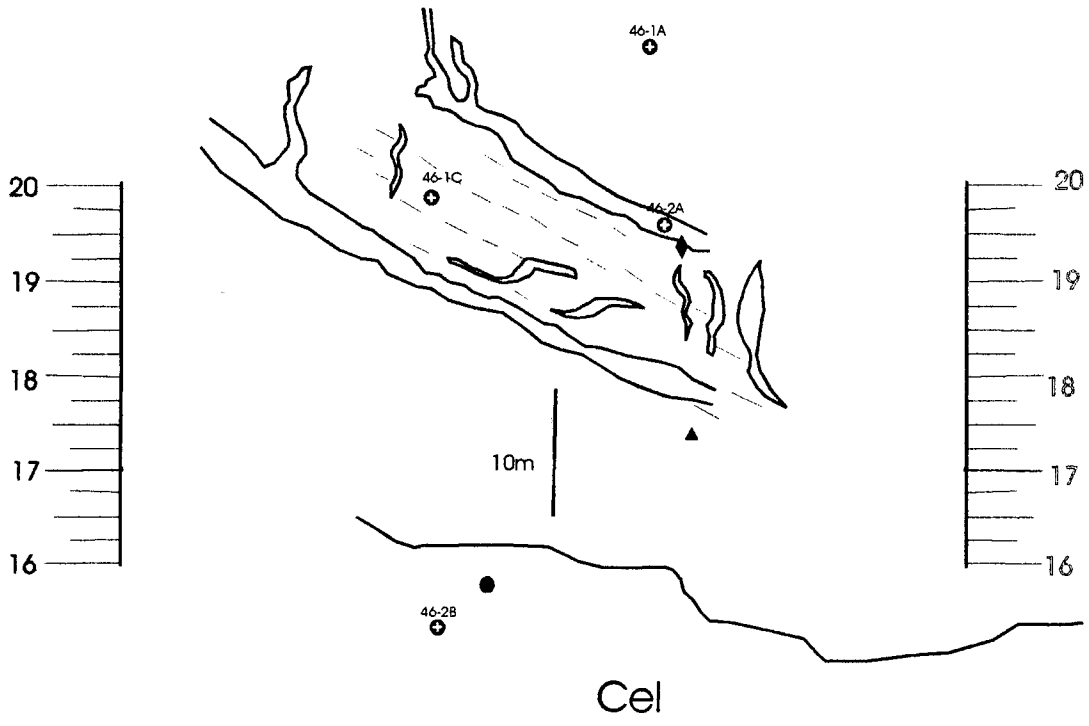

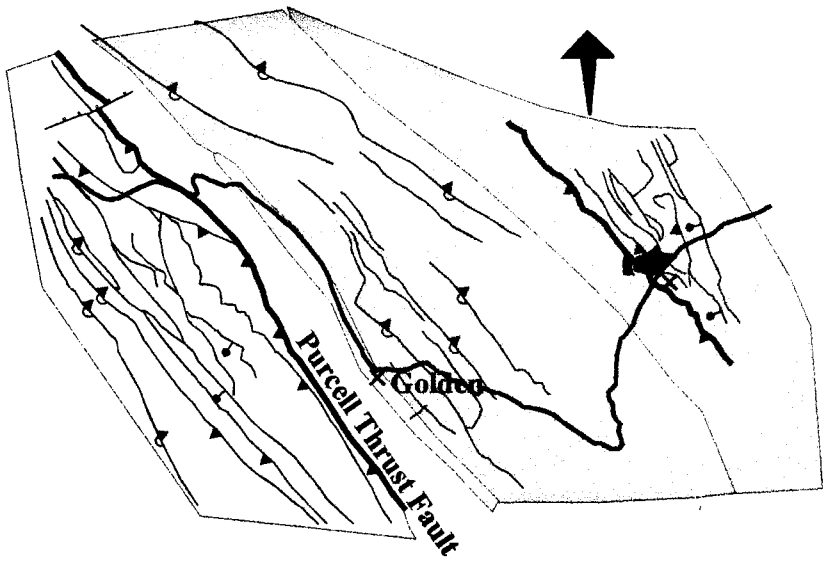
Golden
Purcell Thrust Fault

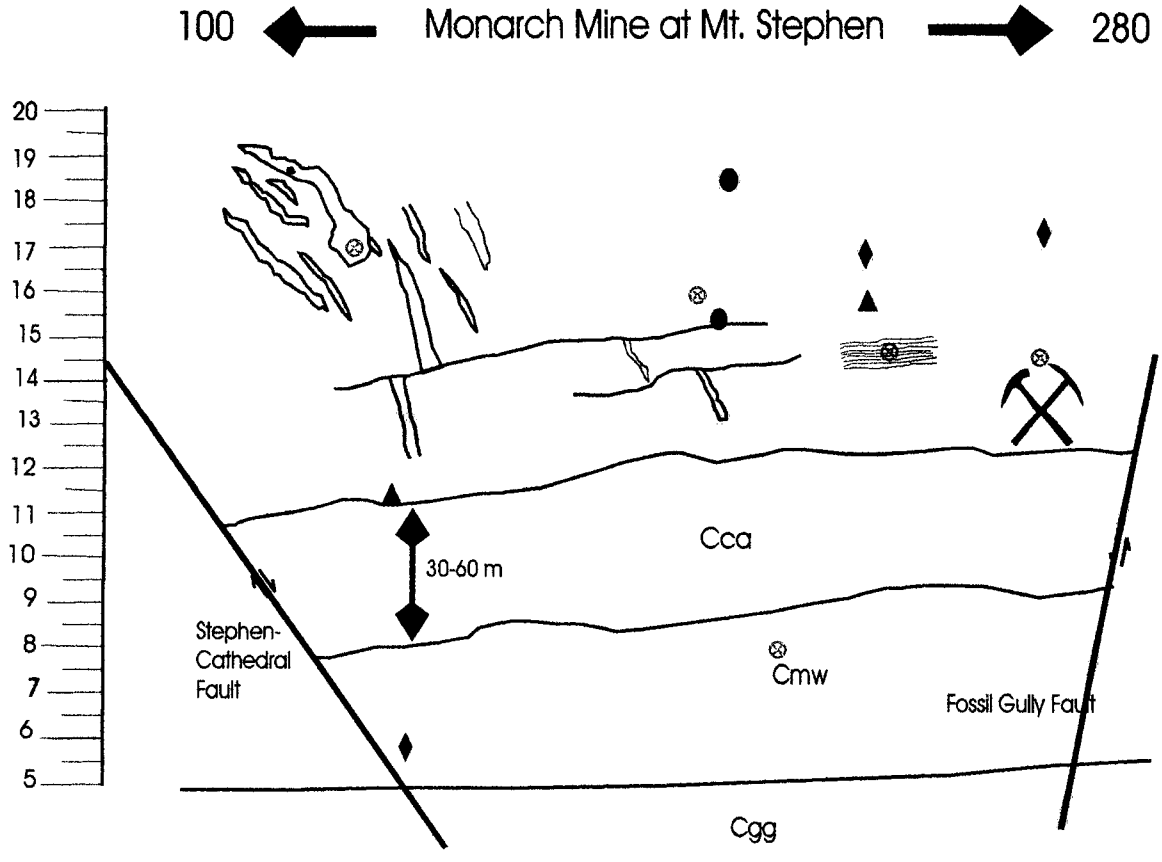
100
Monarch Mine at Mt. Stephen
280
20
19
18
17
16
15
14
13
12
11
10
9
8
7
6
5
Cca
30-60 m
Stephen-
Cathedral
Fault
Cmw
Fossil Gully Fault
Cgg

APPENDIX B

TABULATION OF ISOTOPE VALUES, SAMPLE DESCRIPTIONS, AND ESTIMATED MINERAL MODE IN SILICATES

APPENDIX B1

DOGTOOTH RANGE				Rock Composition (vol. %)				d18O(measured)	d18O(qtz.)	d13C(PDB)	dH(VSMOW)
Locality	Sample	Mineral	Description	Qtz	Musc	Chl	Plag./Ksp.		(370C)		
Copperstain Syncline	42-1A-WR	calcite	limestone					15.4		1.5	
	42-4C-WR	calcite	calcareous siltstone					15.8		0.9	
	42-4B-VQ	quartz	Type I: sigmoidal vein					18.9	18.9		
	42-4A-VC	calcite	s/a					16.0		3.0	
	42-4A-VQ	quartz	s/a					19.7			
	42-5B-WR	silicate	phyllite	20	80	0	0	16.5	19.9		
				10	90	0	0		20.2		
	42-5C-VQ	quartz	Type II: cleavage-parallel vein					18.2			
	42-5C-VH2	muscovite	phyllite								-84
	42-5C-VH	chlorite	Type II: cleavage-parallel vein								-64
Heather Mountain Thrust at Quartz Creek	17-3C-WR	silicate	calcareous slate	5	60	35	0	10.8	15.1		
				5	55	40	0		15.1		
	17-3C-WR	calcite	s/a					15.7		-2.8	
	17-3D-WR	silicate	phyllite	0	80	20	0	13.7	18.1		
				0	60	40	0		18.3		
	17-3E-VQ	quartz	Type I: antitaxial vein					15.7			
	17-3E-VC	calcite	s/a					13.8		-2.4	
	17-3E-WR	dolomite	dolostone					17.3		-0.9	
	17-3F-WR	silicate	sandstone	90	0	0	10	13.6	13.8		
				95	0	0	5		13.7		
hw	17-3F-VQ	quartz	quartz veinlet					13.9			
fw	17-3G-WR	silicate	chlorite phyllite	0	70	30	0	9.5	14		
				0	95	5	0		13.7		
	17-3H-WR	chlorite	chlorite phyllite	0	0	100	0	9.3	14.5		
	17-3K-WR	silicate	chlorite phyllite	20	5	75	0	10.2	14.2		
				40	5	55	0		13.2		
Heather Mountain Thrust at Heather Mountain	16-2B-WR	silicate	sandstone	95	5	0	0	13.4	13.6		
				100	0	0	0		13.4		
	16-2D-WR	silicate	phyllite	5	55	40	0	10.0	14.3		
				25	55	30	0		13.4		
fw	16-2E-WR	silicate	quartzite	85	0	0	15	12.5	12.8		
				95	0	0	5		12.6		
	16-2G-WR	silicate	quartzite	40	55	0	5	11.1	13.5		
				60	35	0	5		12.6		
	16-2I-WR	silicate	quartzite	80	15	0	5	11.9	12.6		
				90	10	0	0		12.3		
	16-2I-VQ	quartz	Type I: antitaxial vein					13.1			
	16-3B-VC	calcite	Type I: antitaxial vein					16.3		-0.4	
	16-3B-VH	muscovite	s/a								-110
Prairie Hills Thrust-hw	16-3B-WR	dolomite	dolostone					15.5		1.6	
	16-1A-WR	silicate	quartzite	85	15	0	0	12.3	12.9		
fw				95	5	0	0		12.5		
Quartz Creek Thrust	43-4A-WR	silicate	Type III vein: shear zone	90	10	0	0	13.1	13.5		

DOGTOOTH RANGE				Rock Composition (vol. %)				d18O(measured)	d18O(qtz.)	d13C(PDB)	dH(VSMOW)
Locality	Sample	Mineral	Description	Qtz	Musc	Chl	Plag./Ksp.		(370C)		
				80	20	0	0		13.9		
at Dauntless Ridge	43-4B-WR	quartz	quartzite					12.5			
Quartz Creek Thrust	34-1C-WR	silicate	phyllite	15	85	0	0	12.2	15.7		
				5	95	0	0		16.2		
at Kinbasket Lake	34-2B-VQ	quartz	Type III: cleavage/fault-parallel vein					14.7			
	34-2B-VC	calcite	s/a					14.1		-11.6	
fw	34-2A-WR	silicate	foliated quartzite	80	15	0	5	14.2	15		
				90	5	0	5		14.5		
	34-2A-WR	calcite	s/a					14.7		-9.9	
	34-3B-VQ	quartz	Type II: cleavage-parallel vein					14.5			
	34-3C-VQ	quartz	Type II: cleavage-parallel vein					14.5			
Unnamed Fault	18-2G-WR	silicate	quartzite	95	5	0	0	12.9	13.1		
				85	15	0	0		13.5		
(footwall of Wall Creek Thru	18-2E-WR	silicate	quartzite	95	5	0	0	12.7	12.9		
				90	10	0	0		13.1		
	18-2E-VQ	quartz	Type I: fibrous vein					18.8			
	18-2A-WR	silicate	quartzite	90	5	0	5	12.3	12.5		
				85	10	0	5		12.7		
	18-3B-VQ	quartz	Type II: cleavage-parallel vein					13.4			
	18-3B-WR	silicate	slate	0	90	10	0	10.5	14.7		
hw				0	95	5	0		14.7		
fw	18-3C-VQ	quartz	Type I: fibrous, a-c vein					12.9			
	18-3C-WR	silicate	foliated quartzite	65	30	0	5	11.8	13.2		
				80	15	0	5		12.5		
	18-3D-VN	chlorite/quartz	matrix within foliated vein	90	0	10	0	11.7	12.2		
				70	5	25	0		13.2		
	18-3D-VQ	quartz	Type II: deformed, crack-seal vein					12.5			
	18-3E-WR	silicate	foliated quartzite	90	10	0	0	11.1	11.5		
				80	20	0	0		11.9		
	18-3E-VQ	quartz	Type I: fibrous vein					12.7			
Cirque Creek Thrust	23-3C-VQ	quartz	Type III: 3 m wide vein					13.1			
Wiseman Creek Thrust	14-3A-WR	silicate	foliated grit	90	8	0	2	14.9	15.3		
				95	3	0	2		15.1		
at Kinbasket Lake	14-2A-VQ	quartz	vein/quartzite-fault zone					14.9			
	14-4C-WR	silicate	foliated sandstone	60	35	5	0	12.8	14.5		
				50	45	5	0		14.9		
	14-4A-WR	silicate	foliated sandstone	75	25	0	0	13.8	14.8		
				60	40	0	0		15.4		
	14-1F-WR	silicate	foliated sandstone	60	40	0	0	11.9	13.5		
				40	60	0	0		14.4		
Wiseman Creek Thrust	9-2E-WR	silicate	sandstone	95	5	0	0	13.2	13.4		
				85	15	0	0		13.8		
at Oldman Creek	9-1D-WR	calcite	limestone					15.3		4.2	
	13-1A-WR	silicate	calcareous slate	33	33	33	0	15.1	18.2		
				50	50	0	0		17.1		
hw				0	100	0	0		19.3		

DOGTOOTH RANGE				Rock Composition (vol. %)				d18O(measured)	d18O(qtz.)	d13C(PDB)	dH(VSMOW)
Locality	Sample	Mineral	Description	Qtz	Musc	Chl	Plag./Ksp.		(370C)		
fw	13-4A-VQ	quartz	massive quartz vein at fault					14.1			
	13-4B-WR	quartz	quartzite matrix	100	0	0	0	13.9	13.9		
				95	5	0	0		14.1		
	13-4B-VQ	quartz	massive quartz vein/ 7m from fault					13.1			
	13-4C-WR	silicate	quartzite matrix	85	15	0	0	12.2	12.8		
				95	5	0	0		12.4		
	8-2-WR	quartz	quartzite protolith	100	0	0	0	13.2	13.2		
				95	3	0	2		13.4		
	48-5A-WR	quartz	quartzite					14.7			

APPENDIX B2

WESTERN RANGES				Rock composition (vol. %)				d18O(measured)	d18O(qtz)	d13C(PDB)
Locality	Sample	Mineral	Description	qtz	musc	chl	plag/ksp		370C	
Purcell Thrust Fault	11-1B-WR	silicate	siliceous slate	60	40	0	0	14.7	16.3	
				45	55	0	0		17	
	10-5C-WR	silicate	slate (50 cm from hanging wall splay)	60	40	0	0	13.8	15.4	
				0	100	0	0		18	
				35	35	30	0		16.8	
	10-5C-VQ	quartz	fault parallel vein					18.1		
	10-5A-VQ	quartz	fault parallel, crack-seal vein					18.3		
	10-5A-VC	calcite	s/a					16.2		-1.9
	34-4A-WR	calcite	calcareous siltstone					16.0		-1.9
	34-4A-VC	calcite	sigmoidal tension gash					16.0		-2.2
	11-4C-VC	calcite	en echelon tension gash					16.2		-2.7
	35-1A-VC	calcite	en echelon tension gash					16.3		-2.5
hw	34-5C-WR	silicate	phyllite	0	100	0	0	15.6	19.8	
fw	34-5A-VQ	quartz	fault-parallel, laminated vein					18.0		
	34-5A-VC	calcite	s/a					16.2		-2.7
	34-5B-VQ	silicate	s/a (1 meter away along strike)					18.7		
	34-5B-VC	calcite	s/a					16.2		-2.7
	34-6B-WR	calcite	calcareous slate					17.9		-2.4
	12-2C-VC	calcite	bedding-parallel/laminated vein					16.5		-0.6
	35-3B-VQ	quartz	fault-parallel vein (footwall splay)					19.0		
	35-3B-VC	calcite	s/a					16.5		-0.4
	12-3C-WR	silicate	siliceous slate	60	30	10	0	15.7	17.4	
				70	30	0	0		16.9	
McKay-Canyon Creek Contact	41-1B-WR	calcite	limestone					19.0		0.3
Rocky Mountain Trench	41-1C-WR	calcite	calcareous siltstone					19.2		-0.1
	41-1C-VC	calcite	cross-cutting/folded vein					18.9		-0.2
	41-1D-WR	calcite	slate					18.8		-0.1
	41-2A-VC	calcite	fault-parallel vein					19.1		-0.3
McKay Group	41-2A-WR	calcite	sparry limestone					19.1		0.3
Canyon Creek Formation	41-3B-WR	calcite	calcareous slate					18.1		0.4
McKay Group at Mitchell Rd.	96MRA4	calcite	micrite					18.5		-1.2
Rocky Mountain Trench	96MRA4	quartz	cross-cutting/folded vein					20.6		
	96MRA4	calcite	s/a					18.1		-1.1
	96MRB1	calcite	micrite					18.0		0.7
	96MRB4	calcite	micrite					18.3		-1.2
	96MRB7	calcite	crack-seal, cleavage-parallel/orthogonal vein					18.2		-1.0
	96MRB7	quartz	s/a					20.5		
	96MRB5	calcite	Boudinaged, cleavage-parallel vein					18.1		-1.2
	96MRB6	calcite	s/a					18.1		-1.2
	96MRC3	calcite	micrite					18.6		-1.2
	96MRC3N	calcite	bleached nodule					17.8		-0.3
	96MRC5	calcite	cleavage-parallel vein					17.9		-1.5
	96MRC6	calcite	fault-parallel vein					18.0		-1.5
	96MRC8	calcite	cleavage-parallel vein					18.0		-1.6

WESTERN RANGES				Rock composition (vol. %)				d18O(measured)	d18O(qtz)	d13C(PDB)
Locality	Sample	Mineral	Description	qtz	musc	chl	plag/ksp		370C	
	96MRD4	calcite	micrite					18.5		-1.8
	96MRD1	calcite	fault-parallel vein					18.0		-1.1
	96MRD2	calcite	fault-parallel vein					18.3		-1.4
	96MRD7	calcite	tensile cracks (mode I)					18.1		-1.1
McKay Group (Unit 4)	41-4A-VQ	quartz	tensile cracks (mode I)					22.3		
4.5 km east of Golden(Hwy 1)	41-4A-VC	calcite	s/a					20.0		-0.3
	41-4A-WR	calcite	limestone					20.1		-0.2
	41-4B-WR	calcite	calcareous slate					20.4		-0.3
Unnamed Fault-Beaverfoot Fm.	49-2A-WRV	dolomite	vein (breccia)					21.8		-2.6
at Mt. Moberly	49-2A-WRV	calcite	vein (breccia)					23.1		-2.7
	49-2A-WRM	dolomite	matix (breccia)					22.4		-0.9
	49-2A-WRM	calcite	matrix (breccia)					23.1		-1.0
	49-1A-WR	dolomite	dolostone (protolith)					22.9		-0.7
Unnamed Fault-Beaverfoot Fm.	36-1B-WRV	calcite	vein (breccia)					22.5		-1.3
at Trans-Canada Hwy.	36-1B-WRV	dolomite	vein (breccia)					22.3		-1.1
	36-1B-WRM	calcite	matix (breccia)					25.1		-0.6
	36-1B-WRM	dolomite	matrix (breccia)					24.1		-0.4
	36-1A-WR	calcite	dolostone (hw)					23.8		-1.5
	36-1B-WR	calcite	lime/dolostone (fw-protolith)					26.2		-0.7
Unnamed Fault-McKay Group	29-1H-WR	calcite	limestone (5 m from fault)					20.8		-1.5
hw	29-1A-WR	calcite	limestone (30 cm from fault)					20.8		-1.7
	29-1D-WR	calcite	matrix (breccia)					20.0		-1.6
	29-1D-VC	calcite	vein (breccia)					19.8		-1.3
fw	29-1G-WR	calcite	limestone (1 m from fault)					20.9		-1.4
	29-1F-WR	calcite	limestone (3 m from fault)					20.7		-1.7

APPENDIX B3

MAIN RANGES				Rock composition (vol. %)				d18O(measured)	d18O(qtz)	d13C(PDB)	dH(VSMOW)
	Sample	Mineral	Description	qtz	musc	chl	plag/ksp		(370C)		
Martin Creek Thrust	31-2D-WR	silicate	slate (25 m from fault)	0	75	25	0	14.1	18.5		
at Mt. Burgess (14)				0	40	60	0		18.9		
	31-2B-WR	silicate	slate (10 m from fault)	45	10	45	0	12.8	15.5		
				70	10	20	0		14.2		
hw	31-2B-VQ	quartz	cleavage-parallel vein					18.5			
	31-2E-VQ	quartz	fault/cleavage-parallel vein					11.8			
fw	31-2G-WR	quartz	slate (50 m from fault)	100	0	0	0	18.8	18.8		
				90	10	0	0		19.2		
	31-3C-WR	calcite	micrite (300 m from fault)					18.8		0.1	
Middle Chancellor outcrop	25-3B-WR	calcite	micrite					20.4		-0.5	
near trace of Martin Creek	25-3A-WR	silicate	calcareous slate					17.5	18.3		
Thrust and Emerald Lake (15)	25-3D-VC	calcite	fault-parallel vein					19.1		-0.8	
	25-3D-WR	calcite	recrystallized slate at fault					19.0		-0.9	
	25-3D-VQ	quartz	fault-parallel vein					21.4			
	25-2M-VQ	quartz	pyrite pressure shadow					19.6			
	25-2J-WR	calcite	calcareous slate					19.4		-0.3	
	44-4B-VC	calcite	fault-parallel vein					19.3		-1.0	
	44-4B-VQ	quartz	s/a					21.5			
	25-2J-VQ	quartz	distended, cleavage-parallel vn					16.2			
	25-2J-VC	calcite	s/a					18.8		-1.0	
	25-2A-WR(l)	calcite	micrite (protolith)					19.4		-0.6	
	25-2A-WR(d)	calcite	darker material (graphite dissol'n seams)					20.6		-0.6	
	25-2A-VC	calcite	bedding-parallel vein					19.9		-0.4	
Caranarvon Thrust (16)	45-1B-WR	calcite	flaggy limestone					20.1		-0.4	
	45-2B-VQ	quartz	laminated, fault-parallel vein					21.7			
	45-2B-VC	calcite	s/a					20.1		-0.9	
	45-3B-WR	calcite	calcareous slate					19.9		-0.4	
Facies Contact (17)	46-2A-VC	calcite	sigmoidal/cleavage-parallel vein					17.3		-2.4	
	46-2A-VQ	quartz	s/a					19.3			
	46-2A-VH	chlorite	s/a								-62
	46-1A-WR	calcite	calcareous phyllite					15.6		-2.4	
Monarch Mine	38-2A-WR	dolomite	dolostone-Cathedral Fm.					15.5		-0.9	
Platform carbonates (18)	47-2A-WR	calcite	calcareous slate - Mt. Whyte Fm.					18.5		0.1	
	38-2C-VC	dolomite	sigmoidal tension gash					11.2		-2.0	
	38-2C-VQ	quartz	s/a					5.9			
	38-2G-VQ	quartz	laminated, bedding-parallel vein					16.9			
	38-2G-VC	calcite	s/a					15.9		-1.9	
	38-2F-VQ	quartz	ore zone vein					17.2			
Gog Gp. near Dennis Pass	47-1A-WR	silicate	quartzite	80	20	0	0	13.1	13.9		
				95	5	0	0		13.3		

APPENDIX C

CALCITE-DOLOMITE SOLVUS GEOTHERMOMETRY

APPENDIX C
Results of calcite-dolomite solvus geothermometry

sample	source	oxide sum	NbCat st Mg	NbCat st Ca	Temp(C)
173E-2	vn cc	100.00	0.018	0.982	**328.58**
173E-5	vn cc	100.00	0.014	0.986	**269.22**
173E-7	vn cc	100.00	0.008	0.992	**61.21**
173E-9	vn cc	100.00	0.009	0.991	**135.01**
173E-11	vn cc	100.00	0.011	0.989	**200.17**
173E-14	vn cc	100.00	0.010	0.990	**161.50**
173E-15	vn cc	100.00	0.020	0.980	**349.87**
173E-16	vn cc	100.00	0.018	0.982	**325.98**
173E-18	vn cc	100.00	0.015	0.985	**278.80**
173E-19	vn cc	100.00	0.029	0.971	**424.91**
173E-20	vn cc	100.00	0.014	0.986	**262.95**
173E-23	vn cc	100.00	0.012	0.988	**223.13**
173E-24	vn cc	100.00	0.023	0.977	**374.20**
173E-25	vn cc	100.00	0.018	0.982	**327.45**
173E-26	vn cc	100.00	0.015	0.985	**277.57**
361B-4	vn cc	100.00	0.081	0.919	**628.24**
361B-8	vn cc	100.00	0.013	0.987	**240.48**
361B-10	vn cc	100.00	0.042	0.958	**493.06**
361B-20	vn cc	100.00	0.015	0.985	**291.71**
361B-24	vn cc	100.00	0.014	0.986	**259.06**
361B-26	vn cc	100.00	0.010	0.990	**178.15**
291D-4	mx(vn?)cc	100.00	0.010	0.990	**179.90**
291D-7	mx cc	100.00	0.009	0.991	**139.09**
291D-31	mx cc(?)	100.00	0.008	0.992	**78.78**
291D-32	mx cc	100.00	0.011	0.989	**189.68**

vn cc = vein calcite; mx cc = matrix calcite
Mg+Ca are restandardized to 1; T calc: Anovitz and Essene